# The effects of passing seagoing vessels on the inland ships in the outer harbour and locks of Hansweert

D. Heijboer

# The effects of passing seagoing vessels on the inland ships in the outer harbour and locks of Hansweert

## Master Thesis

To obtain the degree of Master of Science
at the Delft University of Technology
to be defended publicly on February 28, 2024

by

# D. (Dick) Heijboer

| | | |
|---|---|---|
| Student number: | 4728769 | |
| Project duration: | June 2023 - February 2024 | |
| Thesis committee: | Prof. dr. ir. M (Mark) van Koningsveld | TU Delft |
| | Ir. L. (Lex) de Boom | Witteveen+Bos/TU Delft |
| | Ir. A.J. (Arne) van der Hout | TU Delft |
| | Dr. M.F.S. (Marion) Tissier | TU Delft |

An electronic version of this thesis is available at http://repository.tudelft.nl.

Cover photo: Container ship on open ocean (Prat, 2011).

# Preface

Before you lies the thesis "The effects of passing seagoing vessels on the inland ships in the outer harbour and locks of Hansweert". It has been written to fulfil the graduation requirements of the Master's program in Hydraulic Engineering at the Delft University of Technology. This work, conducted at Witteveen+Bos, would not be complete without acknowledging all the people who supported me in this achievement.

First and foremost, I am grateful for my thesis committee: Lex de Boom, my daily supervisor at Witteveen+Bos, for his consistent guidance and support throughout this journey, Mark van Koningsveld, for serving as the chair of the committee and for offering valuable feedback, Arne van der Hout, whose input and enthusiasm for this field of research have been invaluable and motivating and Marion Tissier as her insightful comments on the methods and the report enriched the overall quality of the thesis.

My sincere thanks go to Matthijs Schouten and Manon Evers of Rijkswaterstaat for their essential role in this project, providing opportunities for site visits, interviews, and crucial data. Without them, this research would not have been possible. Special thanks to all the participants of the interviews and site visits, including inland skippers, pilots, lock operators, and traffic managers. Their contributions helped shape a clear understanding of the problems and provided valuable insights into potential solution directions.

My heartfelt appreciation goes to my parents for their love and support throughout this endeavour. Their encouragement and readiness to lend a helping hand, including lending their car for trips to Hansweert, have been priceless. To my family and friends, thank you for your support, encouragement, and understanding. Your willingness to read and review this document, as well as providing much-needed distractions from the thesis, have been greatly appreciated.

Overall, I am grateful for the journey, and I am pleased with the results achieved. This thesis represents the culmination of months of hard work, dedication, and collaboration, and I hope it serves as a contribution to the improvement of nautical safety.

Dick Heijboer

Rijssen, February 16, 2024

# Abstract

The lock of Hansweert, located in the province of Zeeland in the Netherlands, serves as a crucial inland shipping node between the Western Scheldt estuary and the Rhine Delta. The outer harbour of the lock complex provides the connection to the Western Scheldt and accommodates waiting facilities for inland ships. The Western Scheldt is a vital gateway for maritime traffic, linking the Port of Antwerp to the North Sea. As the navigation channel of the Western Scheldt is located close to the outer harbour of Hansweert, multiple ship incidents at this location are attributed to the water motions generated by passing seagoing vessels on the Western Scheldt. This research investigates how the water motions induced by passing vessels in the Western Scheldt contribute to unsafe situations in the outer harbour and locks of Hansweert, and what preventative measures can be identified to effectively minimize incidents and mitigate risks.

Investigating the incident records reveals that the key contributors are the primary water motions generated by the passing vessels in the Western Scheldt. The phenomenon, experienced as a sudden lowering of the water level and suction forces, can lead to the breakage of mooring lines and uncontrolled movements of inland ships, resulting in a range of safety hazards and operational disruptions. Several documented incidents, field studies and interviews highlight the urgency for effective measures to mitigate the potentially harmful effects of passing vessels on the ships in the Hansweert outer harbour and locks.

A seven-week measurement campaign, involving 1281 passages of so-called oversized vessels, reveals distinct patterns of water level fluctuations during a vessel's passage. A vessel is considered oversized if its length exceeds 210 metres or if its draught is larger than 10 metres. These patterns are described as a translatory drawdown wave travelling into the harbour, reflecting against the lock complex and oscillating back and forth in the outer harbour until dampened. The key parameter characterizing this wave is the lowering of the water level, referred to as the drawdown height. The average measured drawdown height approximates 6 centimetres, with maximum observations up to 40 centimetres. The main factors influencing the drawdown height are the vessel's passing distance to the outer harbour, its speed relative to the currents and its dimensions, shown by a correlation analysis between the parameters describing the passing vessel and the generated drawdown height. Extreme drawdown events were exclusively observed during a combination of a relatively high speed through the water of the seagoing vessel and small passing distances relative to the harbour's entrance.

The impact of the drawdown effects on the inland ships is determined by the forces generated by the pressure difference along the ships, caused by the inclination of the water level. A critical drawdown height of 12 centimetres is set, based on existing force criteria and the linear relation between the drawdown height and water level slope. To improve on the existing drawdown height prediction methods, a site-specific drawdown height prediction equation has been derived:

$$\Delta h = 0.58 \frac{V_s^2}{2g} \left( \frac{A_s}{d_s h_{\text{channel}}} \right)^{0.93} \left( \frac{L_s}{d_s} \right)^{0.70} \sqrt[4]{\frac{h_s}{h_{\text{harbour}}}}$$

where $\Delta h$ is the drawdown height, $V_s$ is the vessel speed through the water, $g$ is the gravitational acceleration, $A_s$ is the underwater cross-section amidships, $d_s$ is the passing distance, $h_{\text{channel}}$ is the channel depth, $L_s$ is the length of the vessel, $h_s$ is the depth at the vessel location and $h_{\text{harbour}}$ is the depth in the outer harbour. Validation of this equation using the observations made during the measurement campaign yields a Pearson correlation coefficient of 0.81 and an Mean Absolute Error score of 2.2 centimetres.

Preventative measures are identified, aiming to minimize incidents and mitigate the risks related to the water motions induced by passing vessels. The predicted drawdown, generated by the passing vessel, is kept below the critical level by recommending a maximum speed related to the passing distance and dimensions of the vessel. Practically, this measure could be applied as a calculation tool or as an overlay on the pilot's electronic sea chart. Coupling this information with awareness campaigns for pilots will contribute to minimizing the adverse effects on the ships in the outer harbour. The resilience against drawdown-induced risks could be strengthened by restricting the maximum combined width of ships moored alongside. Furthermore, by limiting the excessive slack in the lines of the moored ships, through signage and floating bollards, the movements of the ships will be restricted, reducing the risk of line breakage. Notifications of anticipated critical drawdowns would allow traffic controllers or lock operators to caution the inland ships and delay the lock chamber door openings, whilst alerting the passing vessel. Incorporating the mitigation measures recommended in this research could positively impact the safety of navigation in the Hansweert outer harbour and locks.

# Samenvatting

De sluis van Hansweert, gelegen in de provincie Zeeland in Nederland, dient als een cruciaal knooppunt tussen de Westerschelde en de Rijn-Maas-Schelde Delta. De buitenhaven verbindt de sluis met de Westerschelde en faciliteert wachtplaatsen voor binnenvaartschepen. De Westerschelde is een essentiële waterweg voor maritiem verkeer, dat de haven van Antwerpen verbindt met de Noordzee. Aangezien de vaarweg van de Westerschelde zich dicht bij de buitenhaven van Hansweert bevindt, worden meerdere scheepsincidenten op deze locatie toegeschreven aan de waterbewegingen die veroorzaakt worden door passerende zeevaart op de Westerschelde. Dit onderzoek analyseert hoe de waterbewegingen, veroorzaakt door passerende zeevaart in de Westerschelde, bijdragen aan onveilige situaties in de buitenhaven en sluizen van Hansweert, en welke preventieve maatregelen kunnen worden geïdentificeerd om incidenten effectief te minimaliseren en risico's te beperken.

De belangrijkste oorzaak van de incidenten zijn de primaire waterbewegingen van de passerende zeevaart in de Westerschelde, zo blijkt uit incidentrapporten. Dit fenomeen, dat ervaren wordt als een plotselinge daling van het waterniveau en/of zuiging, kan leiden tot trosbreuken en ongecontroleerde bewegingen van binnenvaartschepen, die resulteren in een reeks veiligheidsrisico's en operationele verstoringen. Verschillende incidentrapporten, veldstudies en interviews benadrukken de urgentie van effectieve maatregelen om de potentieel schadelijke effecten van passerende zeevaart op de schepen in de buitenhaven en sluizen van Hansweert te beperken.

Een meetcampagne van zeven weken, betreffende 1281 passages van bovenmaatse schepen, onthult een duidelijke fenomeen van waterniveauschommelingen tijdens de passage van een schip. Dit fenomeen wordt beschreven als een translatiegolf die de haven in beweegt, tegen het sluizencomplex reflecteert en heen en weer oscilleert in de buitenhaven, totdat deze gedempt is. De belangrijkste parameter die deze golf kenmerkt is de waterdaling. De gemiddelde gemeten waterdaling tijdens de passages, bedraagt ongeveer 6 centimeter, met maximale waarnemingen tot 40 centimeter. De factoren die de waterdaling het sterkst beïnvloeden zijn de afstand van het passerende schip tot de buitenhaven, de snelheid van het schip ten opzichte van de stroming en de afmetingen van het schip, aangetoond door een correlatieanalyse tussen de gemeten waterdaling en de parameters die het passerende schip beschrijven. Extreme waterdalingen werden uitsluitend waargenomen tijdens een combinatie van een relatief hoge vaarsnelheid van het schip (ten opzichte van de stroming) en kleine passeerafstanden ten opzichte van de monding van de buitenhaven.

De impact van de waterdaling op de binnenvaartschepen is bepaald door de krachten die worden gegenereerd door het drukverschil langs de schepen, veroorzaakt door de helling van het waterniveau. Een kritieke daling van 12 centimeter is vastgesteld, gebaseerd op bestaande krachtcriteria en de lineaire relatie tussen de waterdaling en de helling van het waterniveau. Ter verbetering van de bestaande methoden voor het voorspellen van de daling, is een locatiespecifieke vergelijking afgeleid:

$$\Delta h = 0.58 \frac{V_s^2}{2g} \left( \frac{A_s}{d_s h_{\text{vaarweg}}} \right)^{0.93} \left( \frac{L_s}{d_s} \right)^{0.70} \sqrt[4]{\frac{h_s}{h_{\text{buitenhaven}}}}$$

waar $\Delta h$ de waterdaling is, $V_s$ de snelheid van het schip ten opzichte van de stroming, $g$ de zwaartekrachtsversnelling, $A_s$ de onderwaterdwarsdoorsnede van het schip, $d_s$ de passeerafstand, $h_{\text{vaarweg}}$ de diepte van de vaarweg, $L_s$ de lengte van het schip, $h_s$ de diepte op de locatie van het schip en $h_{\text{buitenhaven}}$ de diepte van de buitenhaven. Validatie van deze vergelijking met behulp van de waarnemingen tijdens de meetcampagne levert een Pearson-correlatiecoëfficiënt op van 0,81 en een gemiddelde absolute fout van 2,2 centimeter.

Preventieve maatregelen zijn aanbevolen met als doel de kans op incidenten te minimaliseren en de risico's, gerelateerd aan de waterbewegingen veroorzaakt door passerende zeevaart, te verminderen. De voorspelde waterdaling, gegenereerd door een passerend schip, wordt onder het kritieke niveau gehouden door het aanbevelen van een maximale snelheid, specifiek bepaald voor de passeerafstand en afmetingen van het schip. Praktisch gezien kan deze maatregel worden toegepast als een berekeningsinstrument of als een layover op de elektronische zeekaart van de loodsen. Deze informatie, samen met bewustmakingscampagnes voor de loodsen, zal bijdragen aan het minimaliseren van de hinderlijke effecten op de scheepvaart in de buitenhaven. De risicobestendigheid kan worden versterkt door de maximale toegestane afmeerbreedte te beperken. Tevens, door het beperken van overtollige speling in de trossen van de afgemeerde schepen, via beborting en drijvende bolders, kunnen de bewegingen van de schepen worden verminderd, waardoor het risico op trosbreuken wordt verkleind. Meldingen van verwachte kritieke waterdalingen zouden verkeersbegeleiders of sluismeesters in staat stellen om binnenvaartschepen te waarschuwen en de opening van de sluisdeuren uit te stellen, terwijl het passerende schip wordt geattendeerd. Implementatie van de aanbevolen maatregelen in dit onderzoek kan een positieve invloed hebben op de veiligheid van het vaarverkeer in de buitenhaven en sluizen van Hansweert.

# Contents

# Chapter 1: Introduction

## 1.1 Problem statement and research objective

With the presence of the two biggest ports in Europe, the ports of Rotterdam and Antwerp, the Rhine, Meuse and Scheldt Delta can be considered one of the largest port systems in the world, serving a significant share of the European hinterland. In 2021, this system handled a total maritime cargo volume of about 924 million tons and container traffic of approximately 29.9 million TEU, with an estimated combined direct and indirect value of more than 34 billion euro (ING, 2022; Erasmus UPT, 2021; NBB, 2022). An important route in this port system is the Western Scheldt estuary, acting as the access route for the ports of Flushing, Terneuzen and Antwerp, making it one of the busiest waterways in the world, shown in Figure 1.1. In 2022, the Western Scheldt facilitated access to more than 20 thousand seagoing vessels towards the port of Antwerp, accommodating the throughput of 287 million tons of cargo (Port of Antwerp-Bruges, 2023b). The Western Scheldt and Eastern Scheldt are linked by the Canal through Zuid-Beveland, allowing for the passage of inland ships and smaller seagoing ships. In the South, the canal connects to the Western Scheldt through a lock complex at Hansweert, shown in Figure 1.2. Waiting facilities for inland ships are situated in the outer harbour, south of the complex.



Figure 1.1: Map illustrating the shipping network around the Western Scheldt with the maritime routes marked in dark blue and the inland shipping routes marked orange.

As the navigation channel of the Western Scheldt is located close to the outer harbour of Hansweert, the passing seagoing vessels are suspected of causing severe water level depressions in the outer harbour, affecting the ships at the mooring places and in the lock chambers. Multiple incidents related to these water level depressions have been reported, both at the mooring places and in the lock chambers. In March 2023, a seagoing vessel was declared guilty by the Court of Appeal in The Hague, for the damage to two inland ships and the lock gate (Court of Appeal in The Hague, 2023). The court deemed that due to the excessive speed of the passing seagoing vessel, the mooring lines of the inland ships broke, causing the ships to collide with each other and with the lock gate. This research aims to gain an understanding of the hydrodynamic interactions between the passing vessels in the Western Scheldt and the ships in the outer harbour and locks of the Hansweert lock such that recommendations can be provided to proactively prevent future incidents from taking place.

Figure 1.2: Satellite image of the intersection between the Canal through Zuid-Beveland and the Western Scheldt (Google Earth, 2023).

## 1.2 The shipping network

### 1.2.1 The Hansweert lock as a node in the inland shipping network

The lock of Hansweert is part of the southern corridor of the Dutch inland shipping network, together with the Volkeraklock, Kreekraklock and Krammerlock (Rijkswaterstaat, 2021). The lock as it is currently was commissioned in 1987 and consists of two chambers with a width of 24 metres and a length of 275 metres allowing for the passage of CEMT class VIb ships (Rijkswaterstaat, 2023). Mainly, the lock welcomes CEMT class Va and IV size ships, with a length of 135 and 105 metres respectively, shown in Figure 1.3a.



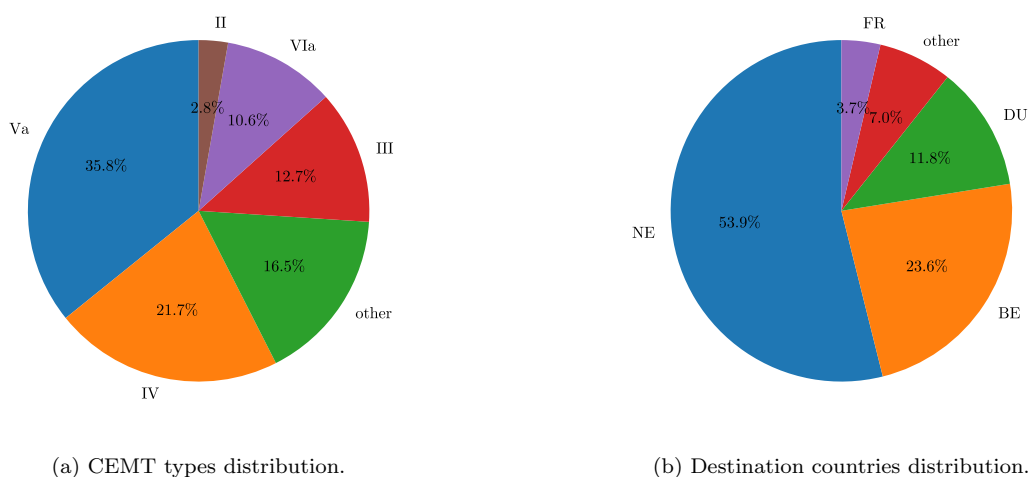(a) CEMT types distribution.



(b) Destination countries distribution.

Figure 1.3: Share of the different CEMT types (a) and the share of the country of destination (b) of the ships that passed the Hansweert lock complex in the period 01/01/2021 - 27/05/2023 as recorded by Rijkswaterstaat.

As the lock provides a connection between the Western Scheldt estuary and the Rhine Delta, most traffic passing the node from North to South originates from ports found in the Rhine Delta such as Rotterdam, Amsterdam, Moerdijk, Dordrecht, Vlaardingen and Duisburg (DE). In the other direction, the prominent ports of departure are those of Ghent (BE), Flushing, Terneuzen, Antwerpen (BE), Sluiskil and Breskens. Although Antwerp is

the main destination for inland shipping from the Rhine Delta travelling South, in practice, most traffic uses the significantly shorter Scheldt-Rhine connection via the Kreekrak locks. Figure 1.3b shows that more than half of the destinations of the passing ships lie within the Netherlands. On average (as recorded in the period 01/01/2021 - 27/05/2023), the lock welcomes 114 ships per day, of which approximately half travels North and half South. Figure 1.4 shows that most passages are made during the daytime and that the peak movement in the southerly direction (towards the Western Scheldt) lies a few hours before the peak in the northerly direction.
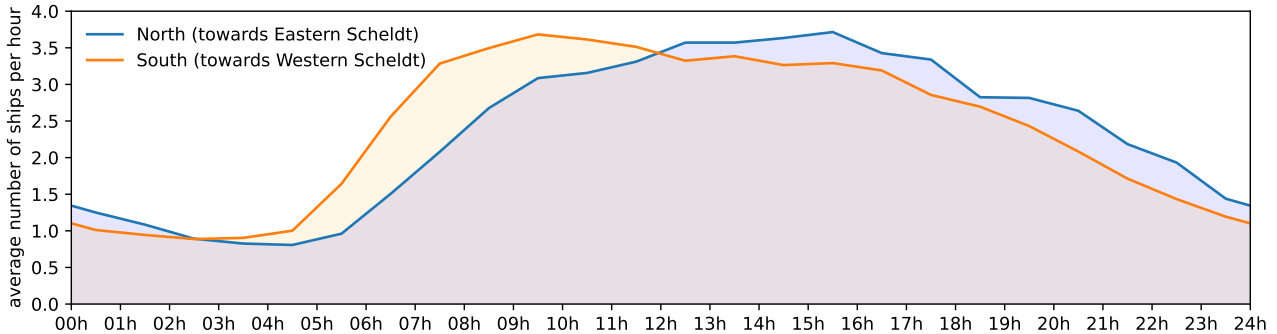


Figure 1.4: Distribution of the average number of ships per hour per direction over a day recorded in the period 01/01/2021 - 27/05/2023 by Rijkswaterstaat.

Rijkswaterstaat (2021) expects the growth of mass transported by inland shipping to be between 18 and 34% in the period between 2014 and 2040, with 2014 as the reference year. For the lock at Hansweert, an increase of 23 to 37% in ship passages is estimated despite the slight decrease seen in commercial traffic intensity in the period 2007 to 2021, shown in Figure 1.5. Figure 1.5 shows that the amount of traffic has reduced more than the amount of payload, indicating an increase in the size of the average ship.
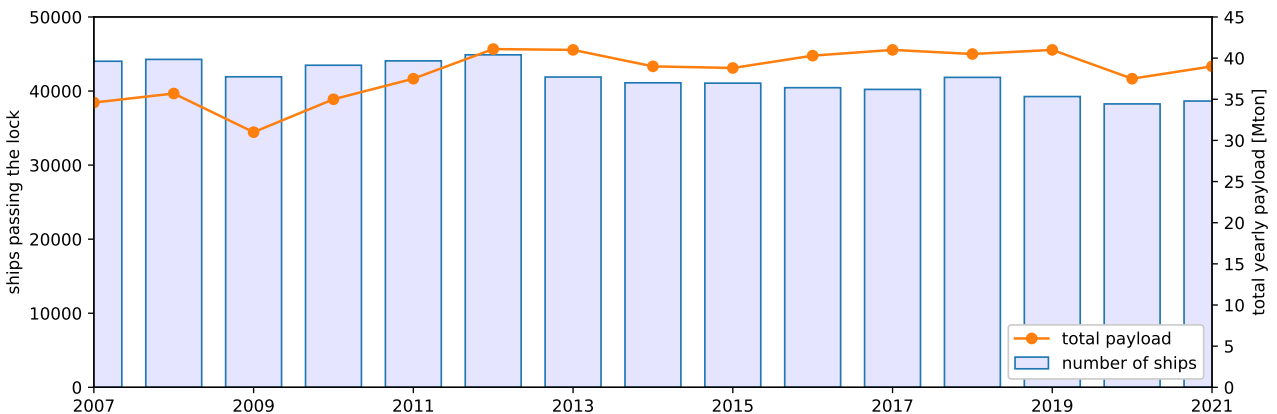


Figure 1.5: Commericial traffic intensity and total payload of the inland ships passing through the lock of Hansweert, abstracted from the openly available shipping maps of the years 2007 to 2021 by VTS-Scheldt.

### 1.2.2 Mooring places in the outer harbour of Hansweert

In the outer harbour of Hansweert, on the South side of the lock complex, mooring places are located with a maximum theoretical capacity of 20 inland waterway ships with a maximum length of 135 metres (RWS, 2023). These waiting areas are intended as berths for the night or weekend or as a refuge in bad weather. Ships also dock here to wait for their time slot in one of the surrounding locks or the dissipation of other delays in the network. In order to reach the capacity, the ships have to be moored alongside each other, with a maximum combined width of 40 metres. The most southern spots are reserved for ships carrying dangerous or harmful substances, so-called 'kegelschepen'. On the North side of the complex, in the Canal through Zuid-Beveland, an additional 22 waiting places are situated, creating a total of 42. Research by Schouten (2023) indicated that on average 22 of 42 spots are occupied at night, based on counts conducted in 2022.

### 1.2.3 The Western Scheldt as the access route to the Port of Antwerp

Throughout its long history, the Western Scheldt has served as a crucial gateway for maritime traffic, connecting the Port of Antwerp with the rest of the world. As part of the Treaty of London (1839), in which the Netherlands recognized Belgium's independence, it was laid down that the Netherlands had to guarantee free passage between the North Sea and the Port of Antwerp across the Western Scheldt (Sanger and Norton, 1915). Therefore, unlike the Eastern Scheldt and the other Dutch estuaries, this estuary was not closed as part of the Delta Works (Marchand, 2006). Instead of a closure, the safety of the land surrounding the Western Scheldt was ensured by reinforcing the dikes.

As of 2022, the merger of the ports of Antwerp and Bruges has resulted in the unified entity known as the Port of Antwerp-Bruges, making them the 13th largest container port of the world, with a throughput of 13.500.000 TEU in that year (Port of Antwerp-Bruges, 2023a). Besides container transport, the port processed 90 million tons of liquid bulk, 17 million of dry bulk, 13 million tons of breakbulk and 20 million tons of rolling stock in 2022. The Port of Antwerp-Bruges (2023a) states that the port is accessible at all times for vessels with draughts up to 13.1 metres. Using a tidal window, the port is accessible for vessels with draughts up to 16.0 metres in the upstream direction and 15.2 metres in the downstream direction. The port regularly welcomes ULCV type containerships, characterized by a capacity above 18,000 TEU's, a length of 399 metres and a width of 60 metres. As shown in Figure 1.6, even though the number of seagoing vessels decreases, the total capacity transport increases, showcasing the up-scaling in size of the seagoing vessels towards the port of Antwerp.
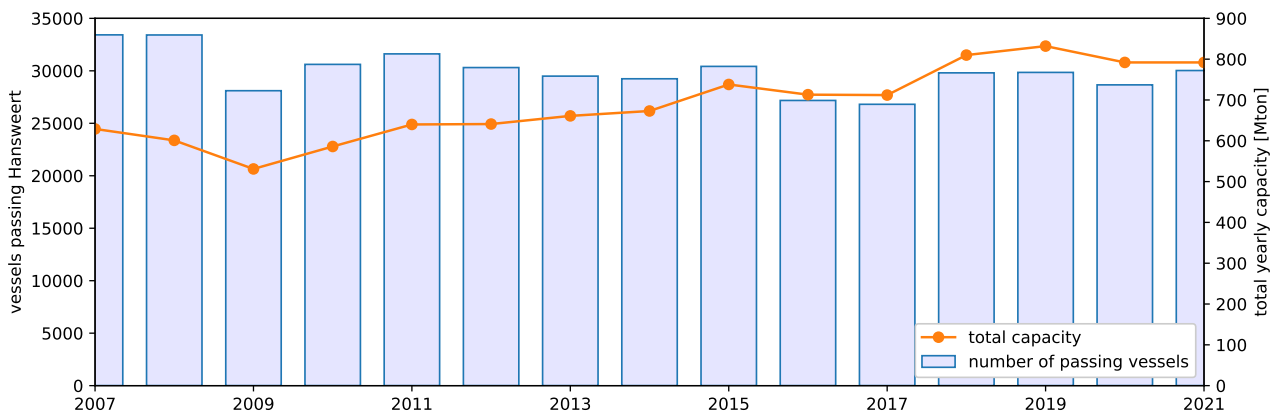


Figure 1.6: Traffic intensity and total capacity of the maritime vessels passing through the Western Scheldt past the outer harbour of Hansweert, abstracted from the openly available shipping maps of the years 2007 to 2021 by VTS-Scheldt.

Data collected by the Joint Flemish-Dutch Management and Exploitation Team (BET) shows that on average 0.74 vessels longer than 210 metres pass the outer harbour at Hansweert per hour. Figure 1.7 shows that the passage time of the vessels is affected by an external influence such that maxima occur every four hours, possibly associated with the shift work schedules in the Port of Antwerp (Marin, 2020).
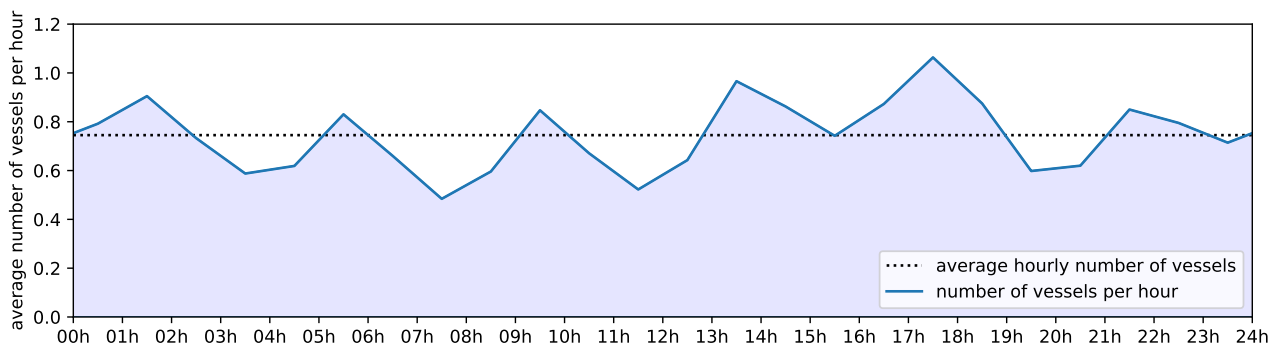


Figure 1.7: Distribution of the average number of ships longer than 210 metres sailing past the outer harbour of Hansweert retrieved from AIS data collected by The Joint Flemish-Dutch Management and Exploitation Team (BET) managing the systems of the Scheldt Radar Chain (SRK) for the period 01/01/2021 - 23/08/2023.

### 1.2.4 Observed nautical safety issues

The connection between the lock of Hansweert and the Western Scheldt is a critical node in the shipping network, hosting a wide range of vessel types and sizes. As moving vessels naturally create disturbances in the water, nearby ships occasionally may encounter disruptions due to these water movements. In recent years, multiple incidents related to water movements created by another vessel at the intersection between the lock of Hansweert and the Western Scheldt have been recorded. On average 24 incidents have been reported yearly, of which in 89% of the cases a seagoing vessel is involved, shown in Figure 1.8.
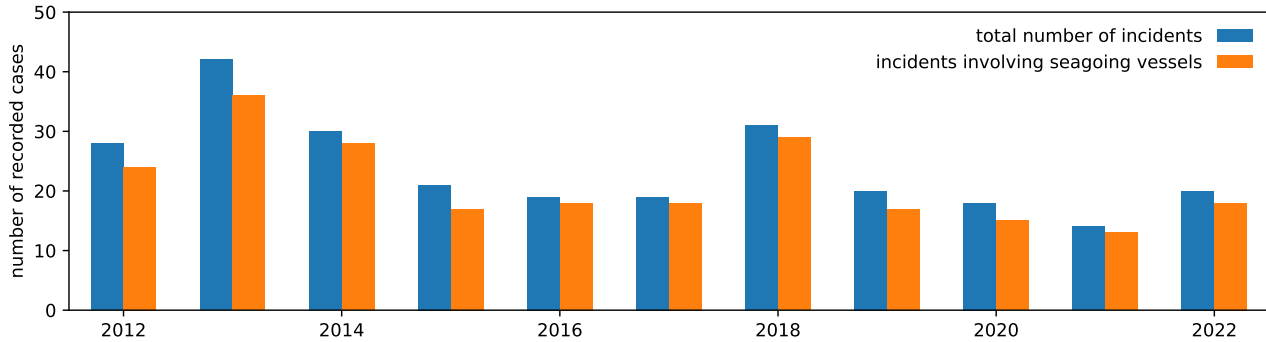


Figure 1.8: Cases of undesirable ship-ship interactions due to water movements caused by another vessel at the intersection between the lock of Hansweert and the Western Scheldt as recorded by Rijkswaterstaat (2022).

## 1.3 Research questions

The aim of the research is to gain an understanding of the hydrodynamic interactions between the passing vessels in the Western Scheldt and the ships in the outer harbour and locks of Hansweert such that recommendations can be provided to proactively prevent future incidents from taking place. The main research question is formulated as follows:

---

**"How do the water motions induced by passing vessels in the Western Scheldt contribute to unsafe situations in the outer harbour and locks of Hansweert, and what preventative measures can be identified to effectively minimize incidents and mitigate risks?"**

---

The main research question is accompanied by the following sub-questions:

1. What physical processes of vessel passages contribute to unsafe situations in the outer harbour and locks of Hansweert?

2. What materials and methods are available to quantify a vessel passage and associated water motions in the outer harbour, and how can these be utilized to predict unsafe conditions?

3. How do the different aspects quantifying a vessel passage relate to the observed water motions in the outer harbour of Hansweert?

4. When are the water motions in the outer harbour generated by passing vessels considered unsafe for inland shipping and how can these motions be predicted?

5. How can the predicted water motions be limited to safe levels and how can resilience against these motions be enhanced?

To maintain a clear overview of the distinctions, in this report, passing seagoing ships sailing over the Western Scheldt are referred to as 'vessels', while the inland ships in the outer harbour and lock chambers at Hansweert are referred to as 'ships'.

## 1.4   Study approach

In addressing the introduced research questions, the initial steps involve enhancing the understanding of the problem through site visits, interviews, and constructing an overview of known relevant events associated with the problem. Based on the understanding of the problem, the relevant literature will be reviewed, concerning the wave generation by the passing vessels and the response of the inland ships in the outer harbour. From the literature study, the data necessary to capture the phenomena is collected, processed and captured by several parameters in a dataset. This dataset summarizes a vessel passage by several parameters, such as the characteristics of the vessel and the phenomena observed in the outer harbour. Based on this data, a prediction model is constructed which predicts the phenomena based on the most influential parameters. A critical threshold is established based on the forces associated with the phenomenon and its alignment with guidelines. In the design of the mitigation measures, this prediction model is applied to give recommendations to reduce the effects of passing vessels in the outer harbour, such that this critical threshold is not exceeded. Besides this, recommendations to increase the resilience of the inland ships against the phenomenon in the outer harbour are given, based on the lessons learned from the practical observations made in the field.

## 1.5   Report structure

Chapter 1 has introduced the problem and research objective. In Chapter 2, the understanding of the problem is enlarged by analysing the recorded incidents and conducting field studies and interviews, answering the first sub-question. Chapter 3 reviews the relevant literature available, concerning the waves generated by ships and ship response to hydrodynamic forcings. The data collection, processing steps and methodology are elaborated in Chapter 4, answering the second sub-question. Subsequently, Chapter 5 answers the third sub-question by providing an analysis of the data collected, including visualizations of the observations and a correlation analysis of the parameters expected to be associated with the phenomenon. Chapter 6 aims to set a threshold after which the phenomenon is considered critical and predict the phenomena in the outer harbour after the passage of a vessel, answering the fourth sub-question. This knowledge is applied in Chapter 7 to draw up mitigation measures to reduce the risk of incidents in the outer harbour and lock of Hansweert due to the passage of vessels in the Western Scheldt, as an answer to the final sub-question. A discussion on the limitations and the contextualization of the study with respect to existing research will be given in Chapter 8. Finally, Chapter 9 concludes the research by answering the main research question and providing recommendations for further research.

# Chapter 2: Problem Analysis

In this chapter, further understanding of the problem is developed. Wallwey and Kajfez (2023) describe qualitative research as a method that investigates phenomena through detailed analysis of non-numerical data, aiming to understand the meanings, perspectives, and experiences of individuals or groups in their natural contexts. Section 2.1 employs this method by presenting insights gathered through field studies and interviews conducted involving individuals associated with the problem. Section 2.2 describes the known relevant events related to disturbance generated by passing seagoing vessels at the outer harbour of the Hansweert lock. Quantitative research, on the other hand, employs numerical data and statistical analysis to quantify relationships, patterns, and trends within a given population or sample (Wallwey and Kajfez, 2023). Understanding the root of the problems allows for the establishment of the framework for conducting quantitative research.

## 2.1 Field study and interviews

Several site visits and interviews with involved individuals have been conducted to gain a comprehensive understanding of the issues surrounding the passing marine traffic at Hansweert. Interviews have been carried out with individuals connected to the anticipated source of the issue (pilots), from the recipient standpoint (inland skippers), and with observers who maintain a relatively neutral position (traffic managers, lock operators, etc.), ensuring a balanced overview. An overview of the site visits and interviews conducted is given in Table 2.1, of which the individual reports are given in Appendix A. This section will present the consolidated findings from these site visits and interviews.

| event | date | report location |
|---|---|---|
| Site visit RWS Goes, Hansweert lock and traffic post | 14/06/2023 | Appendix A.1 |
| Site visit Terneuzen lock and traffic post and Hansweert lock | 13/07/2023 | Appendix A.2 |
| Interview with Ghent–Terneuzen Canal pilots | 04/09/2023 | Appendix A.3 |
| Site visit Hansweert lock control centre | 08/09/2023 | Appendix A.4 |
| Interview with inland skipper | 08/09/2023 | Appendix A.5 |
| Interview with former captain and HSE at GEFO | 20/09/2023 | Appendix A.6 |
| Second visit to the Hansweert traffic post | 05/10/2023 | Appendix A.7 |
| Interview with inland ship captain | 06/10/2023 | Appendix A.8 |
| Interview with Western Scheldt pilot | 29/11/2023 | Appendix A.9 |
| RWS 79 expedition | 05/12/2023 | Appendix A.10 |
| Second interview with Western Scheldt pilot | 13/12/2023 | Appendix A.11 |

Table 2.1: Overview of site visits and interviews conducted.

Inland skippers, lock operators and individuals working on the traffic posts indicated that the breakage of mooring lines due to passing seagoing vessels in the Western Scheldt is common, and many incidents go unrecorded. They stated that this is not an isolated concern exclusive to Hansweert, but also at Terneuzen, Flushing, Walsoorden, the Borssele Sea Jetty and several smaller harbours along the estuary. The harmful phenomenon is mostly described as a significant water level drop which generates strong movements of the moored ships, occasionally strong enough to break mooring lines. This shows that the main issues are related to the water displacement and corresponding suction of the passing vessels. Interviews with the pilots sailing vessels to and from Antwerp indicate that not all pilots are aware of the issues related to the water displacement at Hansweert and therefore not reduce their speed in the bend at Hansweert. At Terneuzen, Walsoorden, the Borssele Sea Jetty and the North Sea/Europe Terminal, the pilots are aware and do adapt their speed and distance subsequently. The (secondary) waves of smaller but faster ships in the outer harbour itself can also cause nuisance, however, this aspect is of lesser importance given the reduced potential for dangerous situations.

### 2.1.1   Problems occurring during the locking process

When a large vessel with significant speed passes the outer harbour and the lock chamber door is open, multiple individuals indicate that the water level can rapidly drop up to 50 centimetres in the chambers, causing the manoeuvring ships to be sucked out of the chamber. This can occur both at Hansweert and at Terneuzen. When the ship is already partially moored in the chamber, this backwards movement can cause great tensions on the mooring lines potentially leading to their breakage. The breakage of a mooring line poses a serious safety hazard and can result in potentially fatal consequences for nearby crew. To compensate for the backwards movement, the ships give engine ahead. The displaced water returning to the chamber, together with the forward propulsion of the engine, accelerates the ship forward, necessitating the application of engine astern. These movements can repeat, resulting in oscillating movements of the ships in the chamber. This can lead to dangerous situations, especially for inexperienced skippers who are unable to anticipate for this effect.

### 2.1.2   Problems at the mooring places

In the Scheldt area is a growing shortage of mooring places for inland ships. Despite this, the mooring places at the South side of the Hansweert lock are underutilized. Indicated reasons for this are the significant tidal range, the rougher seas and also the increased likelihood of breaking loose due to the suction of passing vessels. Due to the great tidal range, it is impossible to keep all lines at tension for a longer period, without having to readjust them frequently. Over-tightening the mooring lines can lead to the ship breaking free during high or low tide. Consequently, often slack in the lines is inevitable when the tide is not extreme. The slack gives the ship a certain degree of freedom of motion. Especially when multiple ships are moored alongside, this freedom of motion allows the ships to build up significant momentum due to the suction force of a passing vessel, which could result in the breakage of the mooring lines.

### 2.1.3   Influencial aspects and significance

The interviews indicate that most critical situations occur at lower water levels. Especially passing vessels with a great draught, sailing at high speed relative to the current velocity cause disturbance. Other parameters of influence mentioned are the width of the passing vessels, length, under keel clearance, the shape of the hull and their distance to the shore. During the locking processes, the size of the affected ship also influences the magnitude of the felt effect, especially the blockage factor. The blockage factor is the ratio between the cross-sectional area of the ship and the cross-sectional area of the chamber. Some individuals indicate that with the increasing size of both the seagoing vessels on the Western Scheldt and the inland ships, the seriousness of the problem is increasing, whereas others mention that it has always been this way.

### 2.1.4   Proposed solutions

The consensus among most interviewees is that (part of) the solution lies in raising awareness among both pilots and inland skippers. Informing pilots through measurements can enable the application of practical measures to mitigate the impact. Inland skippers, on the other hand, should be educated about these phenomena through signage and warnings from traffic posts when a vessel with significant water displacements passes. Suggestions from those involved include having the lock operator delay the opening of the chamber doors when a vessel passes. Some propose implementing measures for passing vessels, such as a potential speed limit based on draught. Additionally, some believe that traffic posts could play a role in enforcing these measures or informing passing vessels about their displacement.

## 2.2   Known relevant events

This section aims to provide a chronological summary of all known significant events and incidents between 2018 and 2023 related to the passages of seagoing vessels at the outer harbour of the Hansweert lock. If not stated otherwise, the information is based on reports by the Commission of Nautical Safety of the Scheldt Area (2020) together with vessel information sourced from the Marine Traffic or Vessel Finder websites.

On **April 17, 2018** a collision took place between an inland motor tanker and another inland cargo ship in the eastern lock chamber at Hansweert where the motor tanker collided with the bow of the cargo ship and the cargo ship collided with its bow with the northern lock gate door. The incident occurred when a seagoing container vessel named MSC Giselle passed the outer harbour of the lock, illustrated in Figure 2.1. The collision resulted in damage to both the inland ships and the lock gate door. The Court of Appeal in The Hague (2023) ruled that the damage can be attributed to the large displacement of water that entered the funnel-shaped outer harbour in front of the lock from the Western Scheldt and then entered the lock chamber (Schuttevaer,

2023; M-info, 2021; Centre for Maritime Law, 2020). The large displacement was attributed to the excessive speed of the container ship and the low water level due to the spring tide. The Shipping Regulations Western Scheldt 1990 commands in Article 6.3 that power-driven ship must reduce their speed if necessary stop if their wave action or suction endangers other ships. The container ship had a length of 300 metres corresponding to a Post-Panamax-I type vessel and was sailing at a speed of 16.5 knots over the ground approximately.



Figure 2.1: Schematization of the incident of April 17, 2018 (not to scale).

On **February 12, 2020** around 20:00 hours, two inland ships, the Cunado and the Duvo (both 110 metres in length) reported damages shortly after each other after the passages of the MSC Santhya and MSC Carouge. The Cunado and Duvo were berthed at piles 55 and 39 respectively in the outer harbour at Hansweert. The MSC Santhya was sailing downstream and is a Panamax-type vessel with a length of 237 metres and a width of 32 metres. The MSC Carouge is a Post Panamax-type vessel with a length of 283 metres and a width of 40 metres, sailing to Antwerp. Reports made by both inland ships note that the wind at the time of the incident was from the east-northeast, force 4 on the Beaufort scale, the water level was 9 dmNAP and the tide was going down.

On **April 20, 2022** a loaded inland motor tanker was moored parallel to two other inland ships to the western mooring piles in the outer harbour of Hansweert, as indicated in Figure 2.2. When a seagoing vessel, named Monaco Maersk, passed the outer harbour, the skipper of the motor tanker stated that two mooring lines broke due to the water displacement and suction caused by the passing vessel. The seagoing vessel had a length of 400 metres, a width of 59 metres and a draft of 13 metres, corresponding to a ULCV type vessel. The report notes that the wind at the time of the incident was from the northeast, force 3 on the Beaufort scale, the water level was 21 dmNAP and the tide was going down. The wave height at the time of the incident was 15 cm.
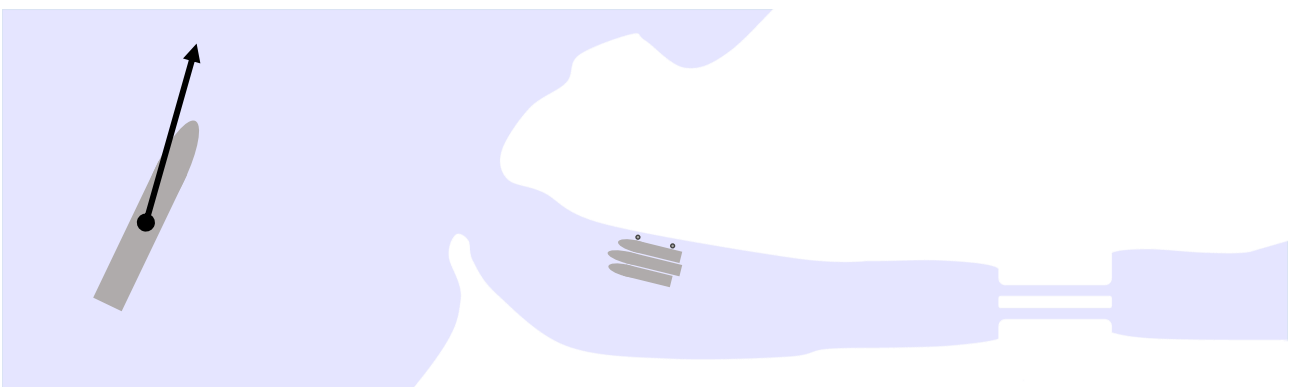


Figure 2.2: Schematization of the incident of April 20, 2022 (not to scale).

On **October 19, 2022** the Commission of Nautical Safety of the Scheldt Area released a statement in which various incidents involving nuisance or damage in ports or locks, on piers or at anchorages due to suction or waves from the passing of large (container) vessels were discussed. The committee stated that the serving pilot(s) and the traffic control centres must be aware that, especially around low tide, the water displacement caused by a passage at the Westerbuitenhaven, the Put van Terneuzen, the sea jetties, the Hansweert outer harbour and the port of Walsoorden can cause a lot of nuisance and even damage to the ships that are anchored

or moored on the sea jetties, waiting areas or in open locks. The serving pilot(s) and the traffic controllers must therefore ensure that all sea-going vessels (in particular oversized vessels) pass the aforementioned locations at an appropriate speed such that no damage is caused. The statement concludes by emphasizing that the Common Nautical Authority must take the impact of the above into account when calculating the sailing plans of the vessels (GNB, 2022).

On **July 10, 2023** inland tanker Liszt reports being sucked out of the lock chamber at Hansweert together with the other ships in the chamber, due to the passage of the Cosco Glory. The Cosco Glory is a New Panamax-type container vessel with a length of 366 metres and a width of 48 metres and was sailing downstream. The pilot on the vessel informed the other skippers he had reduced his speed accordingly. The report notes that the wind at the time of the incident was from the northwest, force 4 on the Beaufort scale and the tide was high.

On **August 10, 2023** the containership named Teno passed the outer harbour with a speed of 17.5 knots, causing broken mooring lines at the tanker ship Typhoon berthed at the south mooring places, Figure 2.3. The Teno is a container vessel with a length of 300 metres and a width of 46 metres. The container vessel was sailing downstream and had a reported draught of 12 metres. The Typhoon has a length of 100 metres and a width of 14 metres and suffered breakage of two 140 metres, 22 tons registered mooring lines at the aft of their ship. The incident report notes that the Typhoon was moored at this location for 14 days before the incident occurred. When the incident occurred, the tanker ship Milano was moored alongside the Typhoon. The Milano's dimensions are 135 metres by 18 metres. The wind at the time of the incident was from the east, force 2 on the Beaufort scale and the tide was low.
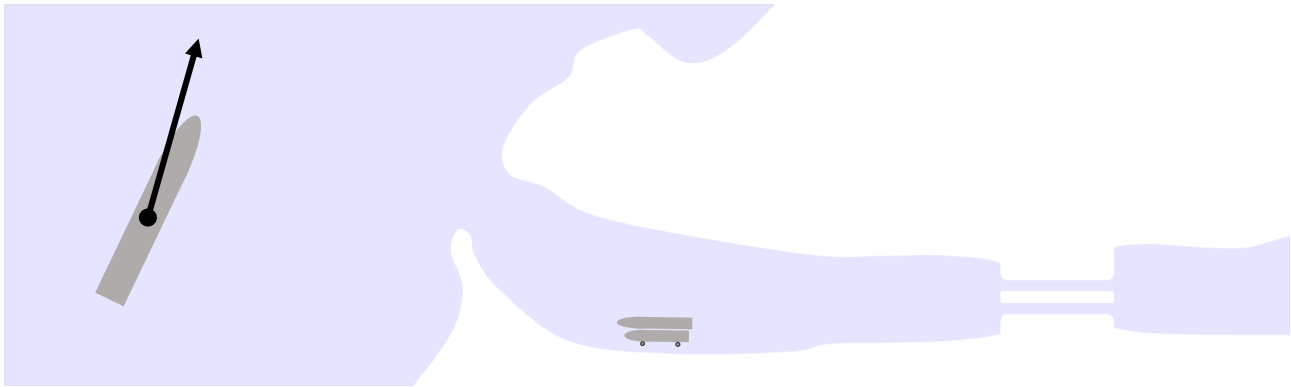


Figure 2.3: Schematization of the incident of August 10, 2023 (not to scale).

On **October 10, 2023** an inland ship is entering a chamber of the Hansweert lock. Simultaneously, the MSC Benedetta XIII passes the outer harbour with a speed of 15 knots at a distance of approximately 480 metres from the harbour entrance, sailing downstream. The MSC Benedetta XIII is a container vessel with a length, width and reported draught of 366, 48 and 14.1 metres respectively. The suction caused by the passing vessel results in a rapid lowering of the water level of 55cm in the lock chamber. The tide at the time of the incident was around 0mNAP.

On **January 11, 2024** a mooring line broke off an inland push barge ship, berthed at the mooring places closest to the Western Scheldt, on the East side of the outer harbour. This occurred when the Finneco 1 passed the outer harbour at an approximate passing distance of 269 metres relative to the entrance of the harbour with a reported speed of 19 knots over the ground, sailing downstream. The Finneco 1 is a ro-ro cargo vessel with a length of 238 metres, a width of 35 metres and a reported draught of 7 metres at the time of passage. The inland ship length, width and draught at the time of the incidents were 135, 11 and 1.5 metres respectively. The wind at the time of the incident was from the east, force 3 on the Beaufort scale, the tide was -2mNAP and the currents 1 metre per second in the downstream direction. The inland push barge combination was moored with four lines registered to a force of 303 kN and reportedly exhibiting minimal slack. No other ships were moored alongside.

## 2.3   Conclusion

In this chapter the following sub-question was treated:

---

"What physical processes of vessel passages contribute to unsafe situations in the outer harbour and locks of Hansweert?"

---

Several site visits, interviews and an analysis of the related incidents revealed that the leading physical process leading to unsafe situations in the outer harbour and locks of Hansweert is the water displaced by the vessels passing the outer harbour and the corresponding suction and the sudden lowering of the water level. This lowering in water level causes (partially) moored inland ships to gain momentum and break through their mooring lines and other undesired ship movements.

In recent years, at the traffic node of the lock of Hansweert and the Western Scheldt, on average 24 incidents have been reported of which in 89% of the cases a seagoing vessel is involved, however involved individuals note that many incidents go unrecorded. These problems are not an isolated concern exclusive to Hansweert, but also to Terneuzen, Flushing, Walsoorden, the Borssele Sea Jetty and several smaller ports along the Western Scheldt, as inland skippers, lock operators and individuals working on the traffic posts indicated that the breakage of mooring lines due to passing seagoing vessels is common at these locations. Interviews with the pilots sailing the passing vessels indicate that not all pilots are aware of the issues related to the water displacement at Hansweert. The incident reports show that in most cases, the incident was triggered by a passing container vessel of significant size, sailing downstream towards the North Sea. The consensus among the interviewees is that mostly passing vessels with a great draught, sailing at a high speed relative to the current velocity cause disturbance, especially during lower water levels.

# Chapter 3: Literature Review

The key physical process leading to unsafe situations in the outer harbour and locks of Hansweert is the water displaced by the passing vessel, concluded in Chapter 2. This chapter aims to gather the available literature concerning the generation of and the response to this water motion. This information is crucial for determining the necessary data to be gathered. The relevant literature concerning the generation of this water motion is discussed in Section 3.1. This section aims to compile an overview of the advancements made in the literature concerning this physical process, to identify the available prediction methods and the key influential parameters. Section 3.2 discusses the response of moored ships to this water motion and provides guidelines to assess the criticality of the forcing.

## 3.1 Waves generated by vessels

A vessel in motion causes variations in pressure and velocity of the surrounding water, as its bow pushes water forward, to the sides, and downward. The resulting current, opposing the sailing direction, returns this water behind the stern of the ship, generating a reduction in pressure alongside the vessel. As the total energy remains constant conforming to Bernoulli's principle, the water level reduces laterally. Around the bow and the stern of the ship the velocity field stagnates generating local pressure increases and thus water level increases (Bhowmik et al., 1981a; Dempwolff et al., 2022a; Van Koningsveld et al., 2023). This variation in water level is called the primary ship wave, consisting of a transversal bow wave, a water level depression along the ship and a transversal stern wave, shown in Figure 3.1. Often, the water level depression caused by the return current is referred to as drawdown (Taylor et al., 2007).
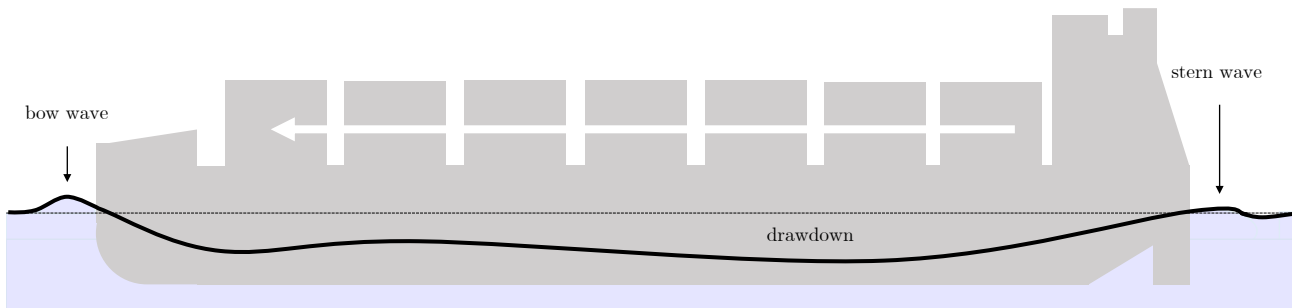


Figure 3.1: Exaggerated schematization of the primary wave along the ship's hull, redrawn after CIRIA (2007).

The secondary water motions are the short waves induced by the discontinuities in the hull of the ship, found at the bow and stern. The motion is composed of a transversal wave moving in the direction of the ship and a divergent wave moving away from the ship (Thomson, 1887; Dempwolff et al., 2022a). Chapter 2 concludes that the water displacement of the passing vessels is the primary concern, therefore, it can be concluded that the primary water motion is the leading phenomenon. For this reason, the literature review continues investigating the drawdown phenomena related to the primary wave.

Multiple efforts have been made to estimate the drawdown caused by vessels, as this primary wave can lead to hazardous movements of moored ships (Swiegers, 2011; Muga and Fang, 1975; Pinkster, 2004), cause erosion at the shorelines of waterways (Sorensen, 1997; Huisman et al., 2011), disrupt the associated ecosystem (Gabel et al., 2017) and have other impacts on structures and ships (Swiegers, 2011). This estimation of the drawdown can be done through measurements, however, the data collected is limited to the timeframe of the measurements and cannot be extrapolated to predict beyond this range. Furthermore, numerical modelling has proven effective in quantifying this primary water motion (David et al., 2017; Jong et al., 2013; Dam et al., 2006; Stockstill and Berger, 2001). Yet, its reliance on specific input data, software proficiency, and significant computational resources often restricts its accessibility. Finally, empirical methods offer a practical alternative, particularly in

pilot studies, shoreline protection design, and long-term wave impact assessment (Almström and Larson, 2020). For the design of embankment protection measures of inland waterways, Dempwolff et al. (2022a) concludes that the generation of primary waves is considered, whereas for larger coastal waterways the impact of drawdown waves remains largely neglected. These empirical methods describing the primary water motion of a vessel have mainly been derived for relatively narrow channels with uniform bathymetry, validated using experimental data. This section will provide an overview of the available empirical methods. The methods of Schijf (1949) and Bhowmik et al. (1981a) are worked out in the main text whereas the additional descriptions are given in Appendix B.

### 3.1.1 Drawdown definition of Schijf

The first attempt to formulate the drawdown or primary water motion a ship creates was based on Bernoulli's theorem and the equation of continuity (Schijf, 1949; Janssen and Schijf, 1953). If the drawdown height is set equal to the head difference, Bernoulli's theorem can be stated as follows:

$$\Delta h = \frac{(V_s + U_r)^2}{2g} - \frac{V_s^2}{2g} \tag{3.1}$$

In this equation, $\Delta h$ represents the drawdown height, $V_s$ the vessel speed, $U_r$ the return current and $g$ the gravitational acceleration. Using a Lagrangian approach, where the observer moves with the ship, the continuity equation requires the following:

$$V_s A_c = (V_s + U_r)(A_c - A_s - W_s \Delta h) \tag{3.2}$$

where:

$$A_c = W_s h \tag{3.3}$$

$$A_s = B_s D_s C_m \tag{3.4}$$

In this equation $A_c$ is the cross-sectional area of the channel, $A_s$ is the underwater cross-section of the vessel amidships and $W_s$ is the undisturbed channel width at the water surface. The cross-sectional area of the channel ($A_c$) is assumed to be rectangular by defining it as the surface width ($W_s$) multiplied by depth $h$, visualized in Figure 3.2. The underwater cross-section of the vessel amidships ($A_s$) is defined as the multiplication of the width of the vessel ($B_s$), the draught of the vessel ($D_s$) and the midship coefficient of the vessel ($C_m$). The midship coefficient is the ratio between the actual underwater area of a midship section and that of a rectangle of the same depth and width (Wärtsilä, 2023). By rewriting Equation 3.2 for the return current ($U_r$) and inserting this in Equation 3.1, an expression for the water level drawdown ($\Delta h$) is observed, which can be solved iteratively:

$$\Delta h = \frac{V_s^2}{2g}\left(\left(\frac{A_c}{A_c - A_s - W_s \Delta h}\right)^2 - 1\right) \tag{3.5}$$

Van Koningsveld et al. (2023) summarizes the assumptions the formulation is based on as follows: (1) the flow can be considered one-dimensional, (2) the sinkage of the ship is equal to the water level depression, (3) the ship uses no trim, (4) the channel is straight, prismatic and infinitely long, (5) the shape of the ship is prismatic, (6) the vessel speed is constant, (7) the ships sails along the channel axis, (8) the return current is uniform in the whole channel, (9) the water level depression is uniform over the channel width, (10) no energy losses and (11) there are no influences of ship-initiated waves.
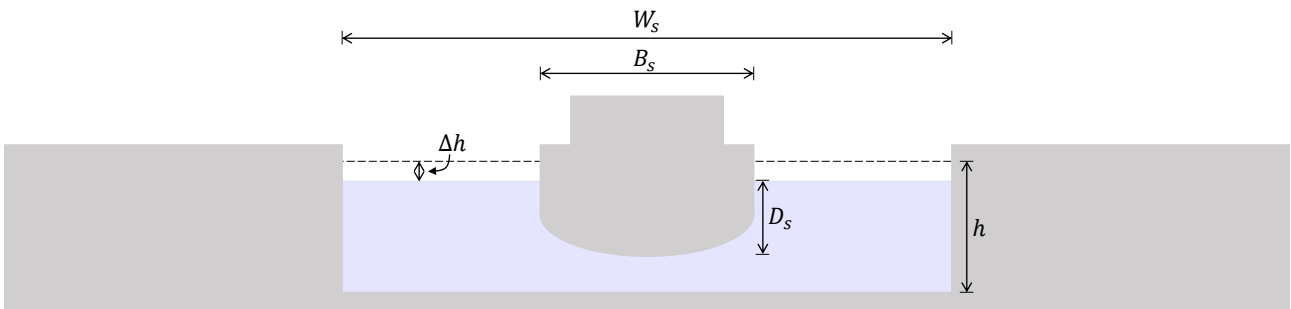


Figure 3.2: Definition of symbols at the amidship's crosssection, redrawn after Van Koningsveld et al. (2023).

### 3.1.2   Drawdown definition of Bhowmik

Bhowmik et al. (1981a) tested the earlier developed empirical equations for drawdown height by Schijf (1949), Gates and Herbich (1966), Dand and White (1978) and Gelencser (1977) using measurements conducted on the Illinois and Mississippi rivers. Dand and White (1978)'s equation is based on a normalized drawdown height using the vessel speed ($V_s$), the gravitational acceleration ($g$) and the blockage ratio ($A_s/A_c$), described in Appendix B.5. The drawdown height is normalized with the velocity head in the Bernoulli equation (Equation 3.1). Bhowmik et al. (1981a) found a better fit for the measurement data by elaborating on Dand and White (1978)'s equation and adding the ratio between the vessel's length ($L_s$) and distance from the ship's sailing line to the shore ($d_s$):

$$\Delta h = 1.03 \frac{V_s^2}{2g} \left(\frac{A_s}{A_c}\right)^{0.81} \left(\frac{L_s}{d_s}\right)^{0.31} \tag{3.6}$$

### 3.1.3   Additional drawdown definitions

Besides the description of Schijf (1949) and Bhowmik et al. (1981a), the additional descriptions are worked out in Appendix B. The definitions of Delft Hydraulics (1953), Gates and Herbich (1977) and the rock manual (CIRIA, 2007) are based on the analytical description of the drawdown given by Schijf (1949). A correction factor is introduced by Delft Hydraulics (1953) and CIRIA (2007) which depends on the ratio between the speed of the ship and its critical velocity. The critical velocity is reached when the return current is supercritical. CIRIA (2007) furthermore includes an expression for a trapezoidal river cross-section. Gates and Herbich (1977) employ the same equation as Schijf (1949), however, the velocity is expressed in knots, the drawdown in feet and the gravitational acceleration is integrated into the constant. Other (empirical) methods are based on scale model tests (Dand and White, 1978; Kriebel et al., 2003), real-world testing (Bhowmik et al., 1981a) or a combination of both (Maynord, 1996; Gelencser, 1977). These methods are mostly focussed on relatively narrow water bodies, as Dand and White (1978)'s experiments are for ships in the Suez Canal, Gelencser (1977) for the St. Lawrence Seaway and Maynord (1996) focusses on the Ohio, Illinois, and Upper Mississippi Rivers. A review of the knowledge and methods related to ship-generated, drawdown waves by Dempwolff et al. (2022a) concludes that current empirical and analytical methods struggle to handle complex bathymetries adequately. As a result, these methods are typically limited to modified waterways or require site-specific input data obtained from experimental data or field measurements.

### 3.1.4   Considered parameters in literature

Table 3.1 summarizes the descriptions made over the years to describe the drawdown caused by the primary ship wave and the parameters used in these descriptions. The parameters used in the analytical and (semi-)empirical descriptions show that the drawdown height depends on the vessel speed, draught and beam together with the water depth and surface width of the channel. Furthermore, the length, distance from the sailing line and channel geometry influence the magnitude of the drawdown in some of the provided methods. The descriptions given in Table 3.1 which are not yet discussed are elaborated and worked out in Appendix B.

| parameter | Schijf 1949 | Schijf corrected 1953 | Gates and Herbich 1966 | Hochstein 1967 | Gelencser 1977 | Dand and White 1978 | Bhowmik 1981 | Maynord 1996 | Kriebel 2003 | CIRIA 2007 |
|---|---|---|---|---|---|---|---|---|---|---|
| ship's speed | ✓ | ✓ | ✓ | ✓ | ✓ | ✓ | ✓ | ✓ | ✓ | ✓ |
| ship's draught | ✓ | ✓ | ✓ | ✓ | ✓ | ✓ | ✓ | ✓ | ✓ | ✓ |
| ship's beam | ✓ | ✓ | ✓ | ✓ | ✓ | ✓ | ✓ | ✓ | | ✓ |
| ship's length | | | | ✓ | | | ✓ | | ✓ | |
| midship coefficient | ✓ | ✓ | ✓ | ✓ | ✓ | ✓ | ✓ | ✓ | | ✓ |
| ship's limit speed | | ✓ | | | | | | ✓ | | ✓ |
| distance | | | | | ✓ | | ✓ | ✓ | | |
| averaged water depth | ✓ | ✓ | ✓ | ✓ | ✓ | ✓ | ✓ | ✓ | ✓ | ✓ |
| channel surface width | ✓ | ✓ | ✓ | ✓ | ✓ | ✓ | ✓ | ✓ | | ✓ |
| block coefficient | | | | | | | | | ✓ | |
| slope of the bank | | | | | | | | | | ✓ |
| gravitational accel. | ✓ | ✓ | | ✓ | | ✓ | ✓ | ✓ | | ✓ |

Table 3.1: Parameters used to calculate the drawdown height in analytical and empirical descriptions.

## 3.2 Ship response to waves

Ships are influenced by the conditions of the water they sail through or are moored in. Waves and currents exert pressures and stresses on a ship, of which the magnitude depends on the characteristics of the waves and currents. The way the ship behaves under the loading of these pressures depends on the features of the ship, such as its dimensions, its draught and its shape. Undesirable ship behaviour could lead to incidents such as the breakage of mooring lines or ship collisions.

### 3.2.1 Hydronamic loading

Multiple descriptions are available on how certain hydrodynamic loadings translate into forcings on ships (Puertos del Estado, 2007; PIANC, 2015). Section 2.1 describes the effects of passing vessels as a suction force and sudden lowering of the water level, related to the primary water motion of the passing vessels, therefore it is assumed that the drawdown wave travels through the outer harbour as a translatory wave. The force on a ship due to a translatory wave generally depends on the slope in the water surface in combination with the weight of the ship (PIANC, 2015). This force ($F_x$) induced by a sudden slope in the water level can be described by the pressure difference between the pressure in the longitudinal direction on the bow of the ship and on the aft of the ship, in the opposing direction, described by the following equation:

$$F_x = \rho_w g \left( \int_0^{h_\text{aft}} A_s(h)\, dh - \int_0^{h_\text{bow}} A_s(h)\, dh \right) \tag{3.7}$$

where the pressure head on the aft and bow is calculated by integrating the underwater cross-section ($A_s$) over the draught at the bow ($h_\text{bow}$) or aft ($h_\text{aft}$) of the ship, schematized in Figure 3.3. The resulting longitudinal force ($F_x$) is then the pressure head difference multiplied by the water density ($\rho_w$) and the gravitational acceleration ($g$). Assuming the difference in draught between the aft ($h_\text{aft}$) and the bow ($h_\text{bow}$) of the ship is $\Delta h$, Equation 3.7 can be rewritten as follows:

$$F_x = \rho_w g B_s C_m D_s \Delta h_\text{ship} \tag{3.8}$$

where $A_s$ is assumed to equal the width of the ship ($B_s$) multiplied by the effective draught ($h_\text{aft}$ or $h_\text{bow}$) and a midship coefficient ($C_m$).
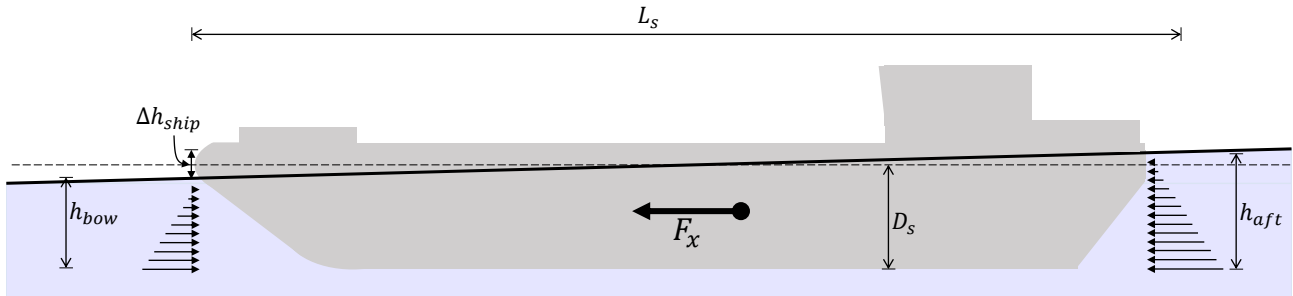


Figure 3.3: Schematization of the pressure difference on a ship induced by a water level slope.

If the wavelength is larger than the length of the vessel, this water level difference along the ship can be expressed using the slope of the water surface ($I$) and the vessel length ($L_s$), as $\Delta h_\text{ship} = I L_s$. Incorporating this in Equation 3.8, the longitudinal force on a ship resulting from a sudden slope in the water level is as follows:

$$F_x = \rho_w g B_s D_s L_s C_m I \tag{3.9}$$

where $F_x$ is the resulting longitudinal force on the ship induced by a slope $I$.

### 3.2.2 Critical loading

When not securely moored, the hydrodynamic loading induces forces on the ship, initiating ship movements. Several guidelines are available which give motion criteria for moored ships (PIANC, 1995, 2023; TNO, 2007), mostly concerning seagoing vessels. If securely moored, the forces on the ship are directly translated into forces in the mooring lines. Reijmerink (2015) provides longitudinal force criteria for ships in lock chambers, based on numerical calculations made using the Lockfill and SCHAT software (developed at Delft Hydraulics), as an extension of the guidelines at that time (Vrijburcht, 1994; Rijkswaterstaat, 2000). These criteria provide an expression for the maximum allowable longitudinal forces on the ship, such that the mooring lines can absorb

them, taking into account the available mooring facilities in a lock. In these guidelines, the critical force ($F_{x,\max}$) is expressed as a promillage of the mass of the displaced water by the ship (WD), multiplied by the gravitational acceleration ($g$):

$$F_{x,\max} = \text{WD} \times g\text{KC} \tag{3.10}$$

where KC is the allowable promillage of the displaced water mass. The mass of the water displaced by the ship (WD) can be expressed by multiplying the width ($B_s$) of the ship, the length ($L_s$), the draught ($D_s$), the blockage factor ($C_B$) and the water density ($\rho_w$), expressed in metric tons. Using the expression of the water displacement, the maximum allowable longitudinal force can be calculated as follows:

$$F_{x,\max} = \rho_w g B_s L_s D_s C_B \text{KC} \tag{3.11}$$

Tabel 3.2 gives the criteria for the different CEMT and RWS ship classes, as presented by Reijmerink (2015). The final column presents the critical force for each ship class, based on the water displacement of a characteristic ship in that class.

| CEMT | MVS | width [m] | length [m] | draught [m] | WD [ton] | criterium [‰] | force [kN] |
|------|------|-----------|------------|-------------|----------|---------------|------------|
| I | M1 | 5.05 | 38.5 | 2.5 | 437 | 4.07 | 17.4 |
| II | M2 | 6.6 | 50 - 55 | 2.6 | 849 | 2.88 | 24.0 |
| | M3 | 7.2 | 55 - 70 | 2.6 | 1179 | 2.43 | 28.1 |
| III | M4 | 8.2 | 67 - 73 | 2.7 | 1455 | 2.18 | 31.1 |
| | M5 | 8.2 | 80 - 85 | 2.7 | 1694 | 2.01 | 33.4 |
| IVa | M6 | 9.5 | 80 - 85 | 2.9 | 2108 | 1.79 | 37.0 |
| | M7 | 9.5 | 105 | 3.0 | 2693 | 1.58 | 41.7 |
| Va | M8 | 11.4 | 110 | 3.5 | 3950 | 1.29 | 50.0 |
| | M9 | 11.4 | 135 | 3.5 | 4848 | 1.16 | 55.2 |
| Vb | BII-2l | 170-190 | 170 - 190 | 3.5 - 4.0 | 6279 | 1.02 | 62.8 |
| | M10 | 13.5 | 110 | 4.0 | 5346 | 1.10 | 57.7 |
| VIa | M11 | 14.2 | 135 | 4.0 | 6901 | 0.97 | 65.7 |
| | M12 | 17.0 | 135 | 4.0 | 8262 | 0.88 | 71.3 |
| VIb | BII-4 | 22.8 | 185 - 195 | 3.5 - 4.0 | 12558 | 0.71 | 87.5 |

Table 3.2: Longitudinal force criteria for the different ship classes conform to the RWS classes, adopted from Reijmerink (2015). The added widths, lengths and (loaded) draughts of the different ship classes are based on the characteristic dimensions given by Rijkswaterstaat (2010).

# Chapter 4: Materials and Methods

In this chapter, the materials and methods used are discussed. Chapter 2 concluded that the primary water motion of the passing vessels is the key physical process leading to unsafe situations in the locks and outer harbour. Subsequently, Chapter 3 explored the methods available in the literature to capture this process. From this exploration, the influential parameters are identified which describe the generation of and response to this phenomenon. Based on these key parameters, the necessary data is collected, described in Section 4.1. Subsequently, Section 4.2 treats the processing done to the different data types. Then, in Section 4.3, the data of the different sources is combined and summarized in a dataset. Finally, the steps taken to predict the drawdown and establish a critical threshold are elaborated in Section 4.4.

## 4.1 Data collection

This section treats the data collection of the six different data types; measurements of the water level fluctuations at three locations in the outer harbour, the calibrated water levels outside the outer harbour, the currents in the fairway outside of the outer harbour, bathymetry, wind data and a dataset describing the passing vessels named AIS data. Figure 4.1 shows an overview of locations at which the different data types are collected. The AIS data and bathymetry are collected for a demarcated area around the outer harbour.
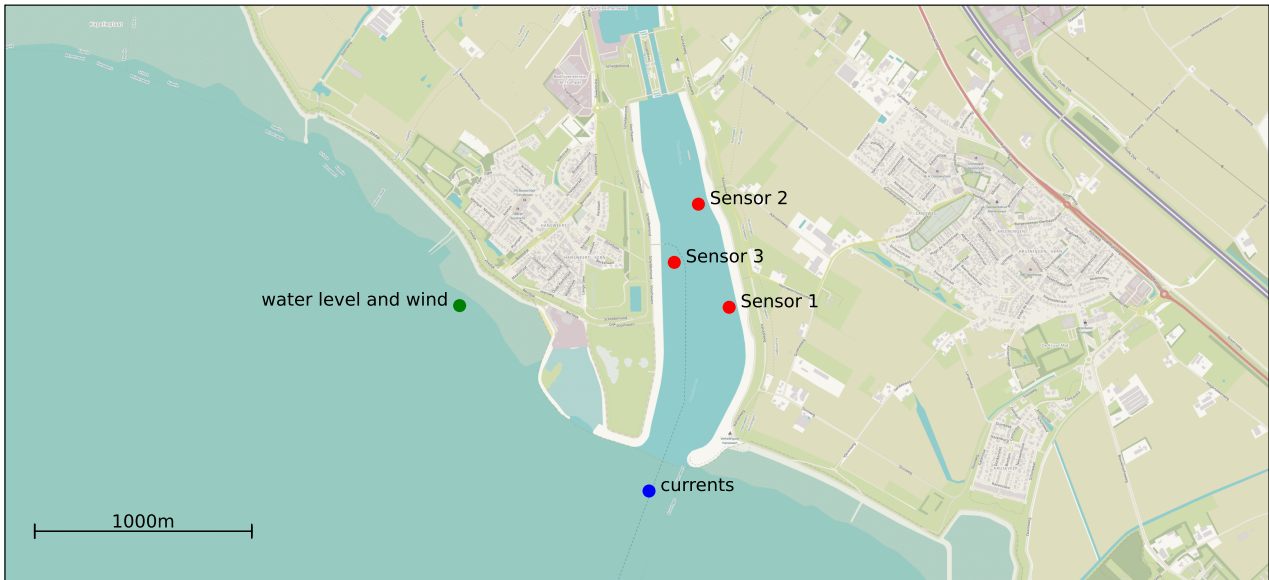


Figure 4.1: Measurement locations of the different types of data.

### 4.1.1 Water level fluctuation measurements

To understand the effects a passing vessel has on the hydrodynamics in the outer harbour, high-frequency measurements of the water level fluctuations have been conducted for seven weeks, in the summer season of 2023. The sensors used to obtain the water level fluctuations in the outer harbour are the Geolux LX-80-15 10Hz non-contact oceanographic radar sensors, taking measurements every second. The instrument was placed above the water surface and measured the distance from its sensor to the surface with a resolution of 0.5mm and an accuracy of ±2mm (Geolux, 2023). The sensors were connected to piles C12, C34 and G23 in the outer harbour, together with a data logger, a solar panel and a battery pack. Sensor 1 is located closest to the Western Scheldt and Sensor 2 is closest to the lock complex, both located at the East side of the harbour. Sensor 3 lies

between Sensors 1 and 2 but is located on the other side of the harbour, on the West side. These locations, pictured as red dots in Figure 4.1, have been chosen as they are significantly spaced apart at approximately equal distances. The data logger, supplied by RMA Hydromet, sends the data in batches of five minutes to a Rijkswaterstaat server. These data batches contain the distance between the instrument and the water level (denoted by L1), the signal-to-noise ratio of the detected signal and the tilt angle of the instrument along both its vertical axis (denoted by A1 and A2). Investigations of the measured data showed that approximately 5% of the data is missing, based on the total number of seconds included in the measurement campaign, and the number of measurements conducted. Furthermore, slight deviations in the tilt angles are observed, for which the measurements were corrected during the processing of the signal, later discussed in Section 4.2.1. The average signal-to-noise ratio indicates a sufficiently clean signal. Figure 4.2 shows the distance between the instrument and the water level for an arbitrary day during the measurement campaign. Appendix C.1 provides more detailed information on the equipment, measurement setup and the collected data.
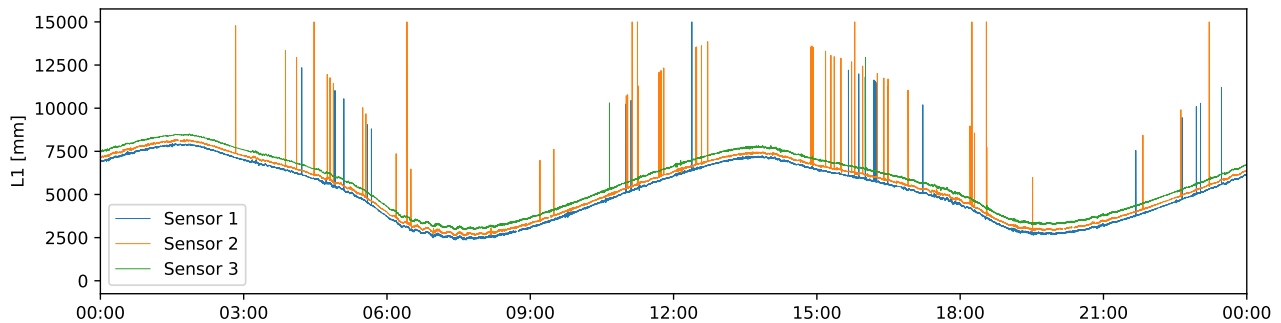


Figure 4.2: Measurements taken during an arbitrary day. L1 represents the distance readings between the sensor and the water surface.

### 4.1.2 Calibrated water levels

As the water level fluctuation measurements are not calibrated to a fixed level, such as the Amsterdam Ordnance Datum (NAP), this data is gathered from a permanent measurement station outside of the outer harbour, represented by the green dot in Figure 4.1. These calibrated water levels are necessary to calculate the depth-related parameters. The data has a sampling period of 10 minutes and is openly available at Rijkswaterstaat Waterinfo. It is downloaded for the measurement period. The time-averaged water level is 0.28 m relative to NAP during the measurement campaign. The maximum and the minimum water levels measured are 3.53 and -2.56 mNAP respectively. In Appendix C.2, the course of the water level during the measurement campaign is visualized.

### 4.1.3 Current data

Current data including direction and depth-averaged magnitude is retrieved from an existing hydrological model, openly available via the Rijkswaterstaat WTZ-viewer. The data is generated every 10 minutes at the location marked blue in Figure 4.1 and was retrieved for the measurement period. Due to the tide-dependent nature of the currents, it alternates between the upstream and downstream directions. Throughout the measurement campaign, the maximum magnitude of the upstream current reaches 2.2 m/s, while the downstream current reaches a maximum of 1.6 m/s. Appendix C.3 provides additional information on how the data was retrieved and visualizes the collected data.

### 4.1.4 Bathymetry

Detailed bathymetry of the project area is provided by Rijkswaterstaat. The data has an accuracy of one by one metre and is openly available at Rijkswaterstaat GeoWeb. The bottom level of the Western Scheldt at the intersection with the outer harbour reaches depths of 30 meters below NAP, shown in Figure 4.3. Appendix C.4 provides additional information and a depth profile of the project location.

### 4.1.5 Wind data

The wind data is measured at the same measurement station as the calibrated water levels, represented as a green dot in Figure 4.1. The data has a sampling period of 10 minutes and is downloaded for the measurement period via Rijkswaterstaat Waterinfo. The average wind speed during this period is 6.2 metres per second

(force 4 on the Beaufort scale) with a maximum of 15.7 metres per second (force 7 on the Beaufort scale). The dominant direction is from the South-West. Appendix C.5 provides additional information and visualizations of the wind climate during the measurement period.



Figure 4.3: Bathymetry data of the project area, retrieved from Rijkswaterstaat GeoWeb.

### 4.1.6 AIS data

AIS, short for Automatic Identification System is an automated vessel tracking system developed as a supplement to the marine radar, as a means to transmit a vessel's location, speed, course and characteristics. This is accomplished by transmitting data at regular intervals via radio signals, allowing vessels and traffic posts in the vicinity to receive and process this information, enhancing situational awareness and navigational safety, and facilitating efficient marine traffic management (IMO, 2015). A sailing vessel transmits these messages every 1-10 seconds. A ship at anchor transmits these messages every 3 minutes. The parameters relevant for this research included in the messages are the position of the vessel, its name, type and unique identification number (MMSI), the speed over ground (SOG), the course over ground (COG), the heading the bow is pointing towards (TH), its length, width, draught and the location of the AIS transmitter relative to the vessel's dimensions. For this research, an alternative value for the vessel draught is included, based on the information system (IVS) of the Joint Nautical Authority of the Scheldt area. All AIS data available was collected for the area surrounding the outer harbour in the period of the measurement campaign. A visualization of the captured AIS transponder locations is given in Figure 4.4. Appendix C.6 provides additional information.
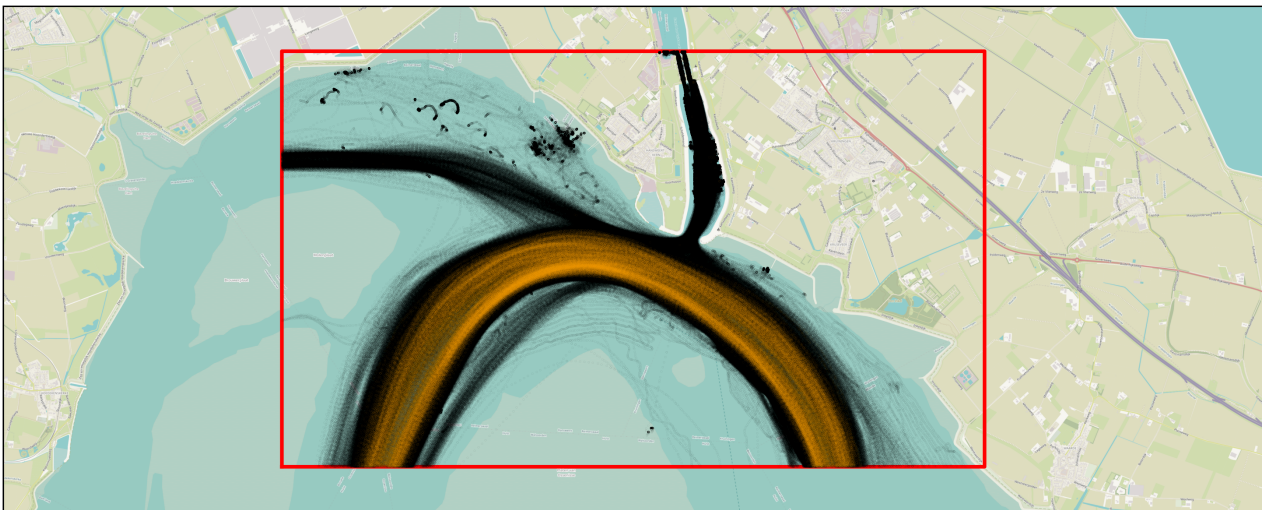


Figure 4.4: AIS transponder locations logged during the measurement campaign plotted on a map. Locations associated with an oversized vessel, defined as vessels longer than 210 metres or deeper than 10 metres, are plotted in orange.

## 4.2 Data processing

This section treats the data processing of the six different data types introduced in Section 4.1. All time-related data is standardized to Central European Summer Time (UTC+02:00) (CEST).

### 4.2.1 Water level fluctuation measurements processing

The processing of the water level fluctuation measurements involves correcting for the tilt angle, the removal of the outliers in the dataset and filtering the frequencies outside of the bandwidth of interest.

**Step 1: Correcting for the tilt angle**

The first step is to correct the measured distance to the sensor (L1) for the tilt angles along both its vertical axis (A1 and A2). As the original signal measured the distance between the sensor and the water surface, the signal is multiplied by minus one, such that greater values represent higher water levels:

$$h = \text{L1} \cos{(\text{A1})} \cos{(\text{A2})} \times -1 \tag{4.1}$$

**Step 2: Outlier removal and filtering of low-frequency oscilations**

The second step is the filtering of low-frequency oscillations and the removal of the outliers, caused by faulty sensor readings. By filtering the signal for the low-frequency oscillations first, the outliers become more straightforward to detect. To determine the appropriate frequency for applying filtering, an estimation of the expected frequency bandwidth of the drawdown phenomena must be made. An initial estimate of the wave period is made by setting the wave period equal to the time it takes a vessel to sail its length. Appendix D.1 shows that the expected period of the drawdown phenomena is between 21 and 100 seconds. The low-frequency oscillations are subtracted from the time series using a rolling overage over 10 minutes, ranging from 5 minutes before to 5 minutes after a certain value:

$$h_{\text{LFF}}(t) = h(t) - \bar{h}(t - 5\text{min} < t < t + 5\text{min}) \tag{4.2}$$

By using a period of 10 minutes, well above the maximum expected period of the drawdown phenomena, the undesired filtering of this phenomenon is prevented. Subsequently, all values above a threshold of 1000mm or below -1000mm are localized, illustrated in the low-frequency filtered signal ($h_{\text{LFF}}$) plot in Figure 4.5. These measurements are then removed from the original time series, and the filtering step is repeated, to remove the influence of the outliers on the rolling average.
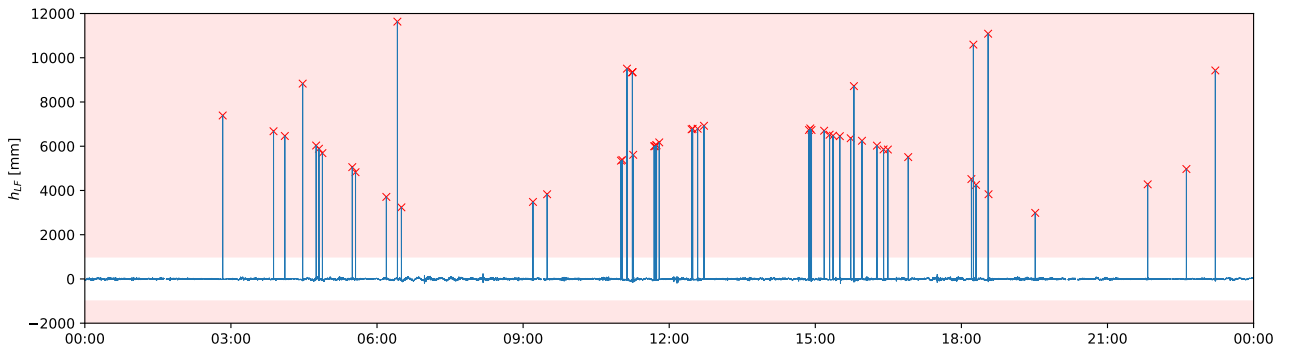


Figure 4.5: The removal of outliers using a 10-minute rolling average using a threshold of 1000mm.

**Step 3: Filtering of high-frequency oscilations**

The minimum expected frequency of the wind-generated waves is 0.35Hz, based on fetch lengths and corrosponding wind speeds, using the Sverdrup-Munk-Bretschneider (SMB) growth curves, calculated in Appendix D.2. The maximum estimated frequency of the ship waves is 0.048Hz, shown in Appendix D.1. To effectively filter the wind waves from the signal data without losing the characteristics of the primary ship waves, a filter has to be applied with a cutoff frequency between these frequencies. A commonly used filter used to eliminate higher frequencies from time series, such as wind-generated waves, is the Butterworth low-pass filter (Floyd, 1969; Baur et al., 2009; Almström and Larson, 2020; Almström et al., 2021; Guo et al., 2022). This filter, also referred to as a maximally flat magnitude filter, is a type of signal processing method designed to have a frequency response

that is as flat as possible in the passband, developed in 1930 by Stephen Butterworth. A fourth-order filter with a cut-off frequency of 0.1 Hz (10s) was found to be suitable to filter the high-frequency oscillations whilst preserving the frequencies of interest. Figure 4.6 shows a two-hour timespan of the low frequency filtered signal ($h_{\mathrm{LFF}}$) and the Butterworth filtered signal ($h_{\mathrm{HFF}}$).
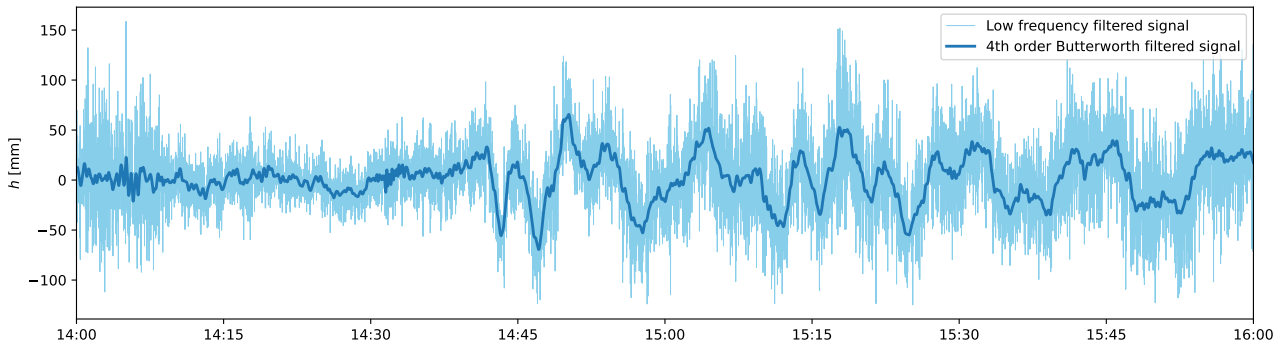


Figure 4.6: The signal before and after the high-frequency filtering using a 4th-order Butterworth filter.

### 4.2.2 Calibrated water levels processing

As the calibrated water level data is sampled at 10-minute intervals, linear interpolation is applied to estimate the water level at the specified time.

### 4.2.3 Current data processing

Similar to the calibrated water level, the current magnitude and direction are linearly interpolated based on the two nearest data points.

### 4.2.4 Bathymetry processing

To make the bathymetrical dataset compatible with the AIS dataset, the coordinate system is converted from the Netherlands RD New (EPSG:28992) coordinate system to the WGS 84 coordinate system, establishing a latitude and longitude for every height data point. Furthermore, as the dataset contains the complete Dutch part of the Western Scheldt, it is narrowed down to only include the area around Hansweert, reducing loading times. For a location of interest, the closest data point to the point of interest is returned, with the corresponding depth value. As the bathymetry has a resolution of one by one metre, no interpolation is deemed necessary.

### 4.2.5 Wind data processing

Similar to the calibrated water level and the current data, the wind data is sampled at 10-minute intervals. Therefore, linear interpolation is applied to estimate the wind direction and magnitude at the time of interest.

### 4.2.6 AIS data processing

The processing for the AIS data steps taken involves correcting data rows with shifted columns to realign them and converting the time zone from UTC to CEST. Based on the location of the AIS transmitter on the vessel, and the time-related coordinates of the transmitter, the coordinates of the bow, middle and aft of the vessel were calculated for every AIS message, elaborated in Appendix E. Unlike parameters such as the width or length of the vessel, which remain constant, the draught of the vessels varies with each trip due to changes in their loading condition. This makes the draught parameter more susceptible to errors or faulty data. The IVS draught of incoming and outgoing vessels recorded by the Joint Nautical Authority of the Scheldt is, among other purposes, used to calculate port dues and pilotage fees. For the continuation of the analysis, the IVS draught will be used as it is considered more reliable since it is formally used. The AIS and IVS draught are compared in Appendix F.

## 4.3 Dataset generation

This section describes the steps taken to combine the data from the different sources in a dataset. The event of a passing vessel is summarized in this dataset by several parameters. These parameters describe the vessel, the environment (wind, currents and water level) and the drawdown occurring in the outer harbour.

### 4.3.1 Vessel and environmental parameters

Before abstracting the parameters describing the vessel's characteristics when passing the outer harbour, the AIS dataset is divided into subsets, containing the data of individual vessel trips. This is done by first listing all the unique vessels in the dataset, based on their MMSI number. Secondly, for every unique oversized vessel, the associated AIS messages are collected. An oversized vessel is defined as a seagoing vessel with a length greater than 210 metres and/or a draught greater than 10.0 metres, adopted from GNB (2019). Smaller vessels are left out from the dataset, aligning with the findings in Chapter 2, where the problem analysis highlighted larger vessels as the primary focus. With this collection of the AIS messages for each oversized vessel, the times between two subsequent messages are analysed. The initiation of a new trip is assumed when the time step with the previous AIS message is greater than 10 minutes. For every individual trip, the data is collected in a separate dataset.

**Time of the passage of the bow, middle and aft of the vessel**

For every time step in the AIS dataset, the coordinates of the bow, middle and aft of the vessel are calculated, explained in Section 4.2.6. Due to the significant size of the vessels passing the outer harbour, three different passage times can be determined, based on the track of the bow of the vessel, the middle and aft. The times of passage are determined by calculating the distance from every coordinate in the track of the bow, middle and aft to the harbour entrance (defined at a latitude of 51.4396° and a longitude of 4.01111°), using the haversine formula. The times at which the distance is minimum for the bow, middle and aft is considered to be the time of passage of the bow ($t_{p,\text{bow}}$), middle ($t_{p,\text{mid}}$) and aft ($t_{p,\text{aft}}$). No interpolation between the two closest points is deemed necessary as the time step between the subsequent AIS messages is sufficiently small, shown in Figures 4.7 and 4.8.



Figure 4.7: Plot showing the track of the coordinates of the middle of an arbitrary vessel passage. The definition of time of passage and passing distance is based on the coordinate with the smallest distance to the harbour entrance.
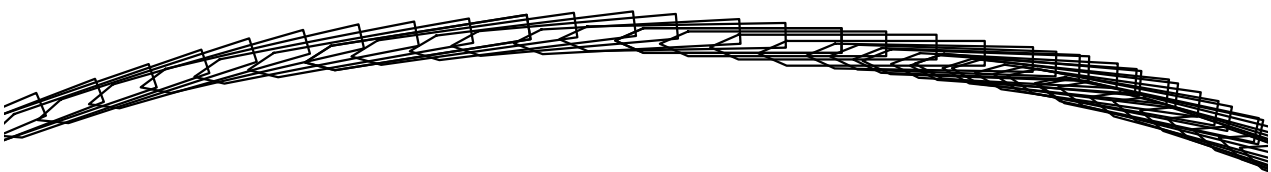


Figure 4.8: Plot illustrating the dimensions of an arbitrary vessel of 293 metres for each timestep, highlighting that the spacial distance between two timesteps is shorter than the vessel's length.

**Passing distance**

From the calculations done to determine the time of the passage of the bow, middle and aft of the vessel, the minimum distances of the bow ($d_{s,\text{bow}}$), middle ($d_{s,\text{mid}}$) and aft ($d_{s,\text{aft}}$) to the harbour entrance are determined simultaneously. The passing distance is defined as follows:

$$d_s = \min\left(d_{s,\text{bow}}, d_{s,\text{mid}}, d_{s,\text{aft}}\right) - 0.5 B_s \tag{4.3}$$

where the actual passing distance ($d_s$) is the subtraction of half the width of the vessel ($B_s$) from the minimum passing distance, comparing the bow, middle and aft of the vessel.

**Water level**

The water level (WL) is defined as the water level at the time of passage of the middle of the vessel ($t_{p,\text{mid}}$). The water level is expressed in metres relative to NAP.

**Bed level**

The bed level (BL) is defined as the bathymetrical elevation at the location of the middle of the vessel at the time of passage ($t_{p,\text{mid}}$). The bed level is expressed in metres relative to NAP.

**Depth**

The depth ($h_s$) in metres is defined as the water level (WL) minus the bed level at the location of the middle of the vessel during passage(BL):

$$h_s = \text{WL} - \text{BL} \tag{4.4}$$

**Under keel clearance**

The under keel clearance (UKC) at the moment of passage of the middle of the vessel is calculated by subtracting the bed level (BL) and the IVS draught ($D_s$) from the water level (WL):

$$\text{UKC} = \text{WL} - \text{BL} - D_s \tag{4.5}$$

where the under keel clearance is expressed in metres.

**Midship and block coefficient**

As the midship ($C_m$) and block ($C_B$) coefficients are not included in the AIS dataset, assumptions of the coefficients are made based on the type of vessel. Table 4.1 shows the coefficients for the vessel types identified in the dataset, adopted from Table 2.6 in Papanikolaou (2014).

|  | cargo | tanker | passenger | other |
|---|---|---|---|---|
| midship coefficient ($C_m$) | 0.975 | 0.995 | 0.940 | 0.970 |
| block coefficient ($C_B$) | 0.650 | 0.840 | 0.550 | 0.600 |

Table 4.1: Midship and block coefficients used in the drawdown height calculations, adopted from Table 2.6 in Papanikolaou (2014).

**Underwater cross-section amidships**

The underwater cross-section amidships ($A_s$) is estimated by multiplying the width ($B_s$) and IVS draught ($D_s$) with the midship coefficient relating to the vessel type ($C_m$):

$$A_s = B_s D_s C_m \tag{4.6}$$

expressed in square metres.

**Water displacement**

The water displacement of the vessel ($\Delta_s$) is estimated by multiplying the length ($L_s$), width ($B_s$) and IVS draught ($D_s$) with the block coefficient relating to the vessel type ($C_B$):

$$\Delta_s = L_s B_s D_s C_B \tag{4.7}$$

expressed in cubic metres.

**Course over ground and true heading**

The course over ground (COG) is the direction the vessel moves towards and the true heading (TH) is the direction the bow of the vessel points towards. Both parameters are determined at the time the middle of the vessel passes the outer harbour ($t_{p,\text{mid}}$).

**Speed over the ground**

The speed over ground (SOG) is defined as the maximum speed over ground recorded between the passage time of the bow ($t_{p_{\text{bow}}}$) and the aft ($t_{p_{\text{aft}}}$) of the vessel in knots. When referring to the speed over ground converted to metres per second, $V_{s,g}$ is used as a symbol.

**Speed through the water**

The speed over the ground can differ significantly from the speed through the water, due to the currents. Using the current data described in Section 4.2.3, an estimation is made of the vessel's speed through the water at the time of passage. This can be done by representing the vessel's course by a vector $\vec{V}_{s,g}$ with magnitude $V_{s,g}$ (speed over ground) and direction $\theta_{s,g}$ (course over ground, also referred to as COG) and the currents as a vector $\vec{U}_c$ with a magnitude $U_c$ and direction $\theta_c$:

$$\vec{V}_s = \vec{V}_{s,g} - \vec{U}_c \tag{4.8}$$

where the vector representing the course of the vessel through the water ($\vec{V}_s$) is the subtraction of the course over the ground from the currents, visualized in Figure 4.9. Using the law of cosines, the magnitude of this vector, which is the speed through water ($V_s$), can be calculated:

$$V_s = |\vec{V}_s| = \sqrt{V_{s,g}^2 + U_c^2 - 2V_{s,g}U_c \cos\left(\theta_{s,g} - \theta_c\right)} \tag{4.9}$$
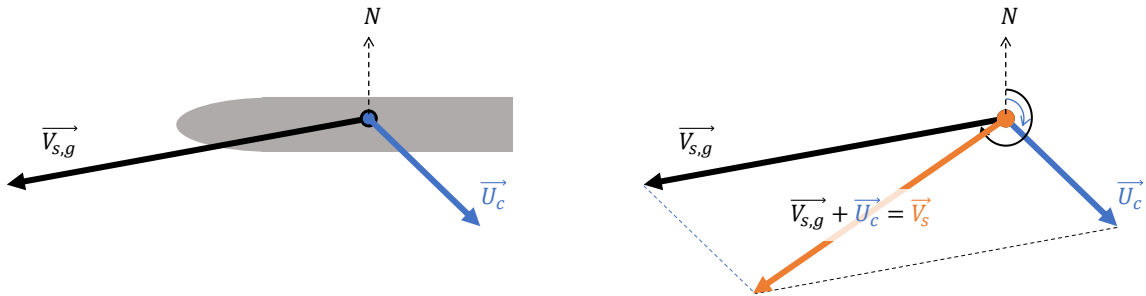


Figure 4.9: The vessel course over the ground and the currents schematized as vectors to calculate the vessel speed through the water.

**Drift angle relative to the vessel**

The drift angle is the difference between the course over ground (COG) and the true heading (TH). A deviation in the course over ground and true heading can be caused by winds, currents or manoeuvring of the vessel. The drift angle is calculated based on a vessel's fixed coordinate system or with respect to the local spatial coordinate system. Within the coordinate system of the vessel, the drift angle is defined as follows:

$$\delta_{s,v} = \text{COG} - \text{TH} \tag{4.10}$$

where $\delta_{s,v}$ is the drift angle relative to the vessel, COG is the course over ground and TH is the true heading. In this frame of reference, positive drift angles are expected for vessels sailing towards the North Sea and negative drift angle for vessels sailing in the direction of Antwerp.

**Drift angle relative to the observer**

Alternatively, the drift angle can be expressed based on the point of view of an observer in a stationary coordinate system. Figure 4.10 shows that negative drift is defined as when the bow of the passing vessel points away from the observer's point of view, relative to the course over ground the vessel moves. Positive drift on the other hand is defined as when the bow is pointing towards the observer. The drift angle calculation relies on the observer's

positioning relative to the passing vessel, distinguishing between the starboard and port sides, described as follows:

$$\delta_{s,o} = \begin{cases} TH - COG, & \text{if } \theta_o < TH < \theta_o + \pi \\ COG - TH, & \text{if } \theta_o - \pi < TH < \theta_o \end{cases} \tag{4.11}$$

where $\theta_o$ is the orientation of the observer relative to the path of the passing vessel. For this study, an orientation of 215 degrees North is used, perpendicular to the channel. Because the outer harbour lies in the outer bend of the route through the Western Scheldt, mostly negative drift angles are expected based on this reference frame.



(a) Negative drift.      (b) Positive drift.
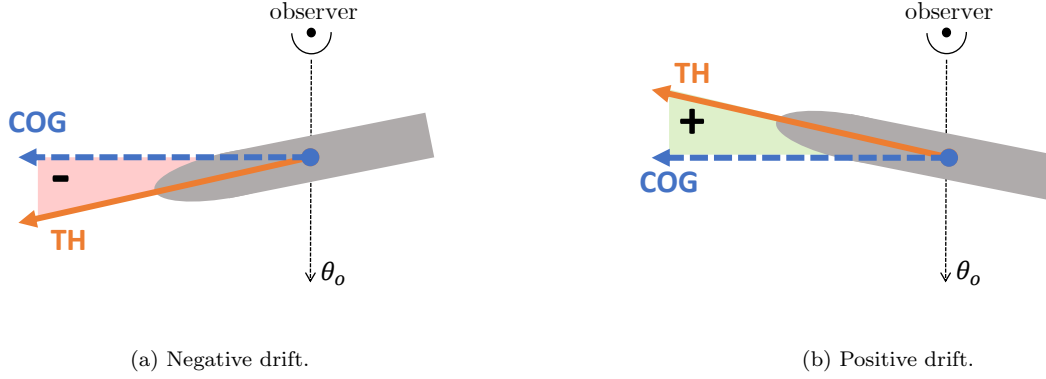
Figure 4.10: Schematization of the definitions of a positive and a negative drift angle with respect to the observation location.

## 4.3.2 Drawdown parameters

The processing and filtering done to the water level fluctuation measurements is explained in Section 4.2.1. Using this filtered signal, the drawdown phenomena occurring in the outer harbour related to a passage of a vessel is characterized by several parameters, based on the wave schematization shown in Figure 4.11. These parameters are calculated by examining three key points in the time series of water level fluctuations. The first point is a local maximum ($h_{max,1}$) corresponding to the bow wave in front of the vessel, elaborated in Section 3.1 and Figure 3.1. The second point is a local minimum ($h_{min}$) corresponding to the drawdown generated by the reduced pressure along the vessel's hull. The final point is the second local maximum ($h_{max,2}$) corresponding to the stern wave at the aft of the vessel. These points are determined based on the time of passage of the vessel and the expected arrival time of the bow, drawdown and aft wave, further elaborated upon in Appendix G.
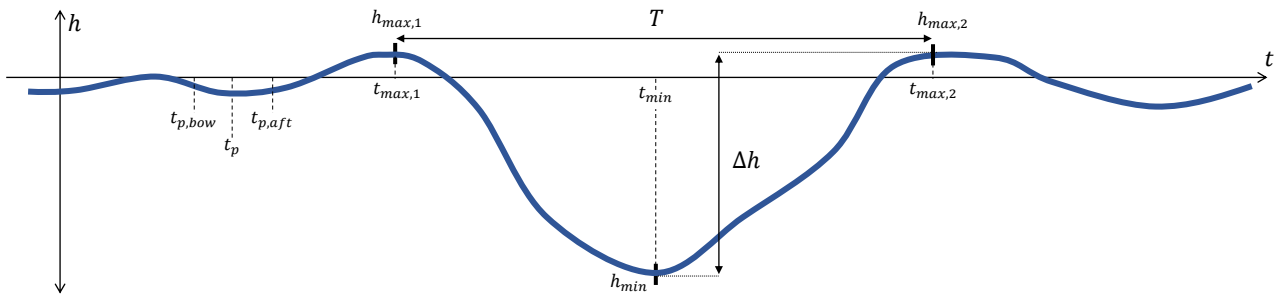


Figure 4.11: Schematization of the Butterworth filtered water elevation fluctuations measured due to the primary wave of a passing vessel.

**Drawdown height**

The drawdown height ($\Delta h$) is defined as the difference between the second local maximum corresponding to the aft wave and the minimum water level:

$$\Delta h = h_{max,2} - h_{min} \tag{4.12}$$

The second local maximum is used as the aft wave acts more predictably than the bow wave, also discussed in Appendix G.

**Drawdown period**

The wave period $(T)$ is defined as the time difference between the initial and the secondary local maximum:

$$T = t_{max,2} - t_{max,1} \tag{4.13}$$

**Water level slope**

The slope of the water level is based on the water level difference and the effective distance between two sensors. As the drawdown is assumed to travel through the outer harbour as a translatory wave, the effective distance is the distance the crest of the wave travels between two points in the longitudinal direction of the outer harbour, visualized in Figure 4.12. This effective distance longitudinal to the harbour is approximately 220 metres between Sensors 1 and 3 and 280 metres between Sensors 3 and 2. For hypothetical Sensors $k$ and $l$ (assuming that Sensor $k$ is located closer to the passing vessel than Sensor $l$), the slope is then defined as follows:

$$I_{k,l} = \max \left( \frac{h_k(t) - h_l(t)}{\Delta l_{k,l}} \right) \quad \text{for} \quad t \in [t_{k,max,1}, t_{l,max,2}] \tag{4.14}$$

where the maximum slope between the two sensors is identified at all timesteps between the time at which the initial maximum water level is observed at Sensor $k$ ($t_{k,max,1}$) and the time at which the secondary maximum water level is observed at Sensor $l$ ($t_{l,max,2}$), as schematized in Figure 4.11.
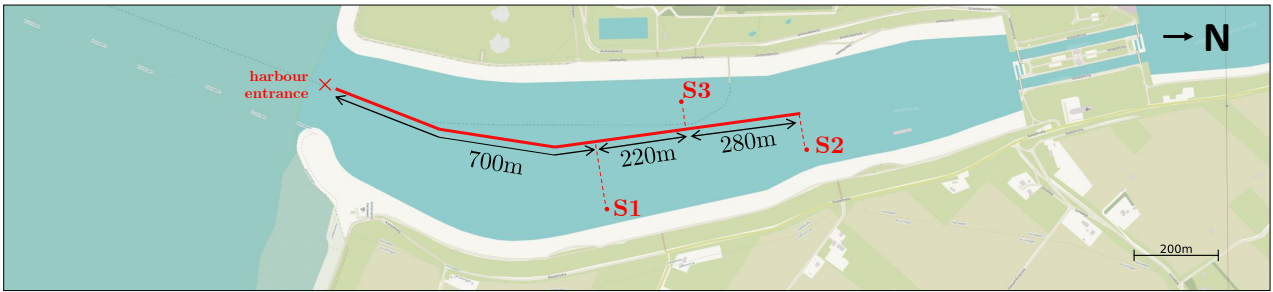


Figure 4.12: Visualization of the effective distances between the sensors and the location chosen to be the mouth of the other harbour. The red line is the assumed path the wave travels through the outer harbour.

### 4.3.3 Dataset overview

An overview of all the relevant parameters collected for every individual passage of an oversized vessel is given in Table 4.2. The static vessel parameters are the parameters which do not change over the course of a trip, based on the AIS data. The environmental parameters describe the water level, currents and wind at the time the vessel passes the outer harbour. The dynamic vessel parameters describe the vessel at the time of passage, calculated in Section 4.3.1. Finally, the drawdown parameters describe the hydrodynamic effects measured in the outer harbour, defined in Section 4.3.2. Appendix H provides sample data for eight arbitrary passages.

| static vessel parameters | | |
|---|---|---|
| vessel name | - | - |
| MMSI number | - | - |
| vessel type | - | - |
| vessel length | $L_s$ | m |
| vessel width | $B_s$ | m |
| vessel draught | $D_s$ | m |
| midship coefficient | $C_m$ | - |
| block coefficient | $C_B$ | - |
| underwater cross-section | $A_s$ | m$^2$ |
| water displacement | $\Delta_s$ | m$^3$ |

| dynamic vessel parameters | | |
|---|---|---|
| passage times | $t_p$ | - |
| passing distance | $d_s$ | m |
| depth | $h_s$ | m |
| speed over ground | $V_{s,g}$ | m/s |
| speed through the water | $V_s$ | m/s |
| course over ground | COG | deg |
| under keel clearance | UKC | m |
| drift angle | $\delta_s$ | deg |

| drawdown parameters | | |
|---|---|---|
| drawdown height | $\Delta h$ | m |
| drawdown period | $T$ | s |
| water level slope | $I$ | - |

| environmental parameters | | |
|---|---|---|
| water level | WL | mNAP |
| current magnitude | $U_c$ | m/s |
| current direction | $\theta_c$ | deg |
| wind magnitude | $U_w$ | m/sc |
| wind direction | $\theta_w$ | deg |

Table 4.2: Set of parameters describing the passing vessel and the environment at the time of passage.

## 4.4 Drawdown prediciton

### 4.4.1 Removal of disturbed observations

The water level fluctuations in the outer harbour can be disturbed before a vessel's passage, influencing the drawdown parameters. This disturbance is mostly induced by a previous passing vessel. For this reason, passages for which the measured oscillations before the time of passage are above a set threshold are removed from the dataset. This is done by analysing the water level fluctuations from 10 minutes before the middle of the vessel passes the outer harbour ($t_{p,mid}$ - 10min) to the time when the vessel passes ($t_{p,mid}$). If the difference between the maximum measured water level and the minimum measured water level measured in this interval is greater than a set threshold, this passage is excluded from further analysis. For this analysis, a threshold of 10 centimetres proved to filter out unreliable observations. Furthermore, vessels with a length greater than 400 metres are removed, as inspections revealed inaccuracies in the length information within their AIS data. Finally, passages with a calculated passing distance greater than 800 metres or less than 200 metres are removed, as inspections of these cases revealed incorrect or incomplete AIS tracks.

### 4.4.2 Corrolation analysis

Literature shows that the key parameter to describe the drawdown related to a vessel passage is the drop in water level, referred to as the drawdown height. In this next step, the influence the vessel and environmental parameters have on the drawdown height is explored. This is done by visual inspection through scatterplots and by calculating the statistical dependence. The statistical dependence between the different parameters is expressed using Spearman's rank correlation coefficient ($\rho$), as this assessment can effectively capture non-linear relationships (Sedgwick, 2014). This provides an overview of the most influential parameters related to the drawdown height. Furthermore, the mutual dependence of the drawdown height versus the drawdown period and slope is analysed. As the slope is significantly correlated with the drawdown height, a formulation relating these two parameters to each other is constructed.

### 4.4.3 Critical drawdown slope and height

Using the longitudinal force criteria for inland ships introduced in Section 3.2.2, the maximum water level slope, generating a critical force for a certain type of inland ship or ship combination, can be calculated, by setting the calculated longitudinal force equal to the critical longitudinal force:

$$\underbrace{\rho_w g B_s D_s L_s C_m I}_{\text{Equation 3.9}} = \underbrace{\rho_w g B_s L_s D_s C_B \text{KC}}_{\text{Equation 3.11}} \tag{4.15}$$

As the mass criterium (KC) is expressed as promillage of the displaced weight, a combination of Equations 3.9 and 3.11 gives the critical slope ($I_{\text{critical}}$) expressed using the mass criterium of a certain ship type:

$$I_{\text{critical}} = \frac{C_B}{C_m} \text{KC}. \tag{4.16}$$

The critical drawdown height can be expressed using the mass criterium, as the drawdown height relates to the water level slope, elaborated in Section 4.4.2. This was used to calculate the maximum allowable drawdown height for every ship type introduced in Table 3.2. Furthermore, the scenario in which multiple ships are moored alongside is analysed in the same way, by analysing the total combined water displacement tonnage of the ships. The ship or ship combinations requiring the lowest drawdown height to fulfil the longitudinal force criteria are taken, and this drawdown height is set as the critical drawdown height.

### 4.4.4 Drawdown height prediction using existing descriptions

In order to predict the criticality of a vessel passage, the drawdown height is predicted and held against the criteria derived in the previous section. In this step, the predictive capability of the drawdown height descriptions introduced in Section 3.1 are tested against the measurement data. This is done by visual inspection through scatterplots where the predicted drawdown height is plotted against the predicted drawdown height based on the empirical equation. To quantify the predictive capacity of a certain method, the Pearson correlation coefficient and Mean Absolute Error (MAE) are used. The Pearson correlation coefficient (r) assesses the linear correlation between the measured and predicted values; 1 means perfect positive correlation, 0 means no correlation and -1 means perfect negative correlation. This coefficient captures the linear dependability between the measurements and predictions without being distorted due to the magnitude difference. This magnitude difference is then captured by the MAE. The MAE is the average difference between predicted and actual values, so higher values indicate a greater mean deviation.

The empirical drawdown height descriptions are based on a schematization of the channel cross-section. Excluding the description by CIRIA (2007), the descriptions schematize the channel cross-section to be rectangular. The cross-section at the passing location is schematized to have a depth of 23 metres relative to NAP and a width of 900 metres, shown in Figure 4.13. The description of CIRIA (2007) uses a trapezoidal schematization for the channel cross-section. The assumed profile has a bottom width of 800 metres, at a depth of 23 metres relative to NAP. By assuming a slope of 9 degrees at both sides, the width at 0mNAP is 1200 metres. The Python code used to calculate the drawdown height is available via a GitHub repository. Appendix H provides sample calculations for eight arbitrary passages.
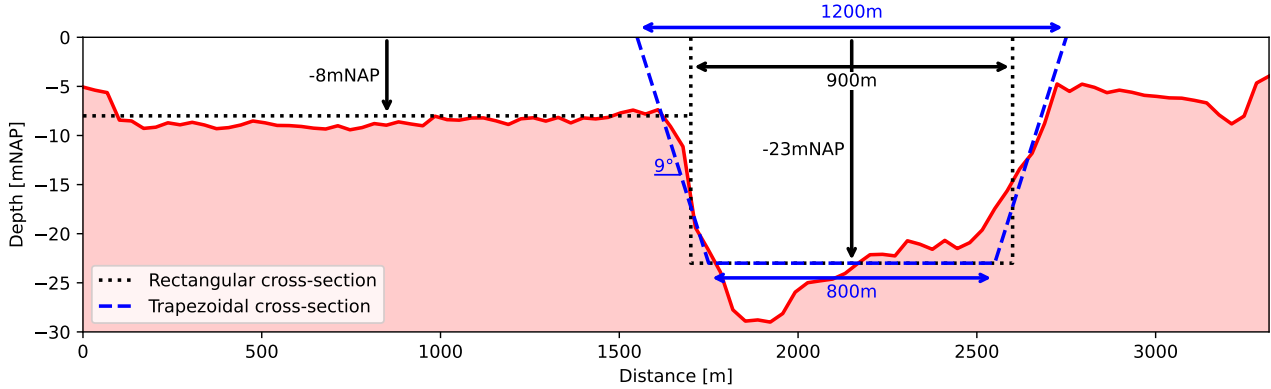


Figure 4.13: The assumed rectangular and trapezoidal channel cross-sections, based on the channel profile given in Figure C.12. The lock complex is situated on the left side of the figure.

### 4.4.5 Site specific drawdown height prediction

To improve the predictive accuracy of existing equations, a new empirical equation is derived based on non-dimensional quantities of the influential parameters, similar to the approach of Almström and Larson (2020). By reducing the number of dimensions, it becomes feasible to calibrate an equation with exponents without introducing incorrect units. Similar to most other empirical drawdown equations found in literature, the drawdown height is expressed as a non-dimensional factor using the vessel speed ($V_s$) and the gravitational acceleration ($g$), hereafter referred to as the dimensionless drawdown height:

$$\frac{2g\Delta h}{V_s^2} \rightarrow \frac{[\text{ms}^{-2}] \times [\text{m}]}{[\text{ms}^{-1}]^2} = \frac{\text{m}^2\text{s}^{-2}}{\text{m}^2\text{s}^{-2}} \tag{4.17}$$

The non-dimensional drawdown height is expressed using a power relationship which includes a number of non-dimensional quantities ($f_{1,2,3,...,n}$), of which the magnitude of their influence on the non-dimensional drawdown height is set using a coefficient, corresponding to a factor $C_{1,2,3,...,n}$, shown in Equation 4.18. The greater the coefficient, the greater the influence of that quantity on the non-dimensional drawdown height. Finally, the factor $C_0$ scales the multiplication of factors.

$$\frac{2g\Delta h}{V_s^2} = C_0 \times f_1^{C_1} \times f_2^{C_2} \times f_3^{C_3} \times ... \times f_n^{C_n} \tag{4.18}$$

**Non-dimensional quantities**

The non-dimensional quantities analysed are based on the quantities used in earlier explored equations, factors taken from Almström and Larson (2020) and newly constructed ratios. The explored quantities include the blockage factor ($A_s/A_c$), the ratio between the length of the vessel and the passing distance ($L_s/d_s$), the ratio between the width of the vessel and the passing distance ($B_s/d_s$), the ratio between the draught and the depth ($D_s/h_s$) and the non-dimensional limit speed ($V_{lim}/\sqrt{gh}$). The limit speed ($V_{lim}$) is defined in Appendix B. Also, a one-sided blockage factor is considered focusing solely on the channel cross-section between the passing vessel to the harbour entrance, denoted as $A_s/(d_s h_{\text{channel}})$. In this quantify, $h_{\text{channel}}$ is the generalized depth of the channel. Finally, an amplification factor is explored, to incorporate the increase in amplitude of waves as they transition from deeper waters in the channel into the shallower regions of the outer harbour. By neglecting refraction, dissipation or reflection effects, Bosboom and Stive (2021) explain that the wave heights at two arbitrary locations can be related as follows:

$$\frac{H_1}{H_2} = \sqrt{\frac{c_1}{c_2}\frac{n_1}{n_2}} \tag{4.19}$$

where $H$ are the wave heights, $c$ are the wave celerities and $n$ are the ratios between the group and individual wave celerities. The subscripts indicate the location at which the parameters are evaluated. By assuming the wave acts in the shallow water regime at both locations, the wave celerity can be expressed using the depth ($\sqrt{gh}$) and $n$ at both locations equals 1. Therefore, a wave height amplification factor is derived, which only relates to the depths:

$$\frac{H_1}{H_2} = \sqrt{\frac{\sqrt{gh_1}}{\sqrt{gh_2}}} = \sqrt[4]{\frac{h_1}{h_2}} \tag{4.20}$$

This amplification factor is applied as a non-dimensional quantity $\sqrt[4]{h_s/h_{\text{harbour}}}$ describing the depth-induced increase in drawdown height between the location where the wave is generated (with a depth $h_s$) and the outer harbour (with a generalized depth $h_{\text{harbour}}$). The factors used in the final equation are chosen iteratively, based on the best-performing combination of non-dimensional quantities. The optimum coefficient values for these dimensionless quantities are obtained through regression analysis involving the observed drawdown heights.

**Regression analysis**

The steps taken in the regression analysis are as follows. The first step is to generate random initial coefficient values, based on a normal distribution around zero with a standard deviation of one. Then, the predictive capability of this newly created power relationship is quantified by analysing the predicted drawdown height against the observed drawdown height, using the Pearson correlation coefficient. This step is repeated until a correlation coefficient above the set initial value is found. In that case, the coefficients of this run are saved and used as the mean of the normal distribution the coefficients for the subsequent runs are determined with. Furthermore, every ten runs, the standard deviation of the normal distribution narrows, such that the solution is directed towards the optimum coefficient values. After several runs (100-1000), the optimum coefficient values are returned. As higher coefficients indicate a greater influence on the non-dimensional drawdown height, this method provides insight into which non-dimensional quantities are the most influential.
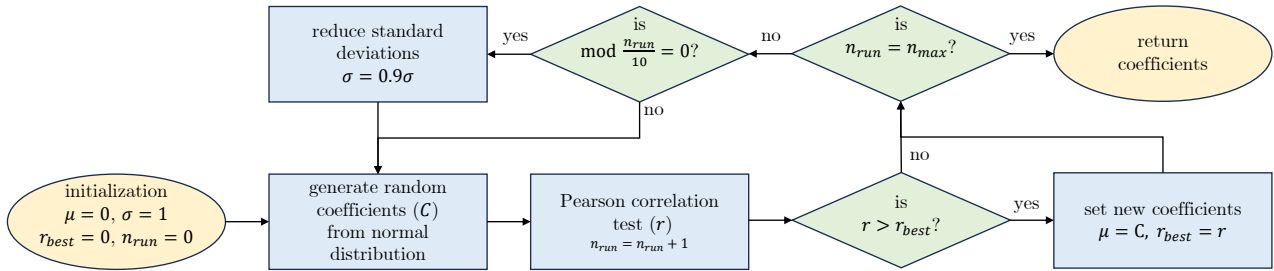


Figure 4.14: Flow chart of the regression analysis methodology. In this figure, $\mu$ and $\sigma$ are the mean and standard deviation describing the normal distribution used to generate the constants $C$. $n_{run}$ describes the number of runs executed and $n_{max}$ the maximum number of runs to be executed.

**Calibration and validation**

This method is used to analyse a number of different power relations with different non-dimensional quantities. The coefficients of the statistically best-performing power relation are then calibrated using the previously introduced methodology, by only considering half of the dataset. This newly formed power relationship describing the drawdown height is subsequently validated using the other half of the dataset. To quantify the predictive capacity of this method, again, the Pearson correlation coefficient and MAE are used.

## 4.4.6   Design of risk mitigation measures

Based on the gained understanding of the problems, mitigation measures are drawn up. The design of the mitigation measures is both focussed on the reduction of the drawdown wave and additional measures to reduce the risk in the outer harbour due to passing vessels in the outer harbour. The first set of measures focuses on the passing vessels, to reduce the drawdown in the outer harbour below the set critical level. The second set focuses on the alternative solution directions, by focusing on the traffic system as a whole and the resilience of the inland ships in the outer harbour against the drawdown phenomena. The applicability of all these measures is tested against the practical knowledge gained in the problem analysis.

## 4.5 Conclusion

In this chapter the following sub-question was treated:

---

"What materials and methods are available to quantify a vessel passage and associated water motions in the outer harbour, and how can these be utilized to predict unsafe conditions?"

---

The materials used to investigate the problems include high-frequency water level measurements in the outer harbour, calibrated water level data, fairway currents data, bathymetry information, wind data, and an AIS dataset describing the passing vessels, all taken over a period of seven weeks. The measurement data was filtered to remove the tide and wind waves from the signal. Using the collected data, a dataset quantifying a vessel passage and associated water motions in the outer harbour was generated. These parameters include (but are not limited to) the dimensions of the vessel passing the outer harbour, the time of passage, the passing distance, the under-keel clearance at the passage location, the speed over ground and through the water of the vessel and the drift angle. The parameters describing the water motions in the outer harbour include the lowering of the water, referred to as the drawdown height, the time scale of the water lowering, referred to as the drawdown period, and the slope in the water level due to this drawdown.

The methodology employed to predict unsafe conditions resulting from the drawdown of vessels passing the outer harbour involves developing a method to predict drawdown heights and establishing a critical drawdown height threshold. If this threshold is surpassed, the water motions in the outer harbour are deemed unsafe. This threshold is established by relating the drawdown heights to longitudinal force criteria for inland ships, through the relation the slope of the water level has with the drawdown height. Using existing longitudinal force criteria for inland ships, the maximum drawdown height, generating a critical force for a certain type of inland ship or ship combination is calculated. Then, the drawdown height is predicted using existing empirical equations. Improvement in prediction accuracy is achieved by developing a site-specific drawdown height equation through regression analysis of the measured drawdown heights. This site-specific drawdown height equation is calibrated and validated using the collected data. Utilizing the drawdown prediction method and the knowledge of the critical drawdown, mitigation measures can be devised to maintain the drawdown height and its associated slope below a predefined maximum.

# Chapter 5: Data Analysis

In this chapter, the data collected for every passing vessel is analysed. Section 5.1 describes and visualizes the drawdown phenomena observed. An overview of the data collected is given in Section 5.2. In Section 5.3, correlation analysis is conducted between the vessel and environmental parameters and the drawdown.

## 5.1 Observations

The analysis of the water level fluctuations measurements obtained from the sensors in the outer harbour during the passage of an oversized vessel reveals distinct patterns. Figures 5.1, 5.2, and 5.3 demonstrate similar behaviour in the filtered water level fluctuations following the passage of an oversized vessel. Roughly one minute after the passage, Sensor 1 registers an abrupt decline in water level, plotted in black. After a few seconds, first Sensor 3 (blue line) and then Sensor 2 (red line) record a similar reduction. This aligns with the expectations, given that Sensor 1 is located in the southernmost region, nearest to passing vessels, Sensor 3 is situated in the middle, and Sensor 2 in the North, closest to the lock chamber (see also Figure 4.1). The wave gets reflected by the northern end of the outer harbour and returns, passing Sensors 2, 3 and 1 respectively. The minutes after the passage are characterized by the more irregular dampening of the water movements. In the figures, the grey lines display the signal of Sensor 1, before the filtering of the higher frequencies.
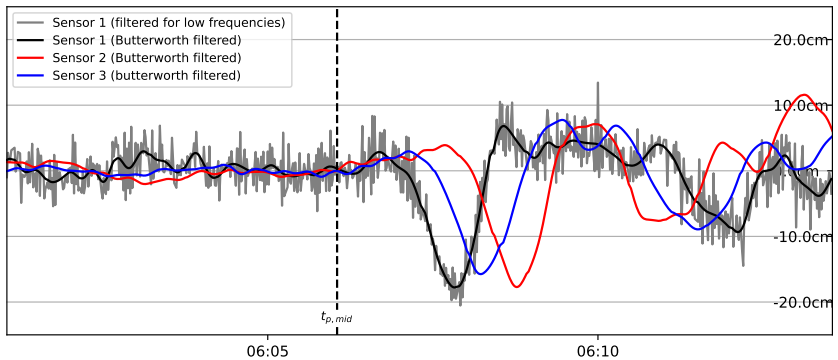


| date and time | 2023-08-01 06:06 |
| --- | --- |
| vessel name | CSCL Neptune |
| vessel length | 366m |
| vessel width | 52m |
| vessel draught | 12.9m |
| speed over ground | 8.2m/s (15.9kts) |
| speed through water | 6.9m/s (13.4kts) |
| passing distance | 328m downstream |
| under keel clearance | 14.0m |
| water level | 0.8mNAP |
| current speed/dir | 1.3m/s at 284° |
| wind speed | 7.6m/s |

Figure 5.1: Water level fluctuations as measured during the passage of the CSCL Neptune on the 1st of August.
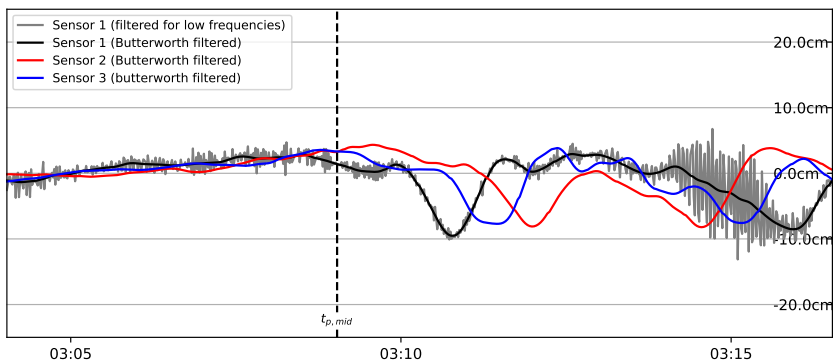


| date and time | 2023-07-08 03:09 |
| --- | --- |
| vessel name | Hudson Express |
| vessel length | 305m |
| vessel width | 40m |
| vessel draught | 11.6m |
| speed over ground | 8.5m/s (16.5kts) |
| speed through water | 7.8m/s (15.2kts) |
| passing distance | 487m upstream |
| under keel clearance | 11.0m |
| water level | -1.59mNAP |
| current speed/dir | 0.7m/s at 107° |
| wind speed | 3.4m/s |

Figure 5.2: Water level fluctuations as measured during the passage of the Hudson Express on the 8th of July.
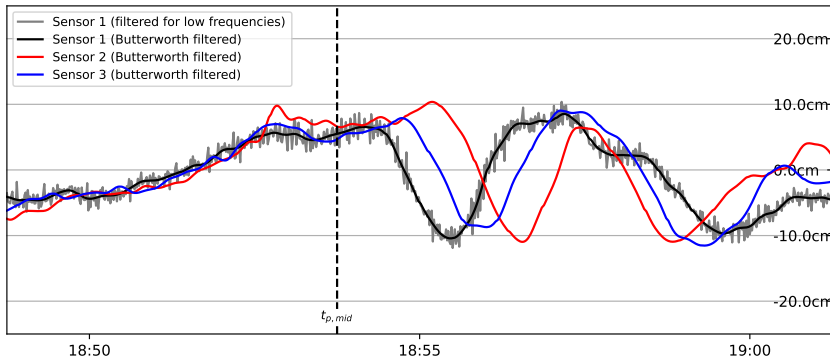
| | |
|---|---|
| date and time | 2023-07-10 18:54 |
| vessel name | Cosco Glory |
| vessel length | 366m |
| vessel width | 48m |
| vessel draught | 14.1m |
| speed over ground | 5.6m/s (10.9kts) |
| speed through water | 6.7m/s (13.0kts) |
| passing distance | 329m downstream |
| under keel clearance | 12.6m |
| water level | 0.2mNAP |
| current speed/dir | 1.1m/s at 106° |
| wind speed | 3.0m/s |

Figure 5.3: Water level fluctuations as measured during the passage of the Cosco Glory on the 10th of July.

Figure 5.4 and 5.5 illustrate that this effect is not consistently observed for every passage. In Figure 5.4 after the passage of the MSC Maureen, visually, no drawdown effect can be noted. Alternatively, already before the passage of the MSC Aino in Figure 5.5, significant disturbance in the water level is observed, with the vessel's passage seemingly having minimal impact on the measurements. In this case, the oscillations can be related to the passage by another vessel passing the outer harbour 35 minutes prior. Using the methodology described in Section 4.4.1, observations like this are removed from the dataset, as the oscillations measured are not related to the passage of this vessel.
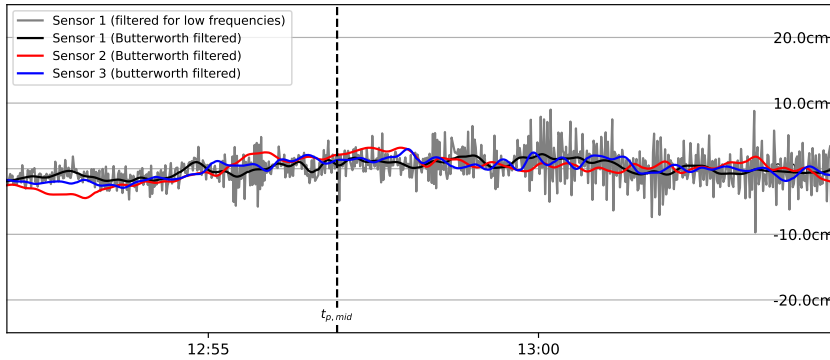


| | |
|---|---|
| date and time | 2023-07-14 12:57 |
| vessel name | MSC Maureen |
| vessel length | 300m |
| vessel width | 40m |
| vessel draught | 11.1m |
| speed over ground | 4.7m/s (9.1kts) |
| speed through water | 6.0m/s (11.7kts) |
| passing distance | 427m downstream |
| under keel clearance | 16.3m |
| water level | 2.0mNAP |
| current speed/dir | 1.4m/s at 104° |
| wind speed | 3.8m/s |

Figure 5.4: Water level fluctuations as measured during the passage of the MSC Maureen on the 14th of July.
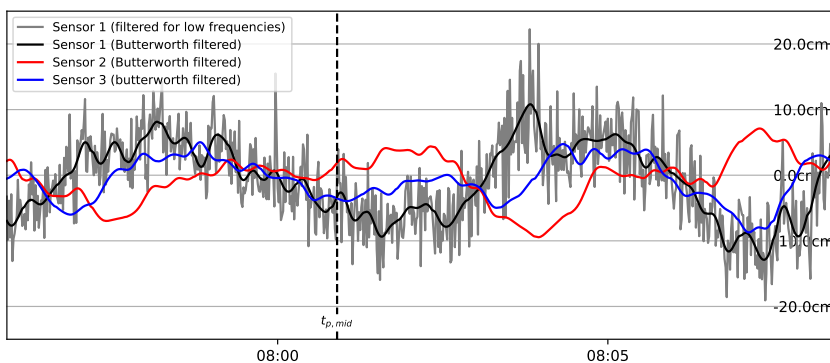


| | |
|---|---|
| date and time | 2023-07-30 08:01 |
| vessel name | MSC Aino |
| vessel length | 328m |
| vessel width | 48m |
| vessel draught | 11.2m |
| speed over ground | 5.6m/s (10.9kts) |
| speed through water | 5.0m/s (9.7kts) |
| passing distance | 375m downstream |
| under keel clearance | 11.6m |
| water level | -1.5mNAP |
| current speed/dir | 0.6m/s at 289° |
| wind speed | 9.5m/s |

Figure 5.5: Water level fluctuations as measured during the passage of the MSC Aino on the 30th of July.

To demonstrate the connection between a passing vessel and notable water level fluctuations, Figure 5.6 displays a density plot of the water level fluctuations measured by Sensor 1 relative to the passage time, for all oversized vessels that passed the outer harbour during the measurement campaign. This thus includes the passages where no drawdown effect is observed and the passages that are removed from further analysis due to oscillations prior to the passage. The density plot emphasises the observed pattern. In the 10 minutes before the passage of a vessel, the water level is relatively constant. Between the time of passage and the following 2 minutes, a clear lowering in the water level can be observed. Sensors 2 and 3 show similar behaviour, although the lowering in water level occurs later.
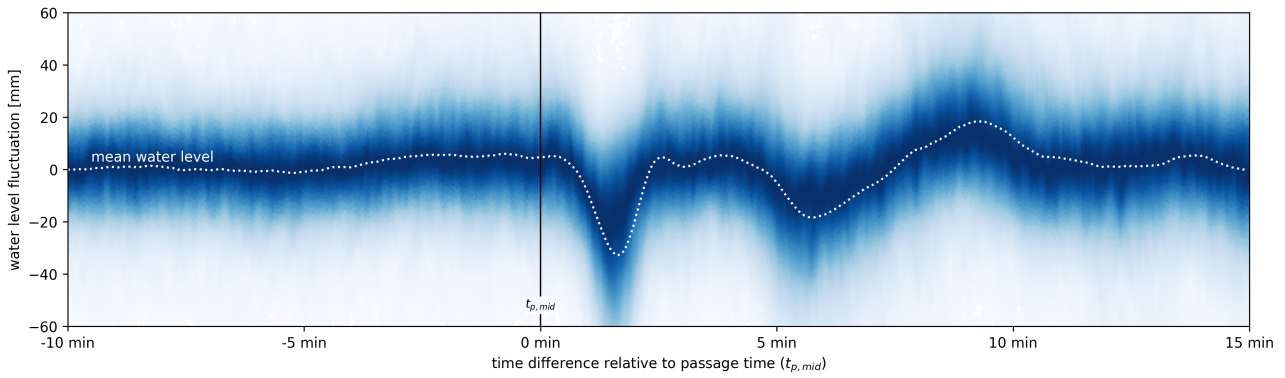
Figure 5.6: Density plot of the fluctuations in water level as measured by Sensor 1, ranging from 10 minutes before passage to 15 minutes after passage, for every oversized vessel passage in the measurement period.

## 5.2 Overview of passage parameters

In total 1281 passages of oversized vessels are observed, in the 7-week measurement campaign. From these 1281 passages, 299 unreliable observations are removed following the methodology described in Section 4.4.1, with 982 observations remaining. These observations are described by the vessel, environmental and drawdown parameters introduced in Table 4.2. As expected, the vessels sailing upstream, towards Antwerp, mostly use the inner bend of the channel, shown in Figure 5.7. The vessels sailing towards the North Sea, mostly use the outer bend, reducing the distance at which they pass the outer harbour. Figure 5.8 shows that the distribution of the speed over the ground compared to the speed through the water shows similar shapes. The average passage speed is around 7 metres per second (14 knots).
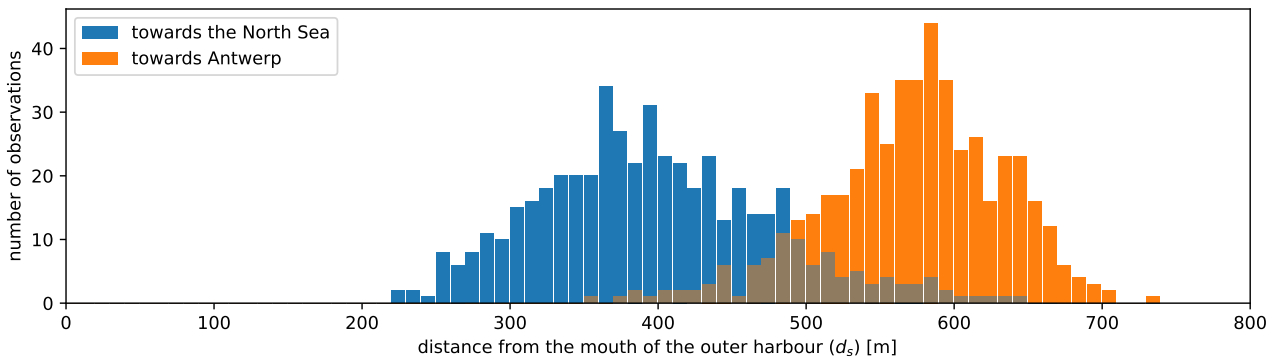


Figure 5.7: Distribution of the passing distances of the oversized vessels passing the outer harbour during the measurement campaign.
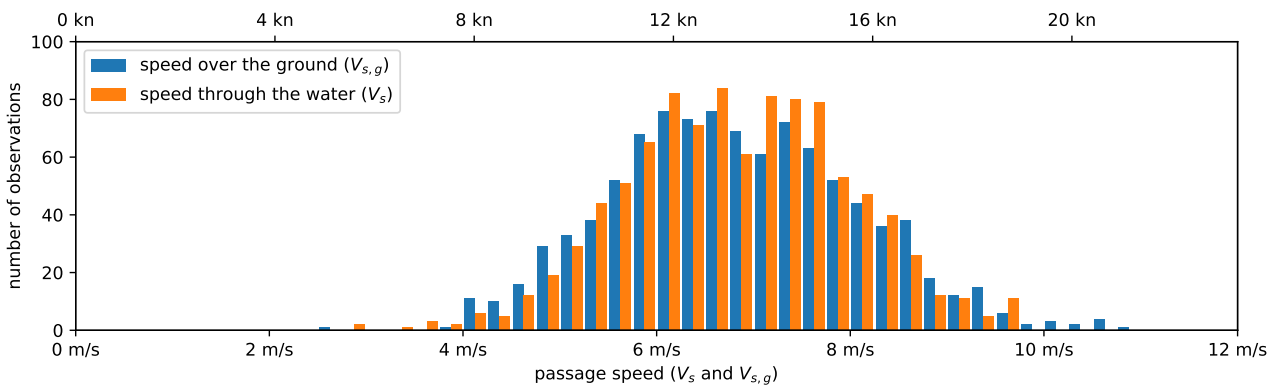


Figure 5.8: Distribution of the speeds over the ground of the oversized vessels passing the outer harbour during the measurement campaign.

The characteristics of the primary waves caused by the passing oversized vessels are displayed in Figures 5.9, 5.10 and 5.11 for the drawdown height ($\Delta h$), drawdown period ($T$) and water level slope ($I$) respectively. The average drawdown height approximates 6 centimeters at Sensor 1, and slightly decreases for the sensors further North, shown by Figure 5.9. In most cases the drawdown height does not exceed 20 centimetres, nevertheless, maximum values reach twice this value. Figure 5.10 shows that the drawdown period is normally distributed around an average duration of 2.5 minutes, more than twice the expected period, calculated in Appendix D.1. The slope in the water level caused by the drawdown wave decreases, as the average slope is higher from Sensor 1 to 3 compared to the slope from Sensor 3 to 2, shown in Figure 5.11. On average, the slope in the water level during a drawdown event is 1 centimetre per 100 metres, however, extreme observations show slopes up to 15 centimetres for the same distance. Appendix I visualizes the distributions of the vessel's dimensions, drift angles, depths and under keel clearances of the passing vessels in the dataset.
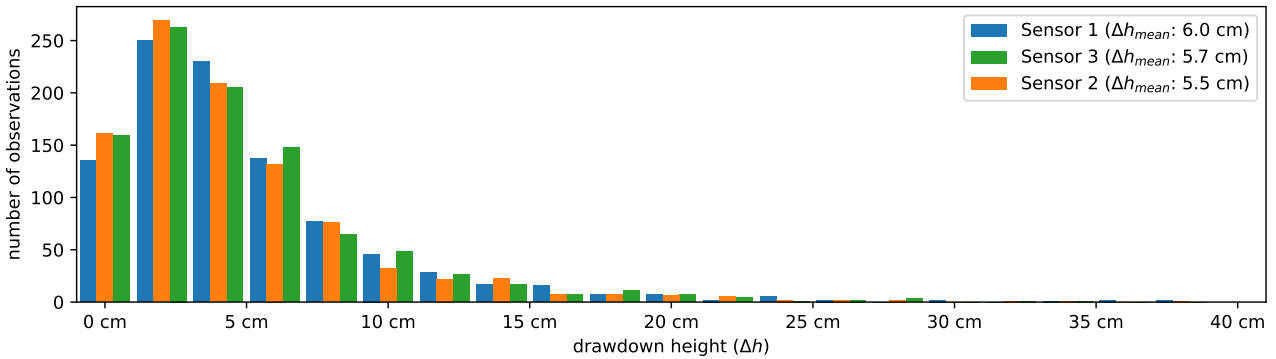


Figure 5.9: Distribution of the drawdown heights related to the passage of oversized vessels during the measurement campaign.
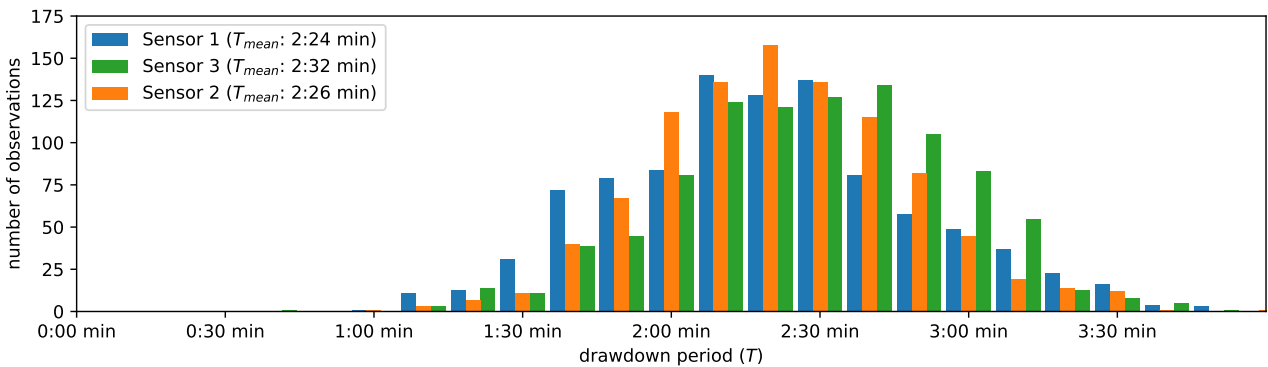


Figure 5.10: Distribution of the drawdown periods related to the passage of oversized vessels during the measurement campaign.
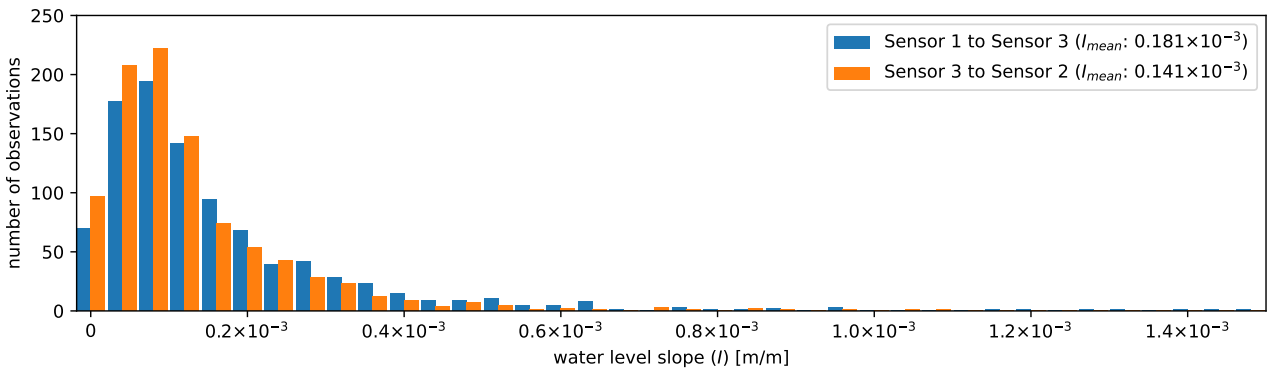


Figure 5.11: Distribution of the drawdown water level slopes related to the passage of oversized vessels during the measurement campaign.

## 5.3 Correlation analysis

This section discusses how the characteristics of the passing vessels and the environmental variables impact the drawdown height. The relations are presented at all three sensor locations. Note that Sensor 1 is located South, closest to the passing vessel, Sensor 3 in the middle and Sensor 2 North, closest to the lock. As explained in the methodology in Section 4.4.2, the statistical dependence between the different parameters is expressed using Spearman's rank correlation coefficient ($\rho$). Furthermore, the mutual dependence between the drawdown height against the drawdown period and slope will be analysed.

### 5.3.1 Drawdown height

Based on the problem analysis in Chapter 2 and the literature study in Chapter 3, several parameters are anticipated to exert influence on the drawdown height, of which the most noteworthy are shown in this section. The remainder is visualized in Appendix J.1. In these figures, the colour scale visualizes the scatter density. One of the parameters expected to influence the magnitude of the drawdown effect is the type of vessel. Two main vessel types are present in the dataset; 'cargo' and 'tanker', of which the 'cargo' type generated the greatest average drawdown height, shown in Figure 5.12.
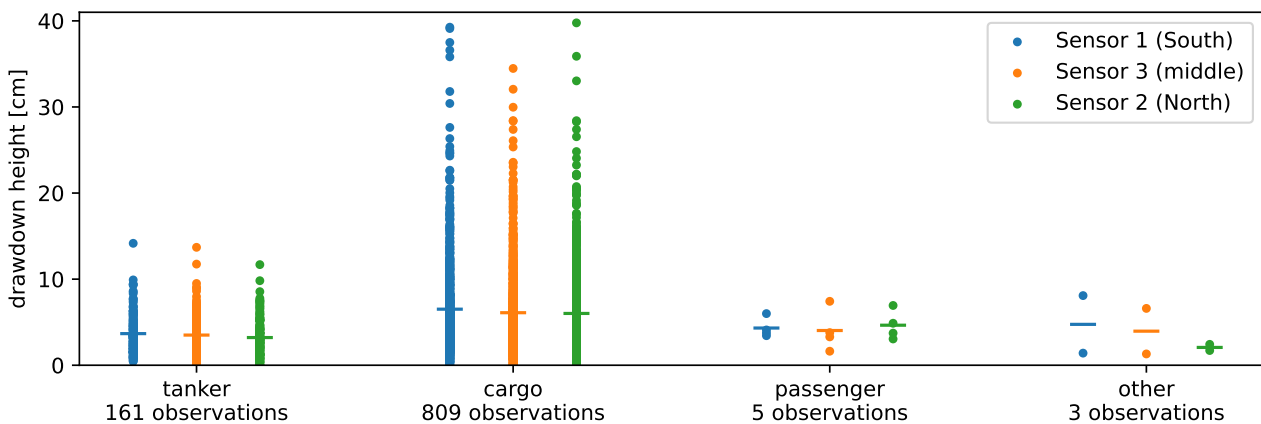


Figure 5.12: Drawdown height versus the different vessel types. The vertical lines indicate the average values.

For all the existing drawdown descriptions in the literature discussed in Section 3.1, the speed through the water ($V_s$) is one of the main parameters influencing the drawdown. A quadratic or higher order relation is expected between $\Delta h$ and $V_s$. When comparing the drawdown height against the calculated speed through the water ($V_s$), Figure 5.13 shows that in general higher speeds tend to increase the drawdown height, although significant variability is observed. The variability indicates that factors beyond vessel speed through the water influence the drawdown height.
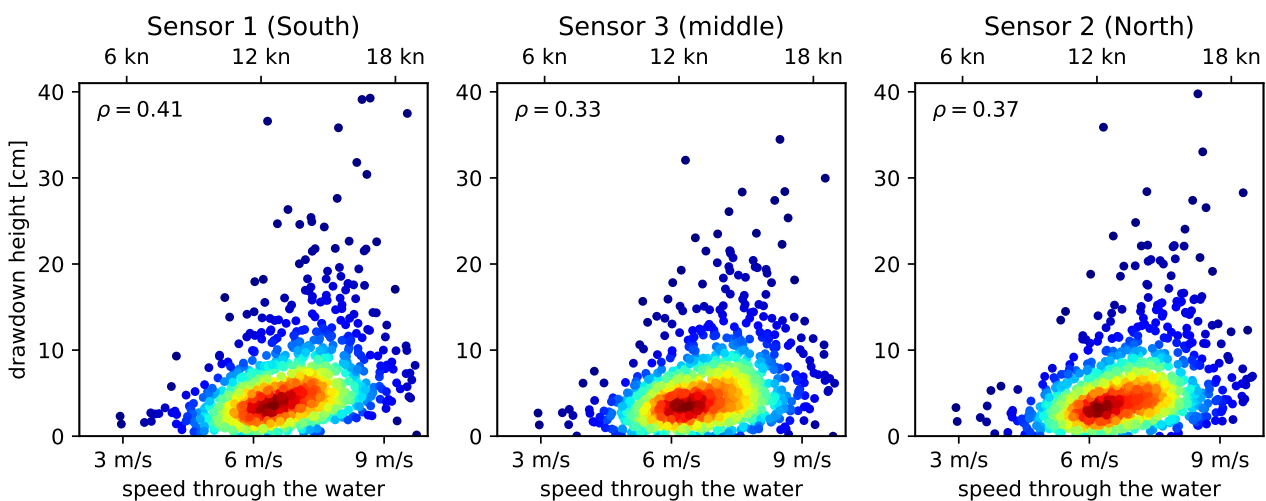


Figure 5.13: Density plot of the drawdown height versus calculated speed through the water for Sensors 1, 3 and 2.

Given that most of the drawdown equations discussed in Section 3.1 are primarily developed for narrow channels, they typically do not account for the distance from the sailing line or passing distance ($d_s$). Nevertheless, in the case of a wider water body such as the Western Scheldt, the impact of the distance is expected to become more pronounced. Figure 5.14 visualizes the relation between the drawdown height ($\Delta h$) and the passing distance relative to the mouth of the harbour ($d_s$). It indicates that the parameters exhibit notable correlation and that the more extreme drawdown events occur with smaller passing distances.
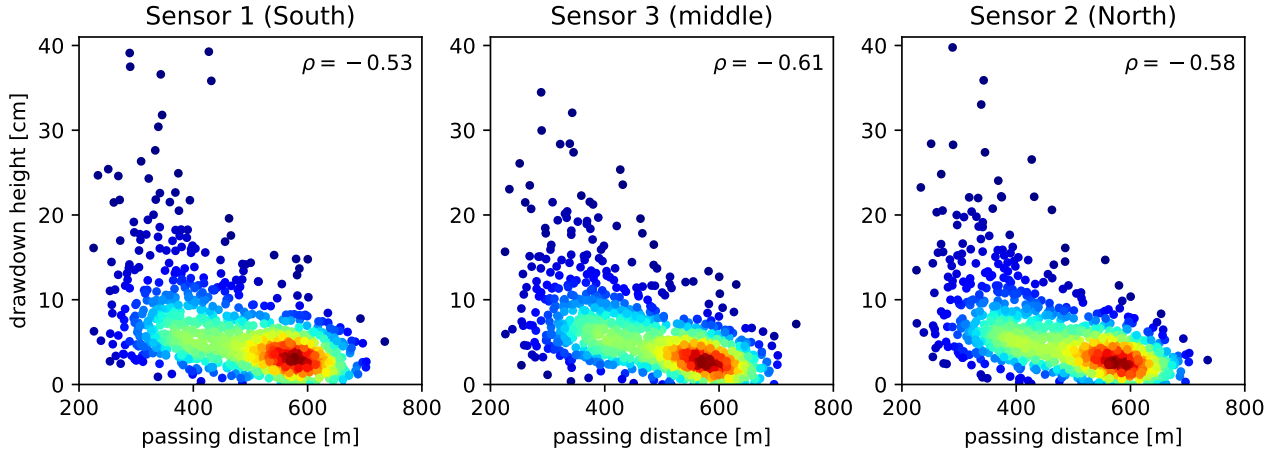


Figure 5.14: Density plot of the drawdown height versus passing distance from the mouth of the harbour ($d_s$) for Sensors 1, 3 and 2.

A relatively significant correlation is noted when comparing the drawdown height against the drift angle relative to the vessel ($\delta_{s,v}$), shown in Figure 5.15. The correlation can be explained by the fact that the drift angle is related to the passing distance, as positive drift angles indicate vessels sailing upstream towards the North Sea and negative drift angles indicate vessels sailing downstream towards Antwerp. The vessels sailing downstream pass the outer harbour at a smaller distance, proven by Figure 5.7. The relationship between the drift angle and the passing distance can be decomposed by analyzing the drift angle based on a stationary coordinate system, as elaborated in Section 4.3.1. When assessing the correlation of the drift angle relative to the outer harbour ($\delta_{s,o}$), the correlation is insignificant, shown in Figure J.8 in Appendix J. This is in line with model tests done by MARIN (2013), which notes that loads experienced due to drawdown at negative drift angles of passing vessels are similar to the loads generated during passages with a drift angle of zero. For this reason, the drift angle is not regarded as one of the primary influential parameters.
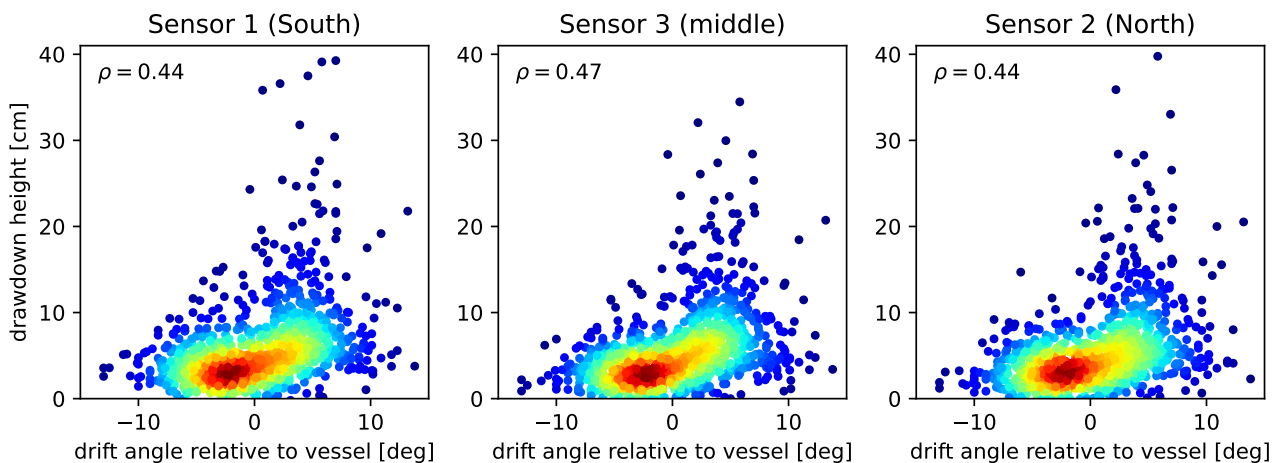


Figure 5.15: Density plot of the drawdown height versus drift angle relative to the vessels coordinate system ($\delta_{s,v}$) for Sensors 1, 3 and 2.

Figure 5.16 compares the drawdown height against the water level (WL), showing minimal correlation. It is noteworthy that the water level does not influence the drawdown height in the outer harbour significantly, although many stakeholders have reported that the problem becomes more pronounced in low-water conditions, described in Section 2.1. As the phenomena itself is not influenced by the water level, the impact it has on the ships in the outer harbour might be intensified during low water conditions. The low correlation is expected, as the existing empirical relations include the water level as part of the wet cross-sectional area of the channel ($A_c$), which remains relatively constant regardless of the water level, thanks to the channel's substantial width and depth.
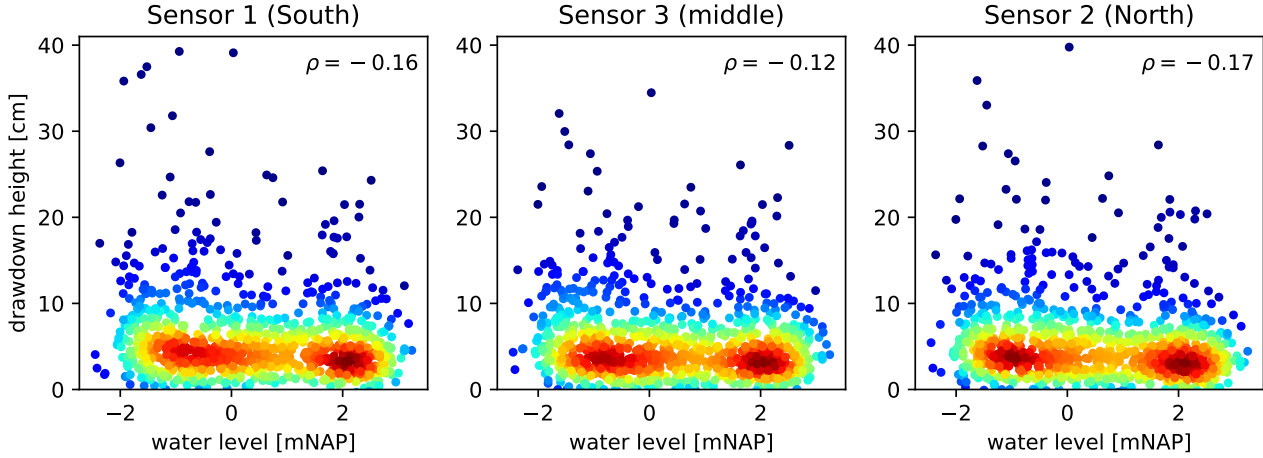


Figure 5.16: Density plot of the drawdown height versus water level (WL) for Sensors 1, 3 and 2.

The remaining comparisons between the drawdown height and parameters of interest are summarized using the Spearman correlation coefficient in Table 5.1 and visualized in Appendix J.1. The table shows that the passing distance, the speed through the water and the dimensions of the vessel are the most influential factors. In the course of the measurement campaign, extreme drawdown events were exclusively observed when there was a combination of high speed through the water and small passing distances. The substantial depth of the channel at the passing location results in a minimal influence of both the depth and the under-keel clearance on the drawdown height. The measurements show no indication that higher windspeeds generate more extreme drawdown heights. Moreover, the drawdown height shows no discernible relation to the current velocity, indicating that the vessels adjust their speed in response to the current velocity, also illustrated in Figure 5.8.

| parameter | symbol | Sensor 1 (South) | Sensor 3 (middle) | Sensor 2 (North) | visualization |
|---|---|---|---|---|---|
| *moderately corollated* | | | | | |
| passing distance | $d_s$ | -0.53 | -0.61 | -0.58 | Figure 5.14 |
| *weakly corollated* | | | | | |
| speed through the water | $V_s$ | 0.41 | 0.33 | 0.37 | Figure 5.13 |
| speed over the ground | SOG | 0.35 | 0.29 | 0.36 | Figure J.1 |
| vessel length | $L_s$ | 0.29 | 0.34 | 0.31 | Figure J.2 |
| vessel width | $B_s$ | 0.27 | 0.32 | 0.27 | Figure J.3 |
| displacement | $\Delta_s$ | 0.26 | 0.32 | 0.26 | Figure J.4 |
| underwater cross-section | $A_s$ | 0.25 | 0.31 | 0.25 | Figure J.5 |
| draught (IVS) | $D_s$ | 0.19 | 0.24 | 0.18 | Figure J.6 |
| *very weakly corollated* | | | | | |
| water level | WL | -0.16 | -0.12 | -0.17 | Figure 5.16 |
| under keel clearance | UKC | -0.13 | -0.13 | -0.10 | Figure J.7 |
| drift angle | $\delta_{s,o}$ | -0.15 | -0.09 | -0.12 | Figure J.8 |
| wind magnitude | $U_w$ | 0.10 | 0.08 | 0.08 | Figure J.9 |
| current magnitude | $U_c$ | -0.08 | -0.09 | -0.05 | Figure J.10 |
| depth | $h_s$ | -0.02 | 0.01 | -0.01 | Figure J.11 |

Table 5.1: The correlation of the vessel characteristics and environmental variables to the drawdown height, expressed using Spearman's correlation coefficient ($\rho$).

### 5.3.2 Drawdown period

Similar to the drawdown height, correlation analysis has been conducted for the drawdown period, described in Appendix J.2. The Spearman correlation values for the drawdown period are generally lower than those for the drawdown height, suggesting a less predictable behaviour of the drawdown period. Further research is required to understand the behaviour of the drawdown period. When examining the relationship between the measured drawdown period and the drawdown height in Figure 5.17, no statistically relevant correlation can be observed between the two parameters.
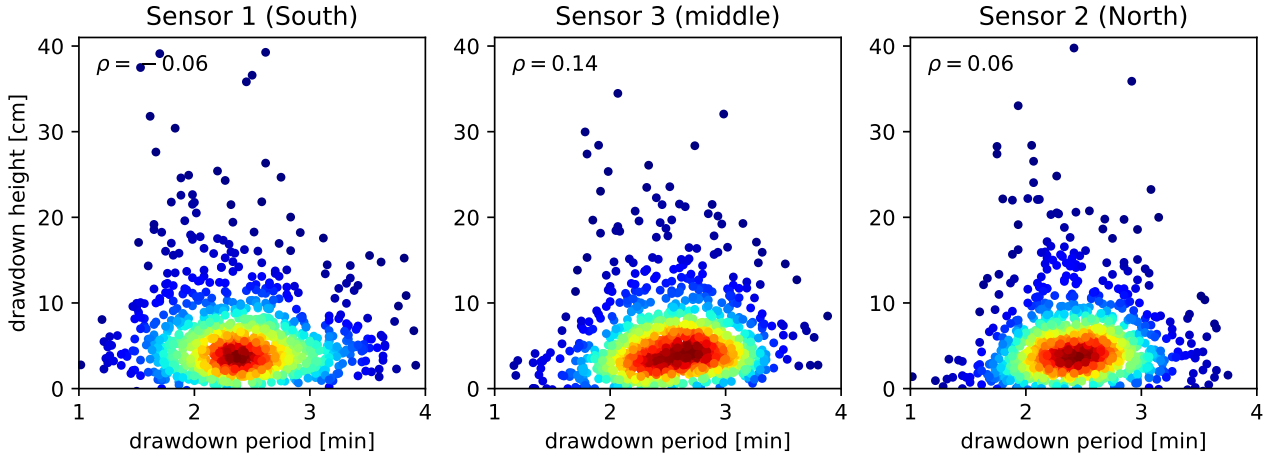


Figure 5.17: Density plot of the drawdown height versus the drawdown period for Sensors 1, 2 and 3.

### 5.3.3 Drawdown slope

In contrast to the drawdown period, the slope in the water level shows a significant correlation with the drawdown height, visualized in Figure 5.18. In this figure, the average drawdown height measured at two sensors is used, as the slope is calculated between these two sensors. Although the drawdown height does not differ significantly at the different measurement locations, the slope in water level does reduce further towards the lock, therefore, the slope of the linear best-fit line differs for the two stretches. Since the water level slope is closely linked to the drawdown height, the parameters introduced in Table 5.1 also exert influence on the water level slope. Figures 5.18 show that the slope in the water level is steeper in the stretch from Sensor 1 to 3 than from Sensor 3 to 2, therefore, for both stretches an expression is written, based on the linear best fit:

$$I_{13} = \frac{1}{282}\Delta h \qquad\qquad I_{32} = \frac{1}{357}\Delta h \tag{5.1}$$

where the slope ($I$) is dimensionless ([m/m]), and the drawdown height ($\Delta h$) is expressed in metres.
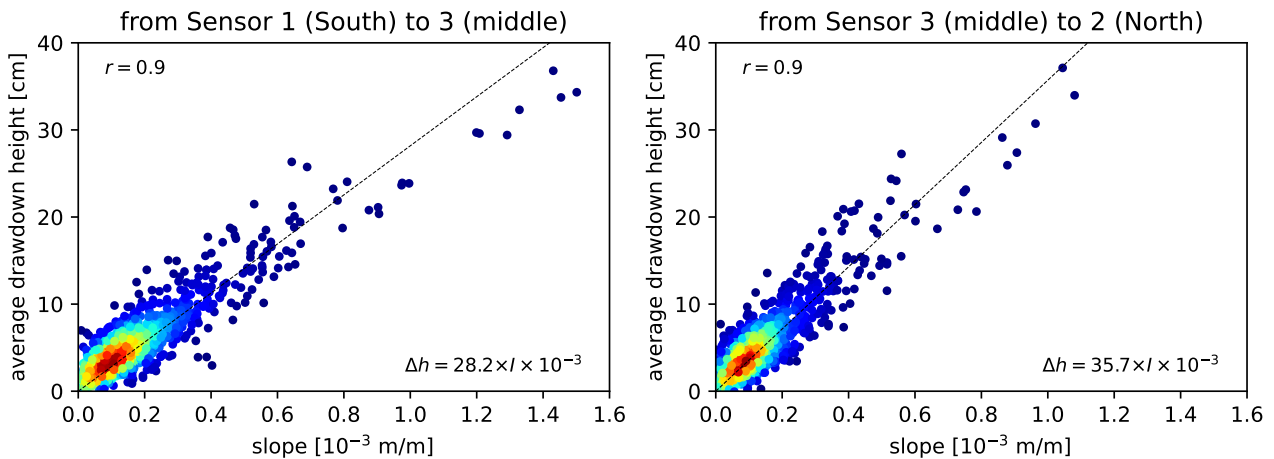


Figure 5.18: Density plot of the drawdown height versus the drawdown slope for Sensors 1, 2 and 3. The linear best fit is plotted as a dotted line.

## 5.4   Conclusion

In this chapter the following sub-question was treated:

---

"How do the different aspects quantifying a vessel passage relate to the observed water motions in the outer harbour of Hansweert?"

---

The main parameter used to describe the water motions in the outer harbour due to the passage of a vessel is the drawdown height. The aspects quantifying a vessel passage which are most influential to the drawdown height are the distance the vessel passes the outer harbour, the speed through the water and the dimensions of the passing vessel, quantified using the Spearman correlation coefficient. In the course of the measurement campaign, extreme drawdown events were exclusively observed when there was a combination of high speed through the water and small passing distances. In general, larger dimensions of a passing vessel also result in a greater drawdown. Aspects showing less correlation with respect to the drawdown height are the water level, the under keel clearance, drift angle, the winds, currents and the depth at the location of the vessel.

A passage involving relatively high vessel speeds, small passing distances or large dimensions reveals distinct patterns in the water motions of the outer harbour. Approximately one minute after the vessel passes, the sensor located closest to the passing vessel detects a sudden drop in water level, followed by similar reductions recorded by the sensor in the middle of the outer harbour and then the sensor closest to the lock after a few seconds. The wave reflects off the northern end of the outer harbour, returning in sequence past the sensors in the opposite direction. The minutes following the passage are characterized by irregular dampening of water movement.

Of the 982 observations, the average drawdown height measured in the outer harbour ranges from 5.5 to 6.0 centimetres, with maximum values reaching up to 40 centimetres. The drawdown period is normally distributed around an average duration of 2.5 minutes. The slope in the water level caused by the drawdown wave decreases as the drawdown wave travels further towards the lock. On average, the slope in the water level during a drawdown event is 1 centimetre per 100 metres, however, extreme observations show slopes up to 15 centimetres for the same distance. The correlation values relating the passage aspects to the drawdown are consistently lower for the drawdown period than those associated with the drawdown height. Furthermore, the observed drawdown height and period do not exhibit mutual influence. On the contrary, the slope in the water level displays a significant correlation with the drawdown height, and can be described as a linear relationship as follows:

$$I_{13} = \frac{1}{282}\Delta h \qquad\qquad I_{32} = \frac{1}{357}\Delta h \tag{5.2}$$

where the slope ($I$) is dimensionless and the drawdown height ($\Delta h$) is expressed in metres.

# Chapter 6: Drawdown Prediction

This chapter aims to set a draw up a critical drawdown level, after which the forces on the inland ships exceed the critical levels and subsequently predict the drawdown phenomena in the outer harbour observed after the passage of a vessel. First, Section 6.1 uses the longitudinal force requirements found in literature and the relation between the drawdown height and slope to determine the critical drawdown height. Subsequently, Section 6.2 uses the existing methods to predict the drawdown height. In Section 6.3, the predictive accuracy is improved, by implementing a new empirical equation for the drawdown height. The method used to determine the criticality is verified by analysing the predicted drawdown slope versus the observed slope and by recalculating the expected drawdown related to known incidents in the outer harbour in Section 6.4. Finally, Section 6.5 discusses the performance of the prediction method and the critical threshold based on the observations made during the measurement campaign.

## 6.1 Critical drawdown height

The key parameter used in literature to describe the drawdown phenomena is the drop in water level, referred to as the drawdown height. This section aims to justify a maximum drawdown height in the outer harbour, ensuring that the resultant forces on all ships within the outer harbour remain below a critical threshold. For this, the longitudinal force criteria introduced in Section 3.2.2 are used. The methodology in Section 4.4.3 explains that by combining Equation 3.8 and 3.11, the longitudinal force criteria (KC) for inland ships can be expressed as a critical slope ($I_{\mathrm{critical}}$) in the water level, shown in Equation 4.16. When the slope in the water level is greater than the critical slope, the force criteria are exceeded. Equations 5.1 relate the water level slope to the drawdown height, therefore, the critical drawdown height can be expressed using the mass criterium:

$$\Delta h_{13}^{\mathrm{crit}} = 282\frac{C_B}{C_m}\mathrm{KC} \qquad\qquad \Delta h_{32}^{\mathrm{crit}} = 357\frac{C_B}{C_m}\mathrm{KC} \qquad\qquad (6.1)$$

where KC is the mass criterium, given as a promillage and $C_B$ and $C_m$ are the block and midship coefficients of the inland ship respectively.

### 6.1.1 Critical drawdown height for individual ships

In Table 6.1 the critical drawdown heights for the different ship classes that can pass through the lock, both on the stretch from Sensor 1 to 3 and from Sensor 3 to 2. For these calculations, it is assumed that $C_B$ is equal to $C_m$ for the inland ships. In practice, $C_B$ is often slightly smaller than $C_m$ for inland ships, reducing the critical drawdown height after which the force criteria are exceeded. The table shows that for the increasing size of the ship, as the force criterium decreases, the critical drawdown height reduces. Furthermore, the critical drawdown height between Sensors 1 and 3 is smaller than the drawdown height between Sensors 3 and 2, as the average slope is steeper between these sensors. The minimum critical drawdown height is observed in the case of a RWS class BII-4 push barge combination, the largest ship allowed to pass the lock chamber, being 20 centimetres. The largest ship allowed to occupy the mooring places is the RWS class M12 ship, requiring a maximum drawdown height of 25 centimetres, after which the longitudinal force criteria are surpassed.

### 6.1.2 Critical drawdown height for multiple ships moored alongside

The minimum critical drawdown height reduces further when considering multiple ships moored alongside each other at the berthing places. The waiting areas allow the mooring of up to three inland ships 135 metres in length side by side with a total combined width of 40 metres (Section 1.2). The most stringent configuration considered is two RWS M12-class ships moored side by side, having a length of 135 metres and a combined width of 34 metres. In this case, the total water displaced is doubled, however, the force criterion considers only one ship as only one ship is moored to the shore. Therefore, in this case, the critical slope and drawdown heights are halved, compared to the case with a single M12-class ship. This sets the critical drawdown height between

| CEMT | MVS | WD [ton] | KC [‰] | force [kN] | $\Delta h_{13}^{\text{crit}}$ [cm] | $\Delta h_{32}^{\text{crit}}$ [cm] |
|------|-----|----------|--------|------------|------|------|
| I | M1 | 437 | 4.07 | 17.4 | 115 | 145 |
| II | M2 | 849 | 2.88 | 24.0 | 81 | 103 |
| | M3 | 1179 | 2.43 | 28.1 | 69 | 87 |
| III | M4 | 1455 | 2.18 | 31.1 | 61 | 78 |
| | M5 | 1694 | 2.01 | 33.4 | 57 | 72 |
| IVa | M6 | 2108 | 1.79 | 37.0 | 50 | 64 |
| | M7 | 2693 | 1.58 | 41.7 | 45 | 56 |
| Va | M8 | 3950 | 1.29 | 50.0 | 36 | 46 |
| | M9 | 4848 | 1.16 | 55.2 | 33 | 41 |
| Vb | BII-2l | 6279 | 1.02 | 62.8 | 29 | 36 |
| | M10 | 5346 | 1.10 | 57.7 | 31 | 39 |
| VIa | M11 | 6901 | 0.97 | 65.7 | 27 | 35 |
| | M12 | 8262 | 0.88 | 71.3 | 25 | 31 |
| VIb | BII-4 | 12558 | 0.71 | 87.5 | **20** | 25 |

Table 6.1: Drawdown height criteria for the different ship classes conform to the RWS classes, based on their longitudinal force criteria as given by Reijmerink (2015), as an expansion on Table 3.2.

Sensors 1 and 3 to 12 centimetres. As this configuration results in the smallest critical drawdown height, this critical level of 12 centimetres will be adopted for the continuation of this research.

## 6.2 Drawdown height prediction through existing methods

As the critical drawdown height is set, the subsequent step involves predicting this drawdown height, such that critical situations can be identified. As elaborated by the methodology laid out in Section 4.4.4, the drawdown height is predicted for every oversized vessel passage in the dataset, using the existing drawdown height definitions introduced in Section 3.1. The descriptions of Schijf and Bhowmik are visualized in this section, and the additional descriptions are visualized in Appendix K. The predicted drawdown height is visually compared with the observed drawdown height, and the predictive capacity of a certain method is quantified using the Pearson correlation coefficient (r) and Mean Absolute Error (MAE).

### 6.2.1 Drawdown height prediction of Schijf

Figure 6.1 shows the observed drawdown height against the predicted drawdown height, calculated using the description of Schijf (1949), given in Section 3.1.1. Despite being entirely analytical, Schijf's method exhibits considerable predictive capabilities. As this method assumes a narrow channel, the predicted drawdown is generally greater than the observed drawdown. In a narrow channel, the lowering of the water level would act more uniform over the cross-section compared to a wider estuary, such as the Western Scheldt. When incorporating a correction factor for the ratio between the vessel's actual and limit speed in the drawdown description, as outlined in Appendix B.1, the degree of overprediction becomes even more pronounced, shown in Figure K.1.

### 6.2.2 Drawdown height prediction of Bhowmik

Figure 6.2 shows the best-statistically-performing prediction method, using the method developed by Bhowmik (1981), worked out in Section 3.1.2. Bhowmik's drawdown height prediction consists of a relatively straightforward equation, including the ratio between the channel and vessel's cross-sectional area and the ratio between the length of the vessel and the passing distance, given in Equation 3.6. While it provides accurate estimates for lower observed drawdowns on average, Bhowmik's method tends to underpredict drawdown heights in more extreme scenarios.

### 6.2.3 Additional drawdown height prediction methods

Table 6.2 gives the r and MAE values for the drawdown descriptions considered, ordered in chronological order. The visualizations corresponding to the drawdown descriptions not treated in the main report are given in Appendix K. The descriptions which include a correction factor ($\alpha_S$), Schijf corrected (Figure K.1) and CIRIA (Figure K.7), overpredict the drawdown height significantly, also shown by their MAE values. Furthermore, the descriptions which include the distance from the sailing line ($d_s$), Gelencser (1977), Bhowmik (1981) and
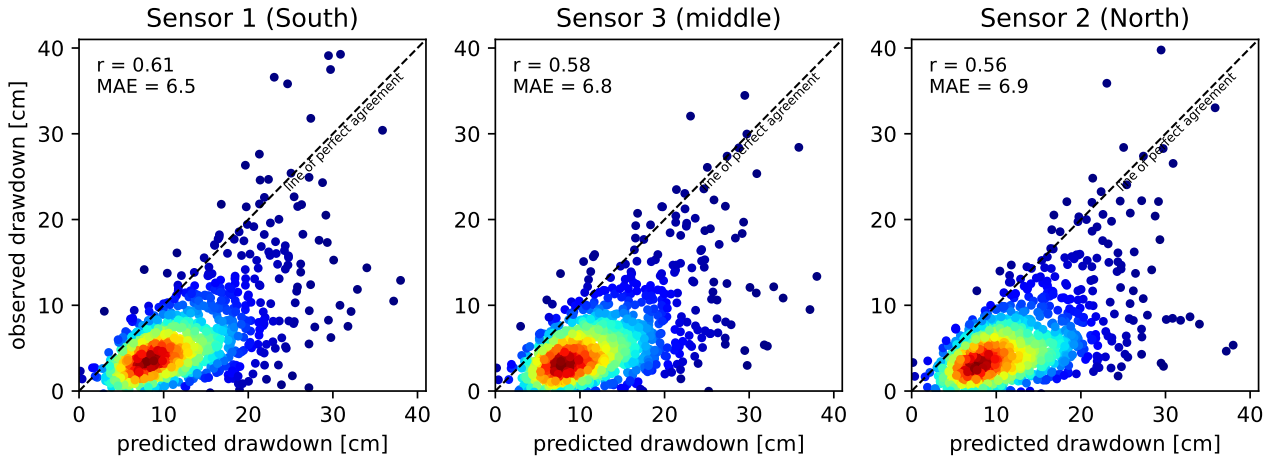
Figure 6.1: The observed drawdown height versus the drawdown height predicted using Schijf (1949).
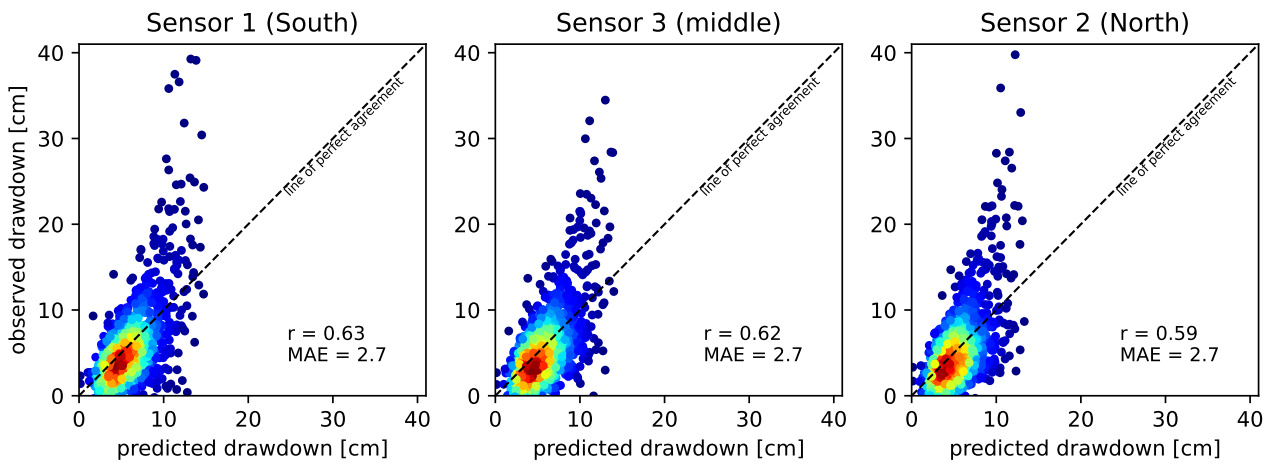


Figure 6.2: The observed drawdown height versus the drawdown height predicted using Bhowmik (1981).

Maynord (1996), do not necessarily predict more accurately than the descriptions without the distance included. Maynord (1996)'s description is most influenced by the passing distance, as at Sensor 1 the drawdown is overpredicted and at Sensor 2 underpredicted, shown in Figure K.5.

## 6.3 Site-specific drawdown height prediction

To improve the predictive accuracy of existing equations presented in Section 6.2, a new semi-empirical equation is derived, based on non-dimensional quantities of the influential parameters. The methodology laid out in Section 4.4.5 explains that by using non-dimensional quantities, it becomes feasible to calibrate an equation with exponents without introducing incorrect units. The dimensionless drawdown height is expressed using the vessel speed ($V_s$) and the gravitational acceleration ($g$).

### 6.3.1 Establishing the non-dimensional quantities

Power relationships, formed by combinations of non-dimensional quantities, are tested for their predictive capabilities. The predictive capabilities of the constructed power relationship are quantified using the regression analysis laid out in the methodology, resulting in a Pearson correlation coefficient. The following combination of quantities yields the highest correlation coefficient: a one-sided blockage factor, defined as $A_s/(d_s h_{\text{channel}})$, the ratio between the length of the vessel and the passing distance ($L_s/d_s$) and an amplification factor related to the depth at the location where the wave is generated and outer harbour ($\sqrt[4]{h_s/h_{\text{harbour}}}$). These quantities capture the main parameters related to the drawdown height, as concluded in Section 5.3.1. Substituting the

| description | Sensor 1 (South) | | Sensor 3 (middle) | | Sensor 2 (North) | | visualization |
|---|---|---|---|---|---|---|---|
| | r | MAE | r | MAE | r | MAE | |
| Schijf (1949) | 0.61 | 6.5 | 0.58 | 6.8 | 0.56 | 6.9 | Figure 6.1 |
| Schijf (1949) corrected | 0.42 | 69.3 | 0.37 | 69.6 | 0.39 | 69.8 | Figure K.1 |
| Hochstein (1967) | 0.59 | 5.4 | 0.58 | 5.6 | 0.56 | 5.7 | Figure K.2 |
| Gelencser (1977) | 0.49 | 10.7 | 0.53 | 8.6 | 0.47 | 7.0 | Figure K.3 |
| Dand and White (1978) | 0.58 | 3.6 | 0.58 | 3.7 | 0.55 | 3.8 | Figure K.4 |
| Bhowmik (1981) | 0.63 | 2.7 | 0.62 | 2.7 | 0.59 | 2.7 | Figure 6.2 |
| Maynord (1996) | 0.59 | 12.1 | 0.66 | 5.6 | 0.59 | 3.9 | Figure K.5 |
| Kriebel (2003) | 0.43 | 19.5 | 0.36 | 19.8 | 0.38 | 20.0 | Figure K.6 |
| CIRIA (2007) | 0.42 | 67.0 | 0.37 | 67.4 | 0.39 | 67.6 | Figure K.7 |

Table 6.2: Overview of the statistical performance of the existing drawdown height descriptions.

quantities into the equation for the non-dimensional drawdown height results in the following expression:

$$\frac{2g\Delta h}{V_s^2} = C_0 \times \left(\frac{A_s}{d_s h_{\text{channel}}}\right)^{C_1} \times \left(\frac{L_s}{d_s}\right)^{C_2} \times \sqrt[4]{\frac{h_s}{h_{\text{harbour}}}} \tag{6.2}$$

### 6.3.2 Calibration

Once the non-dimensional quantities are identified, the regression analysis is revisited to fine-tune the coefficients. This calibration is done by using a random subset containing half of the total dataset, establishing optimum coefficient values for $C_0$, $C_1$ and $C_2$. The constants providing the sufficiently reliable results are 0.58, 0.93 and 0.70 for $C_0$, $C_1$ and $C_2$ respectively, generating the following equation for the drawdown height:

$$\Delta h = 0.58 \frac{V_s^2}{2g} \left(\frac{A_s}{d_s h_{\text{channel}}}\right)^{0.93} \left(\frac{L_s}{d_s}\right)^{0.70} \sqrt[4]{\frac{h_s}{h_{\text{harbour}}}} \tag{6.3}$$

where:

- $\Delta h$: drawdown height [m]
- $V_s$: vessel speed through the water [m/s]
- $g$: gravitational acceleration [m/s$^2$]
- $A_s$: underwater cross-section amidships [m$^2$]
- $d_s$: passing distance from the entrance of the outer harbour [m]
- $h_{\text{channel}}$: generalized channel depth [m]
- $L_s$: length of the vessel [m]
- $h_s$: depth at the vessel location at the time of passage [m]
- $h_{\text{harbour}}$: generalized depth in the outer harbour [m]

The vessel speed through the water ($V_s$) is calculated based on the vessel's speed over the ground and the currents, elaborated in Section 4.3.1. The underwater cross-section amidships ($A_s$) is defined as the width ($B_s$) and the draught ($D_s$) of the vessel multiplied by the midship coefficient ($C_m$), elaborated in Section 4.3.1 as well. The generalized depth of the channel ($h_{\text{channel}}$) and outer harbour ($h_{\text{harbour}}$), are assumed to be relative to a bed level of -23mNAP in the channel and -8mNAP in the outer harbour. Figure 6.3 visualizes the predicted drawdown height against the observed drawdown heights for Sensors 1, 3 and 2, using Equation 6.3.

### 6.3.3 Validation

The other half of the dataset is used for the validation of the equation, shown in Figure 6.4. For both the calibration and validation datasets, the statistical values quantifying the predictive capacity showcase the applicability of the equation. The prediction of some extreme drawdowns, especially those of the calibration dataset measured at Sensor 1, show significant deviations from the observed values. Section 8.2.4 discusses these outliers in further detail.
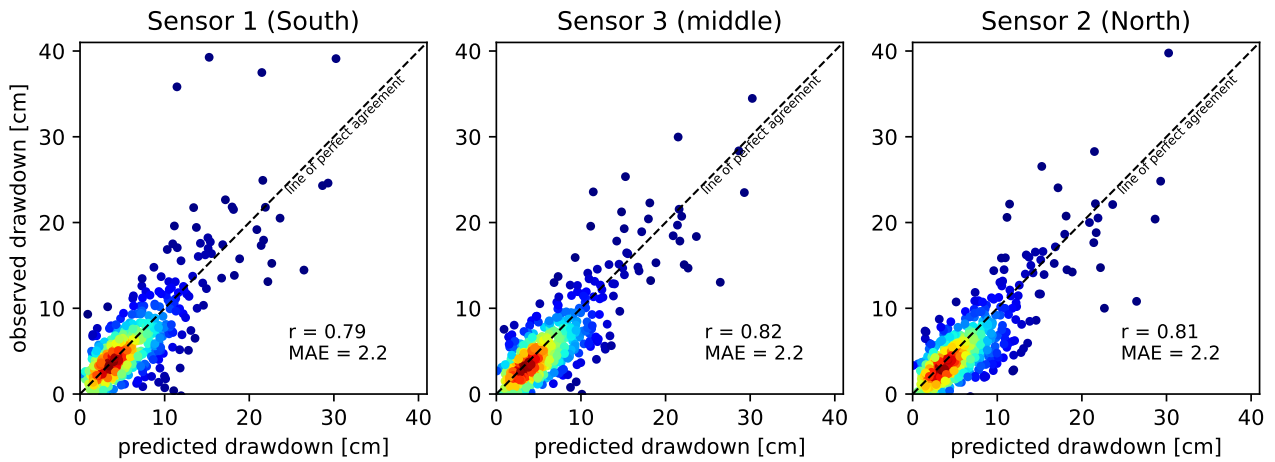
Figure 6.3: The observed drawdown height versus the predicted drawdown height for the calibration dataset.
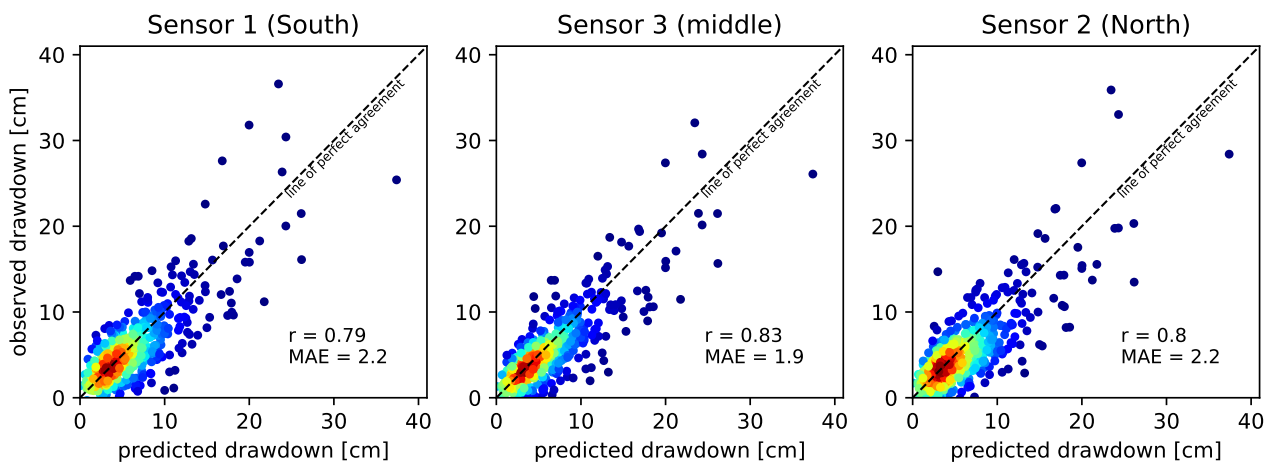


Figure 6.4: The observed drawdown height versus the predicted drawdown height for the validation dataset.

## 6.4 Verification of the method

The method is verified in two ways. First, the predicted slope is compared to the observed slope, as the slope of the water level is used to assess the criticality of a passage. Secondly, the expected drawdown heights that occurred during the known incidents are calculated and held against the criteria.

### 6.4.1 Drawdown slope prediction

The relation between the drawdown height and the slope of the water level is used to draw up a critical drawdown height in Section 6.1. To validate this approach, the relations described by Equations 5.1 and the drawdown height prediction, Equation 6.3, is used to predict the slope of the water level and compare this to the observed slope, of the passages captured during the measurement campaign. Figure 6.5 visualizes the predicted slope using Equation 5.1 and 6.3 against the observed slope on the two stretches. The predictive capability is captured by the Pearson correlation coefficients of 0.76 and a MAE score of 0.1, however, some predictions concerning extremer slopes show significant deviation from the observed values.

### 6.4.2 Drawdown prediction of known incidents

When recalculating the drawdown height that occurred during the incidents introduced in Section 1.2.4, Appendix L shows that in all, except for one case, this critical drawdown height is considerably exceeded. In the case that the criterion was not surpassed, the report states that the incident is attributed to two vessels passing the outer harbour in quick succession. The drawdown wave related to the passage of the second vessel possibly intensified the wave of the initial vessel.
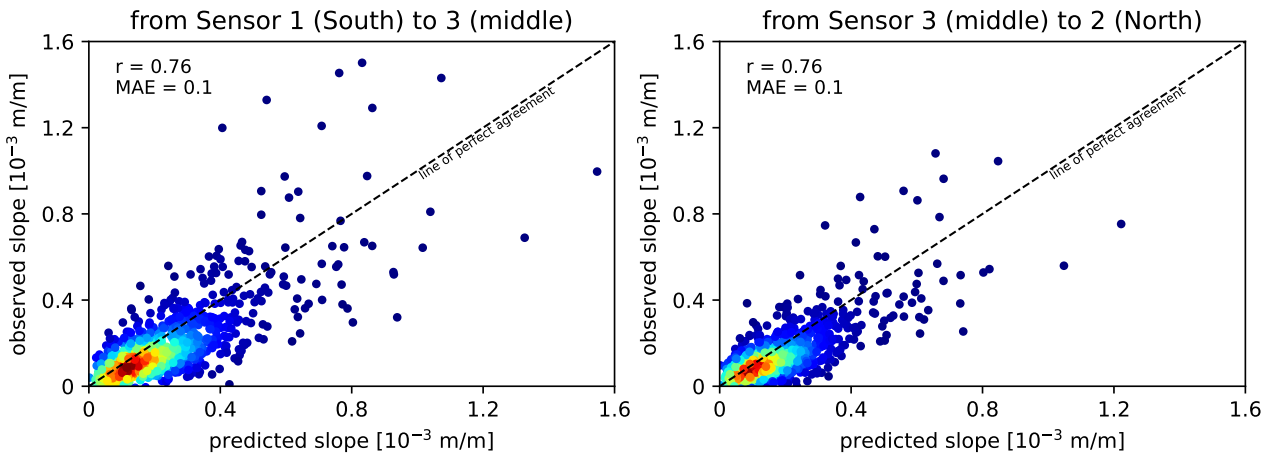
Figure 6.5: The observed drawdown slope versus the predicted drawdown slope.

## 6.5 Prediction reliability

In this chapter, an approach is introduced for determining drawdown height within the outer harbour of Hansweert and a critical drawdown threshold is established, after which force criteria for the inland ships are exceeded. Figure 6.6 shows a scatter plot of the observed drawdown height versus the predicted drawdown height using the site-specific drawdown equation. The vertical and horizontal lines indicate the critical drawdown height of 12 centimetres. Approximately 88 % of the drawdown heights related to the passage during this period are both predicted and observed to fall below the critical limit, coloured green. The red coloured dots indicate the 6% of the observations that are both observed and predicted to be exceeding this limit. The observations that are predicted to fall below the limit, but in reality exceed the limit are plotted in orange, being approximately 2.5% of all passages. Of 3.5% of the passages, the predicted height exceeds the limit although the observed height falls below the limit.
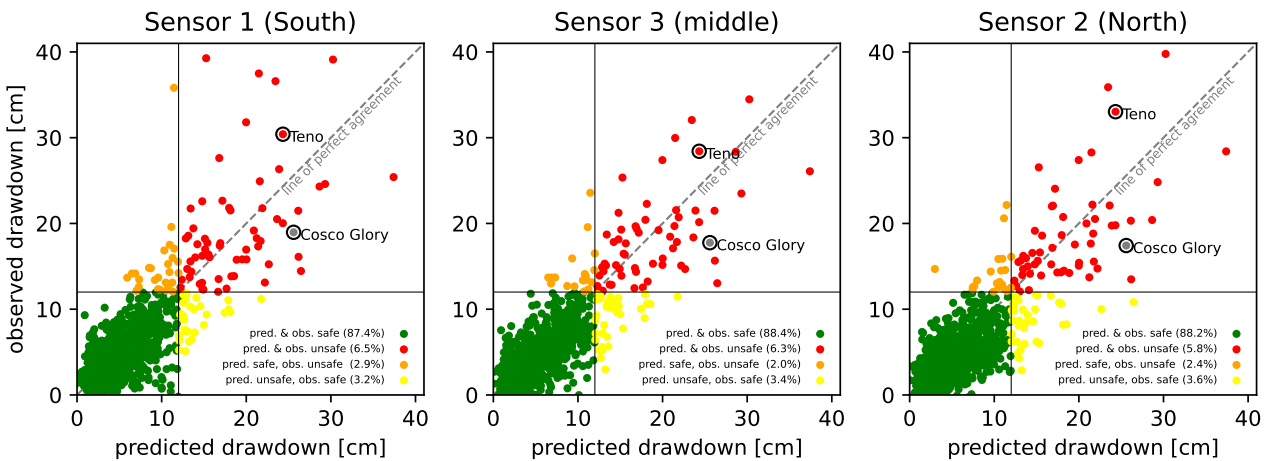


Figure 6.6: The observed drawdown height versus the drawdown height predicted using the site-specific equation for the complete dataset, with the two incidents during the measurement period highlighted.

The observations involving the incidents of the Cosco Glory and Teno are depicted in Figure 6.6, as they occurred during the measurement period. The predicted and observed drawdown heights in both cases surpass the critical level. The data point representing the observation of the Cosco Glory is presented in grey, as this observation was excluded from the analysis due to its classification as unreliable, conforming to the method detailed in Section 4.4.1. The water level fluctuations related to the passages of the Cosco Glory and the Teno are visualized in Figure 5.3 and M.1 respectively. To demonstrate the efficacy of the method used to eliminate unreliable observations, the Pearson correlation coefficient for the entire dataset is computed without any excluded data. The resulting average Pearson correlation coefficient is 0.32, with a MAE of 3.2 centimetres, visualized in Figure M.2. This underscores a notably inferior performance compared to the validation dataset, having an average Pearson correlation coefficient of 0.81, with a MAE of 2.2 centimetres.

## 6.6 Conclusion

In this chapter the following sub-question was treated:

---

"When are the water motions in the outer harbour generated by passing vessels considered unsafe for inland shipping and how can these motions be predicted?"

---

The criticality of the water motions in the outer harbour is based on the longitudinal forces inland ships, generated by the slope in the water level. This inclination of the water level is caused by the translatory drawdown wave related to the vessel's passage and is significantly correlated with the drawdown height. Using the existing longitudinal force requirements and this relation between the slope and the drawdown height, the maximum drawdown height for different types of moored ships or ship combinations is drawn up. The analysis concludes that the most stringent scenario occurs when two RWS M12-class ships are moored alongside, requiring a maximum drawdown height of 12 centimetres, to not surpass the force criteria. When this limit is exceeded, the water motions in the outer harbour generated by passing vessels are considered unsafe for inland shipping.

Analysing existing drawdown height descriptions found in literature, the description by Bhowmik et al. (1981b) proves to be the best-statistically-performing method to predict the drawdown height in the outer harbour. When comparing the observed drawdown height against the predicted drawdown height, this method generates a Pearson correlation coefficient of 0.62 on average for the three measurement locations, and a MAE score of 2.7 centimetres. To predict the drawdown more accurately, a site-specific drawdown height prediction equation is derived:

$$\Delta h = 0.58 \frac{V_s^2}{2g} \left( \frac{A_s}{d_s h_{\text{channel}}} \right)^{0.93} \left( \frac{L_s}{d_s} \right)^{0.70} \sqrt[4]{\frac{h_s}{h_{\text{harbour}}}} \tag{6.4}$$

where $\Delta h$ is the drawdown height [m], $V_s$ is the vessel speed through the water [m/s], $g$ is the gravitational acceleration [m/s$^2$], $A_s$ is the underwater cross-section amidships [m$^2$], $d_s$ it the passing distance from the entrance of the outer harbour [m], $h_{\text{channel}}$ is the generalized channel depth [m], $L_s$ is the length of the vessel [m], $h_s$ is the depth at the vessel location at the time of passage [m] and $h_{\text{harbour}}$ is the generalized depth in the outer harbour [m]. This equation yields an average Pearson correlation coefficient and MAE score of 0.81 and 2.2 centimetres respectively, for both the calibration and validation dataset.

The method is verified by analysing the predicted drawdown slope versus the observed slope and by recalculating the expected drawdown related to known incidents in the outer harbour. The predicted drawdown slope generates an average Pearson correlation coefficient of 0.76 and MAE score of $10^{-4}$ m/m. The calculated drawdown heights that occurred during the recorded incidents exceed the set critical drawdown height, for all but one incident. This incident is attributed to the combined effect of the passage of two vessels in close succession.

# Chapter 7: Mitigation Measures

In this chapter, possible mitigation measures are drawn up to reduce the risk of incidents in the outer harbour and locks of Hansweert due to the passage of vessels in the Western Scheldt, based on the gained knowledge in this research. Additional mitigation measures might exist, such as changes in the layout of the outer harbour, but extend beyond the scope of this research. The recommendations given are divided into two parts; the reduction of the drawdown wave, discussed in Section 7.1, and the enhancement of the resilience against the risks caused by the drawdown, discussed in Section 7.2.

## 7.1 Recommendations to reduce drawdown

Using the gained understanding of the drawdown phenomena in the outer harbour and the factors influencing it, suggestions can be given to limit the expected drawdown height to the critical level of 12 centimetres. In Chapter 5, it is concluded that the distance the passing vessels have from the outer harbour and the speed of these vessels relative to the current velocity are the main parameters influencing the magnitude of the drawdown. Therefore, a restriction based solely on these individual parameters was examined to limit the drawdown height. Appendix N.1 shows that the speed through the water of the passing vessels has to be reduced to 10 knots (5.1 m/s) or the passing distance increased to 600 metres, to limit the drawdown height to the critical level, based on the observations made during the measurement period. Both restrictions are deemed unrealistically stringent and practically unattainable, therefore, a recommendation based on both parameters is formulated.

By reformulating the site-specific equation for the drawdown height (Equation 6.3), a relationship between water speed and passing distance can be established, ensuring that the drawdown height remains below the predefined maximum of 12 centimetres, shown in Appendix N.2. This relationship can be established by specifying the parameters for vessel dimensions and shape ($B_s$, $D_s$, $L_s$, and $C_m$), as well as the water level (WL) and the depth under the vessel ($h_s$) and can be used as a tool to calculate the maximum passing speed. Figure 7.1 illustrates a possible alternative implementation of this relationship, where recommended passing speeds are calculated for three distinct ranges of passing distances. For this example, the passing speeds are calculated using the most extreme vessel dimensions, minimum water level and maximum depth found during the measurement period, thereby representing the most stringent scenario. These ranges are subsequently drawn on the section of the fairway closest to the outer harbour.
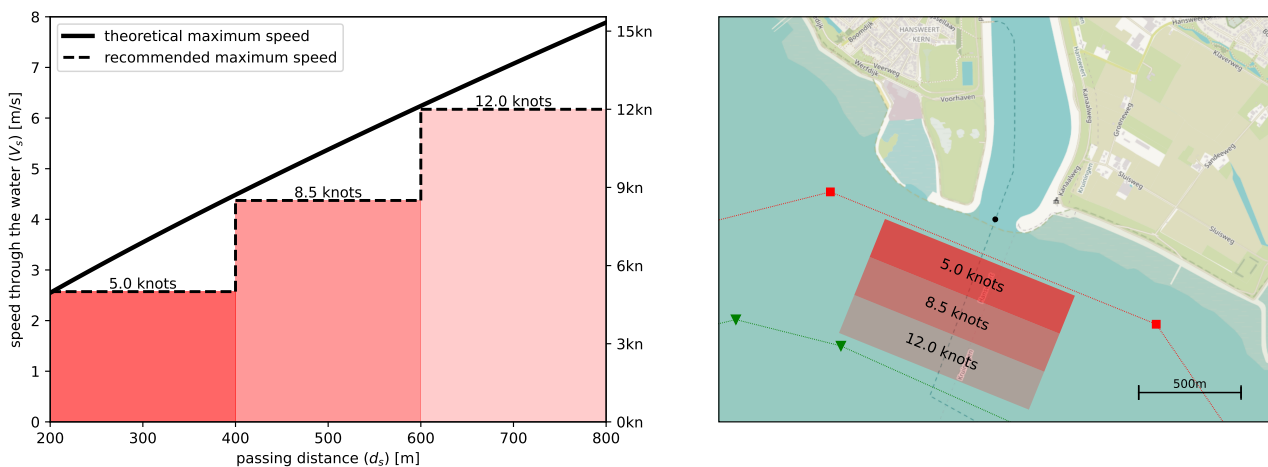


Figure 7.1: Critical passing speed relative to the passing distance required to keep the drawdown height below the set maximum drawdown height. For the calculation of this example, the most extreme parameters are used: $B_s = 65$m, $D_s = 16$m, $L_s = 400$m, $C_m = 0.975$, WL = -2mNAP, $h_s = 26$m and $\Delta h_{\max} = 12$cm.

Using the most stringent recommendation outlined in Figure 7.1, the observations reveal that vessels adhering to this recommended maximum speed have drawdown levels consistently below the established threshold. However, since these measures are derived for the most extreme scenario, the majority of passing vessels' speeds surpassed the recommended maximum, without exceeding the drawdown threshold, shown in Figure N.3. Therefore, it is advisable to calculate the maximum recommended passing speed and distances for each vessel (class) individually to tailor them, based on their dimensions and the water level. Appendix N.2 shows how the recommended maximum speed changes for different vessel dimensions and water levels.

The recommended speed zones shown in the figures could be added as an overlay to the electronic sea charts the pilots used to navigate. By calculating the maximum speeds for the specific vessel and tide in real-time, the resulting speeds are more lenient compared to those introduced in the most extreme case depicted in Figure 7.1. Based on the field research findings (Section 2.1), it is recommended to present these speed limits as guidance to the pilots instead of enforcing a strict speed limit, considering the practical challenges associated with implementing a rigid measure. The calculated recommended maximum speeds tend to become notably high with smaller vessels and increasing passing distances. It is important to note that these recommended speeds only account for the drawdown effect and disregard other practical considerations and traffic navigation safety. This informational provision, combined with multiple awareness campaigns among the pilots, can work towards reducing the drawdown effects below critical levels in the outer harbour of Hansweert.

## 7.2 Recommendations to increase resilience

Besides reducing the drawdown in the outer harbour, recommendations are given to increase the resilience against the drawdown effect in the outer harbour of Hansweert, based on the knowledge gained from the field studies, interviews and the literature review. These recommendations are divided into practical measures concerning the mooring places south of the lock, and measures to reduce the risk during the locking process.

### 7.2.1 Increase of resilience at the mooring places

The forcing on the inland ships is caused by the slope in the water level generated by the drawdown wave, elaborated in Section 3.2.1. Besides the drawdown height, multiple factors influence the magnitude of the force. Having multiple ships moored alongside increases the total water displaced, and thus also the force generated due to the slope in water level. Limiting the maximum combined ship width at the mooring places will increase the allowable drawdown height, conforming to the methodology followed in Section 6.1. This is especially effective for the most southern places, as the slope in the water level (thus generated force) is greater for this section of the outer harbour, shown in Section 5.3.3. The problem analysis revealed that due to the great tidal range at the mooring places, the inland ships often have slack in their mooring lines. The slack in the lines allows the ship to move, potentially building up significant momentum caused by the slope in the water level, posing a risk of mooring line breakage. Installing signage at the mooring places could serve to alert inland shippers about this effect and instruct them to regularly readjust the mooring lines. Another method to minimize the slack in the mooring lines of ships is by using floating bollards, which enables secure mooring without requiring frequent adjustments for the tide.

### 7.2.2 Increase of resilience during the locking process

Reducing the risk during the locking process, in addition to restricting drawdown height, lies in identifying potentially hazardous situations and responding proactively. Identifying potentially hazardous situations can be achieved by employing real-time calculations of the expected drawdown height for the passing vessel, using the site-specific calculation method, given in Section 6.3. When the expected drawdown height surpasses the critical threshold, the personnel at the traffic post and/or at the lock control centre should be notified. This allows them to caution the inland ships or postpone the opening of the chamber doors until the oscillations have reduced. To avoid delays in inland shipping traffic, this occurrence of this postponement should be infrequent. The drawdown predicting method can also be utilized to caution vessels approaching the outer harbour at excessive speeds and to address them accordingly.

## 7.3    Conclusion

In this chapter the following sub-question was treated:

---

"How can the predicted water motions be limited to safe levels and how can resilience against these motions
be enhanced?"

---

The predicted water motions are deemed to remain within safe levels when the critical drawdown height of 12
centimetres is not surpassed. The anticipated drawdown height could be limited by calculating a maximum
speed for specific ranges of passing distances, calculated for the vessel of interest. This measure could be
applied as a calculation tool or as an overlay on the pilot's electronic sea chart. When the vessel adheres to
the recommended speed and distances, the anticipated drawdown height will stay within the predefined critical
height of 12 centimetres. This informational provision, combined with multiple awareness campaigns among
the pilots, works towards reducing the harmful effects.

Resilience against the risk induced by these water motions in the outer harbour can be enhanced by limiting the
maximum combined ship width at the mooring places and addressing issues related to slack in mooring lines
through signage and the use of floating bollards. Notifications of expected critical drawdown heights during the
locking process enable personnel to caution inland ships or delay chamber door openings, and caution passing
vessels approaching the outer harbour at excessive speeds.

# Chapter 8: Discussion

## 8.1  Contextualization

This section aims to contextualize this study within the existing research. The literature study concluded that the existing empirical methods struggle to predict the drawdown in complex bathymetry as they have been mainly derived for narrow and uniform channels. Nevertheless, applying the definitions by Bhowmik et al. (1981a), Schijf (1949) and Dand and White (1978) at the outer harbour of Hansweert reveals some degree of predictive capacity when comparing the predictions to the observations. The developed site-specific equation provides a method to predict the drawdown in the outer harbour with greater accuracy than the existing methods. This equation relates to the approach of Bhowmik, although the blockage factor is adjusted to account for only one side of the fairway. This one-sided blockage factor is not inherently a physical parameter. Its incorporation is justified by its ability to yield a satisfactory fit for the dataset under consideration. Furthermore, an amplification factor was introduced to account for the wave propagation from deeper channel waters to the shallower waters of the outer harbour. This incorporates the assumption that the amplitude of the drawdown wave remains constant after entering the outer harbour. As this equation is tailored to the outer harbour of Hansweert, it cannot be directly applied to other locations. The identification of influential non-dimensional quantities and the calibration process were carried out solely using data from this particular location, as the objective was not to devise a new general equation for the drawdown height. Although the drawdown phenomenon is a well-researched topic, no literature discussing a threshold level was uncovered. To establish the criticality of a drawdown event, a threshold level is calculated based on the longitudinal forces acting on the inland ships in the outer harbour. Even though this threshold is derived based on the site-specific relation between the water level slope and the drawdown height, it can offer a sense of magnitude at other locations.

## 8.2  Limitations

Limitations arise due to constraints in time and resources. This section discusses the main limitations and their potential influence on the results of the research, serving as a critical examination of the study's constraints and boundaries. The limitations are divided across the different sections of the reseach, exploring their potential impact on the conclusions drawn.

### 8.2.1  Problem analysis

In the problem analysis, the insights gathered from interviews with implicated individuals can carry a subjective nature. This is because individuals experiencing adverse effects may tend to exaggerate the actual issues. Increasing the number of interview participants can enhance reliability and mitigate bias. Less significant incidents often tend to remain undocumented, which complicates creating a full overview of the problem, leading to an underestimation of the significance of the problems. The reliability of environmental data in incident reports is questionable, as in the incident report concerning the Cosco Glory on July 10, 2023, (Section 2.2), discrepancies in tidal water level and wind speed are observed when compared to the measurement data (Figure 5.3). Incorrect data could impact the recalculation of drawdown heights during the recorded incidents, done as a verification step in Section 6.4, although already a great share of the data for these calculations is estimated (Appendix L). While these limitations of the problem analysis are unlikely to have altered the conclusion regarding the physical processes of vessel passages contributing to unsafe situations, they may have limited the depth of understanding.

### 8.2.2  Data collection

The collected data, while valuable for the analysis, serves as a limited representation of reality, offering a condensed and filtered perspective on the intricacies of the real world. The data period, 7 weeks during the summer, is not able to capture seasonal or longer scale fluctuations. The current data is only available for

a single location in the river and could deviate from the currents at the vessel's position. Furthermore, the current data are not actual measurements but rather come from a hydrological forecasting model and are thus limited by the limitations of that model. As the speed through the water, as one of the most influential parameters, is calculated using the current data, the uncertainties are carried over into this parameter. AIS data may be unreliable due to a variety of factors, including signal interference, human error by the crew, intentional manipulation and technical malfunctions. While the likelihood of occurrence is minimal, these factors can potentially compromise the accuracy of vessel tracking information. An offset in the transmitted longitude and latitude can result in incorrect speed values and wrongly calculated passing distances. During the measurement campaign, the maximum wind speed was 7 on the Beaufort scale (Section 4.1.5). It is therefore unknown how higher wind speeds would influence the behaviour of the passing vessels. As the Western Scheldt is a morphologically dynamic estuary (Dam et al., 2008), the depth-related calculations may contain errors due to the deviations of the actual bathymetry compared to the bathymetrical dataset. As the water level fluctuation signal undergoes several filtering steps, details are removed, potentially hiding processes at play. These limitations could lead to (small) numerical deviations in the quantification of a vessel passage and may underemphasize certain potential influential aspects.

### 8.2.3 Data analysis

The parameters describing the characteristics of the passing vessel are mostly abstracted at the time the middle of the vessel passes the outer harbour, even though parameters like the under keel clearance of the vessel could be more extreme at a different moment during the passage. Although the drawdown effect observed in the outer harbour is generated over an extended period, this research does not investigate the behaviour of the parameters over time but rather describes them as a single value. Not all parameters that could influence the drawdown process have been considered. Parameters calculated using multiple AIS locations, such as the acceleration of the vessel, deceleration and rate of turn have been excluded from the analysis. Moreover, the analysis does not differentiate between vessels sailing upstream and downstream. The AIS database lacks details regarding the hull shape of the vessels. Consequently, assumptions about the midship and block coefficients are made, relying on the vessel type. Since the dataset predominantly comprises 'cargo' and 'tanker' vessel types (excluding eight observations), many vessels share similar midship and block coefficients. This limitation hinders a thorough investigation into the influence of vessel type. Additionally, the site-specific drawdown equation is calibrated based on highly specific midship coefficients. These limitations may result in the underemphasis of certain aspects of a vessel passage that potentially influence the drawdown wave in the outer harbour. Nevertheless, the aspects taken into consideration in this research are sufficiently representative to predict the drawdown accurately.

The search intervals used to determine the initial maximum, the minimum and the secondary maximum of the drawdown wave are calculated using the expected arrival time of the wave and an offset (elaborated in Appendix G). As the drawdown parameters are calculated using the maximums and minimums located in the search intervals, the fine-tuning of the search interval influences the results. In signal data analysis, determining the accurate timestep corresponding to a maximum or minimum value presents a greater challenge compared to identifying the amplitude associated with these extrema. This difficulty arises due to the inherent nature of signal data, particularly in scenarios involving low amplitudes. When analyzing low amplitudes, the signal-to-noise ratio is typically diminished, resulting in increased uncertainty in the precise timing of signal maxima or minima. Consequently, even slight fluctuations or noise in the signal can lead to inaccurate estimations of the exact timestep at which the maximum or minimum occurs. In contrast, while the amplitude may remain relatively consistent across neighbouring data points, the exact timing of these extremes is susceptible to greater variability. For this reason, the search interval significantly impacts the drawdown period during low-amplitude drawdown events with higher noise levels, while its effect on drawdown height is comparatively minimal. Additionally, timestep values located on the edge of the search boundary due to noise in the signal are directly influenced by the expected arrival time. This inaccuracy in determining the drawdown period could be attributed to the unpredictable behaviour of the period as quantified by its low correlation coefficients (in Section 5.3.2). For this reason, the drawdown period is not used in further calculation steps.

As observations are considered unreliable if the difference between the maximum and minimum water level 10 minutes before the passage is greater than 10cm (Section 4.4.1), observations which fall inside of the criteria could still be unreliable and the water level fluctuations could not be correlated to the passing vessel. Additionally, alternative hydrodynamic processes, unrelated to a passing vessel, may be present in the signal even after the filtering steps, potentially influencing the observations. Secondary processes such as these contribute to the variability observed in the data, introducing complexity to the understanding of how different aspects quantifying a vessel passage relate to the observed physical processes.

### 8.2.4 Drawdown prediction

The critical drawdown height is calculated using the longitudinal force requirements given in existing guidelines. These non-binding criteria are applied for the forces on the ships at the mooring places, although they were originally designed for ships in lock chambers. Given the longer duration of stay at mooring places compared to the lock chambers, the ships are expected to be moored more securely at the mooring places, allowing for greater longitudinal forces and consequently increasing the allowable drawdown height. In the method provided, the force resulting from the drawdown is related to the pressure difference on the ship caused by the slope in the water level (Section 3.2.1). In addition to the pressure difference, currents can exert a force on the ship, although it is not considered in this analysis. The relationship between the drawdown height and the slope is modelled using a linear assumption, adding additional uncertainty that could potentially impact the determination of the critical drawdown height. The effective distance the wave travels between the sensors is based on the assumed path of the wave crest. As the slope in water level is calculated by dividing the water level difference by the effective distance between two sensors (Section 4.3.2), deviations in the effective distances could lead to different slopes in water level. Variations in the water level slopes could, in turn, contribute to discrepancies in the calculated magnitude of the longitudinal force on inland ships, consequently affecting the critical drawdown heights. The effective distance physically cannot fluctuate extensively, thus the potential impact on the critical drawdown height is limited. Given the inherent uncertainty in the determination of the threshold, it is tested against all known incidents (Section 6.4), confirming its effectiveness.

Given that the measurements are conducted solely in the outer harbour, it remains uncertain how the drawdown height would change upon entering the lock chamber. Furthermore, in this method, no conclusions on the effects of multiple vessels close to each other or passing each other at the outer harbour can given. The measurements show that the effects can both be amplified or reduced. As mentioned in the validation of the site-specific drawdown height equation (Section 6.4), certain instances of extreme drawdown events stand out. Especially at Sensor 1, the predicted drawdown is significantly less than the actual observed drawdown, shown by the observations marked red in Figure 8.1. In these cases, the secondary wave (which determines the drawdown height, see Section 4.3.2) is significantly higher than the primary wave, especially at the sensor located closest to the vessel, shown by the visualizations of the water level fluctuations in Appendix O. Although it is challenging to fully explain the hydrodynamics occurring during these passages, the phenomenon could be associated with low water levels, as the tide was low during all these passages. Despite these outliers, the site-specific drawdown height equation remains a reliable method for prediction, as it accurately forecasts the majority of drawdown events. Even though there may be discrepancies in the predicted magnitude of the drawdown height, these outliers are typically correctly identified as critical for the inland ships in the outer harbour.
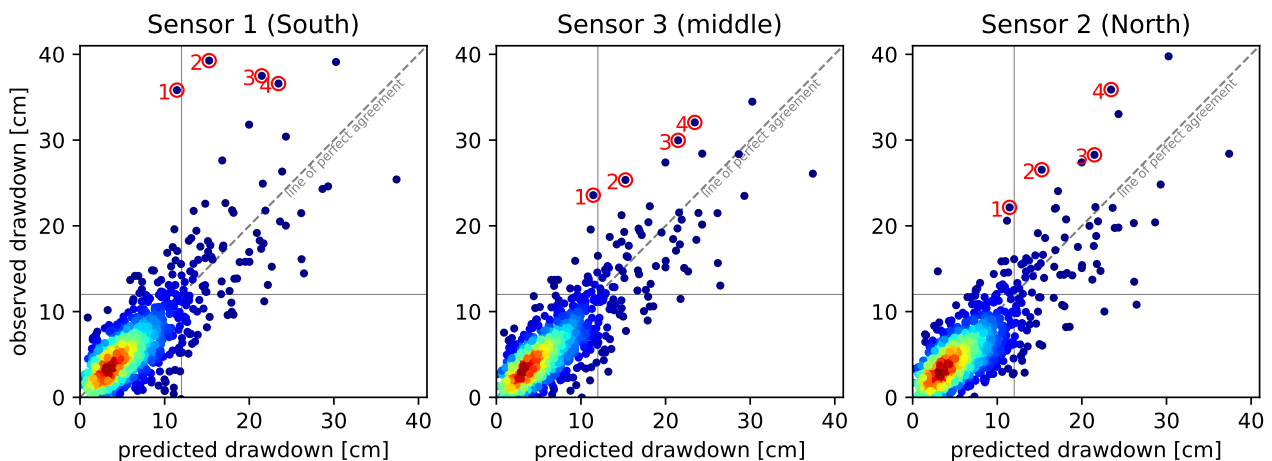


Figure 8.1: Density plot of the observed drawdown height versus the drawdown height predicted using the site-specific equation for the complete dataset. The outliers discussed are marked in red.

# Chapter 9: Conclusion and Recommendations

## 9.1 Conclusion

This research aims to gain an understanding of the hydrodynamic interactions between the passing vessels in the Western Scheldt and the ships in the outer harbour and lock at Hansweert, such that measures can be recommend to proactively prevent future incidents from taking place. The subquestions introduced in the introduction are answered in the conclusion sections of the corresponding chapters. The main research question is as follows:

---

"How do the water motions induced by passing vessels in the Western Scheldt contribute to unsafe situations in the outer harbour and locks of Hansweert, and what preventative measures can be identified to effectively minimize incidents and mitigate risks?"

---

A comprehensive investigation into the water motions induced by passing vessels in the Western Scheldt reveals that the water displaced by the passing vessels is the leading phenomenon contributing to unsafe situations and incidents in the outer harbour and locks of Hansweert. This phenomenon, caused by the primary water motion of the passing vessel, is observed as a translatory drawdown wave travelling into the harbour, reflecting against the lock and oscillating back and forth in the outer harbour until fully dampened. The related effects are experienced as a sudden lowering of the water level and suction forces. The average measured lowering of the water level, referred to as the drawdown height, after the passage of an oversized vessel approximates 6 centimetres, with maximum values up to 40 centimetres. The inclination of the water level, inherent to this drawdown wave, generates a pressure difference along the inland ships, which translates into longitudinal forces on the ships in the outer harbour and locks. These forces can lead to the breakage of mooring lines and the uncontrolled movements of the ships, resulting in a range of safety hazards and operational disruptions. Several documented incidents, field studies and interviews highlight the urgent need for effective measures to mitigate the harmful effects of passing vessels and enhance the safety of navigation in the area.

The main factors influencing the drawdown height are the passing distance relative to the outer harbour, the speed through the water and the dimensions of the vessel, shown by a correlation analysis between the parameters that describe the passage and the drawdown. A critical drawdown height of 12 centimetres is set, based on existing force criteria and the linear relation between the drawdown height and water level slope. When this limit is exceeded, the water motions in the outer harbour generated by passing vessels are considered unsafe for the inland ships. Efforts have been made to predict the drawdown height using existing descriptions. To improve upon the statistically best-performing method, a site-specific drawdown height prediction equation is created.

Preventative measures are identified to minimize incidents and mitigate the risks related to the water motions induced by passing vessels. These measures both focus on limiting the predicted water motions to safe levels and enhancing the resilience against these motions. The predicted water motions are considered within safe limits if the drawdown height remains below 12 centimetres. The anticipated drawdown height could be limited to this threshold by recommending a maximum speed related to specific ranges of passing distances, calculated with the site-specific equation for the vessel of interest. This measure could be applied as a calculation tool or as an overlay on the pilot's electronic sea chart. The resilience against drawdown-induced risks could be strengthened by restricting the maximum combined width of ships moored alongside. Furthermore, by limiting the excessive slack in the lines of the moored ships, through signage and floating bollards, the allowable movements of the ships could be further restricted, reducing the risk of line breakage. Notifications of anticipated critical drawdowns would allow traffic controllers or lock operators to caution the inland ships and delay the lock chamber door openings, whilst alerting the passing vessel. Incorporating these mitigation measures could positively impact the safety of navigation in the Hansweert outer harbour and locks.

## 9.2 Recommendations

This section provides recommendations for further research. The initial set of recommendations focuses on the outer harbour at Hansweert. Subsequently, recommendations are provided for the entirety of the Western Scheldt. Finally, considerations are offered for the broader research field encompassing ship waves.

It is recommended to develop a numerical model of the outer harbour at Hansweert and the related part of the Western Scheld, simulating the hydrodynamics during the passage of a vessel. As this research uses measurements at solely three locations in the outer harbour, a hydrodynamic model could provide insights into the spatial distribution of water motions and localized effects. Software such as XBeach could be used, which is a numerical model allowing for the simulation of ship waves from the ship to the shore (Almström et al., 2021; Jong et al., 2013). Dempwolff et al. (2022b) mention additional models such as HIVEL2D, BOSZ and FUNWAVE-TVD. Using the data captured during the more than 1000 vessel passages collected for this research, such a numerical model could be calibrated and validated with this data. This model could potentially offer a more comprehensive understanding of the intricate water motions at play, including scenarios not considered in the dataset used for this research. This understanding would provide the ability to more accurately predict extreme conditions within the outer harbour, surpassing the limitations of the current approach. Additionally, mitigation measures considering a change in the spatial configuration (for example the orientation of the mooring places or the orientation of the harbour entrance) could be explored, by evaluating how the drawdown wave would be influenced by the spatial change. Alternatively, the prediction accuracy of the drawdown in the outer harbour could be enhanced by developing a neural network using the gathered data on vessel passages and drawdown observations. This approach could provide additional insights into the relationships between different parameters and potentially improve the predictive capabilities.

A numerical model could also be applied to model the response of the inland ships in the outer harbour to the hydrodynamic forcings, in terms of mooring line forces or movements (Nam and Park, 2018). An example of such a model is Quaysim, a time domain moored ship motions model (Terblanche and Van der Molen, 2013). Dobrochinski et al. (2023) mention additional models such as AnySim, Orcaflex, Moses, Ansys AQWA and Ariana which could fit this purpose. Given the current method's reliance on a force approximation tied to the water level slope, a deeper understanding of how passing vessels influence forces on inland ships will lead to the design of more precise mitigation measures. High-frequency water level fluctuation measurements in the lock chambers at Hansweert could enhance the understanding of the transition of the drawdown wave from the outer harbour into the lock chamber, without the need for a numerical model. This understanding would allow for more accurate mitigation measures to reduce the risks during the locking process. Practically, these measurements could be used to write a relation between the expected drawdown height in the outer harbour and the drawdown in the lock chambers, as an amplification factor. Alternatively, these measurements could be used to calibrate a hydrodynamic model of the outer harbour and lock chambers.

Finally, it is recommended to extend the scope of the study to include measurements at alternative locations along the Western Scheldt where problems related to the water displacement of vessels occur, such as (outer) harbours at Terneuzen and Walsoorden. This will provide a broader perspective on the problems, allowing for the identification of common trends and region-specific considerations. Understanding the problems related to drawdown over the full Western Scheldt trajectory provides the opportunity to draw up a general drawdown risk mitigation strategy covering the whole estuary. Measurements at Hansweert and alternative locations along the Western Scheldt or other rivers could provide an opportunity to form a new general drawdown height description for wide rivers. Drawdown descriptions in literature are predominantly constructed with the consideration of relatively narrow channels. A newly formed description in which the passing distance is a key parameter, which is calibrated and validated using measurements taken at a set of locations, could be applied at locations along wider rivers and estuaries, for which no measurements can be taken.

# Bibliography

Almström, B., Roelvink, D., and Larson, M. (2021). Predicting ship waves in sheltered waterways–an application of xbeach to the stockholm archipelago, sweden. *Coastal Engineering*, 170:104026.

Almström, B. and Larson, M. (2020). Measurements and Analysis of Primary Ship Waves in the Stockholm Archipelago, Sweden. *Journal of Marine Science and Engineering*, 8(10).

Almström, B., Roelvink, D., and Larson, M. (2021). Predicting ship waves in sheltered waterways – An application of XBeach to the Stockholm Archipelago, Sweden. *Coastal Engineering*, 170:104026.

Baur, T., Peters, K., and Teschke, U. (2009). Practical analysis methodology for ship-induced waves in estuaties. In *Coastal Engineering 2008: (In 5 Volumes)*, pages 748–760. World Scientific.

Bhowmik, N. G., Demissie, M., and Guo, C. Y. (1981a). Waves and Drawdown Generated by River Traffic on the Illinois and Mississippi Rivers. Technical report, University of Illinois Water Resources Center, Champaign, USA.

Bhowmik, N. G., Soong, T. W., Reichelt, W., and Bogner, W. C. (1981b). Waves Generated by Recreational Traffic on the Upper Mississippi River System. Technical report, Illinois State Water Survey.

Bosboom, J. and Stive, M. J. (2021). *Coastal dynamics*. TU Delft Open.

Bretschneider, C. L. (1952). The generation and decay of wind waves in deep water. *Eos, Transactions American Geophysical Union*, 33(3):381–389.

Butterworth, S. (1930). On the theory of filter amplifiers. *Experimental wireless and the wireless engineer*, 7:536–541.

Centre for Maritime Law (2020). Fluvius Kft v Ooms Tanktransporten BV. `https://cmlcmidatabase.org/fluvius-kft-v-ooms-tanktransporten-bv`. Online; accessed 12-December-2023.

CIRIA (2007). *The Rock Manual. The use of rock in hydraulic engineering (2nd edition)*. C683, CIRIA, Londen, United Kingdom.

Court of Appeal in The Hague (2023). Aanvaring in de sluis van Hansweert tussen twee binnenvaartschepen waarvan een de sluisdeur raakt, kort nadat een zeeschip de sluis passeerde op de Westerschelde. `http://deeplink.rechtspraak.nl/uitspraak?id=ECLI:NL:GHDHA:2023:530`. Online; accessed 7-June-2023.

Dam, G., Bliek, A., Labeur, R., Ides, S., and Plancke, Y. (2008). Long term process-based morphological model of the western scheldt estuary.

Dam, K. T., Tanimoto, K., Nguyen, B. T., and Akagawa, Y. (2006). Numerical study of propagation of ship waves on a sloping coast. *Ocean Engineering*, 33(3-4):350–364.

Dand, I. W. and White, W. K. (1978). Design of navigation canels. *Proceedings of the Symposium on Aspects of Navigability of Constraint Waterways Including Harbour Entrances*, 2(3). Delft, the Netherlands.

David, C. G., Roeber, V., Goseberg, N., and Schlurmann, T. (2017). Generation and propagation of ship-borne waves - Solutions from a Boussinesq-type model. *Coastal Engineering*, 127:170–187.

Delft Hydraulics (1953). Verschijnselen bij de vaart van een of twee schepen in een kanaal. Technical report, Waterloopkundig Laboratorium Delft, the Netherlands.

Dempwolff, L., Melling, G., Windt, C., Lojek, O., Martin, T., Holzwarth, I., Bihs, H., and Goseberg, N. (2022a). Loads and effects of ship-generated, drawdown waves in confined waterways - A review of current knowledge and methods. *Journal of Coastal and Hydraulic Structures*, 2(13).

Dempwolff, L.-C., Windt, C., Melling, G., Martin, T., Bihs, H., Holzwarth, I., and Goseberg, N. (2022b). The influence of the hull representation for modelling of primary ship waves with a shallow-water equation solver. *Ocean Engineering*, 266:113163.

Dobrochinski, J. P., van Deyzen, A., Zijlema, M., and van der Hout, A. (2023). Combining numerical tools to determine wave forces on moored ships. *Coastal Engineering*, 179:104224.

Erasmus UPT (2021). Havenmonitor 2021- De economische betekenis van Nederlandse zeehavens. Technical report, Erasmus University Rotterdam.

Floyd, G. F. (1969). Gravimeter filters. *Geophysics*, 34(6):968–973.

Gabel, F., Lorenz, S., and Stoll, S. (2017). Effects of ship-induced waves on aquatic ecosystems. *Science of The Total Environment*, 601-602:926–939.

Gates, E. D. and Herbich, J. (1977). Mathematical model to predict behavior of deep-draft vessels in restricted waterways. Technical report, Texas A & M University, College Station, Texas. US Army Corps of Engineers Report No. 200.

Gelencser, G. J. (1977). Drawdown surge and slope protection, experimental results. Technical report, PIANC. Proceedings of the 24th International Navigation Congress, Leningrad.

Gemeenschappelijke Nautische Autoriteit Scheldegebied (2019). Bekendmaking aan de Scheepsvaart ScheldeGebied - Aanduiding bovenmaats zeeschepen. `https://www.vts-scheldt.net/Alsic.Web.FileStorage.ashx?fileID=fdd844dc-af7c-4096-a25d-a1a150d3e2ba`. Online; accessed 21-September-2023.

Gemeenschappelijke Nautische Autoriteit Scheldegebied (2020). Overzicht incidenten 2020-2022.

Gemeenschappelijke Nautische Autoriteit Scheldegebied (2022). Gezamelijke verklaring 01-2022: Overlast/schade ontstaan door zuiging of golfslag na passage van grote (container)schepen. `https://www.vts-scheldt.net/default.aspx?path=Over%20ons/Beleid/CNVS_nl&KL=en`. Online; accessed 29-June-2023.

Geolux (2022). LX-80 10 Hz Oceanographic Radar Sensor. `https://www.geolux-radars.com//lx-80-ocean`. Online; accessed 2-October-2023.

Geolux (2023). *LX-80-15 10 Hz Oceanographic Radar Sensor User Manual v2.4.1*. Samobor, Croatia.

Guo, Z., Zhong, L., Wang, K., and Jiang, Z. (2022). Nonlinear air dynamics of a surface effect ship in small-amplitude waves. *Journal of Ocean Engineering and Science*.

Hochstein, A. (1967). *Navigation Use of Industrial Canals; Water Transportation*. Moscow Publishing House.

Holthuijsen, L. H. (2007). *Waves in Oceanic and Coastal Waters*. Cambridge University Press.

Huisman, B., Schroevers, M., van der Wal, M., and Terwindt, J. (2011). Measuring ship induced waves and currents on a tidal flat in the Western Scheldt estuary. Technical report, Deltares and Nortek.

IMO (2015). Revised Guidelines for the Onboard Operational Use of the Shipborne Automatic Identification System (AIS). Technical report, International Maritime Organization.

ING (2022). A Kaleidoscopic View of the Future of the Rhine-Scheldt Delta Port System. Technical report, ING Belgium.

Janssen, P. and Schijf, J. (1953). Rapport XVIIIth International Navigation Congress PIANC. *PIANC 18th congress 1953, Rome*, pages 175–196.

Jong, D., Roelvink, D., Reijmerink, S., and Breederveld, C. (2013). Numerical modelling of passing-ship effects in complex geometries and on shallow water. In *Smart Rivers. Conference. Liege (BE), Maastricht (NL)*, pages 23–27.

Kriebel, D., Seelig, W., and Judge, C. (2003). Development of a unified description of ship-generated waves. *Proceedings of the U.S. Section PIANC Annual Meeting, Roundtable, and Technical Workshops (CD-ROM)*, PIANC USA.

M-info (2021). Passing vessel blamed 100% for collision caused in locks by the suction effect of the water. `https://www.m-info.org/post/passing-vessel-blamed-100-for-collision-caused-in-locks-by-the-suction-effect-of-the-water`. Online; accessed 12-December-2023.

Marchand, M. (2006). Flood risk analysis for the river scheldt estuary. Technical report, FLOODsite.

MARIN (2013). Research on Passing Effects on Moored Ships, ROPES JIP, WP3 modeltests performed by MARIN . Technical report, MARIN, 6700 AA Wageningen, The Netherlands. Report No. 23920-5-BT.

Marin (2020). Analyse gebruik tijdpoorten op de Westerschelde. Report nr. 31852-1-MO-rev.2.

Maynord, S. (1996). Return Velocity and Drawdown in Navigable Waterways; Technical Report HL-96-7. Technical report, US Army Corps of Engineers.

Muga, B. J. and Fang, S. J. (1975). Passing ship effects-from theory and experiment. In *Offshore Technology Conference*, pages OTC–2368. OTC.

Nam, B. and Park, J. (2018). Numerical simulation for a passing ship and a moored barge alongside quay. *International Journal of Naval Architecture and Ocean Engineering*, 10(5):566–582.

NBB (2022). Economic importance of the Belgian maritime and inland ports – Report 2020. Technical report, National Bank of Belgium.

North Sea Port (2018). North Sea Port: A merger between Zeeland Seaports and Port of Ghent. `https://www.inlandports.eu/media/2018.03.27%20North%20Sea%20Port%20Flyer.pdf`. Online; accessed 4-September-2023.

Papanikolaou, A. (2014). *Selection of Main Dimensions and Calculation of Basic Ship Design Values*, pages 69–292. Springer Netherlands, Dordrecht.

PIANC (1995). Criteria for Movements of Moored Ships in Harbours. Technical report, Permanent International Association of Navigation Congresses (PIANC). Report of Working Group no. 24 of the Permanent Technical Committee II.

PIANC (2015). Ship Behaviour in Locks and Lock Approaches. Technical report, Permanent International Association of Navigation Congresses (PIANC). Report N 155 - Inland Navigation Commission.

PIANC (2023). Criteria for Acceptable Movements of Ships at Berths. Technical report, Permanent International Association of Navigation Congresses (PIANC). Report of MarCom Working Group Report N 212 – 2023.

Pinkster, J. A. (2004). The influence of a free surface on passing ship effects. *International Shipbuilding Progress*, 51(4):313–338.

Port of Antwerp-Bruges (2023a). Cijferboekje 2023 Feiten en Cijfers. `https://media.portofantwerpbruges.com/m/cbd0a8ac5e5a4ab/original/BROCHURE_Cijferboekje-2023_NL.pdf`. Online; accessed 8-August-2023.

Port of Antwerp-Bruges (2023b). Port of Antwerp-Bruges stabiel in 2022. `https://newsroom.portofantwerpbruges.com/port-of-antwerp-bruges-stabiel-in-2022#`. Online; accessed 7-June-2023.

Prat, D. (2011). Container ship on open ocean [photograph]. `https://www.istockphoto.com/nl/foto/container-ship-on-open-ocean-gm117145443-15637959?clarity=false`.

Puertos del Estado (2007). ROM 3.1-99: Recommendations for the Design of the Maritime Configuration of Ports, Approach Channels and Harbour Basins. Technical report, Puertos del Estado.

Reijmerink, B. (2015). Revisie en uitbreiding krachtcriteria voor binnenvaartschepen in schutsluizen. Technical report, Deltaris.

Rijkswaterstaat (2000). Handboek Schutsluizen (2 delen). Technical report, Bouwdienst Rijkswaterstaat.

Rijkswaterstaat (2010). Richtlijnen Vaarwegen 2011. Technical report, Rijkswaterstaat, Dienst Verkeer en Scheepvaart.

Rijkswaterstaat (2021). Achtergrondrapportage Vaarwegen Integrale Mobiliteitsanalyse 2021. Technical report, Rijkswaterstaat Water Verkeer en Leefomgeving (WVL).

Rijkswaterstaat (2022). Overzicht hinderlijke waterbeweging veroorzaakt door ander schip.

Rijkswaterstaat (2023). Vaarwegen in Nederland. Technical report, Rijkswaterstaat Centrale Informatievoorziening (CIV).

RWS (2023). Vaarweg informatie sluizencomplex hansweert. `https://www.vaarweginformatie.nl/frp/main/#/geo/map?viewport=51.443630;3.987372;51.457497;4.042304&layers=HARBOUR&layers=BERTH&term=`. Online; accessed 23-August-2023.

Sanger, C. and Norton, H. (1915). England's guarantee to belgium and luxemburg, with the full text of the treaties. *New York: Charles Scribner's Sons*.

Schijf, J. (1949). Protection of embankments and bed in inland and maritime waters, and in overflows or weirs. *PIANC 17th congress 1949, Lisbon*, pages 61–78.

Schouten, M. (2023). Ligplaatsen voor de binnenvaart, een toenemend tekort? onderzoek naar de huidige en toekomstige ligplaatsenbehoefte in de corridor midden-zeeland. Technical report, Rijkswaterstaat Zee en Delta.

Schuttevaer (2023). Welk schip is schuldig aan aanvaring in sluis Hansweert? `https://www.schuttevaer.nl/nieuws/actueel/2023/04/07/welk-schip-is-schuldig-aan-aanvaring-in-sluis-hansweert`. Online; accessed 12-December-2023.

Sedgwick, P. (2014). Spearman's rank correlation coefficient. *BMJ: British Medical Journal*, 349:g7327.

Sorensen, R. (1997). Prediction of vessel-generated waves with reference to vessels common to the Upper Mississippi River system. Technical report, US Army Corps of Engineers, St. Louis, USA.

Stockstill, R. L. and Berger, R. C. (2001). Simulating barge drawdown and currents in channel and backwater areas. *Journal of waterway, port, coastal, and ocean engineering*, 127(5):290–298.

Sverdrup, H. U. and Munk, W. H. (1947). Wind, sea, and swell: theory of relations for forecasting. Technical report, U.S. Hydrographic Office.

Swiegers, P. B. (2011). Calculation of the forces on a moored ship due to a passing container ship. Master's thesis.

Taylor, D., Hall, K., and MacDonald, N. (2007). Investigations into ship induced hydrodynamics and scour in confined shipping channels. *Journal of Coastal Research*, pages 491–496.

Terblanche, L. and Van der Molen, W. (2013). Numerical modelling of long waves and moored ship motions. *Coasts and Ports 2013*, pages 757–762.

Thomson, W. (1887). On ship waves: Proceedings of the institution of mechanical engineers. *Proceedings of the Institution of Mechanical Engineers*, 38(1):409–434.

TNO (2007). Golfhinder: Een relatie tussen bewegingen en hinder op afgemeerde schepen. Technical report, TNO Defensie en Veiligheid.

Van Koningsveld, M., Verheij, H., Taneja, P., and De Vriend, H. (2023). *Ports and Waterways: Navigating the changing world*. Delft University of Technology, Hydraulic engineering, Ports and Waterways, Delft, The Netherlands.

Vrijburcht, A. (1994). Troskrachtcriteria van schutsluizen, rapport Q1443. Technical report, WL — Delft Hydraulics.

VTS-Scheldt (2021). Scheepsvaart in Zeeland 2005, 2006, 2007, 2008, 2009, 2010, 2011, 2012, 2013, 2014, 2015, 2016, 2017, 2018, 2019, 2020 and 2021. `https://www.vts-scheldt.net/default.aspx?path=Nautische%20info/download&KL=en`. Online; accessed 27-June-2023.

Wallwey, C. and Kajfez, R. L. (2023). Quantitative research artifacts as qualitative data collection techniques in a mixed methods research study. *Methods in Psychology*, 8:100115.

Wärtsilä (2023). Coefficients of form. `https://www.wartsila.com/encyclopedia/term/coefficients-of-form`. Online; accessed 15-December-2023.

# List of Figures

# List of Tables

# Acronyms

**AIS** Automatic Identification System. 17, 19, 21–23, 26, 27, 30, 51, 61, 64, 91, 94, 95, 99

**BET** The Joint Flemish-Dutch Management and Exploitation Team (BET) managing the systems of the Scheldt Radar Chain (SRK). 4, 59

**BL** Bed Level relative to NAP. 23, 99

**CEMT** Conférence Européenne des Ministres de Transport. 2, 16, 59, 72, 75

**CEST** Central European Summer Time (UTC+02:00). 20, 21, 85, 87, 88, 90

**COG** Course Over Ground in degrees North. 19, 24, 26, 91

**IVS** Information system of the Joint Nautical Authority of the Scheldt area. 21, 23, 37, 61, 62, 95, 99, 100, 105, 107, 109

**MAE** Mean Absolute Error. ii, 27, 41, 43–46

**MMSI** Maritime Mobile Service Identity. 19, 22, 91, 99

**NAP** Normaal Amsterdams Peil (Amsterdam Ordnance Datum). 9, 10, 18, 23, 26, 28, 31, 32, 43, 47, 60, 62, 63, 89, 96, 99, 116, 117, 119–122

**RWS** Rijkswaterstaat. 16, 40, 46

**SOG** Speed Over Ground in knots. 19, 24, 37, 62, 91, 103, 107

**TEU** Twenty-foot Equivalent Unit. 1, 4

**TH** True Heading in degrees North. 19, 24, 91, 94, 99

**UKC** Under Keel Clearance. 23, 26, 37, 99, 107

**ULCV** Ultra Large Container Vessel. 4, 9

**UTC** Universal Time Coordinated. 21, 91

**WD** Mass of water displaced by a ship. 16, 41

**WL** Water Level relative to NAP. 23, 26, 37, 47, 60, 62, 63, 96, 99, 119, 120

# Appendix A: Field study and interview reports

## A.1   Site visit RWS Goes, Hansweert lock and traffic post

On the 14th of June, 2023 a site visit was conducted to the Rijkswaterstaat office in Goes, to the Hansweert lock complex and the Hansweert marine traffic post.

### A.1.1   Meeting Rijkswaterstaat

The meeting was attended by myself (Dick Heijboer), Richard Amersfoort, Christian Hoek, Manon Everts and Matthijs Schouten. In the meeting, Matthijs explained the motivation for the research. The investigation was initiated after an incident on the 20th of April, 2022, when the mooring lines broke of a waiting ship due to the passage of a seagoing vessel. Besides this event, multiple incidents are recorded (and not recorded) at the waiting areas and in the lock chamber. This ensures that the captains of the inland vessels are reluctant to utilize the waiting areas in the outer harbour of Hansweert lock. Together with the already existing shortage of waiting places, this is an increasing problem. Besides the outer harbour of the Hansweert lock, similar problems occur at the Terneuzen lock and smaller (recreational) ports in the Western Scheldt area.

To investigate this process, it is proposed that three oceanographic radar sensors (type LX-80-15 10Hz) are used to measure the wave height in the outer harbour, at the locations shown in Figure A.1. Furthermore, the already existing wave height sensor in the lock chamber can be used, however, currently, it does not store any data. Measurements are expected to start at the end of June 2023 and will cover a period of 4 weeks. A longer period is not possible as the mooring piles to which the sensors will be connected are expected to undergo maintenance in August 2023. (As maintenance got delayed, measurements were ultimately taken for 7 weeks.)



Figure A.1: Proposed sensor locations.

Several comments were made regarding the measurements. As the sensors will be connected to the pylons at the waiting area, the wave height data will be influenced by the presence of moored ships. Ships in front of the sensor will have a sheltering effect, potentially reducing the wave height. Therefore, it will be important to know the presence of ships during the measurement campaign. Furthermore, the side of the pylon to which the sensor is connected can influence the wave height, as the pylon itself can have a sheltering effect.

It was explained that the main processes causing the breaking of the mooring lines are expected to be the sudden drop in water level elevation, the suction currents towards the ship's propellers and the sudden increase of water level after the passage of an oversized vessel. This water level depression wave and the subsequent water level elevation wave might take up to 2 minutes to reach the lock chambers. As the water level depression reaches the lock gates first and reflects on the lock complex, the depression and elevation wave are expected to meet somewhere in the middle of the outer harbour. An extreme scenario could be if two large vessels pass each other close to the outer harbour, such that the corresponding waves amplify.

Highlighted was the effect of the tidal level and tidal currents on these processes. Furthermore, it was recommended to take wind data into the analysis, as vessels with a large surface area need to increase their speed during strong cross-winds, to prevent an extreme drift angle.

### A.1.2 Visit Hansweert traffic post

A spontaneous visit was conducted to the Hansweert traffic post, the location is shown in Figure A.1. The Hansweert traffic post coordinates the junction between the South outer harbour and the Western Scheldt. The exit into the Western Scheldt and the entry into the South outer port of the lock can be challenging due to the relatively narrow gap, the high tidal (up to 4.5 knots) and the traffic intensity. The crew on duty at the post were aware of the problems at the outer harbour and noted that not only the oversized seagoing vessels were responsible for the occasional breaking of mooring lines but also the smaller ships generating significant wave action in the outer harbour. Furthermore, they explained that in order to keep the correct amount of tension in the mooring lines, the mooring lines of the waiting inland ships at the outer harbour should be readjusted at regular intervals for the changing water level due to the tide. Often the crew allows for more slack in the lines, which reduces the times the mooring lines have to be readjusted. However, more slack makes them more prone to failing in case of high waves or suction currents, as the slack lines allow for more movement of the ship.

During the site visit, multiple aerial pictures were taken using a drone. Figure A.2 shows the passing of MSC Vandya, with a length of 366 metres and a breadth of 48 metres. No significant water level fluctuations were visible in the outer harbour during the passing of this vessel.



Figure A.2: Aerial picture of the MSC Vandya passing the outer harbour of the Hansweert lock.

## A.2 Site visit Terneuzen lock and traffic post and Hansweert lock

On the 11th of July, 2023 a site visit was conducted to the Terneuzen traffic post and lock complex and the Hansweert outer harbour.

### A.2.1 Terneuzen traffic post and lock complex

Myself (Dick Heijboer) and Matthijs Schouten (Rijkswaterstaat) visited the Terneuzen traffic post to gain an understanding of the traffic system and learn about the impacts of increasingly larger vessels sailing through the Western Scheldt. At the Terneuzen traffic post, the locks are operated and the intersecting marine traffic of the Western Scheldt and the outer harbour of the Terneuzen locks is managed, Figure A.3. The crew on duty at the traffic post recognized the issues occurring at the Hansweert lock and stated that during specific circumstances the water level in the outer harbour of the inland shipping lock at Terneuzen could drop to almost a metre after the passage of an oversized vessel. They noted that this often had to do with the speed of the vessel and the moment in the tidal cycle. Broken mooring lines or waves overtopping the low-lying inland barges were not uncommon. They mentioned that most pilots of the oversized vessels are well aware of the issues and slow down accordingly at the critical points along the Western Scheldt in order to prevent problems due to their wave action and suction. Furthermore, a visit was made to the construction site of the new lock chamber at Terneuzen, allowing larger seagoing vessels into the Dutch and Belgium hinterland and reducing the waiting times.



Figure A.3: Map of the Terneuzen lock complex.

The passages of the HMM Helsinki (length 400m, width 61m, reported draught 13.4m and the MSC Michel Cappellini (length 399m, width 61m) were observed during high tide at the outer harbour of the Terneuzen Inland locks. Even though the currents caused by these vessels were visible, no significant lowering of the water level was observed. Later, at the falling tide, the MSC Domitille (length 299m, width 49m, reported draught 11.3m) passed Terneuzen, and significant secondary waves were seen (Figure A.4), however, the effects of the primary wave was minimal.

Figure A.4: Secondary waves caused by the MSC Domitille observed at Terneuzen.

### A.2.2 Outer harbour Hansweert lock

Furthermore, a second visit to the project site at Hansweert was made to inspect the measurement devices (Figure A.5) and to observe the passage of the MSC Rayshmi (length 328m, width 48m). No significant primary waves were observed, although the secondary wave pattern was visible.



Figure A.5: Radar measurement device installed in the outer harbour of the Hansweert lock.

## A.3   Interview with Ghent–Terneuzen Canal pilots

On the 4th of September, 2023, an online interview was organized to discuss the effects of passing seagoing vessels experienced by inland navigation skippers and pilots on the Ghent-Terneuzen Canal. The meeting was attended by myself (Dick Heijboer) and Erik de Ruijter, Christan Hoek, Manon Evers and Matthijs Schouten on behalf of Rijkswaterstaat and two pilots. The inland skippers invited to the meeting were unable to attend. The area of operation for the pilots present at the meeting primarily involves piloting seagoing vessels along the Western Scheldt, through the locks at Terneuzen towards Ghent. Similar to Hansweert, issues are being experienced at Terneuzen due to passing seagoing traffic. Vessels up to 265 metres in length, 37 metres in width and with a draught of 12.5 metres are permitted in the Ghent-Terneuzen Canal (North Sea Port, 2018).

After Matthijs introduced the research, the pilots explained that the effect of passing seagoing vessels with non-adjusted speed is very noticeable whilst entering or exiting the lock chambers at Terneuzen. They were very clear in pointing out that not the waves were the issue for them but the water displacement and the ship-ship interactions. They reported a suction force on the vessel pulling the vessel out of the lock chamber after the passage of a large seagoing vessel and pushing it back in again, resulting in an oscillating motion. If the ship is only partially secured in the lock and the southern lock gate is still open, the drop in water level can be more than half a metre, resulting in occasions when a mooring line breaks due to the movement out of the lock chamber. Therefore, it is important for them, when approaching the lock, to not only look forward but also backward to see if there is a vessel passing by, and to be able to anticipate. This can be done by giving the engine ahead or using a tug to compensate for the force out of the lock. In a rough estimate, they approximated that more than once every month, mooring lines of seagoing vessels break in the lock at Terneuzen due to passing vessels. Even though the pilots report these incidents, most of the time they are not documented. The pilots stated that the passing seagoing vessels towards Antwerp are sometimes unaware of what the effects of their primary wave are in the western outer harbour at Terneuzen. Not only in the lock but also in the turning basin in the outer harbour, the effects are felt, as a passing vessel could result in a strange turning force. The problems seem to have increased but the pilots are unsure whether this is because of the increased speed or size of the passing vessels, the change in layout of the outer harbour at Terneuzen or a combination of these.

Even though the primary wave effects are greater with low tide, the impact on the ship they were piloting remained the same. This is because the ships they sail during low tide are mostly empty, thus a lower mass and less affected by the suction forces. During high tide, the ships they sail have greater draught due to the payload and a more affected by the suction forces. They also mentioned that the impact is felt more on a larger vessel. This, combined with the reduced margins in the lock chamber makes the pilotage of larger vessels into the chamber more challenging and risky. When asked about what characteristics of the passing vessel influence their primary wave the most, they mentioned speed through the water, draught, under-keel clearance, water displacement and passing distance. The type of vessel did not seem to make a noticeable difference for them although they expect the blockage factor to be an important parameter as well.

As a solution, they would not propose a speed limit in the critical passages along the Western Scheldt as this would be difficult to enforce and probably undesirable for all parties. However, more awareness among the pilots sailing to and from Antwerp, and attention from the traffic service regarding these processes so that it can alert fellow waterway users, could significantly reduce this problem.

*Return to Section 2.1.*

## A.4   Site visit Hansweert lock control centre

On the 8th of September, 2023, a site visit was conducted to the Hansweert lock complex. Myself (Dick Heijboer) and Matthijs Schouten (Rijkswaterstaat) visited the control room to investigate the impacts of passing seagoing vessels on the ships in the outer harbour and in the lock. From the control room, the filling and emptying processes of the two chambers are controlled and the waiting places at the South and North sides of the lock are managed.

When asked about the effects of the large passing vessels in the Western Scheldt, the crew at duty explained that at low tide the water level could drop up to 80 centimetres in the chambers, but at half or high tide, no significant effects were visible. They explained that inexperienced skippers, when entering the chamber, would increase the power to battle against the outflowing currents due to the suction of the passing vessel. However, when the current reversed, they would suddenly gain speed unexpectedly and risk collision. Furthermore, they explained that not only the outflowing currents but also the reduced under-keel clearance decreases the effectiveness of the ship's propellor. The lowering of the water level would reach the lock when the passing ship was approximately 4 or 5 ship lengths away after passing. To anticipate for this effect, the operators would wait with the opening of the southern lock gate door until the effects of the passing ship would have reduced to a safe level. They also indicated that the length, draught and especially speed are of influence on the suction the passing vessel generates. When asked about the secondary waves of the passing vessels, they were very clear to point out that those were not the cause of problems for the outer harbour of Hansweert.

As the crew also manages the waiting places, they explained that places on the North side of the lock are more popular than the ones on the South side. Multiple reasons could be identified; the tide is less on the North side, the waves due to the weather are less and there are no effects due to the passing vessels in the Western Scheldt. On the South side, especially when there are multiple ships moored aside, the suction due to the passing of a vessel could result in the breakage of the mooring lines. Often the lines of the ship closest to the shore would be the ones that break as those take the highest load. A part of the problem could also be that the mooring lines used on the inland ships are not always up to standard and the lines are given too much slag, allowing the ship to move. Most skippers are very aware of these effects and usually use extra mooring lines to secure their ship, especially if they stay there for the weekend. On the other hand, it also happens that mooring lines break due to the passage of larger inland ships through the lock.
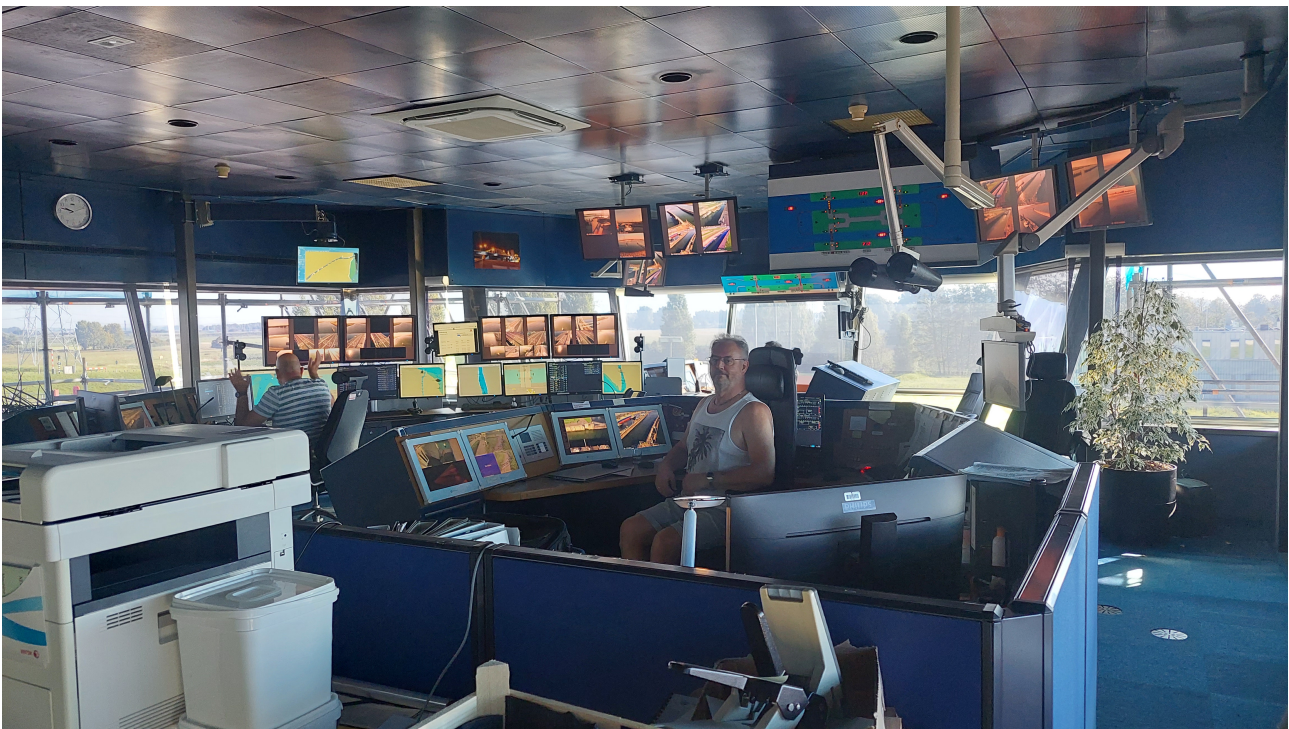


Figure A.6: Control room of the Hansweert lock complex.

## A.5   Interview with inland skipper

On the 8th of September, 2023, an interview was conducted with a skipper of an inland tanker who is well-acquainted with the locks at Hansweert and Terneuzen. Every week, his ship makes the trip between Sluiskil and Germany and back, passing the locks at Hansweert and Terneuzen twice, one time loaded and one time empty. His ship is a CEMT IVa class tanker with a length of 85 metres a width of 9.5 metres and a loaded weight of 2250 tons.

The skipper explained that the water level drop in the lock chamber can be significant when a large vessel passes, due to the suction caused by the vessel. This causes the ship to initially move out of the chamber, but when the water returns it results in an oscillating movement, back and forth, typically four or five times. When the ship is already (partially) moored, this creates high tensions in the ropes. Sometimes the water level would drop up to half a metre, resulting in a high-risk situation where deckhands have to lie down to protect themselves from snapping mooring lines. The skipper emphasizes the seriousness of this problem by stating that a fatal accident is imminent unless the situation improves. A water level drop of 20 to 30 centimetres would still result in the ship having to give engine ahead and astern to compensate for the oscillating movement. A 10-centimetre drop is manageable. He explained that the capacity of the lock chambers has been reduced to anticipate this back-and-forth movement, such that the ships in the chambers do not collide. These problems occur especially at low tide, both at Hansweert and at Terneuzen and have been going on for the last five to ten years. The magnitude of the drop in water level depends on the ship's draft, the depth, the hull shape, and especially the speed. The skipper claims that there might be pressure on the pilots and captains to sail their vessels at excessively high speeds, in order to meet their deadlines or planned times of arrival. Furthermore, some vessels with significant draught have to keep their speed to catch the tide, as their tidal window could be very limited. When asked if it could be the case that ships need to maintain high speed to navigate the turn in order to maintain sufficient pressure on the rudder, he believed that this could not be the case, as higher speed does not necessarily mean better navigation ability. Under normal weather conditions, it should be possible to execute the turn without causing disturbance for the surrounding marine traffic. The majority of pilots are neat and correct individuals, he elaborates, although there are a few who may come across as arrogant and may not be concerned about the consequences of their ship's suction.

Moreover, the skipper avoids the waiting areas on the south side of the Hansweert lock due to the fear of breaking loose at night due to passing maritime traffic. If no spot is available at the protected North side of the lock, he continues his journey to a different location. The underutilization of the waiting areas at the outer harbour of Hansweert due to the passing vessels is an additional problem on top of the shortage of waiting areas already present in the Scheldt region. It happens regularly that ships get pulled loose, especially when multiple ships are moored alongside. This is also the reason why all the old piles in the outer harbour were leaning sideways. It should be noted that the forces on the piles have increased due to the increase in size of both the passing seagoing vessels and the inland ships. When asked if it could also depend on how the ships were moored and the amount of slack on the lines, he did not think this was the reason. He explained the method experienced skippers used to keep the mooring lines in tension whilst not having to readjust them to correct for the tide: by creating a height difference between the mooring lines the tidal movement can be accommodated, as illustrated in Figure A.7.

When asked how often accidents occur, the skipper indicated they happen regularly. He also mentioned that after an incident, things go well for a while, but after it is forgotten the problems resurface. Often incidents are not reported by the skippers as they do feel that no action is taken in response. As a solution, the skipper would prefer to see a speed restriction for the vessels sailing the Western Scheldt. Possibly, this could also be dependent on draught, similar to the canal leading to Ghent. The traffic posts at Hansweert and Terneuzen could oversee whether the seafaring vessels are indeed adhering to the speed limit.
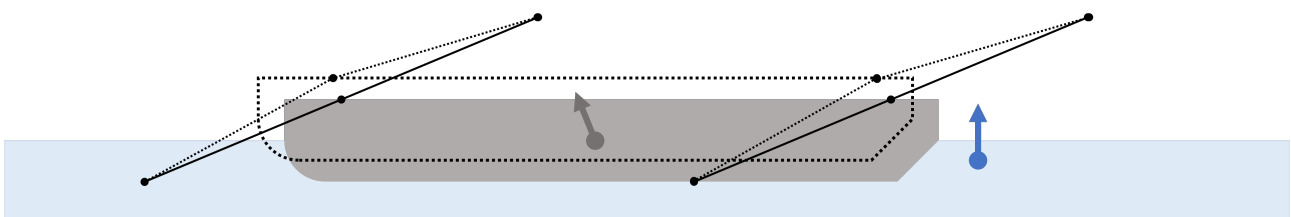


Figure A.7: Schematization of a mooring configuration to accommodate for the tidal movement.

## A.6 Interview with Roel Tukker

On the 20th of September, 2023, an interview was conducted with Roel Tukker, a former captain on an inland tanker and since 2015 part of the Health, Safety and Environment (HSE) department of GEFO Shipping Group. Roel, along with his department, performs audits and conducts investigations into incidents involving vessels of the GEFO fleet.

This interview was prompted by two independent but very similar reports of broken mooring lines of GEFO ships, less than a week apart, due to the suction of a passing ship at the Hansweert Lock. These incidents occurred at the sheltered North side of the lock. The breakages were caused by large inland ships, a 150-metre tanker and a 135-metre containership, which both were leaving the lock at moderately high speed (10.9kmph), sailing North. The GEFO ships with a length of 110 metres were both moored at North jetty designated for vessels ships with dangerous cargo, shown in Figure A.8. Both incidents occurred at night, 1.5 hours after low tide.



Figure A.8: Map showing waiting places designated for ships with dangerous cargo in blue.

Roel explained that inland ships when berthed overnight, typically maintain some slack in their lines to avoid the need for nightly adjustments due to the tide, even with the mooring configuration shown in Figure A.7. This can result in the ships having some leeway to move back and forth. When a large vessel passes by at high speed, the moored ship may be set in such motion to the extent that the ship's motion cannot be fully absorbed by the mooring lines anymore, and the mooring lines break. Especially when multiple ships are moored alongside, only the mooring lines of the ship moored to the piles will have to carry the load of the combined mass and momentum. The greater the slack on the lines, the more leeway the ships have, and the more momentum the ships can get. This makes it challenging to pinpoint liability when the breaking of the mooring lines depends on both the speed of the passing vessel and the mooring of the stationary ship. There is no speed limit on the Canal through Zuid-Beveland, but good seamanship requires consideration for the surrounding ships.

When asked about the waiting places at the South side of the lock and the effects of the passing seagoing vessels, he explains that 2 to 4 times per year, one of the 130 GEFO ships reports an incident of broken mooring lines due to passing seagoing vessels. This is one of the reasons that skippers prefer the waiting places on the North side, together with the reduced tidal fluctuation and the calmer wave conditions. GEFO skippers utilize these waiting places at Hansweert not only for overnight stays but also for waiting until a berth becomes available at their destination, for instance, the DOW chemical plant in Terneuzen. Roel is unaware of issues in the lock chambers at Hansweert concerning the passage of large seagoing vessels in the Western Scheldt.

To reduce the necessary slack on the mooring lines due to tidal fluctuations, the installation of floating bollards could be considered. These bollards would move up and down with the tide to ensure that the mooring lines can always be kept tight, reducing the leeway of the ships and thus also the risk of line breakage. He also indicated that it is important to create awareness among the skippers and pilots of the passing ships, both at the South and North sides of the lock, of the effects the suction of their ship could have on other ships.

## A.7   Second visit to the Hansweert traffic post

On the 5th of October, 2023, a second visit was conducted to the Hansweert traffic post, in which the incident of the 10th of July, 2023 (illustrated in Section 2.2) was discussed.

The traffic controller at duty explained that just before 19:00 hour in the evening, the Cosco Glory, a 366-metre-long container vessel, was bound to pass the outer harbour, sailing downstream. As is customary, the pilot of the container vessel reduced its speed prior to the turn at Hansweert. In this case down to 10.2 knots. After the passage of the vessel, the traffic post received calls from the Liszt, an inland tanker, at that moment in the lock chamber, about the excessive speed of the passing seagoing vessel. The captain of the Liszt asked the post where he could fill in a complaint form, as all ships in the locks were sucked out due to the passing vessel. Later, the lock operators called the traffic post, confirming this statement. The pilot on the Cosco Glory, being aware of this discussion, stated that he had reduced his speed significantly. He expressed his disbelief that the reduction was not sufficient and stated that next time, as speed did not seem to matter, he would pass the outer harbour at high speed. This comment led to a non-substantive discussion between the inland skippers and the pilot. The traffic controller explained that it was generally known that water is sucked out of the outer harbours at Hansweert and Terneuzen due to passing oversized vessels, but in this case, no significant disruption was expected as it was not low tide.

When asked about mooring line breakage at the waiting places, the traffic controller stated that he personally saw one case, a few years back but he is aware from fellow controllers that incidents occur more frequently. Furthermore, he said that the effects are felt greater at Walsoorden, a small port 6.5 kilometres upstream.
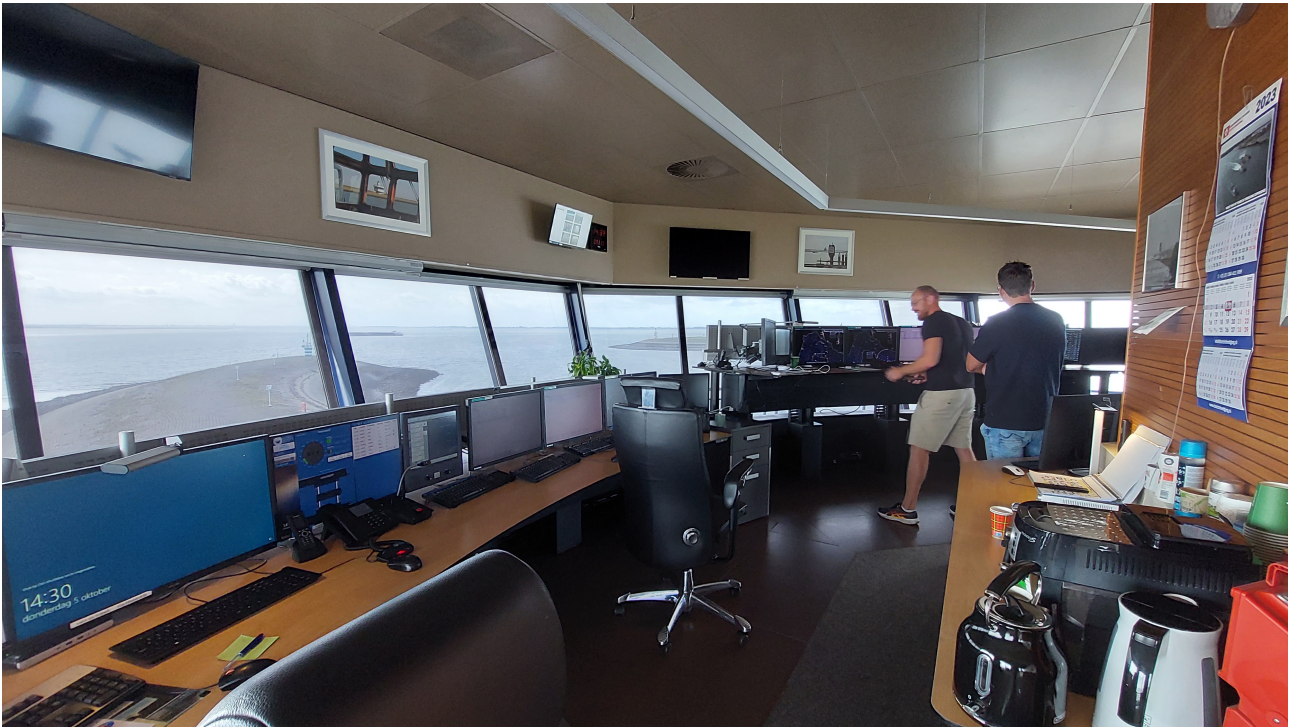


Figure A.9: Inside the Hansweert traffic post.

*Return to Section 2.1.*

## A.8 Interview with Liszt captain

On the 6th of October, 2023, an interview was conducted with the captain of the inland tanker called Liszt. This ship was involved in the incident of the 10th of July, discussed in Section 2.2 and Appendix A.7. The Liszt is an inland tanker with a length of 125 metres and a width of 12 metres, a CEMT Va class ship.

The captain described the incident as follows: The passage of the 366-metre-long Cosco Glory caused significant suction forces on the ships in the lock chamber at Hansweert. At the time of passage, the Liszt and another similarly sized ship were already (partially) moored in the chamber and a larger ship was manoeuvring into position behind them, as sketched in Figure A.10. The southern lock gate was in the process of closing. After the passage, the suction caused the ships to be pushed out of the chamber, and back into the outer harbour. In order to prevent the breakage of lines, the ships gave engines ahead. The captain of the larger ship commanded the lock gate operators to reopen the lock gate, in order to avoid collision. Due to the expertise of the crew members on the ships in the locks, damages could be prevented.

The captain expresses his concern for this issue, stating that this is not an isolated incident but part of a recurring and increasing problem, as the vessels in the Western Scheldt are getting larger, with greater draught. A few months ago he experienced a similar incident at Hansweert. Margins in the lock chamber are sometimes not more than a metre, giving the captains very little room for error. Furthermore, he states that he experiences a decreasing level of attentiveness and understanding from the pilots on the seagoing vessels. Some pilots do not seem to realize the effects that their vessel is having on other ships and appear to be under time pressure. The captain would prefer to see a speed limit based on draught, as he experiences greater effects with greater draught or speed. In practice, this would imply the greater the draught, the lower the maximum speed. He argues that deeper ships are more stable, and thus be navigable at lower speeds.

When asked if the captain sometimes uses the waiting places in the outer harbour, he responded negatively. In his opinion, this is not doable. It would be a waste of mooring lines, as breakage can be expected due to the effects of the passing vessels. In Terneuzen, he never experienced incidents himself, but he is aware from fellow skippers that similar issues are at play here, although he believed that the maritime traffic slows down more at Terneuzen than at Hansweert.
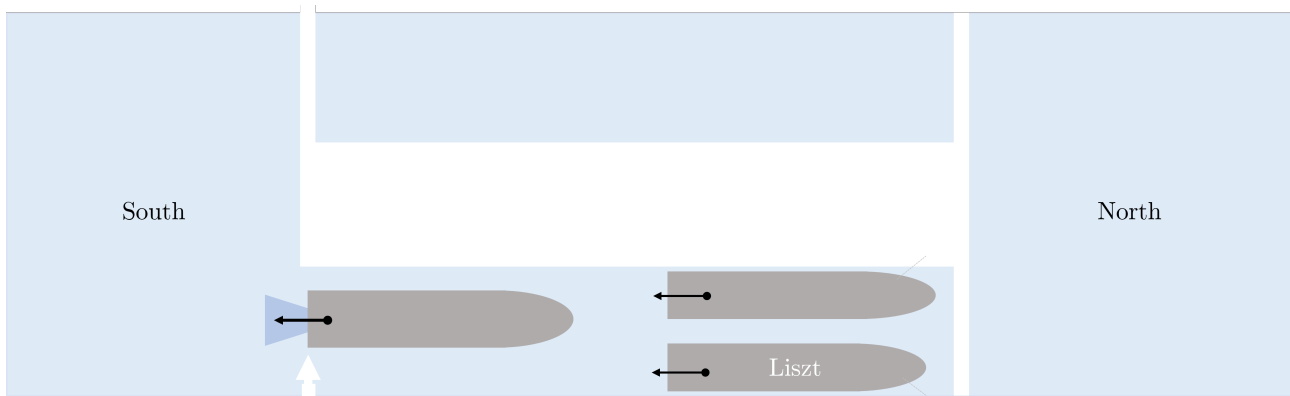


Figure A.10: A schematization of the lock configuration as described by the captain of the Liszt at the time of the incident (not to scale).

## A.9 Interview with Bastiaan Bijvank

On the 29th of November, 2023, an interview was conducted with Bastiaan Bijvank, the operational manager and pilot at the Scheldemonde Pilotage Association and member of the Nautical Safety Committee of the Scheldt area.

### A.9.1 Dutch and Flemish Pilots

Bastiaan explained that all ports at the Dutch part of the Scheldt are covered by Dutch pilots. The Flemish ports, including Antwerp, are served by both Dutch and Flemish pilots, distributed according to an allocation key. In practice, for the vessels passing Hansweert, 77.5% of the pilots are approximately Flemish, 22.5% Dutch. The workforce of the pilotage consists of 170 Dutch pilots and slightly more Flemish pilots.

### A.9.2 Bend at Hansweert

The bend at Hansweert is one of the more straightforward bends in the Western Scheldt trajectory because it is quite wide. Bastiaan mentioned two aspects which can make it challenging. Crosscurrents, occurring approximately 15-20 times per year, generate rotational movements in the water, especially affecting long vessels. Furthermore, the bend can be a busy traffic node, requiring extra attention, with inland ships navigating to and from the lock of Hansweert. Apart from these points, it is generally an easy bend and a good location for overtaking or letting other vessels pass. The Scheldt regulations stipulate that you should keep to the starboard side of the waterway as much as possible, however, when sailing downstream, if there is no oncoming traffic, pilots tend to cut the bend to save time and to increase the passing distance to the outer harbour at Hansweert. For vessels having greater draught, it is preferable to stick to the middle of the channel where the dredged course is located.

### A.9.3 Bend at Bath

In contrast, the river bend at Bath presents a significantly greater challenge. With a width of 300 metres from buoy to buoy, it is vital to prevent large vessels from encountering each other in this stretch. Typically, this is addressed in the traffic planning. If, however, it appears that such an encounter might happen, the pilots of both vessels address the issue in advance, typically, by having the vessel travelling against the current reduce its speed, in accordance with regulations.

### A.9.4 Speed over the ground versus speed through the water

When asked if the pilots use the speed through the water or over the ground for navigation, Bastiaan explained that they read the speed over the ground. However, the pilots have a very clear understanding of the current patterns at various locations and, therefore, a good idea of their speed through the water. For navigation purposes, the speed over the ground is most important.

### A.9.5 Ship waves

Pilots are primarily concerned that the waves generated by their vessels could lead to the separation of push-barge combinations. Especially when boarding at night, it's challenging to know what waves your vessel is generating. In such cases, asking nearby inland vessels or precisely calibrating the radar may bring this to light. The secondary waves heavily depend on the type of vessel, the speed and size and the loading condition. Some vessels generate fewer waves at higher speeds.

### A.9.6 Primary ship wave

The primary wave, and the suction associated with it, are less clearly observable. Although pilots are aware of the effect, the magnitude of the suction they generate is hard to establish. He notes that with the increasing size and speed of the vessel the suction increases as well. Furthermore, the under keel clearance is also influential. If under keel clearance is limited, the physical maximum speed of the vessel is reduced due to these suction effects.

### A.9.7 Problems at the Borssele Sea Jetty

An example of a location where moored ships are affected by this primary water motion is the Borssele Sea Jetty. Especially outbound passing vessels with a limited under-keel clearance push water ahead through the

narrow channel. This water volume reflects against the shore, comes back, and pushes the ships away from the jetty. In the past, they believed that the passing speed here caused the problems. Now they know that if they reduce their speed before entering the narrow stretch of the channel (Pasje van Borssele), the water volume in front of the bow of the ship has more time to disperse, such that the speed at which they pass the jetty does not matter as much.

### A.9.8 Problems at Hansweert

A similar effect could be taking place at Hansweert, Bastiaan elaborated. Due to the orientation of the entrance of the outer harbour, the vessels sailing downstream push a volume of water into the outer harbour. He argues that not only the passing distance but also the upstream or downstream orientation of the passing vessels influence the effects observed in the outer harbour.

### A.9.9 Awareness among pilots

As the pilots themselves do not experience these problems, discussions of known cases are organized to raise awareness. With no set speed limit on the Western Scheldt, the maximum speed is determined by ensuring no hindrance to others. Therefore, it is important for the pilots to understand when they create hindrances.

### A.9.10 Tidal window

Bastiaan explains that a number of locks are required to stay closed when a large vessel passes by. However, as the number of passing large vessels increases, the locking operations are more and more hindered. When asked if vessels have to increase their speed because of a limited tidal window, Bastiaan explains that large vessels have a minimum tidal window margin of 1 hour. This tidal window margin contains an extra 10 minutes to slow down for the harbours and locks along the route, including these at Terneuzen. For vessels sailing upstream, this provides a reasonable margin. For vessels sailing downstream, this margin is smaller due to the current direction. It is problematic to exceed the tidal time window and ultimately fall short of reaching Antwerp or the North Sea. The tidal window could be increased by reducing the loading of the vessels, as that reduces their draught. This is, however, undesirable for the Port of Antwerp.

### A.9.11 Solution direction

Bastiaan believes that the solution lies in awareness for both the pilots and inland skippers. Traffic posts could anticipate by informing inland traffic. Signs, for example, could raise awareness among inland shipping to ensure their mooring lines remain secure in waiting areas. Furthermore, by informing the pilots of the measurements and translating the water elevation readings to actual forces, the pilots can apply this knowledge to practical measures. Bastiaan refers to the harbour at Walsoorden, where after a long trajectory of creating awareness among the pilots, the number of complaints has reduced significantly. A comparable approach might also be effective for Hansweert.

## A.10   RWS 79 expedition

On the 5th of December, 2023, myself (Dick Heijboer) and Matthijs Schouten joined the crew of the RWS 79 vessel on their morning shift, in order to gain further understanding of the generation of primary waves of large seagoing vessels and their effects on the harbours along the Western Scheldt. The crew is well aware of the issues concerning the waves and suction generated by the passing vessels, as the home port of the RWS 79 is the outer harbour of Hansweert. The passage of the tanker named Bro Nissum visually showed currents in the outer harbour, especially visible around the piles. This vessel has a length of 144 metres and a draught of 6.7 metres. The Chennai Express, measuring 304 metres in length, 40 metres in width, and with a draught of 13.6 metres shown in Figure A.11, was followed from the bend at Bath to the bend at Hansweert. Although this vessel did not generate significant secondary waves, the drawdown along the hull of the vessel was visible and the currents were well felt by the 24-metre-long Rijkswaterstaat ship.



Figure A.11: The Chennai Express sailing through the bend at Bath towards the North Sea as observed from the RWS 79 ship.

## A.11 Interview with Tom Hardies and Eric Poirier

On the 13th of December, 2023 an interview was conducted with Tom Hardies, a river pilot at the Flemish pilotage and Eric Poirier, head of the nautical department, concerning the Scheldt river trajectory. Tom has years of experience piloting seagoing vessels along the Western Scheldt to and from Antwerp.

### A.11.1 Bend at Hansweert

When asked about the practicalities at the bend of Hansweert, Tom explained that the crosscurrents occurring during the rising tide can be challenging. During the rising tide, a substantial amount of water flows from the Middelgat into the main channel, affecting both the passing vessels and the inland ships, visualized in Figure A.12. The current forces the ships that leave the outer harbour of Hansweert towards the middle of the fairway. Also, the passing vessels experience this pushing force. Additionally, this location is a busy traffic node with substantial inland shipping traffic and a potential crossing point for other maritime traffic, unlike at Bath and Borssele.
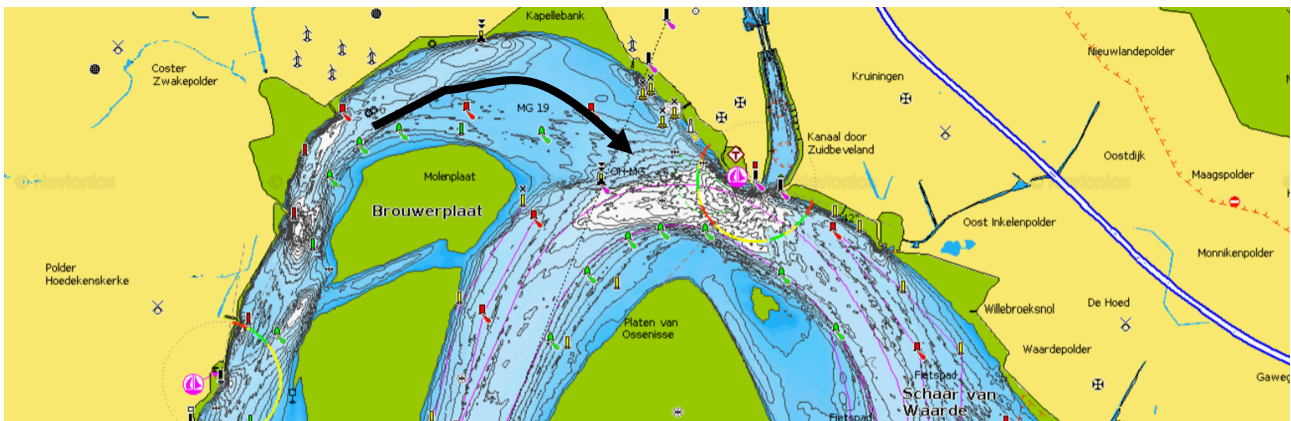


Figure A.12: Additional currents from the Middelgat into the main channel during rising tide (Navionics, 2023).

### A.11.2 Adaptation pilots

Most pilots do not reduce their speed physically before the bend of Hansweert, in contrast to Terneuzen, Walsoorden, and Borssele, where they actively reduce their speed. The passing vessels do naturally lose some of their speed due to the navigation through the bend. The issues at Hansweert are not well-known and not prevalent among most pilots. Tom himself has not heard of a specific incident related to the water displacement at Hansweert. At other locations, issues with suction are more commonly known, such as at the North Sea/Europe terminal. Vessels with a deep draught pass this location at a maximum of 8 knots, even though there is no physical speed limit.

### A.11.3 Waves and water displacement

When asked if the pilots are aware of the waves their vessel generates, Tom explained that this is assessed by looking at the wake of their vessel. However, from the elevated vantage point of a bridge, especially at night, it might be challenging to judge the magnitude. Assessing the water displacement, and the corresponding suction, is more difficult as this effect is not visible on the wider parts of the river and not perceptible on board. On the narrower stretches the drawdown is visible at the banks. Pilots do consider the water displacement their vessel generates, also based on their experience, and take this into account when passing for example the outer harbour of Terneuzen. Especially during low tide, they pay attention to this aspect.

### A.11.4 Tidal window

For the stretch between Flushing and Saeftinghe, the tidal window is calculated using an average speed of 12 knots over the ground. Normally, pilots enter the stretch with two or three hours of margin. If the margin in the tidal window is less than one hour, pilots are not allowed to start the voyage. Besides the tidal window, pilots must adhere to the traffic planning to ensure that vessels do not encounter each other at specific stretches of the route, as that could result in problematic situations.

### A.11.5 Solution direction

Tom and Eric agree that the solution must come from both sides. They strive for safe and efficient shipping transport on the Scheldt. By informing the pilots using clear data of the phenomena and impact of the water displacement at Hansweert, they will adapt their speed and passing distance accordingly. A practical application could be an overlay showing the critical and safe passing distances on the electronic map. On the other hand, inland shipping must ensure that they are securely moored. Eric adds that the southernmost berths might be positioned too close to the fairway, and it is not advisable to moor three ships alongside, especially at this location. He proposes that the lock operator waits with the opening of the chamber doors when a vessel passes, especially in an extreme case when two vessels encounter each other in the bend. If it appears that with the increasing amount and growing size of shipping traffic at the Western Scheldt it is necessary to slow down at the bend of Hansweert, pilots want to and will reduce their speed.

# Appendix B: Overview drawdown descriptions

This appendix gives an overview of the empirical relations given in the literature to describe the drawdown also presented in Table 3.1. The following parameters are used in the equations:

- $\Delta h$: Maximum water level depression related to the primary water motion [m]
- $V_s$: Ship speed [m/s]
- $V_{lim}$: Natural limit speed of the ship [m/s]
- $U_r$: Maximum return current velocity along the ship [m/s]
- $D_s$: Draught of the ship [m]
- $B_s$: Beam of the ship [m]
- $L$: Length of the ship [m]
- $C_m$: Midship coefficient of the ship
- $A_s$: Underwater cross-section of the ship amidships defined as $D_s B_s C_m$ [m$^2$]
- $d_s$: Distance from the sailing line [m]
- $A_c$: Wet cross-sectional area of the undisturbed channel [m$^2$]
- $W_s$: Undisturbed channel width at the water surface [m]
- $h$: Water depth [m]
- $\bar{h}$: Cross-sectionally averaged water depth defined as $A_c/W_s$ [m]
- $\alpha$: Slope of the bank [rad]
- $W_b$: Channel width at the bed level defined as $W_s - 2h \cot \alpha$ [m]
- $C_B$: Block coefficient of the ship
- $g$: Gravitational acceleration [m/s$^2$]

## B.1   Schijf (1949) including a correction factor

Equation 3.1 was modified by introducing a correction factor after tests conducted by Delft Hydraulics (1953) revealed certain deviations from the theory:

$$\Delta h = \alpha_s \frac{(V_s + U_r)^2}{2g} - \frac{V_s^2}{2g} \tag{B.1}$$

where the correction factor is defined as:

$$\alpha_s = 1.4 - 0.4 \frac{V_s}{V_{lim}} \tag{B.2}$$

Similarly to Equation 3.5, an expression for the water level drawdown ($\Delta h$) can be observed by rewriting Equation 3.2 for the return current ($U_r$) and inserting this in Equation B.1.

$$\Delta h = \frac{V_s^2}{2g} \left( \alpha_S \left( \frac{A_c}{A_c - A_s - W_s \Delta h} \right)^2 - 1 \right) \tag{B.3}$$

The correction factor depends on the ratio between the speed of the ship ($V_s$) and the natural limit speed of the ship ($V_{lim}$). Schijf (1949) argues that the natural limit speed of a ship is reached when the return current ($U_r$) is supercritical. A flow is supercritical when the Froude number is equal to one. Van Koningsveld et al. (2023) shows that the limit speed can be iteratively calculated with the following equation:

$$V_{lim} = \sqrt{g\bar{h} \left( 3 \left( \frac{V_{lim}}{\sqrt{g\bar{h}}} \right)^{\frac{2}{3}} - 2 \left( 1 - \frac{A_s}{A_c} \right) \right)} \tag{B.4}$$

## B.2 Gates and Herbich (1966)

Gates and Herbich (1977) developed an equation for drawdown at the Natural Research Council of Canada and the David Taylor Model Basin (Bhowmik et al., 1981b). This is the same equation as Schijf (1949), however, the velocity is expressed in knots, the drawdown in feet and the gravitational acceleration is integrated into the constant.

$$\Delta h = \frac{V_s^2}{22.6}\left(\left(\frac{A_c}{A_c - A_s - W_s\Delta h}\right)^2 - 1\right) \tag{B.5}$$

## B.3 Hochstein (1967)

Hochstein (1967) developed the following relation for drawdown where $K$ is a containment factor which is a function of the ratio of the ship length to beam and the blockage ratio. Almström and Larson (2020) propose that a factor $K = 0.7$ represents the average ship.

$$\Delta h = V_s^2(C_1 - 1)\frac{C_2}{2g} \tag{B.6}$$

where:

$$C_1 = \left(\frac{A_c}{A_c - A_s}\right)^{2.5} \tag{B.7}$$

$$C_2 = \begin{cases} 0.3\exp\left(\frac{1.8V_s}{K\sqrt{g\bar{h}}}\right), & \text{if } \frac{V_s}{K\sqrt{g\bar{h}}} \le 0.65 \\ 1, & \text{if } \frac{V_s}{K\sqrt{g\bar{h}}} > 0.65 \end{cases} \tag{B.8}$$

## B.4 Gelencser (1977)

Another equation was developed by Gelencser (1977) which includes the length of the ship ($L_s$) and the distance of the ship from the shoreline ($d_s$) in its definition. This description was derived from prototype and model tests by fitting the calculated drawdown to the measured drawdown (Bhowmik et al., 1981b).

$$\Delta h = 2 \times 10^{-6}\left(\left(\frac{V_s A_s L^2}{d_s \sqrt{A_c}}\right)^{1/3}\right)^{2.8} \tag{B.9}$$

## B.5 Dand and White (1978)

Dand and White (1978) developed an expression based on scale ship experiments (Bhowmik et al., 1981b):

$$\Delta h = 8.8\left(\frac{A_c}{A_s}\right)^{-1.4}\left(\frac{V_s^2}{2g}\right) \tag{B.10}$$

## B.6 Maynord (1996)

Maynord (1996) developed an elaborate definition, including the limit speed and the distance from the shore:

$$\Delta h = C \times \left(\frac{\left(V_s + \left(V_s\frac{A_c}{A_c - A_s} - V_s\right)\left(1.9 - 1.29\frac{V_s}{V_{lim}}\right)\right)^2}{2g} - \frac{V_s^2}{2g}\right) \times \sqrt{0.75\left(\frac{A_c}{A_s}\right)^{0.18}}$$

$$\exp\left(3\ln\left(\frac{1}{0.75\left(\frac{A_c}{A_s}\right)^{0.18}}\right)\right) \tag{B.11}$$

where $C$ depends on the location of the ship in the fairway, and $V_{lim}$ is the limit speed, which requires to be solved iteratively:

$$C = \begin{cases} 1.65 - 1.3\frac{d_s}{W_s}, & \text{if } \frac{d_s}{W_s} \leq 0.5 \\ 1.35 - 0.7\frac{d_s}{W_s}, & \text{if } \frac{d_s}{W_s} > 0.5 \end{cases} \tag{B.12}$$

$$V_{lim} = \sqrt{2g\bar{h}\left(\frac{A_s}{A_c} + 1.5\left(\frac{V_{lim}^2}{g\bar{h}}\right)^{1/3} - 1\right)} \tag{B.13}$$

## B.7   Kriebel (2003)

The expression of Kriebel et al. (2003) includes the block coefficient of the vessel ($C_B$), and does not consider the river and vessel width:

$$\Delta h = D_s(0.0026C_B - 0.001) \times \exp\left(\left(\frac{-215.8D_s}{L_s} + 26.4\right)\frac{V_s}{\sqrt{gL_s}} \times \exp\left(\frac{2.35(1 - C_B)D_s}{\bar{h}}\right)\right) \tag{B.14}$$

## B.8   CIRIA (2007)

The analytical description by CIRIA (2007) is very similar to that of Schijf (1949) with the correction factor, described in Section B.1, however, it includes an expression for a trapezoidal river cross-section, where $\alpha$ is the slope of the river banks.

$$\Delta h = \frac{V_s^2}{2g}\left(\alpha_s\left(\frac{A_c}{A_c^*}\right)^2 - 1\right) \tag{B.15}$$

$$A_c^* = W_b(h - \Delta h) + \cot\alpha(h - \Delta h)^2 - A_s \tag{B.16}$$

The correction value is calculated by Equation B.2. Furthermore, it includes three methods to calculate the limit speed. The minimum value should be used for further calculations.

$$V_{lim,A} = \sqrt{g\frac{A_c}{W_s}\left(3\left(\frac{V_{lim}}{\sqrt{g\frac{A_c}{W_s}}}\right)^{\frac{2}{3}} - 2\left(1 - \frac{A_s}{A_c}\right)\right)} \tag{B.17}$$

$$V_{lim,B} = \sqrt{\frac{gL_s}{2\pi}} \tag{B.18}$$

$$V_{lim,C} = \sqrt{g\bar{h}} \tag{B.19}$$

$$V_{lim} = \min\left(V_{lim,A}; V_{lim,B}; V_{lim,C}\right) \tag{B.20}$$

# Appendix C: Data collection details

## C.1  Water level fluctuation measurements

This appendix provides additional details and visualizations concerning the measurements of the water level fluctuations in the outer harbour, introduced in Section 4.1.1.

### C.1.1  Equipment

The Geolux LX-80-15 10Hz non-contact oceanographic radar sensor, shown in Figure C.1, measures the distance from the sensor to the water surface, by transmitting a radio wave in an 80GHz frequency range and measuring the shift of the electromagnetic wave reflected from the water surface. This method ensures that the measurement quality is not affected by changes in air temperature or density. The data is transmitted using an NMEA-like protocol, outputting messages containing relevant information. Table C.1 presents the data included in the messages for this measurement campaign. Geolux provides the opportunity to transmit additional types of data, not shown in the table, such as calculated significant wave heights or periods. This capability was intentionally omitted to reduce the data to be transmitted and alleviate the load on the transmitter and server. The signal-to-noise ratio and the tilt angles of the instrument are transmitted to check the reliability of the measurements.



Figure C.1: The Geolux LX-80-15 10Hz non-contact oceanographic radar sensor (images from Geolux website).

| Symbol | Description |
|--------|-------------|
| L1 | The actual distance between the instrument and the water surface |
| L2 | The average filtered distance between the instrument and the water surface |
| S1 | Signal-to-noise ratio of the detected signal |
| A1 | The tilt angle of the instrument along X axis |
| A2 | The tilt angle of the instrument along Y axis |
| MIN | Minimum water level measured in a set time interval |
| MAX | Maximum water level measured in a set time interval |
| AVG | Average water level measured in a set time interval |

Table C.1: Information contained by the NMEA Protocol output messages (Geolux, 2023).

## C.1.2   Measurement setup and data logging

The installation of the sensor, data logger, solar panel and battery pack was timed during high tide to guarantee that the sensors always maintain sufficient clearance above the water level, shown in Figures C.2. The data logger is supplied by RMA Hydromet and sents the data in batches of five minutes to a Rijkswaterstaat FTP-server. The files containing the five-minute data are combined into a single data file. This file is structured such that every row represents a timestep and the parameters L1, L2, S1, A1, A2, MIN, MAX and AVG, introduced in Table C.1, are the columns. The data is timestamped in Central European Summer Time (UTC+02:00) (CEST).



Figure C.2: Pictures of the installation and configuration of the water level fluctuation measurement setup.

## C.1.3   Overview of the data collected

Measurements are conducted for seven weeks, from the 29th of June, 2023 until the 17th of August, 2023. Figure C.3 shows the development of the distance between the instrument and the water surface (L1) for the complete period. When an arbitrary day is displayed, Figure C.4, the tidal cycle is visible.

Approximately 5% of the data is missing, based on the total number of seconds included in the measurement campaign, and the number of measurements conducted. This ratio excludes 9 hours (between 30/06/2023 18:00 and 01/07/2023 03:20) for which the data is lost due to data being overwritten on the FTP server. This missing data can often be related to so-called serial port 2 errors. Besides the missing data, also outliers are observed in Figures C.3 and C.4, ranging from 0mm to the maximum detection distance of 15000mm.
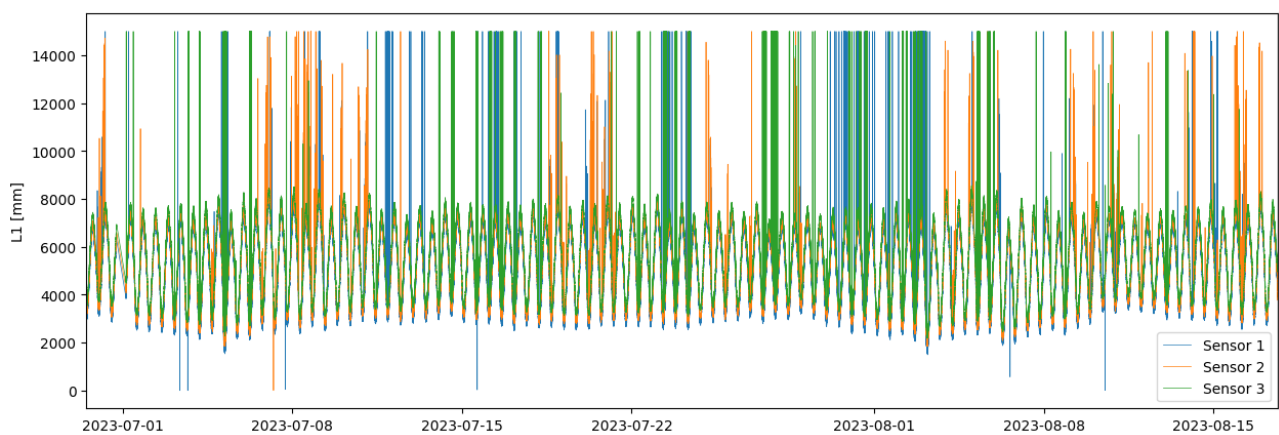


Figure C.3: Raw data recorded by the three sensors in the outer harbour.
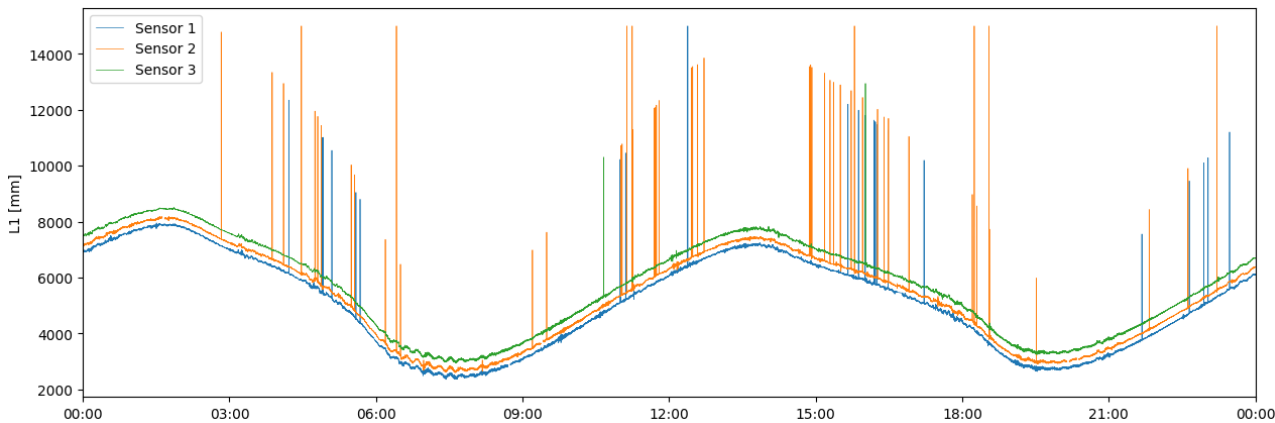
Figure C.4: Raw data recorded by the three sensors in the outer harbour on the 8th of July, 2023.

When investigating the tilt angles along the X-axis, Sensor 1 shows some variability, periodically angles greater than 10 degrees. The averaged tilt angles along the X-axis remain less than one degree. On the Y-axis, the variability in tilt angle is less, however, the averaged angles are 1.8, 3.4 and 3.0 degrees for the sensors respectively. Figures C.6 and C.5 display the development of the tilt angles. It should be noted that the graphs provide a more pronounced view of the outliers, but they primarily represent isolated events and the exceptionally extreme outliers are not consistently observed over extended periods. The signal-to-noise ratio is the difference between the signal level corresponding to the measured distance and the noise floor level, plotted in Figure C.7. Low levels indicate that the measured value may be inaccurate. Table C.2 gives an overview of the collected data.
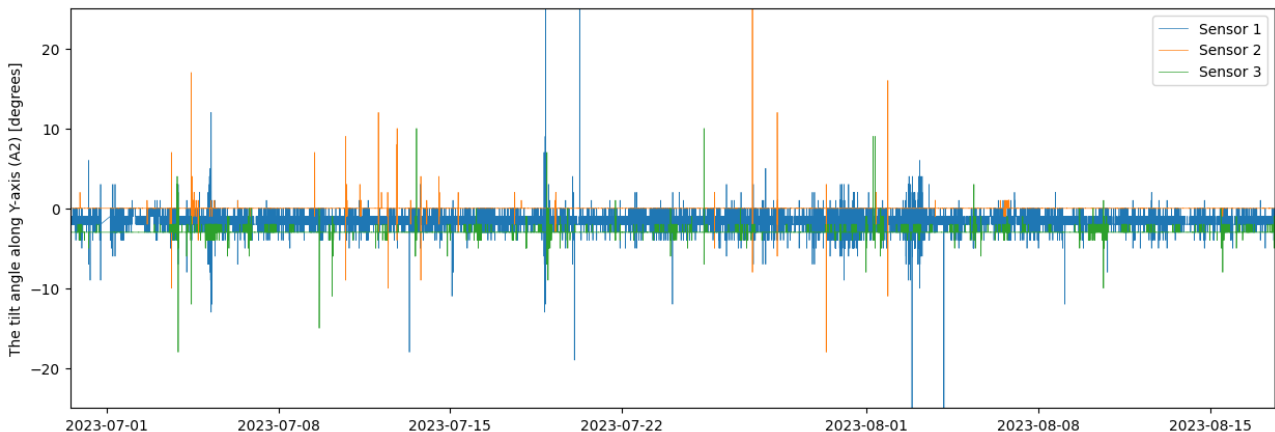


Figure C.5: The development of the tilt angles along the Y-axis for the sensors during the measurement campaign.
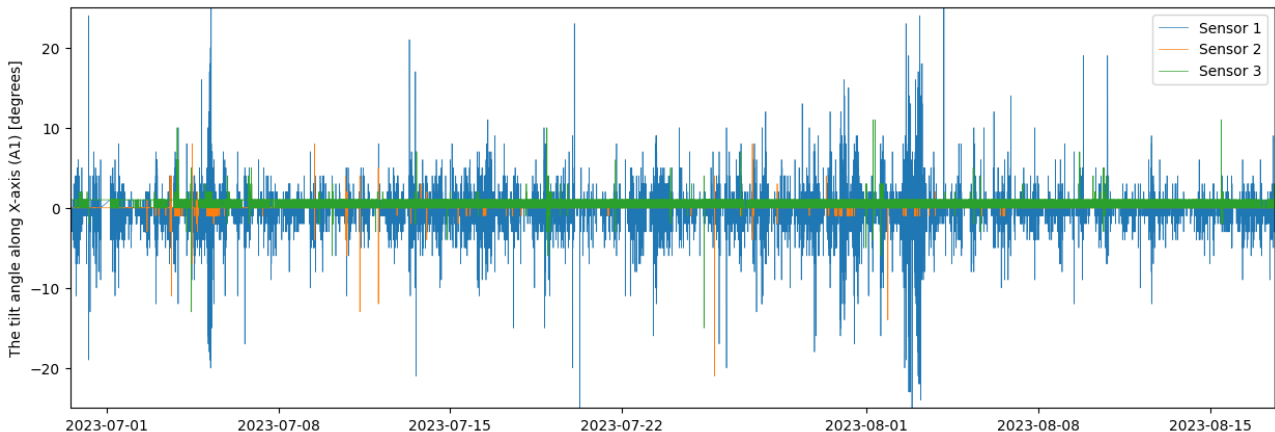


Figure C.6: The development of the tilt angles along the X-axis for the sensors during the measurement campaign.
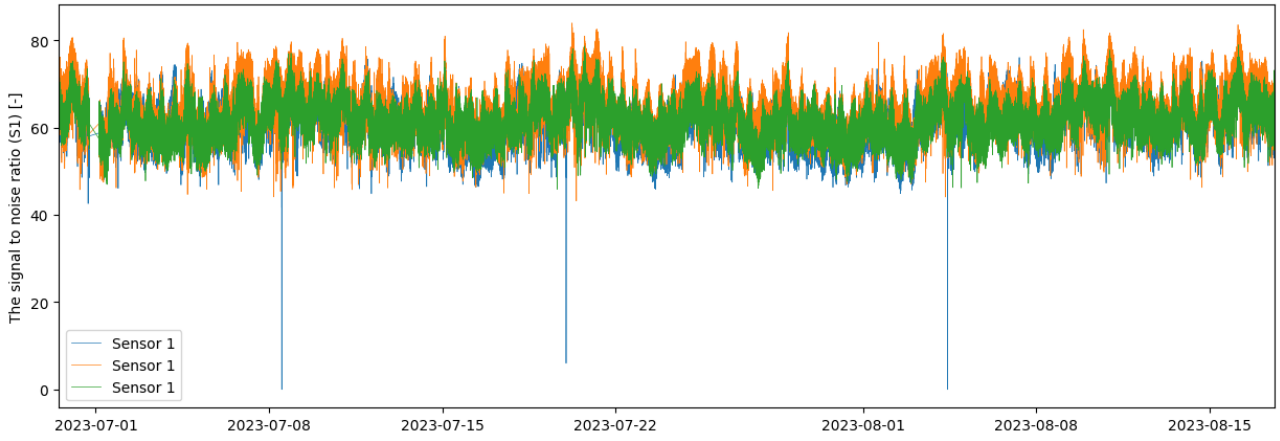
Figure C.7: The development of the signal-to-noise ratio for the sensors during the measurement campaign.

| parameter | Unit | Sensor 1 | Sensor 2 | Sensor 3 |
|---|---|---|---|---|
| Average distance between instrument and water surface | mm | 5034 | 5266 | 5610 |
| Percentage of data missing | - | 4.1% | 4.8% | 4.6% |
| Average tilt angle along X-axis | deg | 0.1 | 0.0 | 0.5 |
| Average tilt angle along Y-axis | deg | 1.8 | 3.4 | 3.0 |
| Average signal-to-noise ratio | - | 62% | 65% | 62% |

Table C.2: Overview of the data measured by the sensor in the measurement period.

## C.2 Calibrated water levels

Figure C.8 visualizes the development of the water level, introduced in Section 4.1.2. The data is downloaded via Rijkswaterstaat Waterinfo for the measurement period, from the 29th of June, 2023 until the 17th of August, 2023. The data is timestamped in Central European Summer Time (UTC+02:00) (CEST).
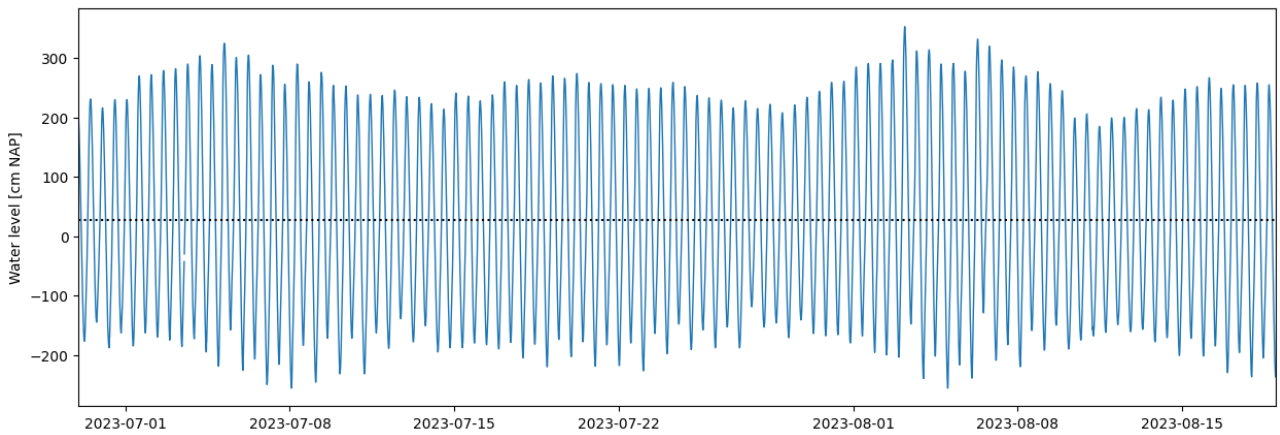


Figure C.8: Development of the water level outside of the outer harbour during the measurement campaign.

## C.3  Current data

This appendix provides additional information on how the data was retrieved and visualizes the collected data. Section 4.1.3 mentions that the current data is downloaded via the Rijkswaterstaat WTZ-viewer. The settings applied to the WTZ-viewer are given in Table C.3. The data is timestamped in Central European Summer Time (UTC+02:00) (CEST). Figure C.9 shows the development of the currents during the measurement period, from the 29th of June, 2023 until the 17th of August, 2023. The relation between the current direction and the current magnitude is shown in Figure C.10.
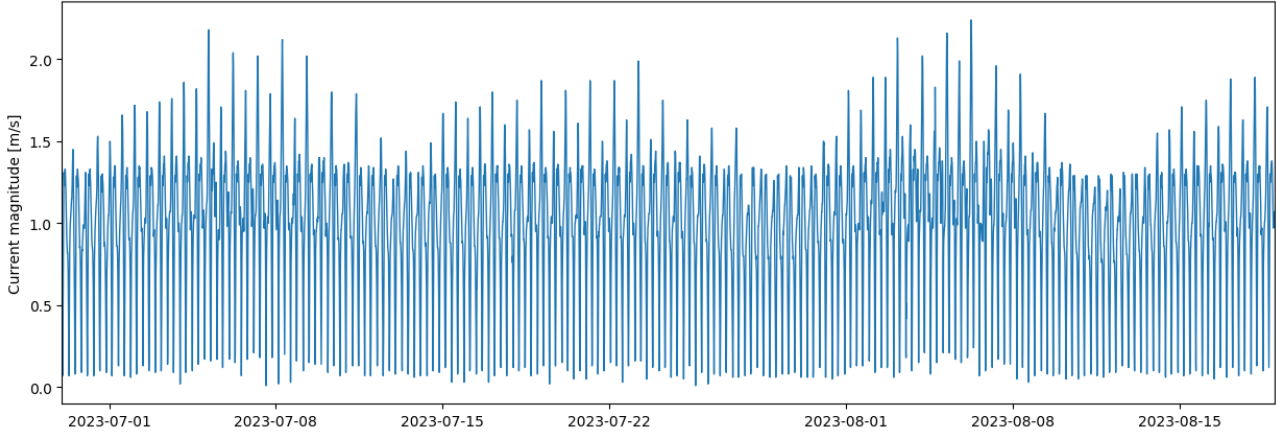


Figure C.9: Development of the currents in the fairway outside of the outer harbour during the measurement campaign.
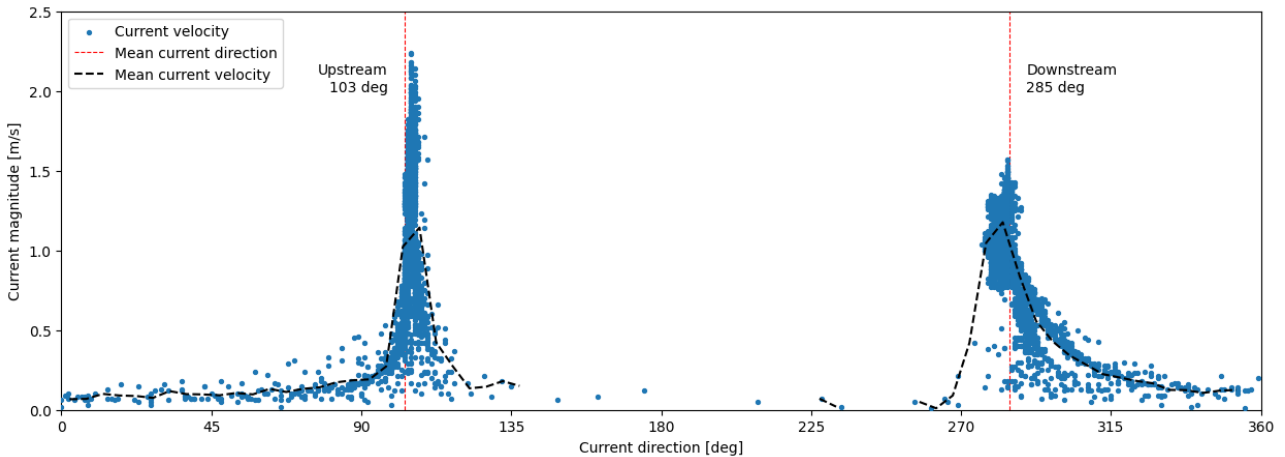


Figure C.10: The current direction versus the magnitude as calculated during the measurement campaign.

| setting | symbol | description |
|---|---|---|
| location | HRWT | Hansweert (59250, 384120 RD) |
| type | SG | current speed and direction (timestep of 10minutes) |
| source | h | HMC prediction |
| fase | 6 | definitive forecast |
| channel | a,b | magnitude, direction |

Table C.3: Rijkswaterstaat WTZ-viewer settings applied to retrieve the current data.

*Return to Section 4.1.3.*

## C.4 Bathymetry

As mentioned in Section 4.1.4, bathymetrical data with an accuracy of one by one metre is downloaded via Rijkswaterstaat GeoWeb. The dataset used for the bathymetrical data includes the Dutch part of the Western Scheldt and is in the Netherlands RD New (EPSG:28992) coordinate system. The units are in metres and the bottom levels are relative to NAP. The source does not provide a time span in which the bathymetrical measurements were taken. Figures C.11 and C.12 show the location of the relatively deeper lying fairway through the Western Scheldt.
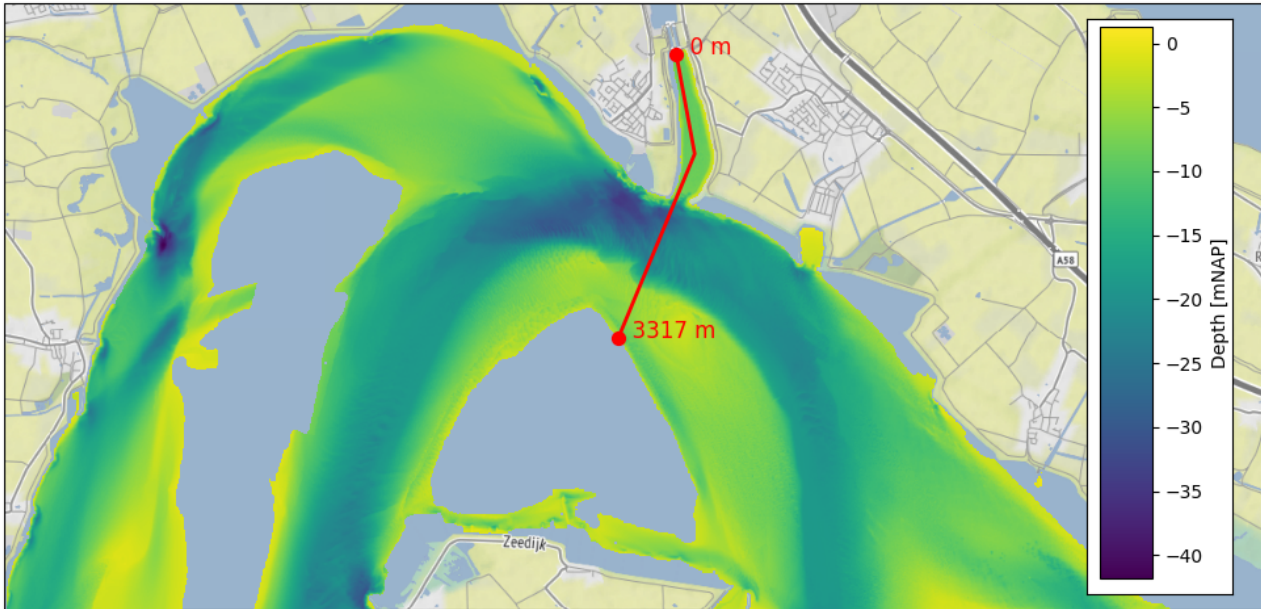


Figure C.11: Bathymetrical data of the project area provided by Rijkwaterstaat.
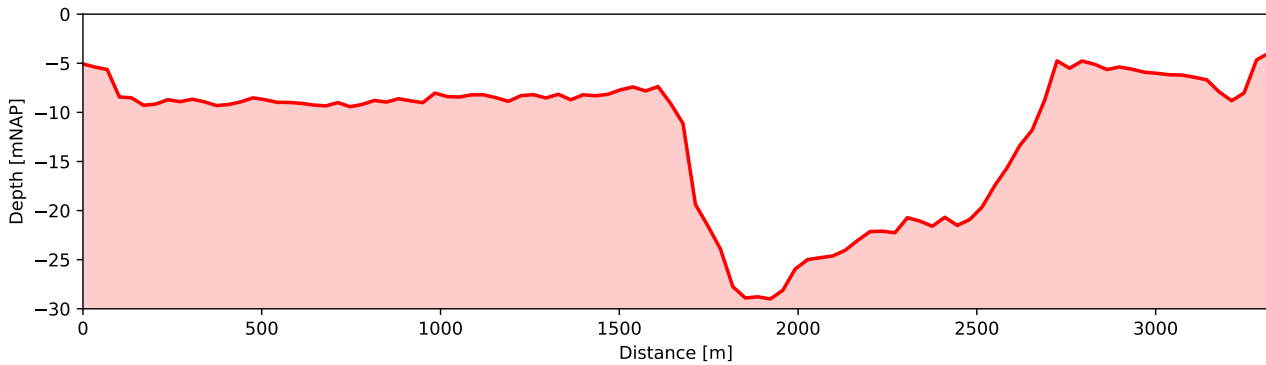


Figure C.12: Depth profile of the path shown in Figure C.11.

*Return to Section 4.1.4.*

## C.5 Wind data

As mentioned in Section 4.1.5, the wind data is downloaded for the measurement period via Rijkswaterstaat Waterinfo, from the 29th of June, 2023 until the 17th of August, 2023. The data is timestamped in Central European Summer Time (UTC+02:00) (CEST). Figure C.13 shows the development of the wind speed over the measurement period. The dominant direction is from the South-West direction, shown by Figure C.14.
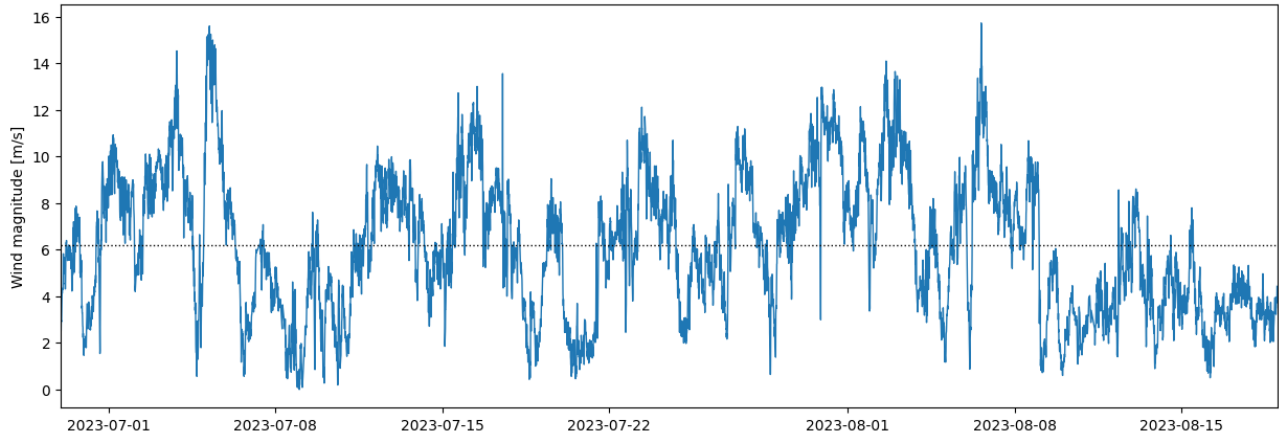


Figure C.13: The development of the wind speed during the measurement campaign.
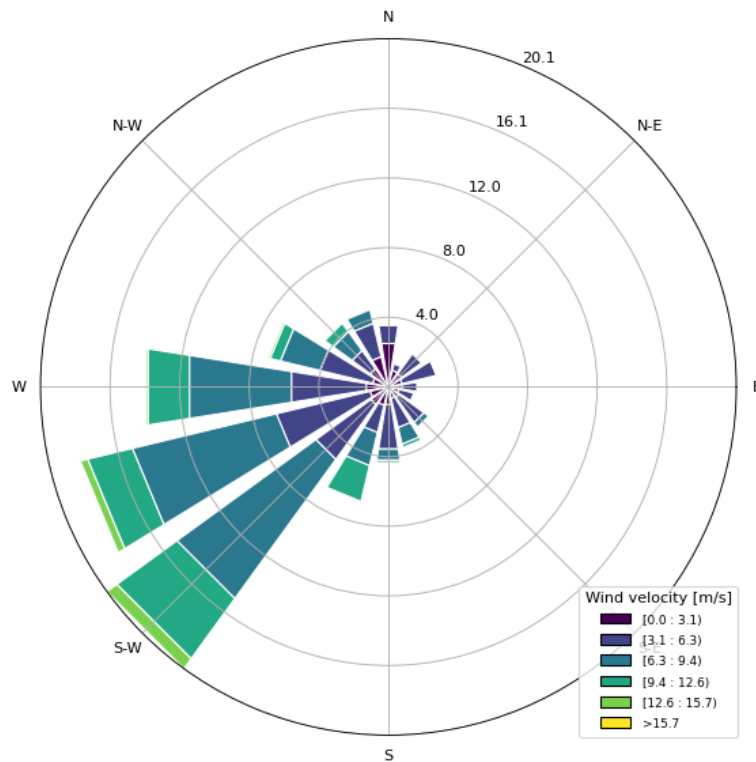


Figure C.14: Wind rose of wind climate during the measurement campaign.

*Return to Section 4.1.5.*

## C.6   AIS data

Section 4.1.6 mentioned that the AIS data was collected for the same period as the measurement campaign of the water level fluctuations, a total of 50 days from 2023-06-29 00:00:00 to 2023-08-18 00:00:00. The area for which the data is collected is defined between the latitudes of 51.4179° and 51.4573° and longitudes of 3.9489° and 4.0559° shown in Figure C.15. The data is timestamped in UTC time. Table C.4 gives an overview of the relevant parameters included in the AIS dataset obtained for this research.
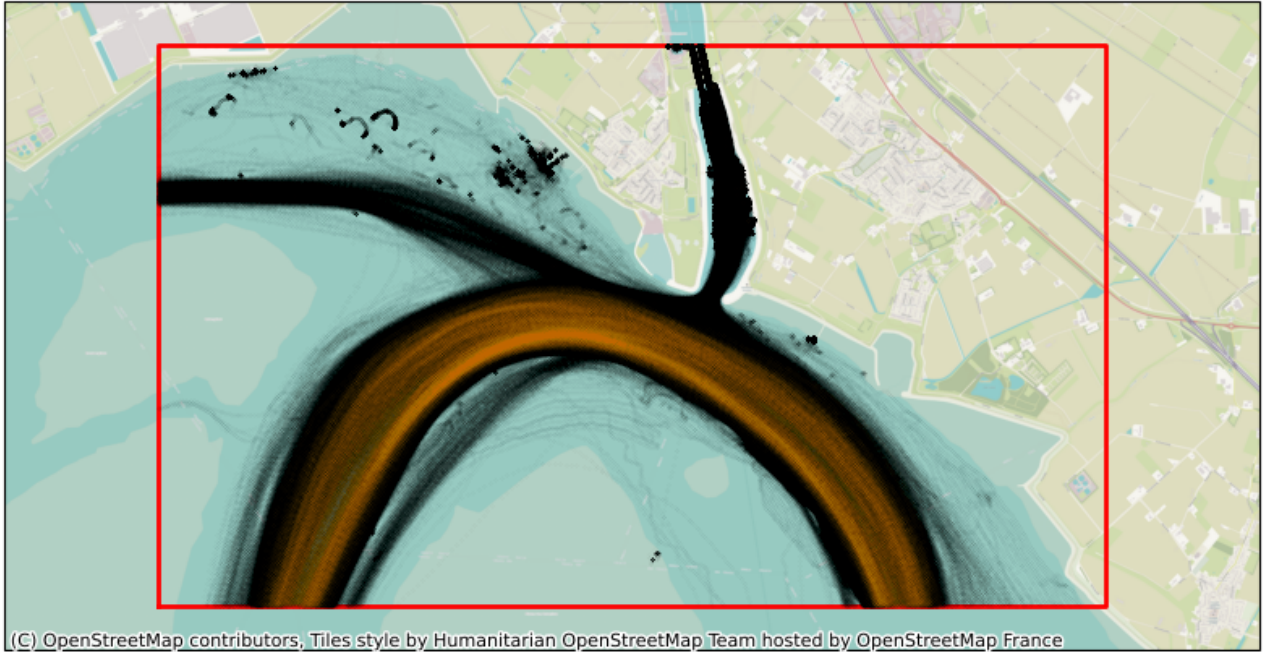


Figure C.15: AIS transponder locations logged during the measurement campaign plotted on a map. Locations associated with an oversized vessel, defined as vessels longer than 210 metres or deeper than 10 metres, are plotted in orange.

| parameter | description | unit/format |
|---|---|---|
| time | the time at which the data is generated | UTC-seconds |
| position | position in longitude and latitude with 0.0001 arcminutes precision | degrees |
| MMSI | a vessel unique nine digit identification number | 9-digit number |
| SOG | speed over ground in 0.1 knots resolution | knots |
| COG | course over ground in 0.1 degree precision | degrees North |
| TH | true heading the bow of the ship is pointing towards | degrees North |
| name | name of the vessel | 20-character or less |
| callsign | international callsign assigned to the vessel | 7-character or less |
| vessel type | type of vessel and/or cargo | text |
| A | distance from the AIS GPS antenna to the bow of the vessel | metres |
| B | distance from the AIS GPS antenna to the aft of the vessel | metres |
| C | distance from the AIS GPS antenna to the port side of the vessel | metres |
| D | distance from the AIS GPS antenna to the starboard side of the vessel | metres |
| length | distance between the forward and aft of the vessel also referred to as LOA | metres |
| width | breadth of the vessel at the broadest point | metres |
| draught | distance between the waterline and the deepest part of the ship | metres |

Table C.4: Parameters included in the AIS messages.

# Appendix D: Expected wave frequencies

This appendix treats the expected frequencies related to the primary ship waves and the wind climate. These are determined to accurately filter the measured signal, without losing the characteristics of interest, as described in Section 4.2.1.

## D.1 Expected drawdown frequency bandwidth

An initial estimate of the frequency of the drawdown phenomena can be made by setting the wave period equal to the time it takes a vessel to sail its own length.

$$f = \frac{1}{T} = \frac{V_s}{L_s} \tag{D.1}$$

where $f$ is the frequency of the wave, $T$ the period, $L_s$ the length of the vessel and $V_s$ the velocity of the vessel. By taking a minimum and maximum vessel speed of 4m/s and 10m/s (Figure 5.8) and minimum and maximum vessel length of 210m and 400m (based on the definition of an oversized vessel), a frequency bandwidth between 0.010Hz and 0.048Hz is observed, shown in Table D.1.

| water depth ($h$) | vessel length ($L$) | wave period ($T$) | frequency ($f$) |
|---|---|---|---|
| min. speed - 4m/s | min. length - 210m | 53s | 0.019Hz |
| min. speed - 4m/s | max. length - 400m | **100s** | **0.010Hz** |
| max. speed - 10m/s | min. length - 210m | **21s** | **0.048Hz** |
| max. speed - 10m/s | max. length - 400m | 40s | 0.025Hz |

Table D.1: Estimation of the frequency bandwidths of a primary ship wave.

## D.2 Expected wind seas

An estimation of the wave height and period of the wind seas in the outer harbour can be made based on wind speeds and corresponding fetches using the Sverdrup-Munk-Bretschneider (SMB) growth curves (Sverdrup and Munk, 1947; Bretschneider, 1952; Holthuijsen, 2007). The SMB growth curves provide a simplified power law for the relation between dimensionless fetch ($\tilde{F}$) and dimensionless wave height ($\tilde{H}$) and wave period ($\tilde{T}$), shown in Equations D.2. The dimensions are removed from the units using the wind speed at 10 metres elevation ($U_{10}$), shown in Equations D.3.

$$\tilde{H} = 2.88 \times 10^{-3} \tilde{F}^{0.45} \qquad \tilde{T} = 0.459 \tilde{F}^{0.27} \tag{D.2}$$

$$\tilde{F} = \frac{gF}{U_{10}^2} \qquad \tilde{H} = \frac{gH}{U_{10}^2} \qquad \tilde{T} = \frac{gT}{U_{10}} \tag{D.3}$$

Using the wind data discussed in Section 4.1.5, the maximum wind speed for every wind direction can be calculated. By taking the fetch and maximum wind speed for every wind direction, the maximum wave height and period corresponding to that direction can be calculated. Figure D.1 shows the fetches in all 360 possible wind directions. The maximum fetch lengths are those in the South direction.
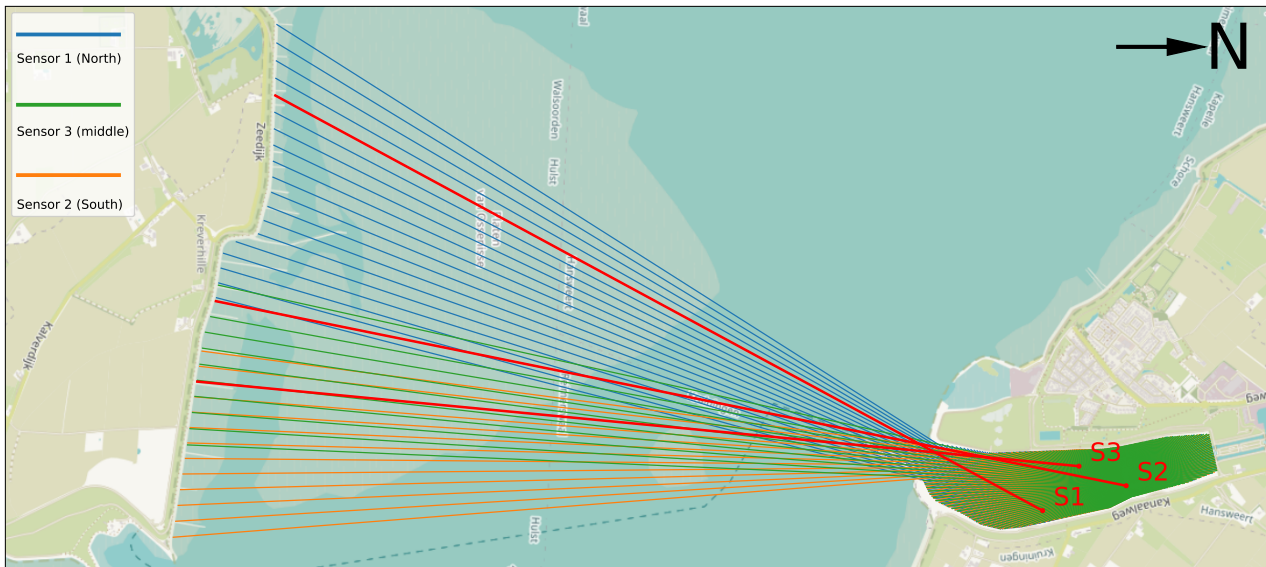
Figure D.1: The calculated fetches for the three different sensors. The red lines indicate the fetches of the maximum wave heights calculated for each of the sensors.

Table D.2 shows for every sensor the maximum estimated wave height and period for the three sensors, and the corresponding wind speed, direction and fetch. Note that the maximum waves do not occur at the maximum wind speed event, but rather result from a combination of fetch and wind speed.

|  | max. wave height | max. wave period | frequency | wind speed | wind direction | fetch |
|---|---|---|---|---|---|---|
| Sensor 1 | **0.65m** | **2.83s** | **0.35Hz** | 13.3m/s | 209deg | 4965m |
| Sensor 3 | 0.57m | 2.70s | 0.37Hz | 11.6m/s | 192deg | 5282m |
| Sensor 2 | 0.53m | 2.61s | 0.38Hz | 11.0m/s | 186deg | 5038m |

Table D.2: The calculated wave height and period and corresponding wind speed, direction and fetch for every sensor.

# Appendix E: Bow, middle and aft coordinates

In this appendix, the calculations conducted to calculate the coordinates of the bow, middle and aft of a vessel are given.

Using the coordinates of AIS transmitter, the true heading and the position of the AIS transmitter relative to the bow, aft, port and starboard side of the vessel (Table C.4 in Appendix C.6), the coordinates of the bow, aft and middle of the vessel can be calculated for every AIS message. Figure E.1 shows a schematization of a vessel where $A$ is the distance between the transmitter and the bow, $B$ between the transmitter and the stern, $C$ the distance between the transmitter and port side and $D$ the distance between the transmitter and the starboard side of the vessel. The true heading (TH) is the direction the bow is pointing towards, relative to the North (N).
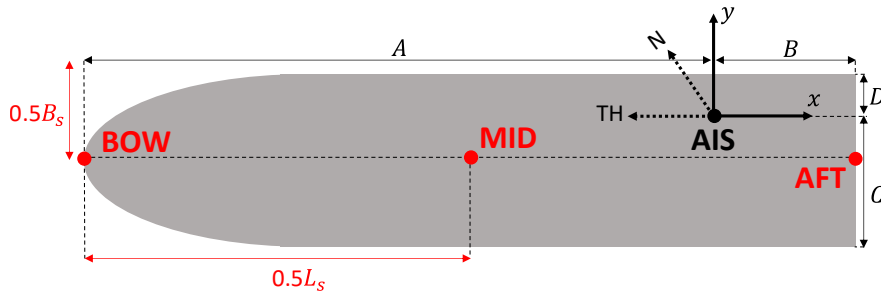


Figure E.1: Schematization of a vessel with the corresponding coordinates.

The coordinates of the bow, aft and middle of the vessel (marked as red dots in Figure E.1) can be calculated based on the distance between the point of interest and the AIS transmitter and the corresponding angle between these locations, relative to the North. The distance and angle between the transmitter and an arbitrary point of interest P can be calculated as follows:

$$r_{\text{P,AIS}} = \sqrt{dy^2 + dx^2} \tag{E.1}$$

$$\phi_{\text{P,AIS}} = \begin{cases} \text{TH} - \arctan\left(\frac{dy}{dx}\right) + \pi, & \text{if } dx > 0 \\ \text{TH} - \pi, & \text{if } dx = 0 \\ \text{TH} - \arctan\left(\frac{dy}{dx}\right), & \text{if } dx < 0 \end{cases} \tag{E.2}$$

Where $dx$ is the distance along the vessel from point P to the transmitter and $dy$ is the distance along the width of the vessel, conform to the coordinate system introduced in Figure E.1. Using the obtained angle and distance, and the location of the transmitter, the longitude and latitude of point P can be calculated, by applying the haversine formula. The haversine formula is a method to calculate the distance of two points on a sphere.

*Return to Section 4.2.6.*

# Appendix F: AIS and IVS recorded draught

Section 4.2.6 describes why the IVS recorded draught is used for the analysis, rather than the AIS draught. This appendix shows the differences between the IVS and AIS for all vessels in the dataset. Figures F.1 and F.2 show the distribution of the recorded AIS and IVS draughts respectively, together with the average deviation of the IVS recorded draughts from the AIS recorded draughts in Figure F.3. Especially ships with a smaller recorded IVS draught have a large deviation in IVS and AIS draught on average.
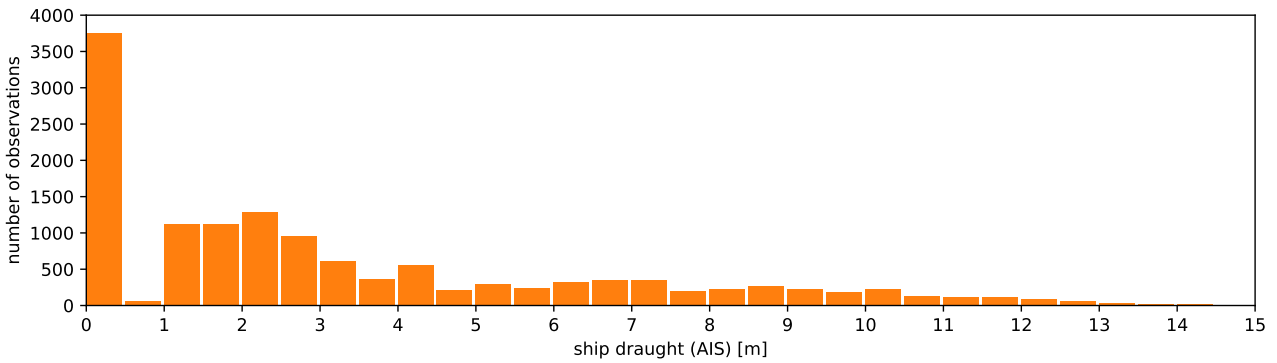


Figure F.1: Distribution of the ship AIS draughts observed during the measurement campaign.
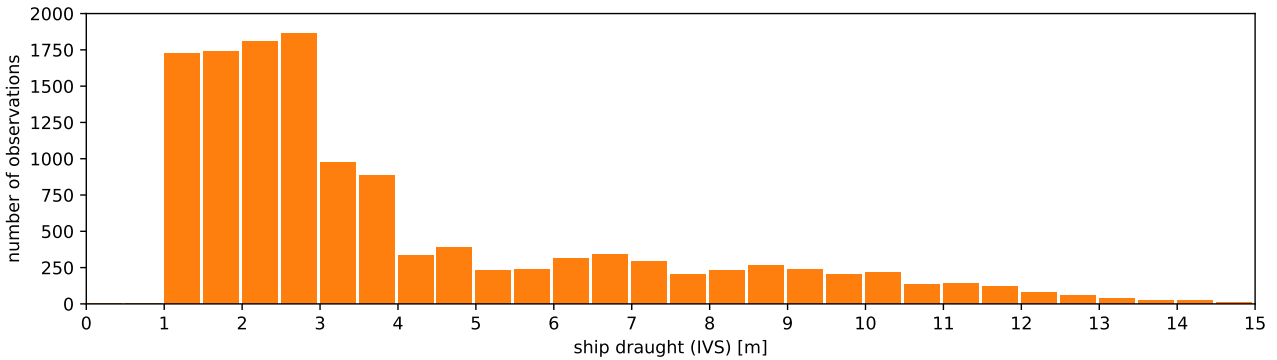


Figure F.2: Distribution of the ship IVS draughts observed during the measurement campaign.
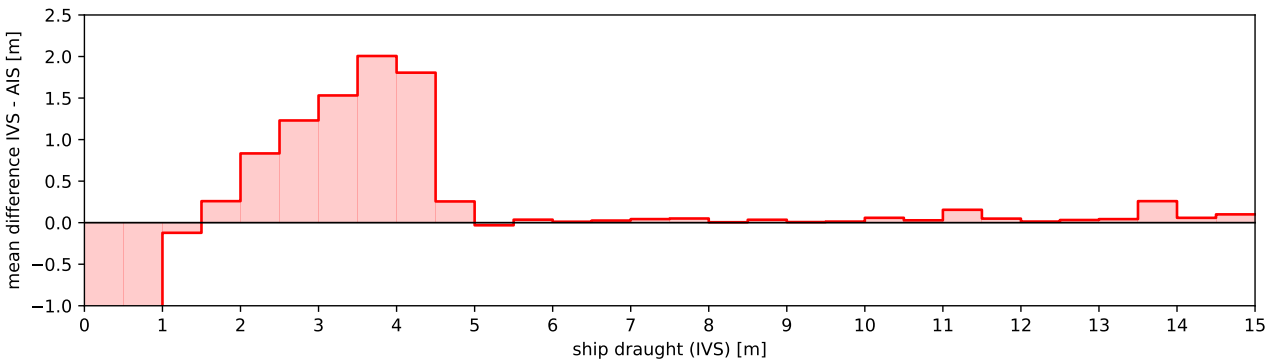


Figure F.3: Distribution of the deviation in IVS and AIS draughts observed during the measurement campaign.

# Appendix G: Drawdown characterization

Section 4.3.2 explains that three key points in the time series of the water level fluctuations are used, in order to express the phenomena with parameters. This appendix explains how these three points are determined. The localization of the initial maximum, the minimum and the secondary maximum is done by setting for each of the points a time interval of 60 seconds in which the maximum or minimum is determined, shown in Figure G.1. The timing of this search interval is calculated based on the expected arrival time of the bow, drawdown and aft wave.
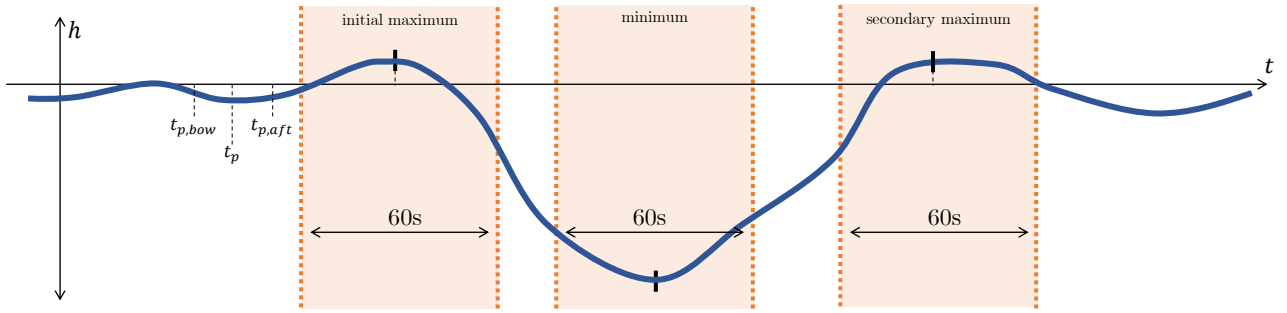


Figure G.1: Schematization of the drawdown wave, including the search intervals for the initial maximum, the minimum and secondary maximum water level.

## G.1 Expected arrival time of the bow, drawdown and aft wave

It is assumed that the initial maximum in water level relates to the bow wave, the minimum relates to the drawdown and the secondary maximum relates to the aft wave, as introduced in Section 3.1, Figure 3.1. A prediction of the expected observation time of initial maximum ($t_{\mathrm{max},1}$), minimum ($t_{\mathrm{min}}$) and secondary maximum ($t_{\mathrm{max},2}$) water level is made, based on the passage time of the bow ($t_{p,\mathrm{bow}}$), middle ($t_{p,\mathrm{mid}}$) and aft ($t_{p,\mathrm{aft}}$) of the vessel (Section 4.3.1) and the time it takes for the wave to travel from the vessel to sensor $S$ ($\Delta t_S$):

$$t_{\mathrm{max},1,S} = t_{p,\mathrm{bow}} + \Delta t_S \tag{G.1}$$

$$t_{\mathrm{min},S} = t_{p,\mathrm{mid}} + \Delta t_S \tag{G.2}$$

$$t_{\mathrm{max},2,S} = t_{p,\mathrm{aft}} + \Delta t_S \tag{G.3}$$

The time it takes for the wave to travel from the vessel to sensor $S$ ($\Delta t_S$) is based on the distance from the passing vessel to the harbour entrance ($d_s$), the effective distance between the entrance and sensor $S$ ($\Delta l_S$) and the wave celerity ($c$). In the shallow water regime, the wave celerity ($c$) can be estimated by taking the square root of the water depth ($h$) multiplied by the gravitational acceleration ($g$) ($c = \sqrt{gh}$) (Holthuijsen, 2007). In this analysis, for the stretch between the vessel and the harbour entrance, a general channel depth ($z_{\mathrm{channel}}$) of -28 mNAP is assumed, based on the profile in Figure C.12. For the stretch between the harbour entrance to the sensors, a harbour depth ($z_{\mathrm{harbour}}$) of -7 mNAP is assumed. Subtracting these values from the water level (WL) at the time of passage provides the depth in the channel and harbour. The effective distances between the entrance and the sensors are based on the assumed path the crest of the waves travel through the harbour, elaborated in Section 4.3.2, Figure 4.12. The distances used are as follows: 700 metres from the entrance to Sensor 1 ($\Delta l_{01}$), 920 metres from the entrance to Sensor 3 ($\Delta l_{03}$) and 1200 metres from the entrance to Sensor 2 ($\Delta l_{02}$). Using these values, the travel time between the vessel and sensor $S$ can be calculated subsequently:

$$\Delta t_S = \frac{d_s}{\sqrt{g(\mathrm{WL} - z_{\mathrm{channel}})}} + \frac{\Delta l_S}{\sqrt{g(\mathrm{WL} - z_{\mathrm{harbour}})}} \tag{G.4}$$

## G.2     Localizing the minimum water level

Although this method simplifies the processes affecting the speed at which drawdown travels from the passing vessel to the measurement locations significantly, it provides a point in time which is dynamically dependent on the relevant parameters influencing the observation time of the minimum, such as water level, passing distance, vessel length and speed. Practical observations show that the observed time of maximum drawdown, $t_{min}$, is best captured by a search interval of 40 seconds before the expected drawdown arrival time and 20 seconds after this time. Furthermore, the start of the search interval of the wave should be after the passage time of the middle of the vessel ($t_p$). Figure G.2 confirms this, as a clear maximum of observations is observed in the middle of the search boundary. Nevertheless, besides the observations captured by the search interval, a notable number of observations are encountered at the boundaries of the search area. This is inevitable due to the noise in the data.
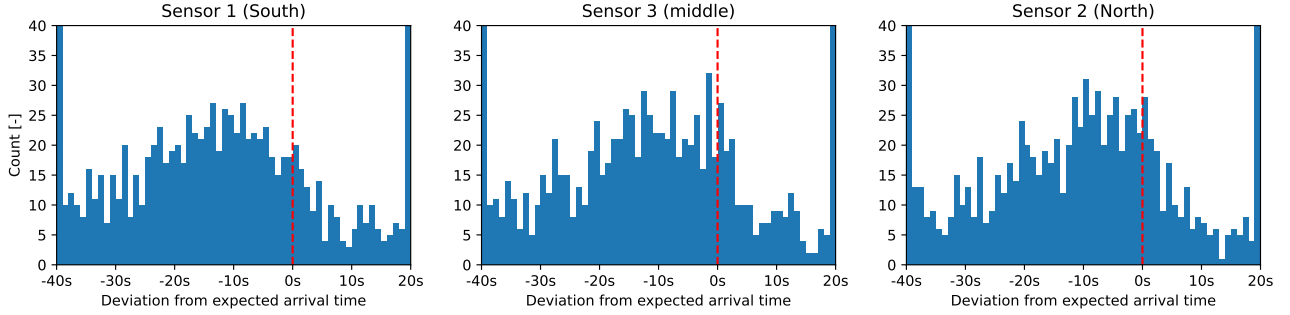


Figure G.2: The positioning of the found minimum water levels in the search interval ($t_{min}$), relative to the expected drawdown arrival time, marked as the red vertical line.

## G.3     Localizing the secondary maximum water level

The secondary maximum water level related to the aft wave of the vessel, $h_{max,2}$, is best captured by a search interval bounded by the expected arrival time of the aft wave, and 60 seconds after this time, shown in Figure G.3. Furthermore, the start of the search interval for the aft wave should be greater than the time of maximum drawdown ($t_{min}$), determined previously.
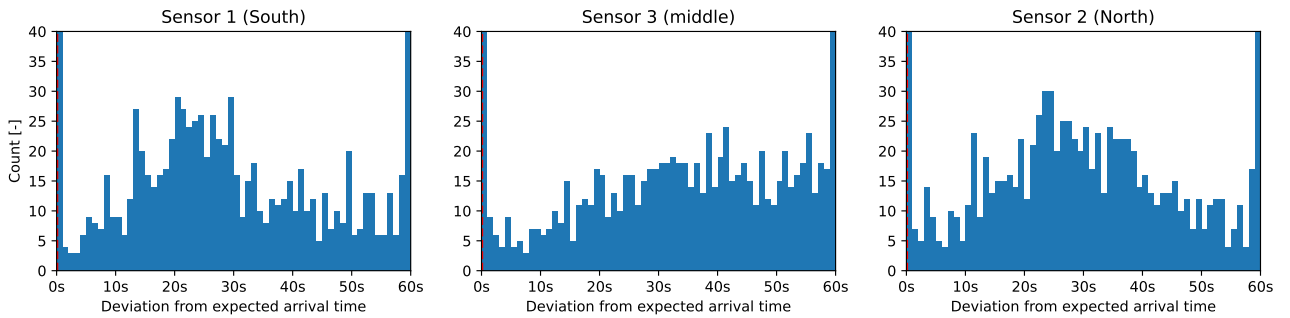


Figure G.3: The positioning of the found secondary maximum water levels in the search interval ($t_{max,2}$), relative to the expected aft wave arrival time.

## G.4     Localizing the initial maximum water level

The observed arrival time of the bow wave, denoted as $h_{max,1}$ in Figure 4.11, deviates significantly from the calculated arrival time. Visual inspection of the time series shows that a search interval ranging from 100 seconds to 40 seconds prior to the anticipated arrival time of the bow wave yields the most precise determination of the maximum. A secondary restriction to the search interval is that the start of the search interval cannot be before the time of passage of the bow of the passing vessel. Furthermore, the end of the search interval should not be greater than the time of maximum drawdown ($t_{min}$), determined previously. Figure G.4 shows a less convincing number of observations in the middle of the search boundary. This can be attributed to the

challenge of distinguishing the bow wave in the time series in cases of limited primary wave magnitude. Apart from this, there is sufficient confidence in the accuracy of this maximum determination, because it is in most cases constrained by both the time of bow passage and the time of minimum water level. However, as confidence is greater in the predictability of the aft wave, the corresponding maximum ($h_{max,2}$) is used to determine the drawdown height. Figure G.5 shows an example of the search intervals and the maxima and minimum being identified within this interval.
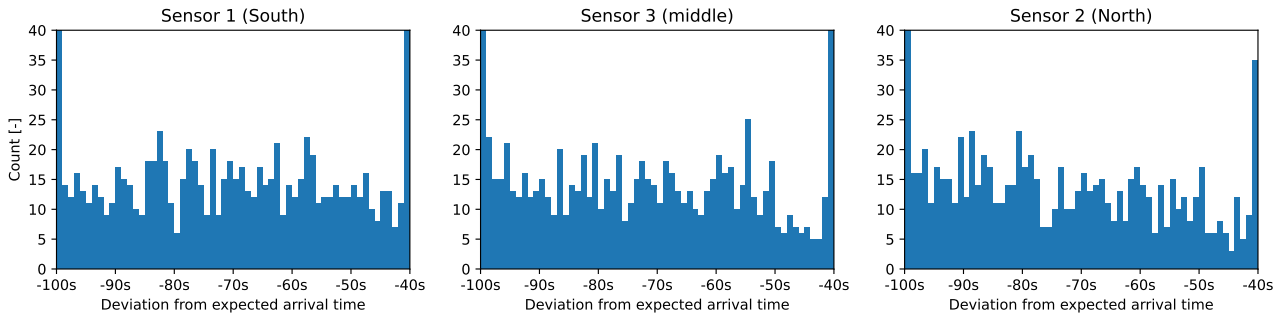


Figure G.4: The positioning of the found primary maximum water levels in the search interval ($t_{max,1}$), relative to the expected bow wave arrival time.
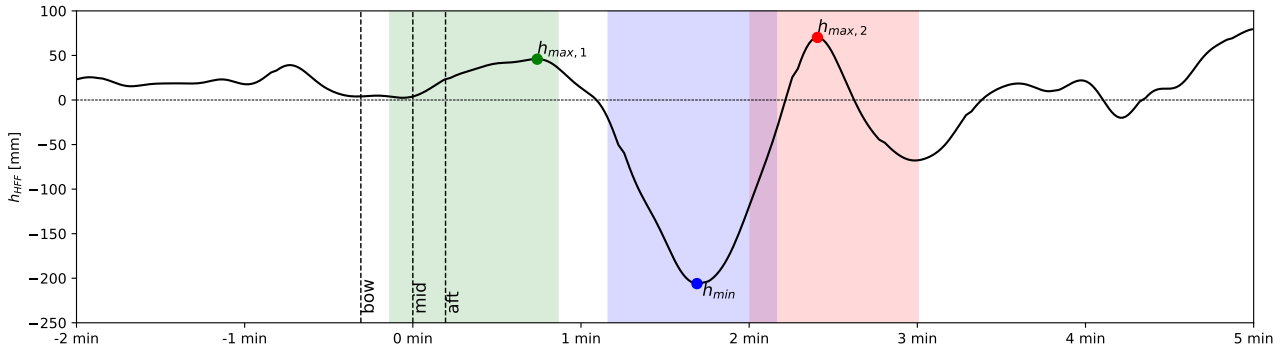


Figure G.5: Example of the search intervals for the initial maximum, minimum and secondary maximum water level.

*Return to Section 4.3.2.*

# Appendix H: Sample data and calculations

Table H.1 shows the parameters retrieved from the different data sources and the calculated parameters for eight arbitrary passages. The Python code used to calculate the drawdown height is available via the https://github.com/DickHeijboer/DrawdownHeightEquations.git repository

| static vessel parameters | | | | | | | | |
|---|---|---|---|---|---|---|---|---|
| MMSI | 215651000 | 636020917 | 566961000 | 372341000 | 566954000 | 373712000 | 353728000 | 636092781 |
| vessel type | cargo | tanker | cargo | tanker | cargo | cargo | cargo | cargo |
| length ($L_s$) [m] | 269 | 183 | 329 | 159 | 398 | 334 | 349 | 300 |
| width ($B_s$) [m] | 32 | 32 | 46 | 27 | 51 | 48 | 44 | 46 |
| draught IVS ($D_s$) [m] | 10.5 | 10.4 | 10.2 | 10.5 | 11.4 | 10.3 | 12.1 | 12 |
| draught AIS [m] | 10.2 | 10.4 | 10.2 | 10.5 | 11.4 | 10.3 | 12.1 | 12 |
| midship coefficient ($C_m$) | 0.975 | 0.995 | 0.975 | 0.995 | 0.975 | 0.975 | 0.975 | 0.975 |
| block coefficient ($C_B$) | 0.65 | 0.84 | 0.65 | 0.84 | 0.65 | 0.65 | 0.65 | 0.65 |
| underwater cross-section ($A_s$) [m$^2$] | 328 | 331 | 457 | 282 | 567 | 482 | 519 | 538 |
| water displacement ($\Delta_s$) [m$^3$] | 58750 | 51158 | 100338 | 37864 | 150408 | 107334 | 120775 | 107640 |
| **dynamic vessel parameters** | | | | | | | | |
| date | 2023-06-29 | 2023-07-07 | 2023-07-10 | 2023-07-14 | 2023-07-22 | 2023-07-26 | 2023-08-06 | 2023-08-10 |
| passage time bow ($t_{p,\text{bow}}$) | 22:25:45 | 15:21:25 | 11:51:31 | 01:38:26 | 01:24:05 | 16:52:30 | 04:25:09 | 15:41:04 |
| passage time mid ($t_{p,\text{mid}}$) | 22:26:04 | 15:21:51 | 11:51:54 | 01:38:47 | 01:24:29 | 16:53:00 | 04:25:31 | 15:41:23 |
| passage time aft ($t_{p,\text{aft}}$) | 22:26:25 | 15:22:07 | 11:52:18 | 01:38:57 | 01:24:59 | 16:53:21 | 04:25:55 | 15:41:41 |
| passing distance ($d_s$) [m] | 405 | 338 | 287 | 617 | 309 | 480 | 289 | 339 |
| speed over ground ($V_{s,g}$) [m/s] | 6.8 | 4.8 | 7.4 | 5.6 | 7.5 | 6.8 | 7.4 | 9.5 |
| course over ground ($\theta_{s,g}$) | 302 | 297 | 296 | 119 | 295 | 297 | 298 | 297 |
| true heading (TH) [deg] | 295 | 290 | 295 | 121 | 290 | 295 | 292 | 290 |
| bed level (BL) [mNAP] | -22.5 | -25.4 | -26.4 | -24.2 | -25.9 | -24.7 | -25.2 | -24.4 |
| depth ($h_s$) [m] | 23.3 | 24.7 | 27.3 | 26.2 | 23.9 | 23.7 | 25.2 | 23 |
| under keel clearance (UKC) [m] | 12.8 | 14.3 | 17.1 | 15.7 | 12.5 | 13.4 | 13.1 | 11 |
| speed through the water ($V_s$) [m/s] | 7.7 | 5.8 | 6.2 | 5.4 | 6.8 | 7.3 | 8.5 | 8.6 |
| drift angle rel. vessel ($\delta_{s,v}$) [deg] | 7 | 7.2 | 1.1 | -2.4 | 5.2 | 2.2 | 5.8 | 6.9 |
| drift angle rel. obsv. ($\delta_{s,o}$) [deg] | -7 | -7.2 | -1.1 | -2.4 | -5.2 | -2.2 | -5.8 | -6.9 |
| **environmental parameters** | | | | | | | | |
| water level (WL) [mNAP] | 0.8 | -0.8 | 0.9 | 2 | -2 | -0.9 | 0 | -1.4 |
| current magnitude ($U_c$) [m/s] | 1 | 1 | 1.3 | 0.2 | 0.7 | 0.5 | 1.1 | 0.9 |
| current direction ($\theta_c$) [deg] | 106 | 104 | 282 | 92 | 286 | 105 | 105 | 280 |
| wind magnitude ($U_w$) [m/s] | 2.4 | 5.3 | 2.3 | 7.4 | 6.9 | 5.1 | 4.3 | 1.6 |
| wind direction ($\theta_w$) [deg] | 343 | 130 | 205 | 232 | 236 | 280 | 161 | 135 |
| **drawdown parameters** | | | | | | | | |
| drawdown height S1 ($\Delta h_1$) [cm] | 7 | 5 | 14 | 2 | 26 | 11 | 39 | 30 |
| drawdown height S3 ($\Delta h_3$) [cm] | 9 | 5 | 15 | 2 | 22 | 9 | 34 | 28 |
| drawdown height S2 ($\Delta h_2$) [cm] | 7 | 3 | 14 | 1 | 20 | 7 | 40 | 33 |
| drawdown period S1 ($T_1$) [s] | 148 | 191 | 162 | 142 | 157 | 193 | 102 | 110 |
| drawdown period S3 ($T_3$) [s] | 151 | 148 | 145 | 144 | 173 | 164 | 124 | 114 |
| drawdown period S2 ($T_2$) [s] | 151 | 154 | 182 | 82 | 171 | 143 | 145 | 116 |
| drawdown slope S13 ($I_{13}$) [$10^{-3}$ m/m] | 0.2 | 0.1 | 0.4 | 0 | 1 | 0.3 | 1.5 | 1.3 |
| drawdown slope S32 ($I_{32}$) [$10^{-3}$ m/m] | 0.1 | 0.1 | 0.3 | 0 | 0.8 | 0.3 | 1.1 | 1 |
| **drawdown height predictions** | | | | | | | | |
| Schijf [cm] | 13 | 7 | 10 | 4 | 20 | 18 | 29 | 36 |
| Schijf corrected [cm] | 90 | 55 | 64 | 48 | 79 | 85 | 113 | 117 |
| Hochstein [cm] | 12 | 6 | 9 | 4 | 19 | 17 | 24 | 28 |
| Gelencser (at S1) [cm] | 14 | 6 | 25 | 3 | 50 | 28 | 44 | 34 |
| Dand and White [cm] | 8 | 5 | 8 | 3 | 15 | 13 | 19 | 22 |
| Bhowmik (at S1) [cm] | 7 | 4 | 6 | 2 | 11 | 9 | 14 | 14 |
| Maynord (at S1) [cm] | 19 | 22 | 26 | 12 | 28 | 20 | 27 | 27 |
| Kriebel [cm] | 35 | 12 | 15 | 9 | 24 | 28 | 57 | 71 |
| CIRIA [cm] | 87 | 54 | 62 | 47 | 76 | 83 | 109 | 112 |
| Site-specific equation [cm] | 7 | 5 | 13 | 1 | 24 | 9 | 30 | 24 |

Table H.1: Sample data from eight arbitrary passages.

# Appendix I: Overview of passage data

This appendix visualizes the additional parameters collected for every passing vessel not treated in Section 5.2.
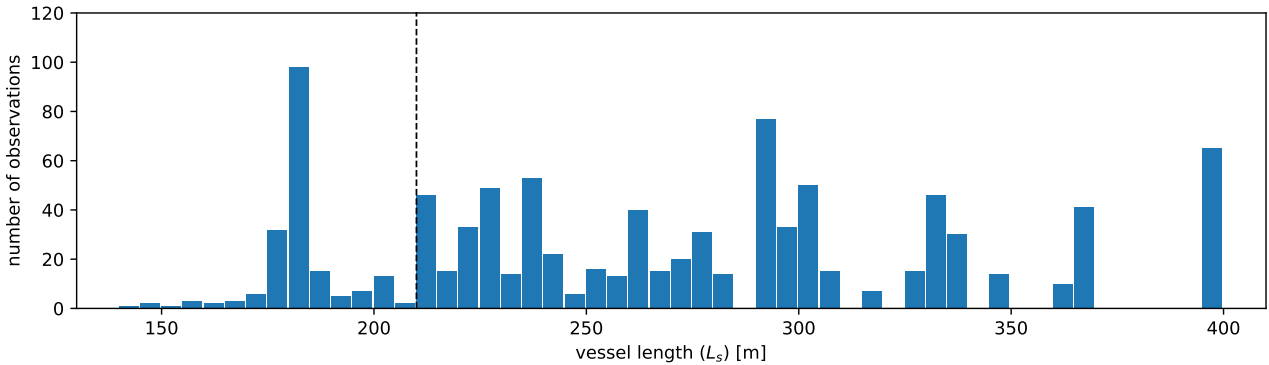


Figure I.1: Distribution of the lengths of the oversized vessels passing the outer harbour during the measurement campaign. The dotted line marks the 210-metre limit, beyond which vessels are classified as oversized; observations to the left represent vessels exceeding 10 metres in draught.
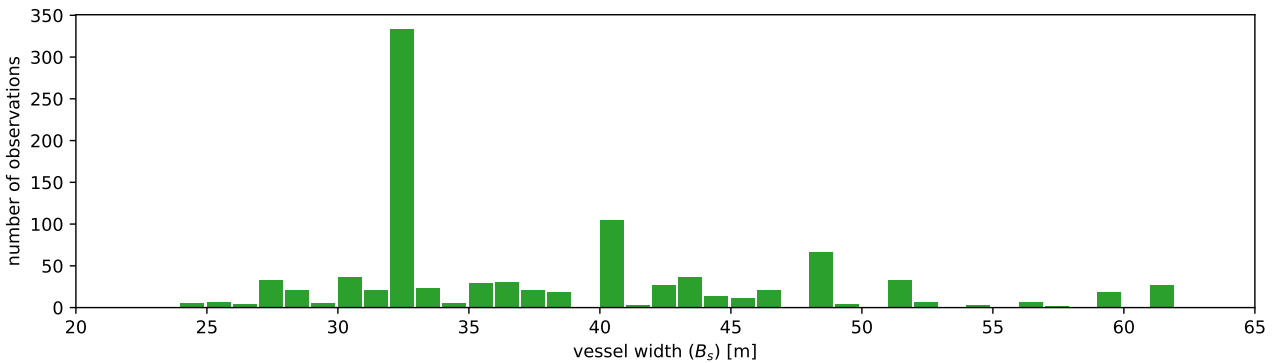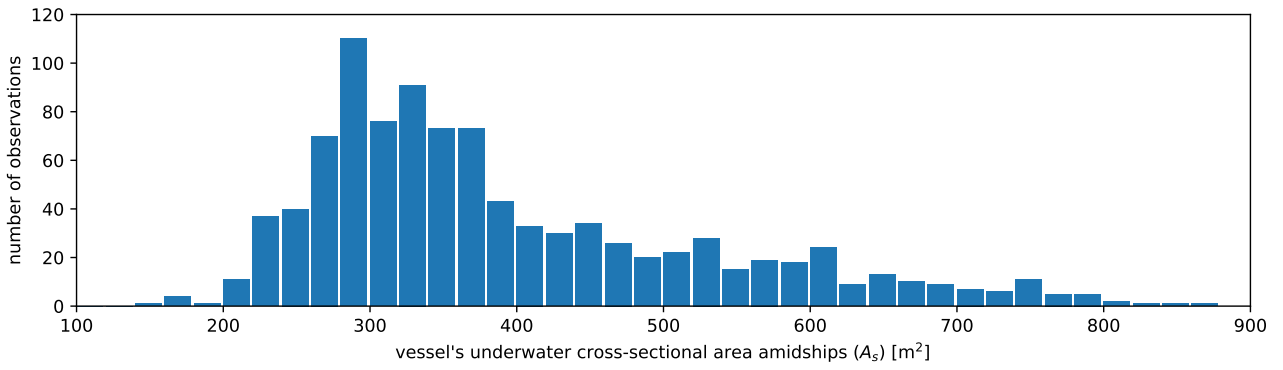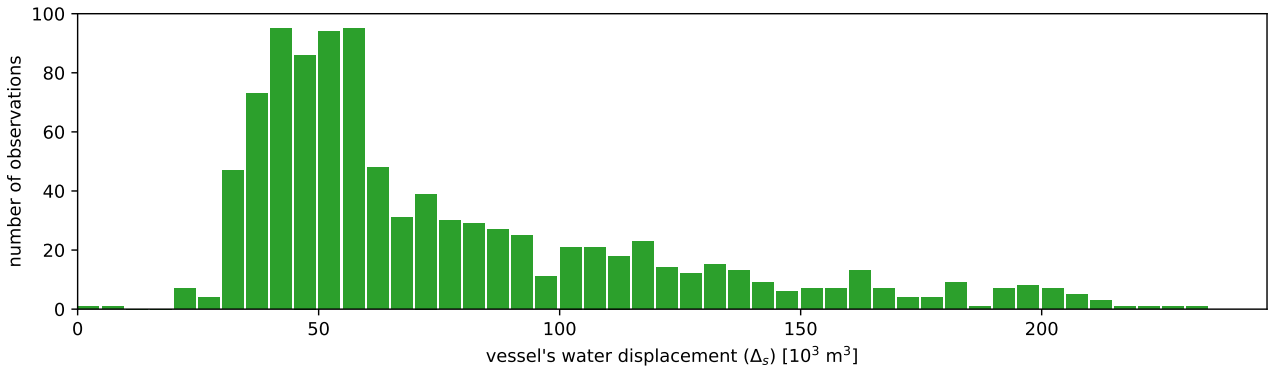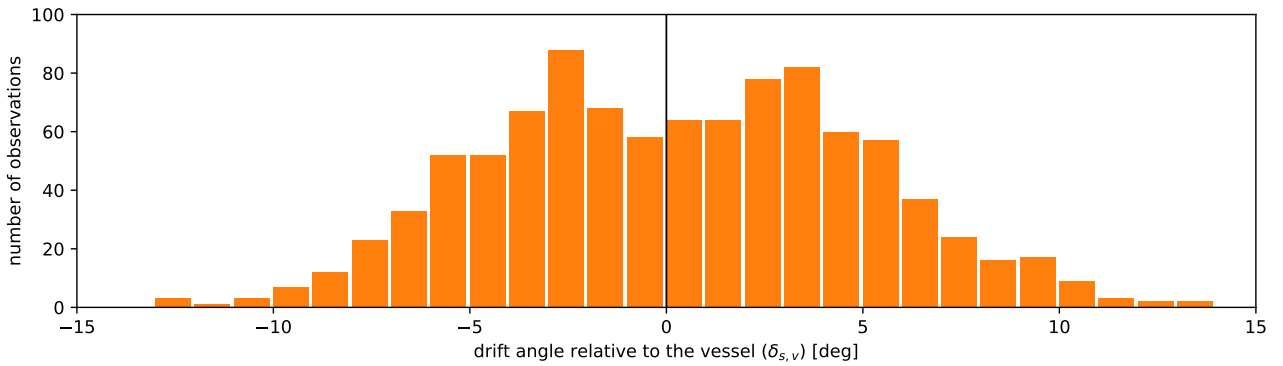


Figure I.2: Distribution of the widths of the oversized vessels passing the outer harbour during the measurement campaign.
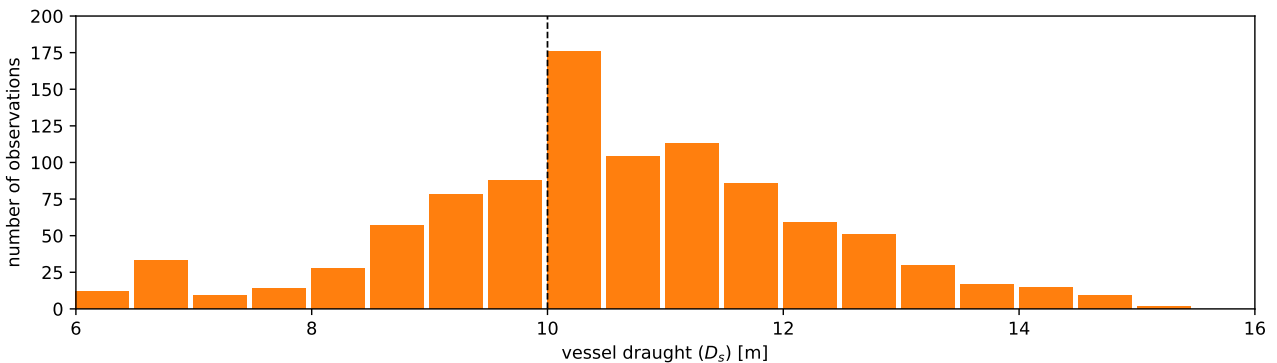


Figure I.3: Distribution of the (IVS) draughts of the oversized vessels passing the outer harbour during the measurement campaign. The dotted line marks the 10-metre limit, beyond which vessels are classified as oversized; observations to the left represent vessels exceeding 210 metres in length.

Figure I.4: Distribution of the underwater cross-sections amidships of the oversized vessels passing the outer harbour during the measurement campaign.



Figure I.5: Distribution of the water displacements of the oversized vessels passing the outer harbour during the measurement campaign.



Figure I.6: Distribution of the drift angles relative to the vessel coordinate system, of the oversized vessels at their time of passage, recorded during the measurement campaign.
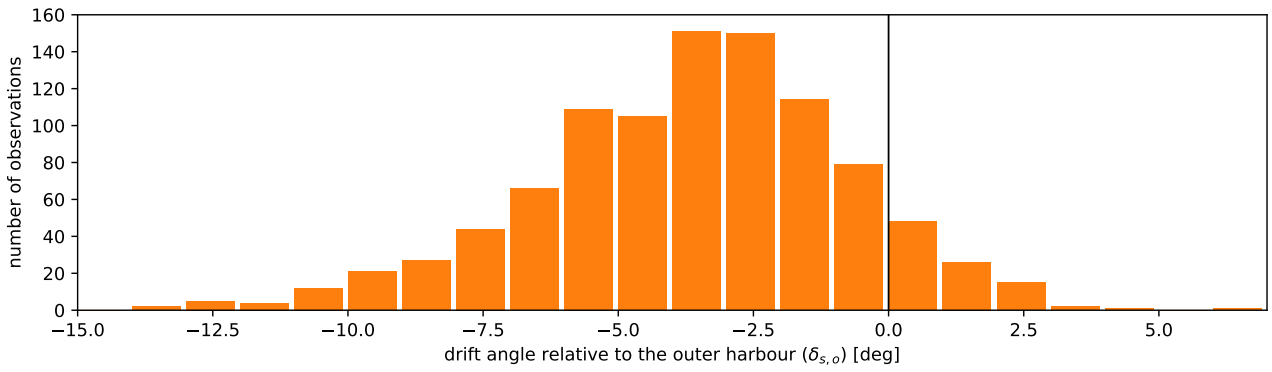
Figure I.7: Distribution of the drift angles relative to the outer harbour, of the oversized vessels at their time of passage, recorded during the measurement campaign.
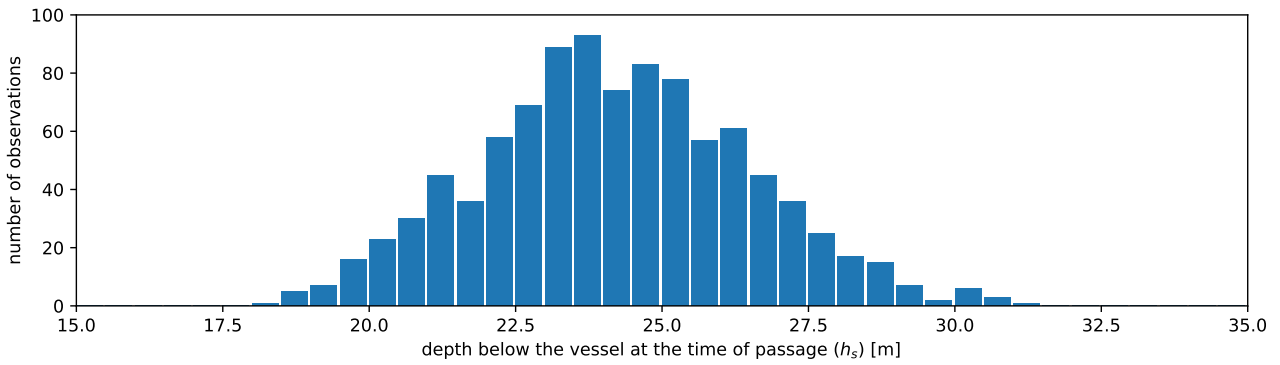


Figure I.8: Distribution of the depths below a passing oversized vessel at their time of passage, recorded during the measurement campaign.
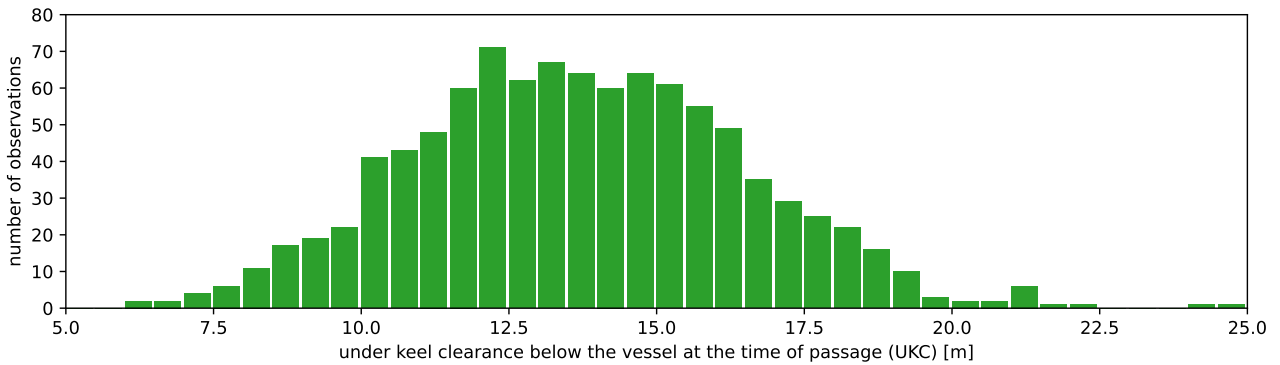


Figure I.9: Distribution of the under keel clearances below a passing oversized vessel at their time of passage, recorded during the measurement campaign.

*Return to Section 5.2.*

# Appendix J: Correlation analysis

This appendix provides the visualizations of the parameters compared against the drawdown height, not treated in Section 5.3. Furthermore, the visualizated correlation between the drawdown period and the other parameters is explored.

## J.1    Drawdown height

Section 5.3.1 discussed the drawdown height ($\Delta h$) in relation to the vessel type, speed through the water, the passing distance, the underwater cross-section and the water level. In this section, the remaining parameters of interest are visualized.
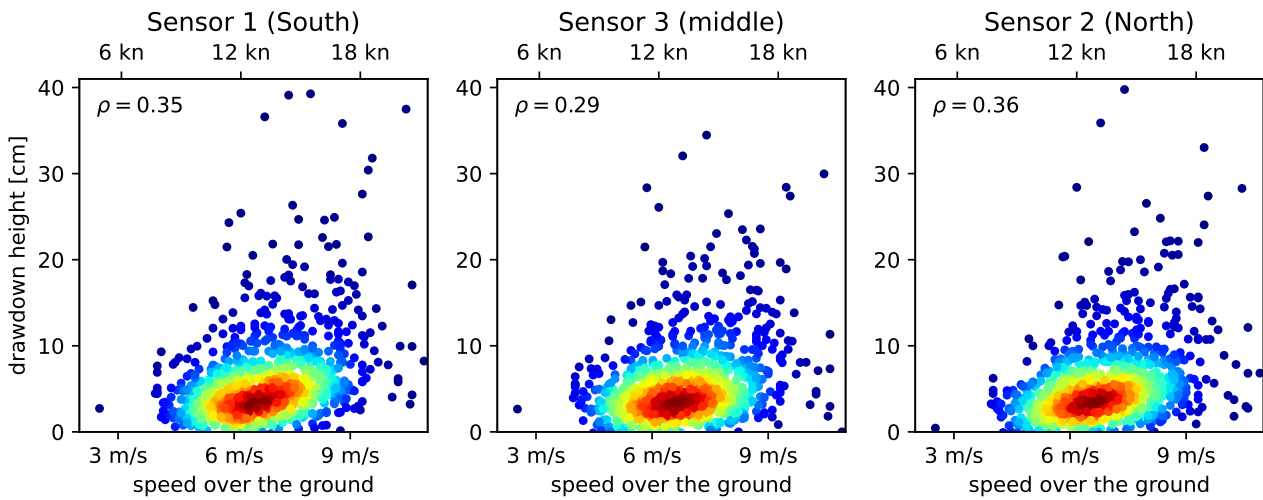


Figure J.1: Drawdown height versus speed over ground (SOG) for sensor 1, 3 and 2.
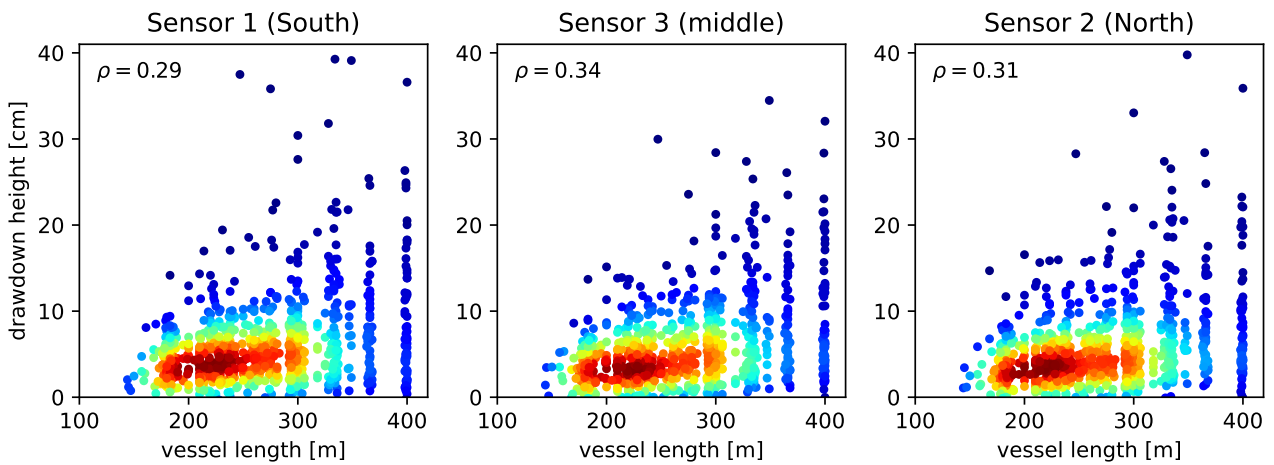


Figure J.2: Drawdown height versus vessel length ($L_s$) for Sensors 1, 3 and 2.
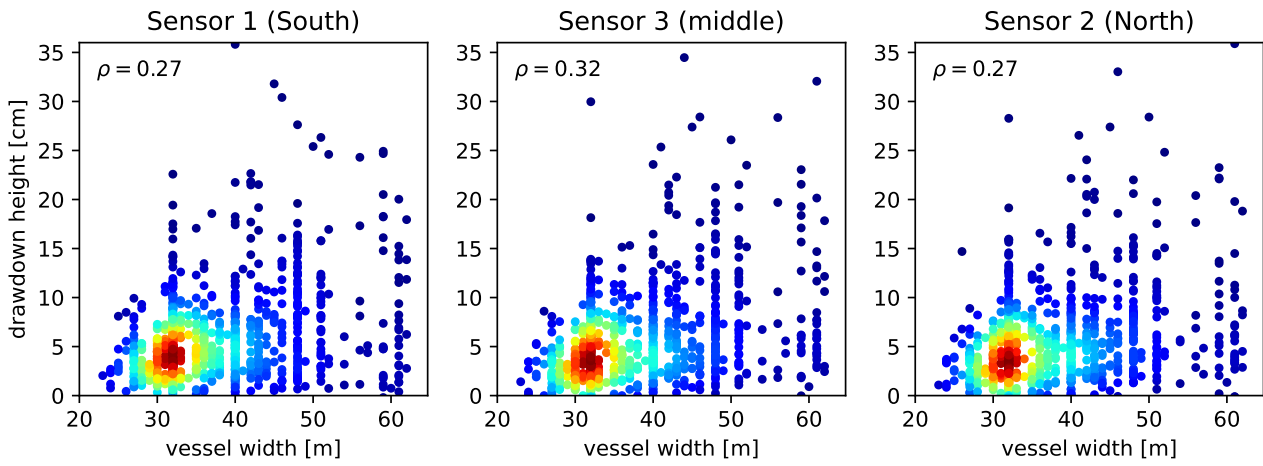
Figure J.3: Drawdown height versus vessel width ($B_s$) for Sensors 1, 3 and 2.
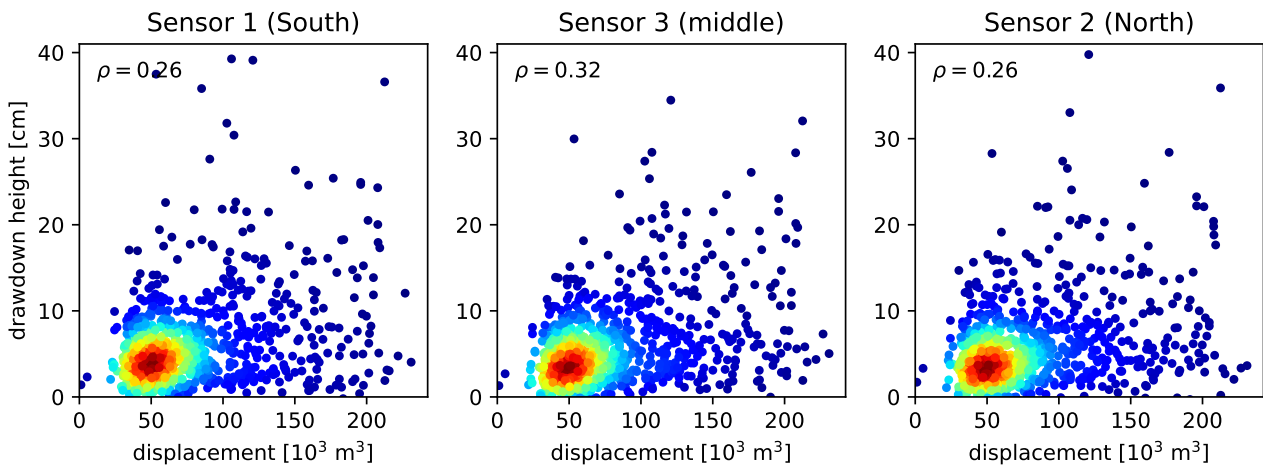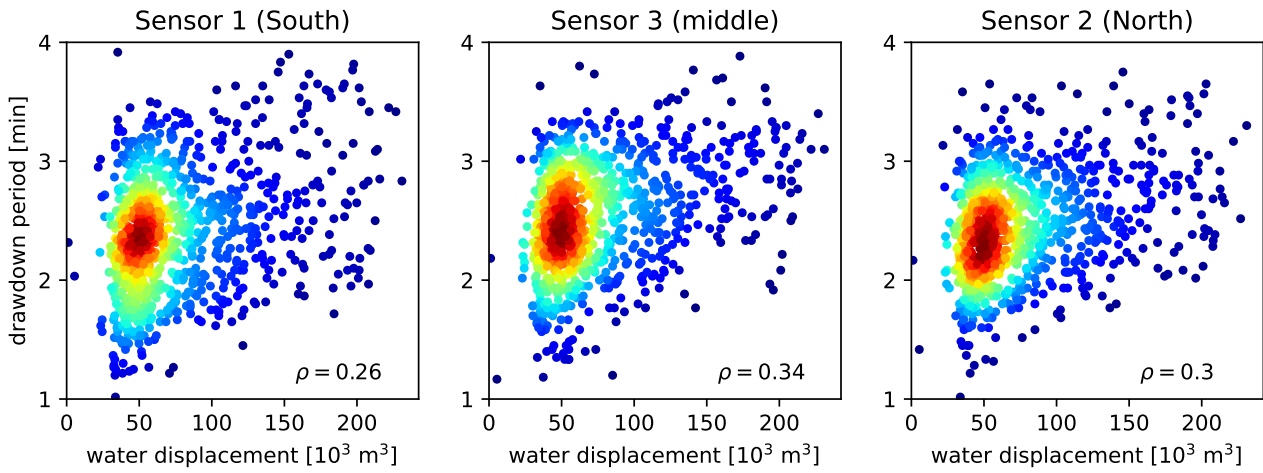


Figure J.4: Drawdown height versus displacement ($\Delta_s$) for Sensors 1, 3 and 2.
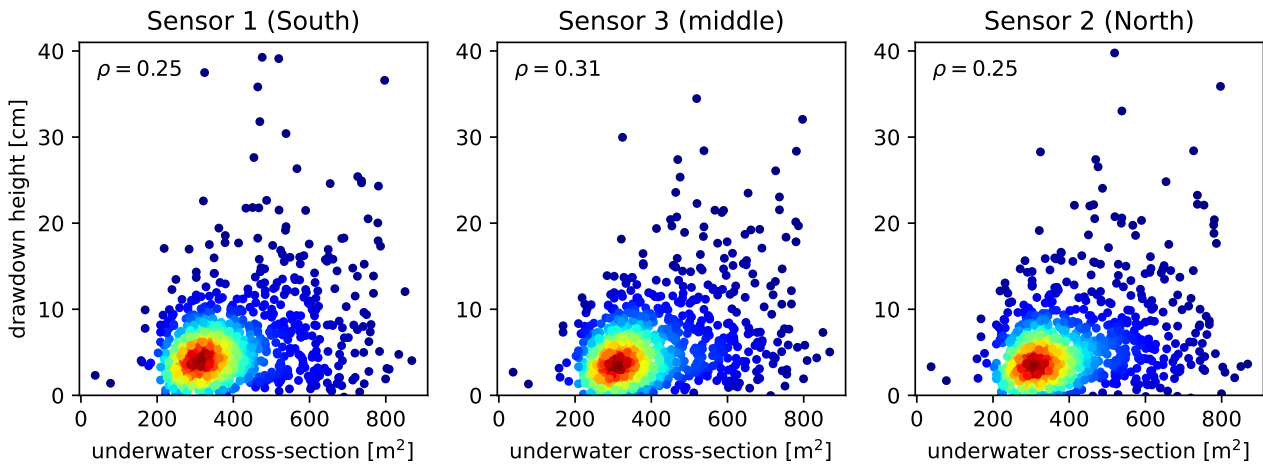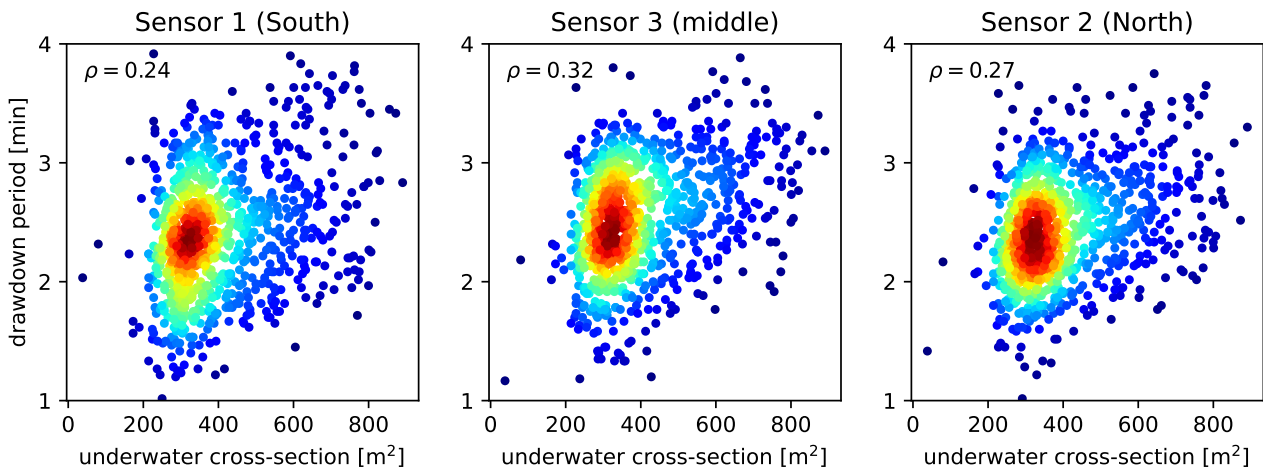


Figure J.5: Drawdown height versus underwater cross-section amidships for Sensors 1, 3 and 2.
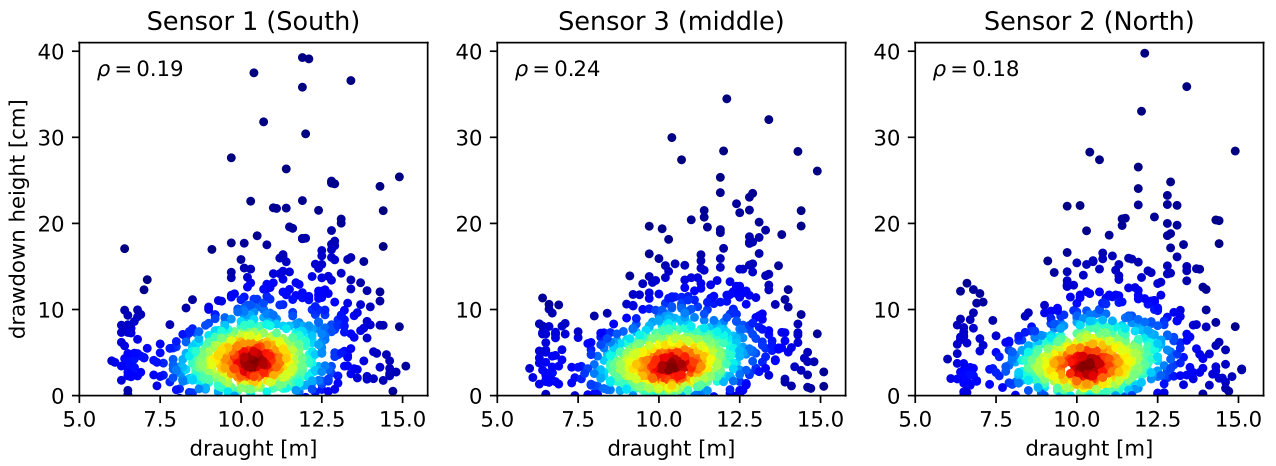
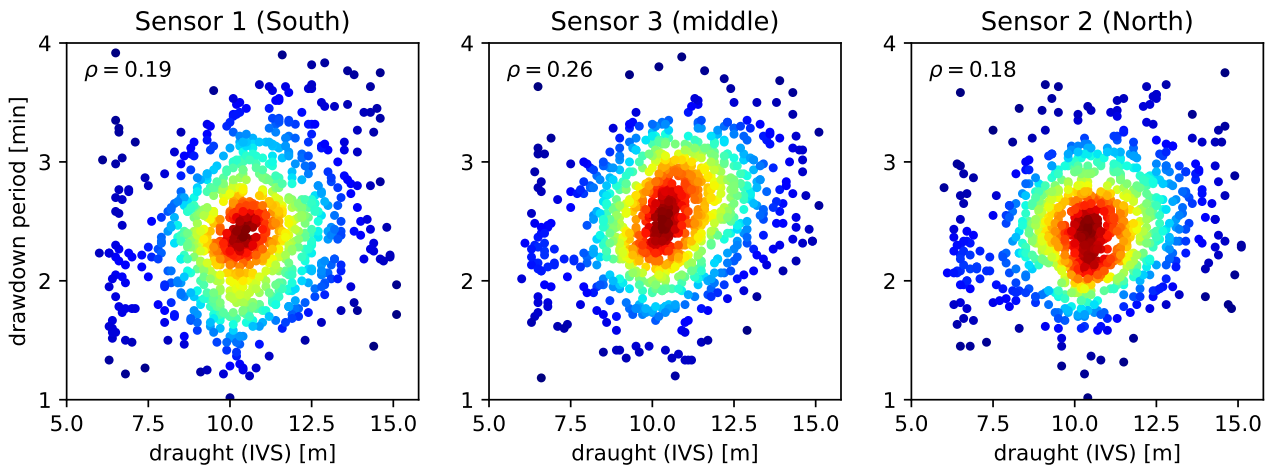Figure J.6: Drawdown height versus (IVS) draught ($D_s$) for Sensors 1, 3 and 2.
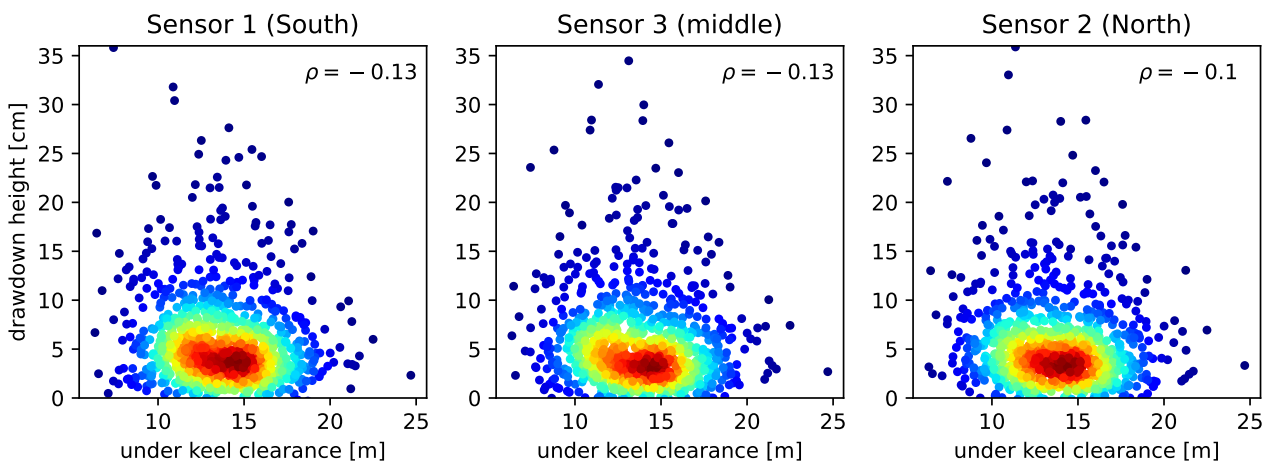


Figure J.7: Drawdown height versus under keel clearance (UKC) for Sensors 1, 3 and 2.
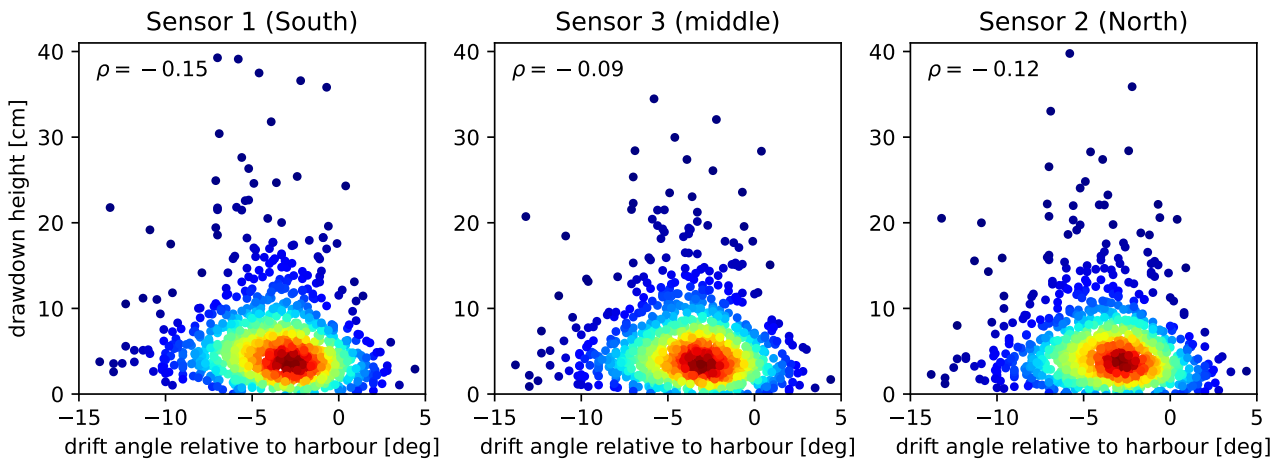


Figure J.8: Drawdown height versus drift angle relative to the outer harbour in a stationary coordinate system ($\delta_{s,o}$) for Sensors 1, 3 and 2.
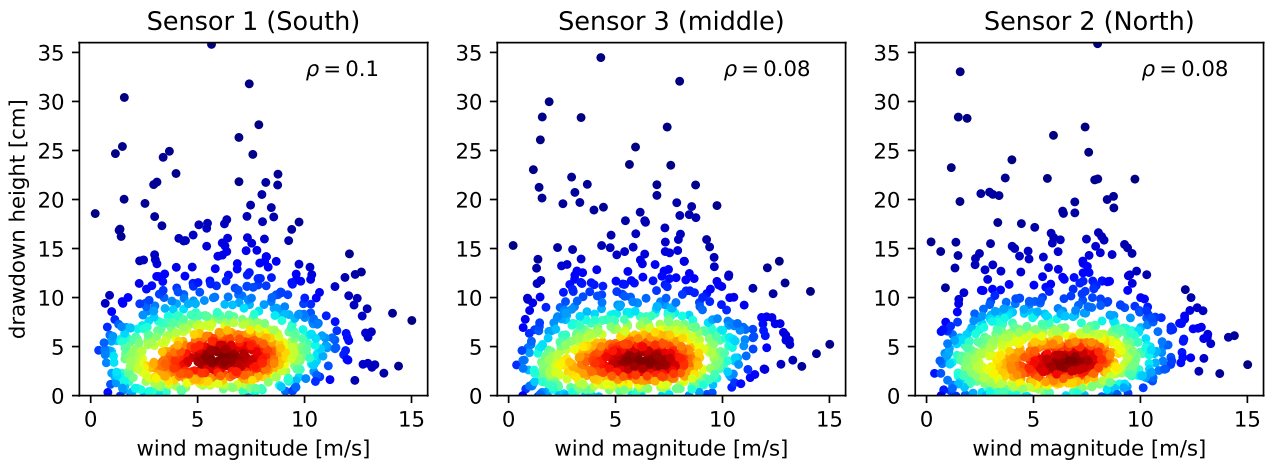
Figure J.9: Drawdown height versus wind magnitude ($U_w$) for Sensors 1, 3 and 2.
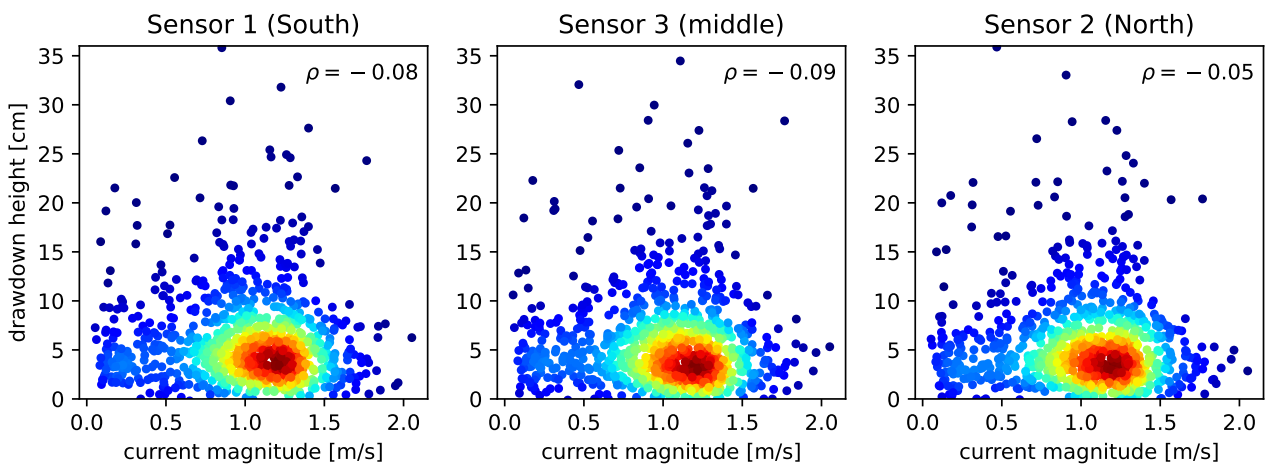


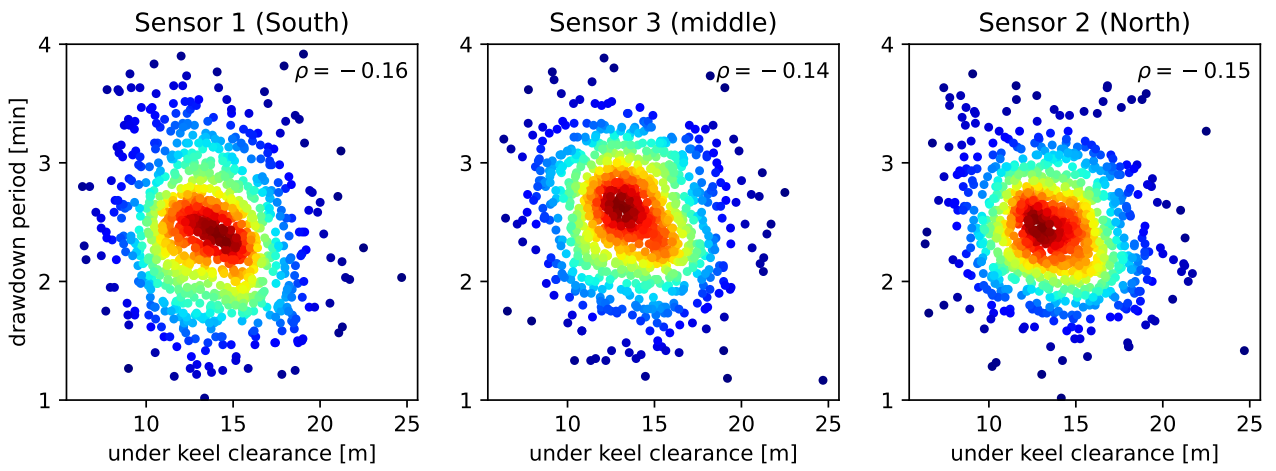Figure J.10: Drawdown height versus current magnitude ($U_c$) for Sensors 1, 3 and 2.
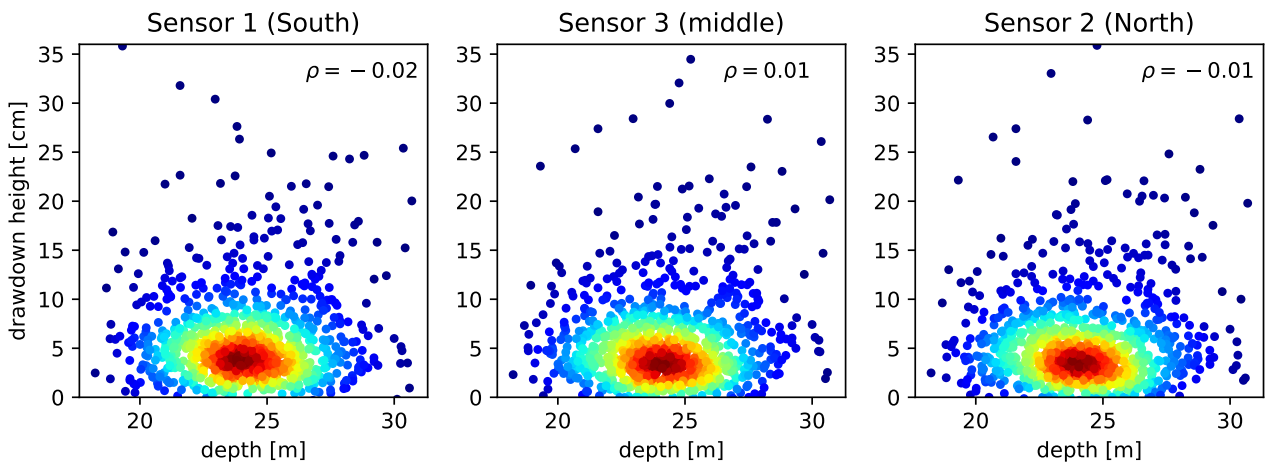


Figure J.11: Drawdown height versus depth at the location of the passing vessel ($h_S$) for Sensors 1, 3 and 2.

## J.2  Drawdown period

As mentioned in Section 5.3.2, similar to the drawdown height, the relation of the drawdown period regarding several parameters is explored. The statistical correlation is expressed as a Spearman correlation coefficient, summarized in Table J.1. The visualizations of the parameters plotted against the drawdown period are given below. The vessel type does visually not affect the drawdown height, shown in Figure J.12.

| parameter | symbol | Sensor 1 (South) | Sensor 3 (middle) | Sensor 2 (North) | visualization |
|---|---|---|---|---|---|
| *weakly corollated* | | | | | |
| speed over the ground | SOG | -0.35 | -0.28 | -0.21 | Figure J.13 |
| displacement | $\Delta_s$ | 0.26 | 0.34 | 0.30 | Figure J.14 |
| underwater cross-section | $A_s$ | 0.24 | 0.32 | 0.27 | Figure J.15 |
| vessel length | $L_s$ | 0.20 | 0.27 | 0.28 | Figure J.16 |
| vessel width | $B_s$ | 0.20 | 0.28 | 0.25 | Figure J.17 |
| draught (IVS) | $D_s$ | 0.19 | 0.26 | 0.18 | Figure J.18 |
| *very weakly corollated* | | | | | |
| speed through the water | $V_s$ | -0.22 | -0.20 | -0.11 | Figure J.19 |
| under keel clearance | UKC | -0.16 | -0.14 | -0.15 | Figure J.20 |
| drift angle | $\delta_s$ | -0.10 | -0.02 | -0.08 | Figure J.21 |
| passing distance | $d_s$ | 0.09 | -0.05 | -0.04 | Figure J.22 |
| depth | $h_s$ | -0.06 | 0.01 | -0.06 | Figure J.23 |
| current magnitude | $U_c$ | 0.04 | 0.05 | 0.04 | Figure J.24 |
| water level | WL | -0.01 | 0.04 | -0.08 | Figure J.25 |
| wind magnitude | $U_w$ | -0.05 | -0.01 | -0.01 | Figure J.26 |

Table J.1: The correlation of the vessel characteristics and environmental variables to the drawdown period, expressed using Spearman's correlation coefficient ($\rho$).
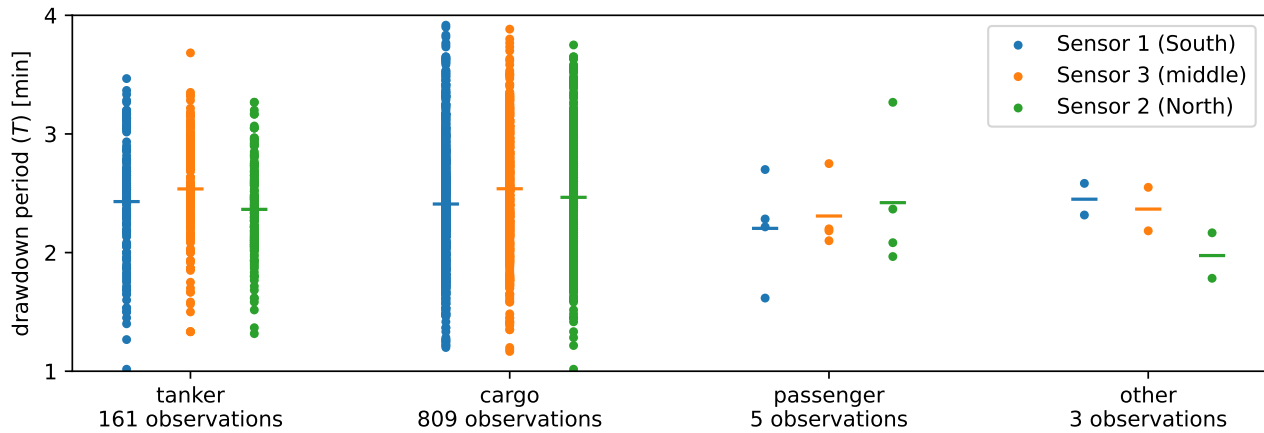


Figure J.12: Drawdown period versus the different vessel types.
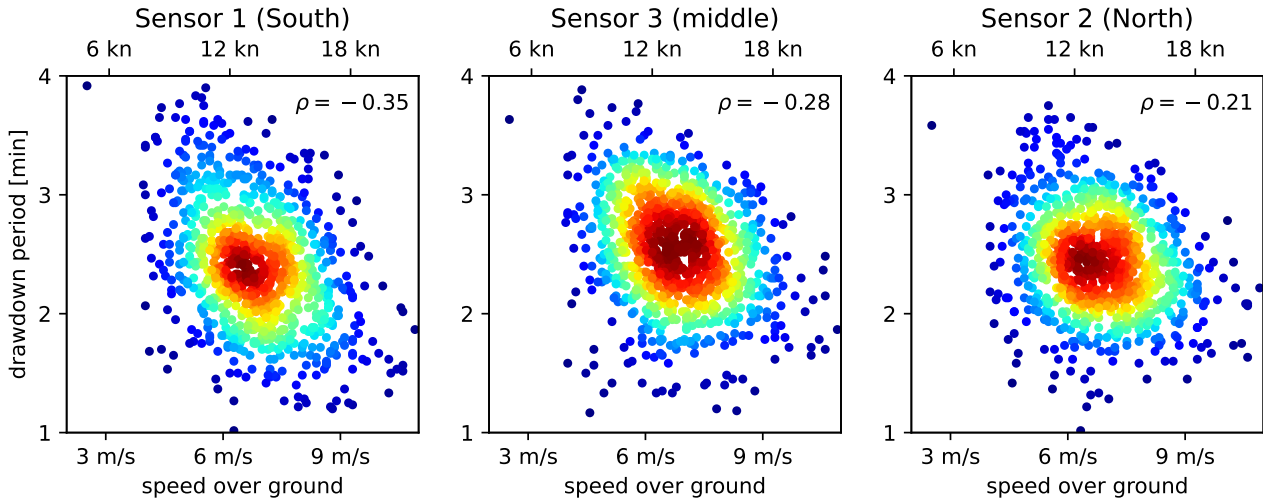
Figure J.13: Drawdown period versus calculated speed over the ground for Sensors 1, 3 and 2.
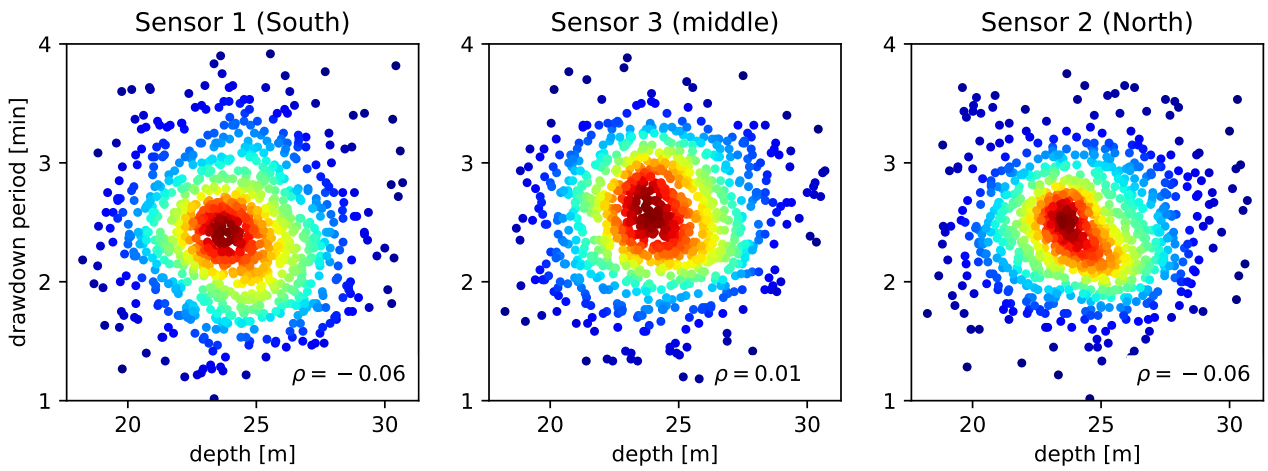


Figure J.14: Drawdown period versus displacement ($\Delta_s$) for Sensors 1, 3 and 2.



Figure J.15: Drawdown period versus underwater cross-section amidships ($A_s$) for Sensors 1, 3 and 2.
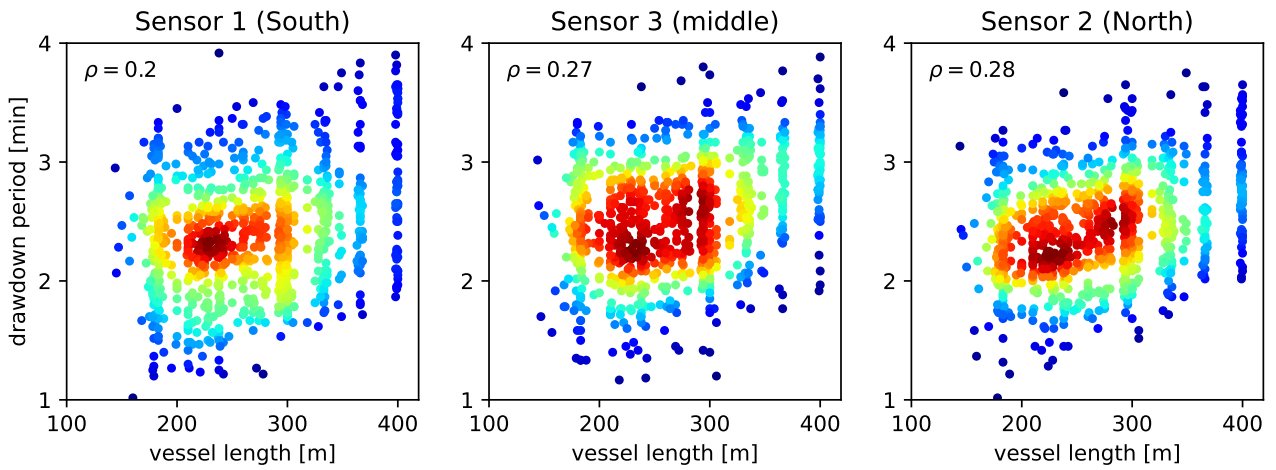
Figure J.16: Drawdown period versus the vessel length for Sensors 1, 3 and 2.
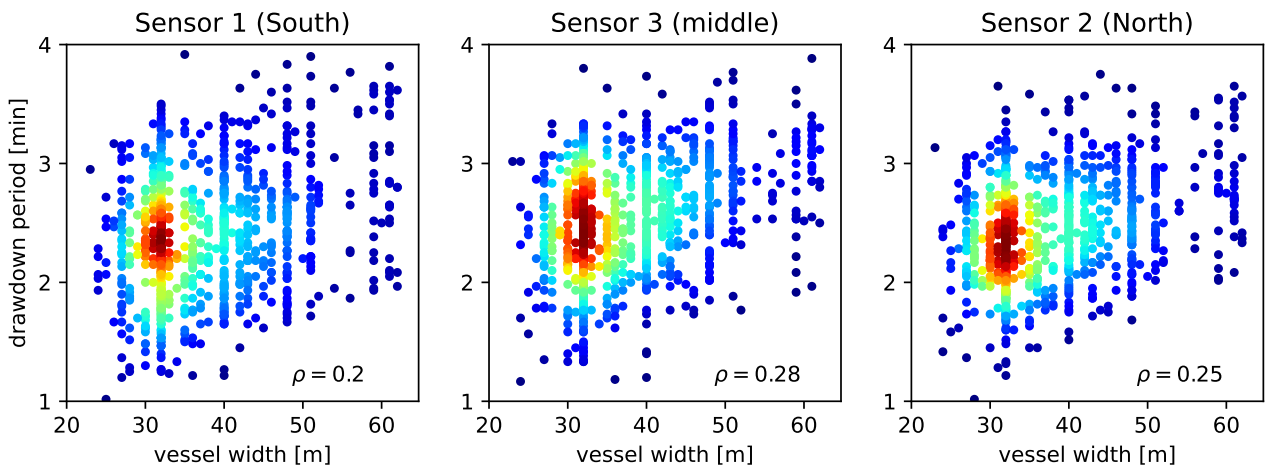


Figure J.17: Drawdown period versus vessel width ($B_s$) for Sensors 1, 3 and 2.



Figure J.18: Drawdown period versus (IVS) draught ($D_s$) for Sensors 1, 3 and 2.
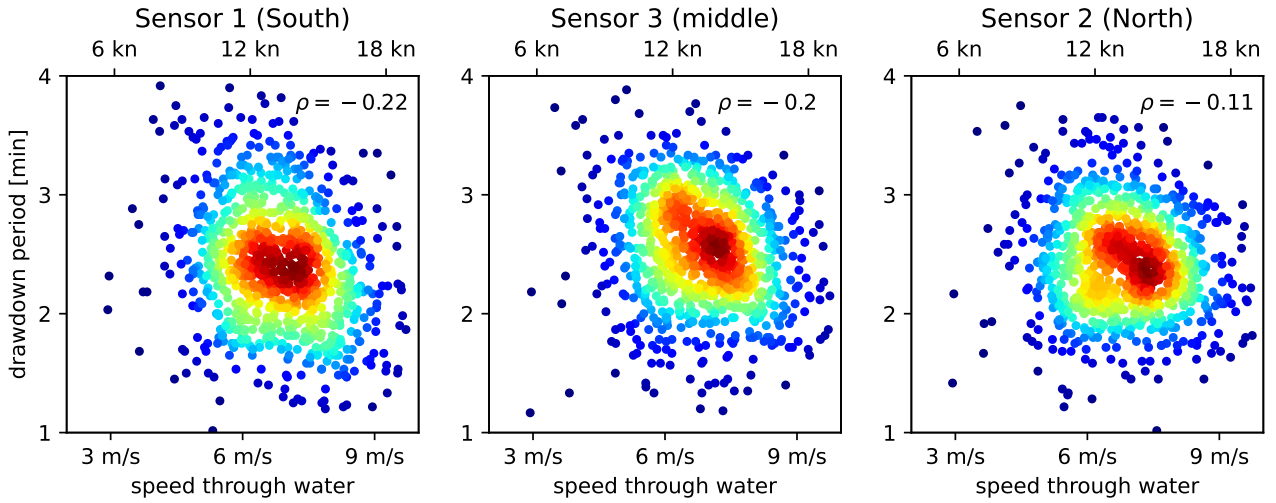
Figure J.19: Drawdown period versus calculated speed through the water ($V_s$) for Sensors 1, 3 and 2.



Figure J.20: Drawdown period versus under keel clearance (UKC) for Sensors 1, 3 and 2.
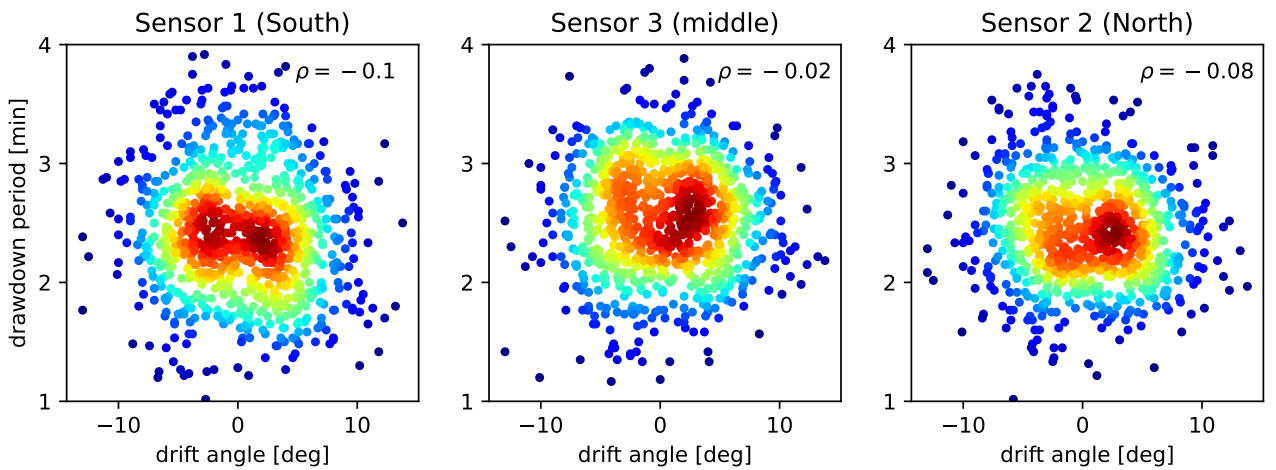


Figure J.21: Drawdown period versus drift angle relative to the vessel ($\delta_{s,v}$) for Sensors 1, 3 and 2.
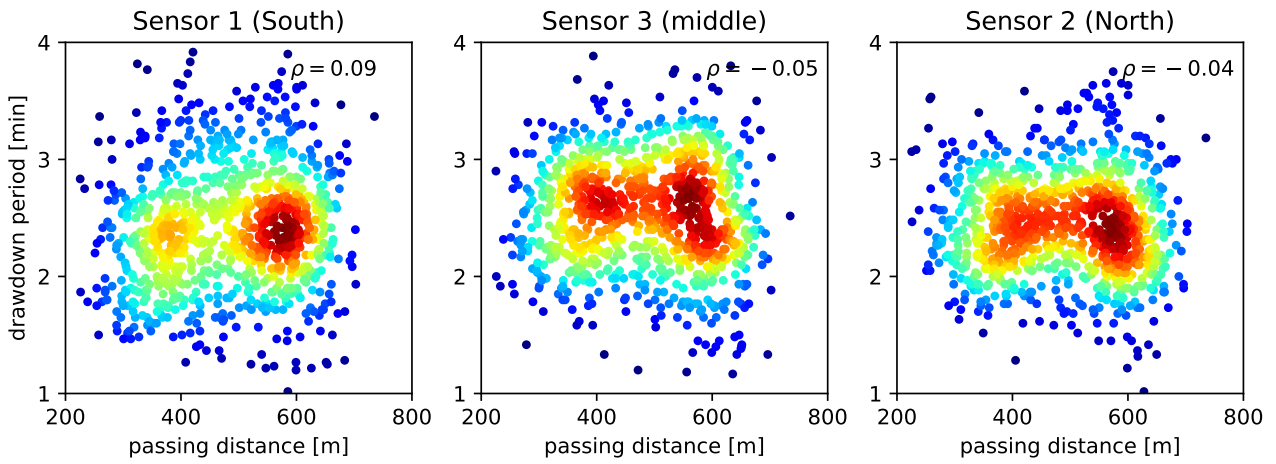
Figure J.22: Drawdown period versus passing distance ($d_s$) for Sensors 1, 3 and 2.



Figure J.23: Drawdown period versus depth at the location of the passing vessel ($h_s$) for Sensors 1, 3 and 2.
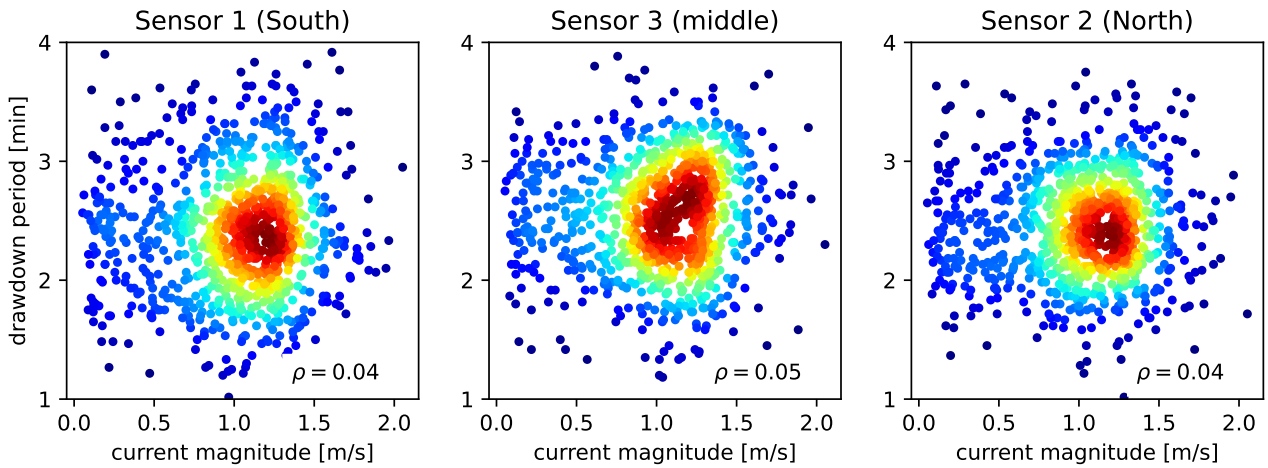


Figure J.24: Drawdown period versus current magnitude ($U_c$) for Sensors 1, 3 and 2.
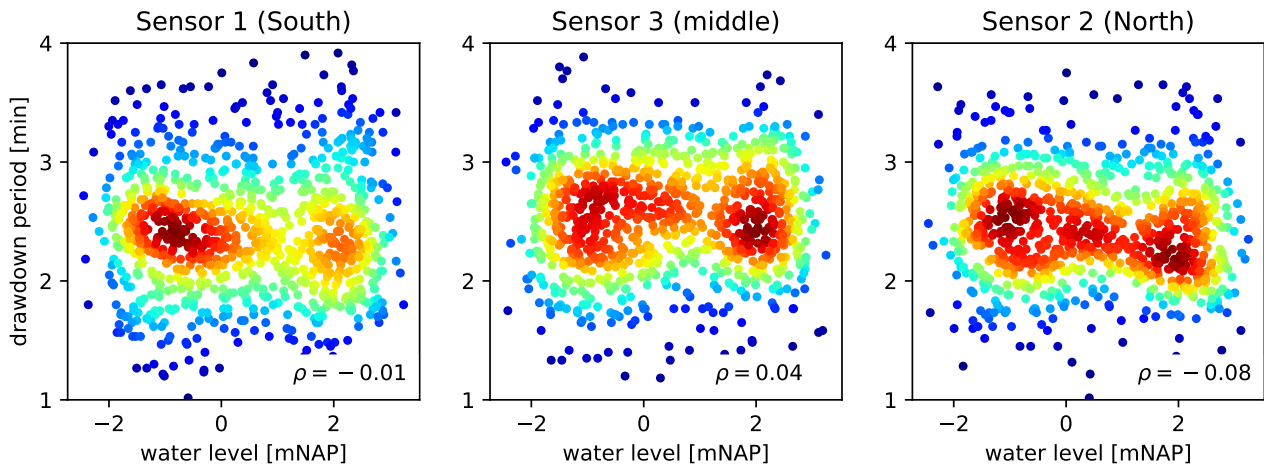
Figure J.25: Drawdown period versus water level (WL) for Sensors 1, 3 and 2.
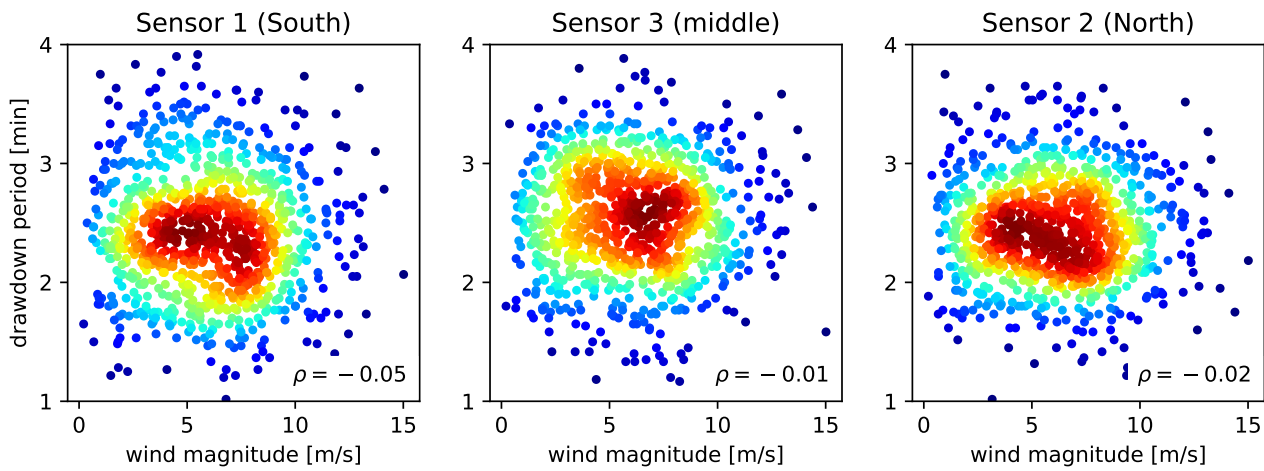


Figure J.26: Drawdown period versus wind magnitude ($U_w$) for Sensors 1, 3 and 2.

# Appendix K: Drawdown height prediction through existing methods

This appendix provides the visualizations of the drawdown height predictions of the methods not visualized in Section 6.2.
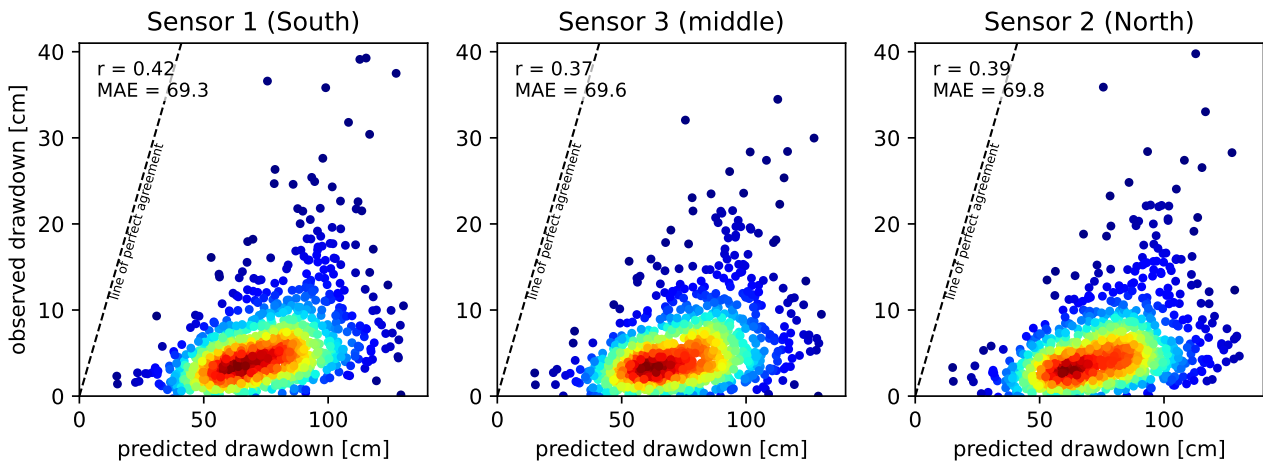


Figure K.1: The observed drawdown height versus the drawdown height predicted using Schijf (1949) including a correction factor.
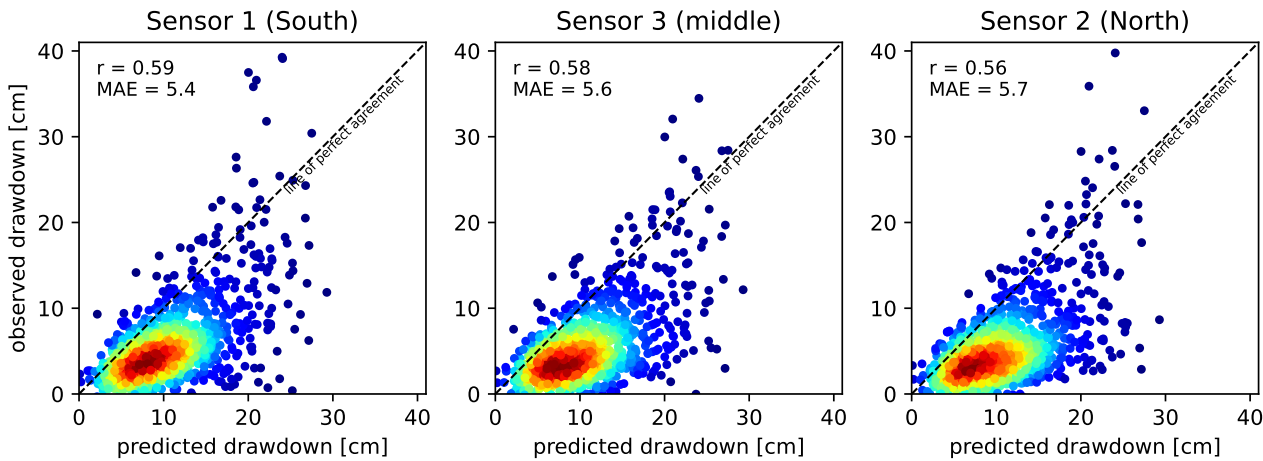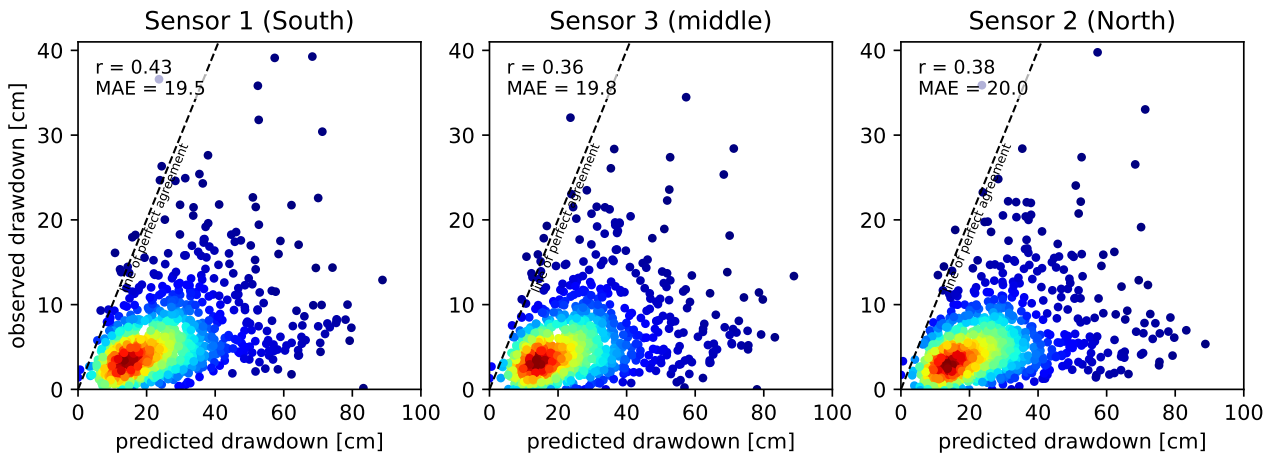


Figure K.2: The observed drawdown height versus the drawdown height predicted using Hochstein (1967).
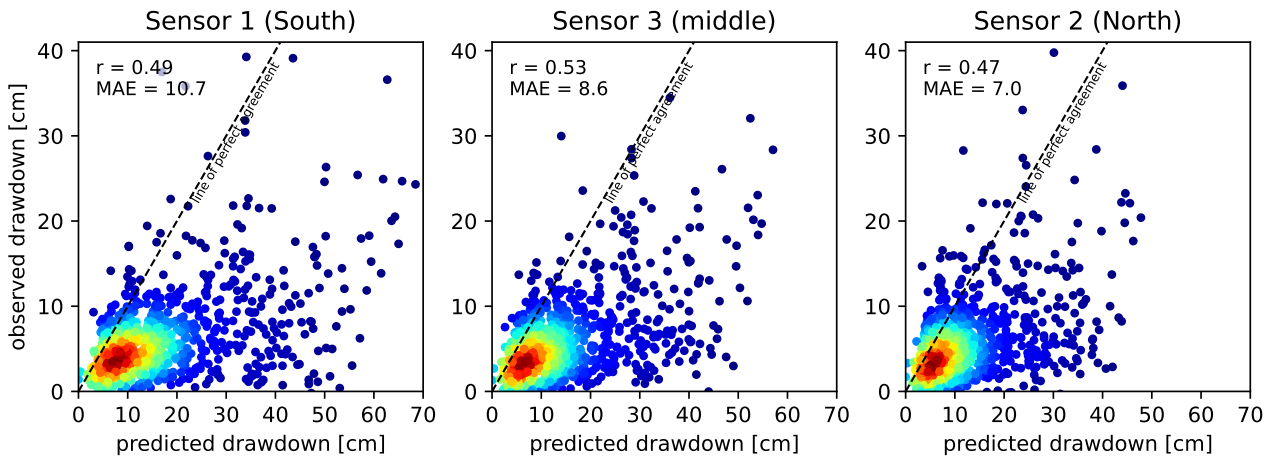
Figure K.3: The observed drawdown height versus the drawdown height predicted using Gelencser (1977).
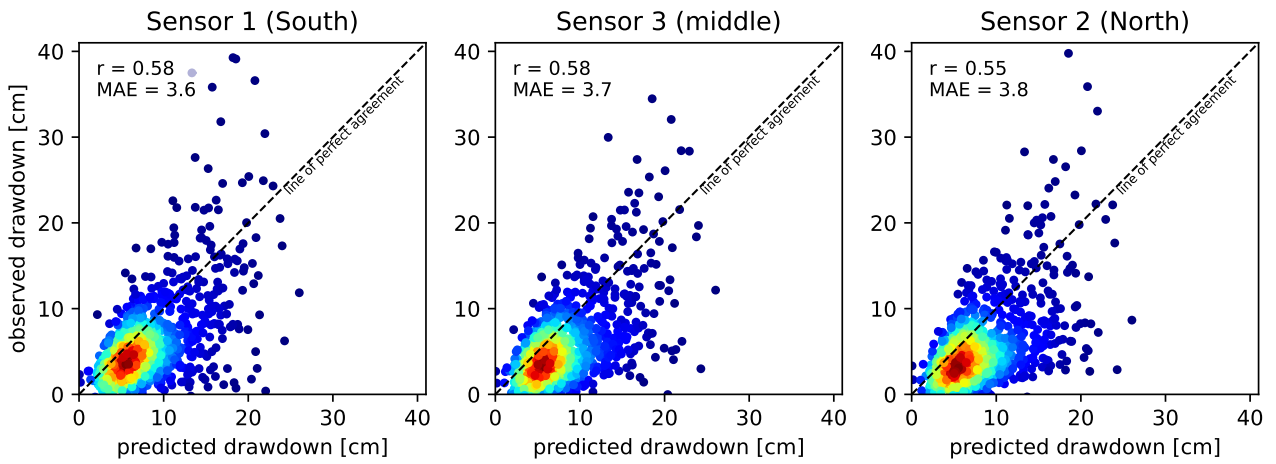


Figure K.4: The observed drawdown height versus the drawdown height predicted using Dand and White (1978).
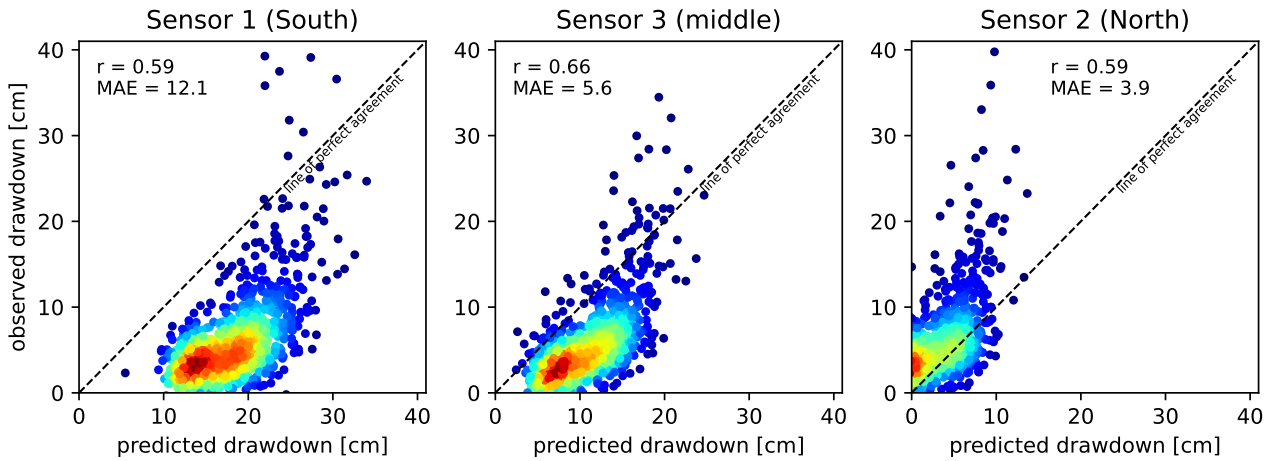


Figure K.5: The observed drawdown height versus the drawdown height predicted using Maynord (1996).

Figure K.6: The observed drawdown height versus the drawdown height predicted using Kriebel (2003).
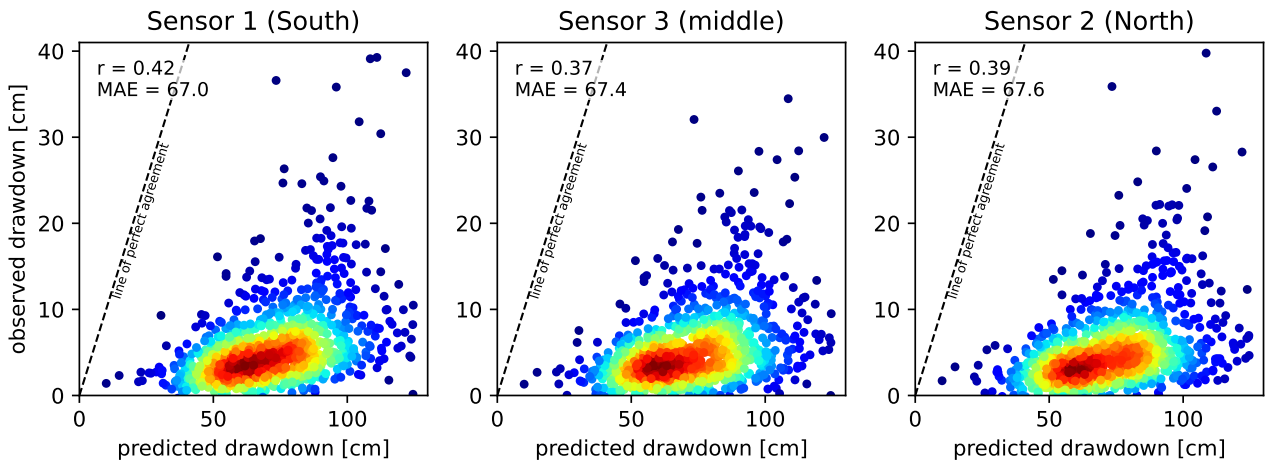


Figure K.7: The observed drawdown height versus the drawdown height predicted using CIRIA (2007).

# Appendix L: Drawdown prediction incidents

In this appendix, the drawdown height generated by the passing vessels during the recorded incidents treated in Section 1.2.4 is predicted, as a verification of the set critical drawdown height, set in Section 6.1.

Table L.1 displays the parameters used to calculate the drawdown height using the site-specific drawdown height equation (Equation 6.3) introduced in Section 6.3. In the table, the red cells denote (partially) assumed values, while the green cells denote trusted values. As the Cosco Glory and the Teno incidents occurred during the measurement campaign, all parameters are known for these cases. The following assumptions have been made for the unknown values:

- For the cases, where the cells containing the value for the speed through the water ($V_s$) of the passing vessel are marked red, the speed through the water cannot be estimated. Therefore, the average speed through the water is used, being approximately 7 [m/s], shown in Figure 5.8 in Section 5.2.

- For the incidents in which the draught of the passing vessel is unknown, the underwater cross-section amidships ($A_s$) of the passing vessel is unknown as well. For these cases, the maximum historic draught of the vessel is used to calculate the cross-section, retrieved from marinetraffic.com.

- In the cases where the passing distances ($d_s$) are unknown, the average passing distance for upstream and downstream sailing vessels is taken, using the passing distance distribution shown in Figure 5.7. The average passing distance for vessels sailing upstream is 580 metres, whereas downstream is 380 metres.

- The average depth under the vessel ($h_s$) found in the dataset is used for the incidents where the depth is unknown, being 23 metres.

- The generalized channel ($h_{channel}$) and harbour ($h_{harbour}$) depths are based on a bed level of -23 and -8mNAP for the channel and bed respectively, as instructed in Section 6.3. For the incident in which the MSC Giselle is involved, the report does not provide information on the water level, therefore, the average water level is used to calculate the generalized depths.

| vessel name | | | MSC Giselle | MSC Santhya | MSC Carouge | Monaco Maersk | Cosco Glory | Teno | MSC Benedetta | Finneco 1 |
|---|---|---|---|---|---|---|---|---|---|---|
| date | | | 17-04-2018 | 12-02-2020 | 12-02-2020 | 20-04-2022 | 10-07-2023 | 10-08-2023 | 21-10-2023 | 11-01-2024 |
| time | | | 11:51 | 20:00 | 20:00 | 10:10 | 18:54 | 15:35 | 4:45 | 21:00 |
| speed through water | $V_s$ | [m/s] | 8.7 | 7 | 7 | 7 | 6.7 | 8.6 | 8.8 | 8.8 |
| cross-section | $A_s$ | [m²] | 683 | 377 | 527 | 743 | 660 | 538 | 677 | 239 |
| passing distance | $d_s$ | [m] | 380 | 380 | 580 | 380 | 282 | 339 | 480 | 269 |
| vessel length | $L_s$ | [m] | 300 | 237 | 283 | 399 | 366 | 300 | 366 | 238 |
| depth | $h_s$ | [m] | 23 | 23 | 23 | 23 | 27.8 | 23.0 | 23 | 23 |
| channel depth | $h_{channel}$ | [m] | 22 | 23.9 | 23.9 | 25.1 | 23.2 | 21.5 | 23 | 21 |
| harbour depth | $h_{harbour}$ | [m] | 7 | 8.9 | 8.9 | 10.1 | 8.2 | 6.5 | 8 | 6 |
| drawdown height | $\Delta h$ | [cm] | 25 | 7 | 6 | 17 | 26 | 24 | 18 | 15 |

Table L.1: Calculation of the drawdown height of the recorded incidents described in Section 1.2.4. Red cells denote (partially) assumed values, while green cells denote trusted values.

For most of the incidents, the predicted drawdown values calculated surpass the set critical maximum drawdown height of 12 centimetres. Only for the incident involving the MSC Santhya and MSC Carouge, the critical level is not exceeded. The incident that occurred could be related to the summed-up drawdown effect of the two vessels passing the outer harbour shortly after each other, as described in Section 1.2.4. Furthermore, the actual vessel speeds and passing distances could be more extreme than the average values used in this calculation.

# Appendix M: Visualizations related to the prediction reliability

In this section, the water level fluctuations measurements taken during the passage of the Teno are visualized in Figure M.1. Figure M.2 visualizes the observed drawdown height versus the drawdown height predicted using the site-specific equation, using the complete dataset, including the unreliable observations.
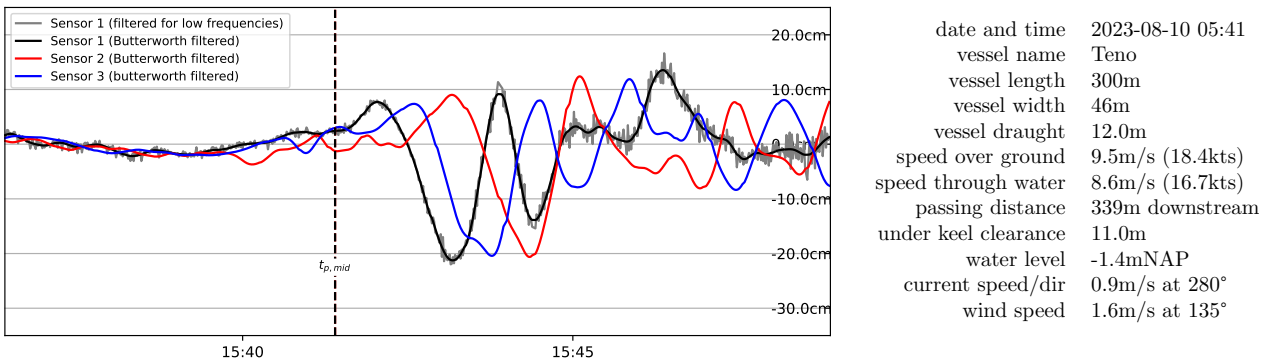


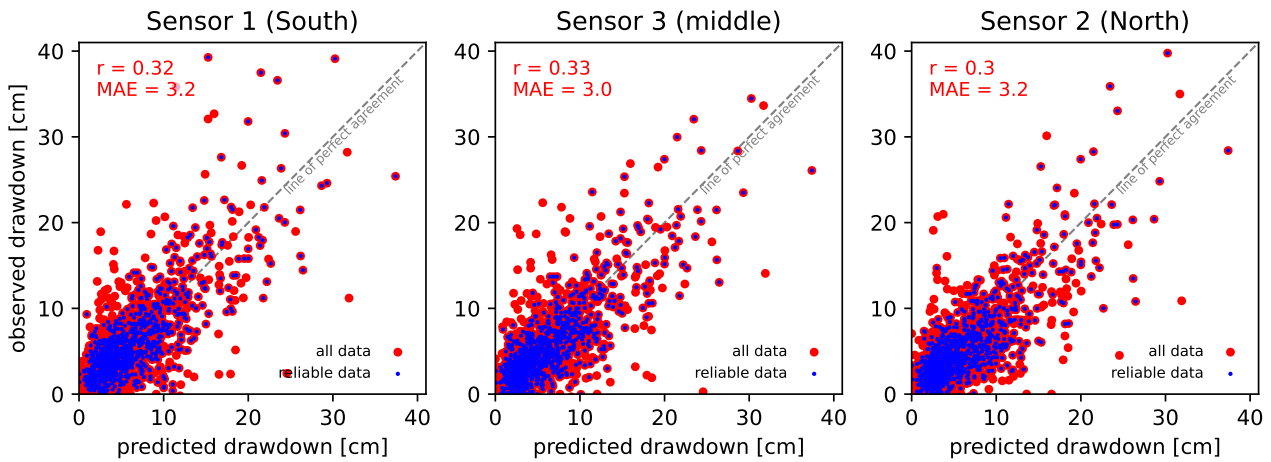Figure M.1: Water level fluctuations as measured during the passage of the Teno on the 10th of August.



Figure M.2: The observed drawdown height versus the drawdown height predicted using the site-specific equation, using the complete dataset, including the unreliable observations.

# Appendix N: Drawdown reduction measures

In this appendix, visualizations are included to support and validate the statements presented in Section 7.1.

## N.1 Individual measures

In the figures, the red line denotes the critical drawdown height of 12 centimetres. Observations generating drawdown heights greater than this limit are dotted in red. The vertical black lines indicate the proposed limits of the speed through the water and the passing distance. The figures show that a restriction based on solely the speed or passing distance is unreaslistic as the gross of the observations surpass the proposed limits.
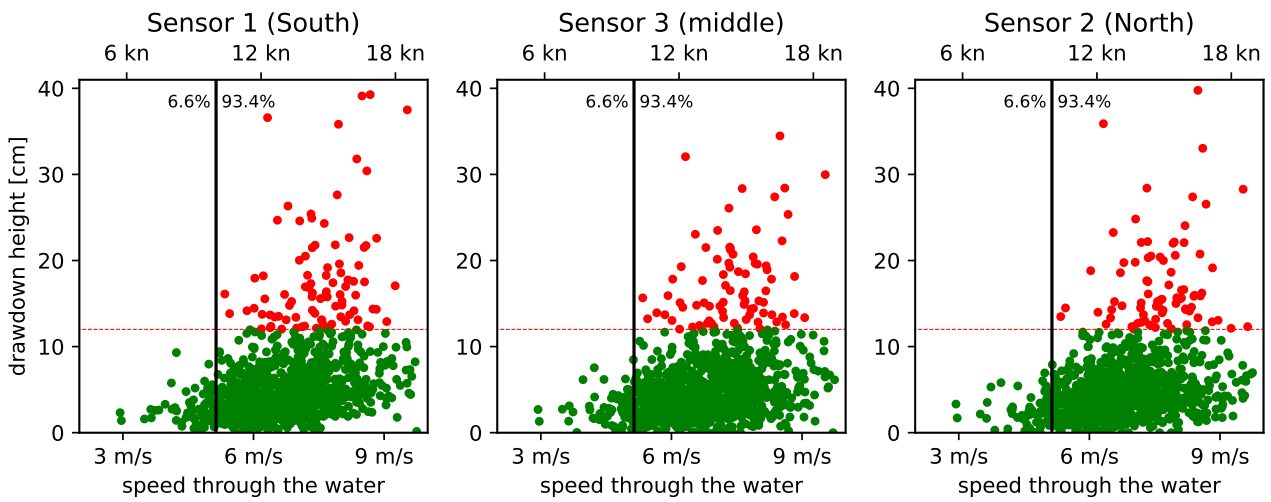
Figure N.1: The observed drawdown height against the speed through the water of the passing vessels, as measured during the measurement campaign.
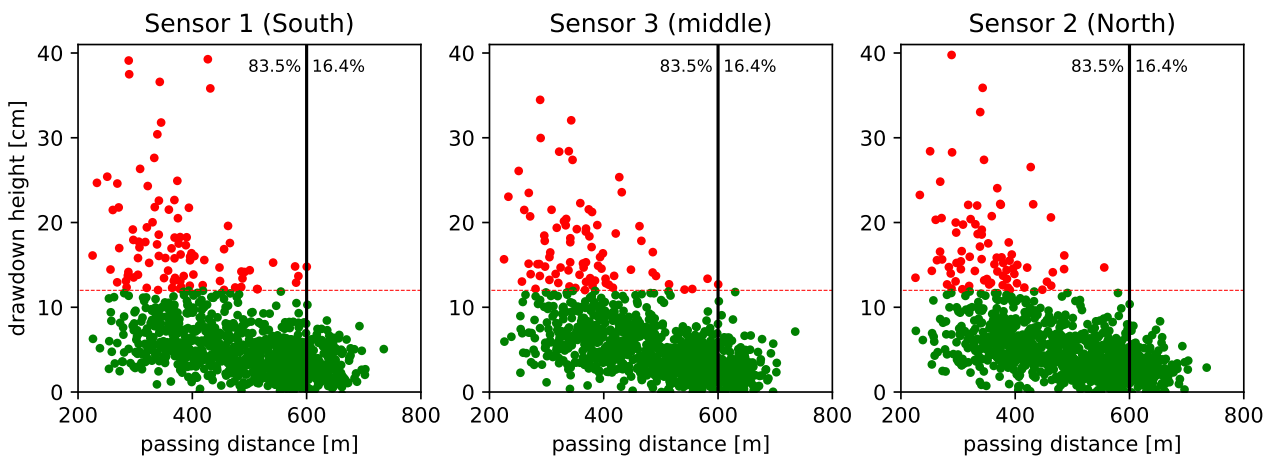
Figure N.2: The observed drawdown height against the passing distance of the passing vessels, as measured during the measurement campaign.

## N.2 Intergrated measures

As elaborated in Section 7.1, Equation 6.3 can be rewritten for the vessel speed through the water. By filling $\Delta h$ equals 0.12m as the critical water level, the submerged cross-sectional area amidships ($A_s$) of the passing vessel, the generalized channel and harbour depth ($h_{\text{channel}}$ and $h_{\text{harbour}}$) based on the water level at the time of passage, the length of the vessel ($L_s$) and the depth under the vessel at the time of passage ($h_s$), a relation between the vessel speed through the water ($V_s$) and the passing distance ($d_s$) is formulated:

$$V_s = \sqrt{\frac{2g}{0.58}\Delta h \left(\frac{A_s}{d_s h_{\text{channel}}}\right)^{-0.93} \left(\frac{L_s}{d_s}\right)^{-0.70} \left(\frac{h_s}{h_{\text{channel}}}\right)^{-0.25}} \tag{N.1}$$

In this equation, the sailing direction does not influence the critical speed. Based on the theoretical maximum speed, speed limits for different passing distance ranges can be given. Figure N.3 shows the drawdown height versus the passing distance, where the passages adhering to the most strict limit introduced in Figure 7.1 are marked green and the violating passages marked light red. However, since these measures are derived for the most extreme scenario, the majority of passing vessels' speeds surpassed the recommended maximum, without exceeding the drawdown threshold.
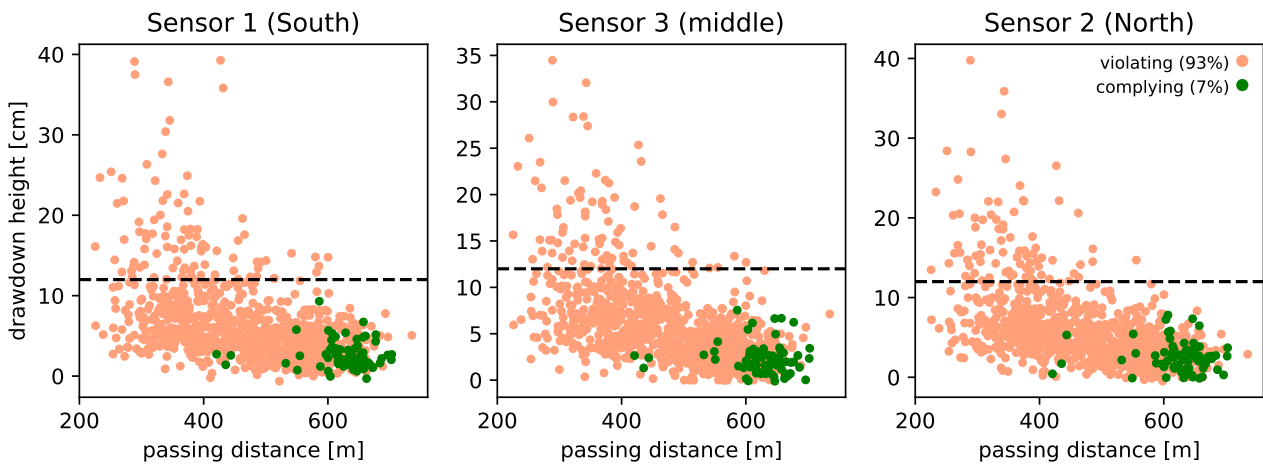


Figure N.3: Drawdown height versus the passing distance, where the passages adhering to the most strict limit are marked green and the violating passages marked light red. For the calculation of the maximum speed, the most extreme parameters are used: $B_s = 65$m, $D_s = 16$m, $L_s = 400$m, $C_m = 0.975$, WL = -2mNAP, $h_s = 26$m and $\Delta h_{\text{max}} = 12$cm.

Figures N.4, N.5 and N.6, show the recommended vessel speed for a relative critical passage, an average passage and a less critical passage, respectively.
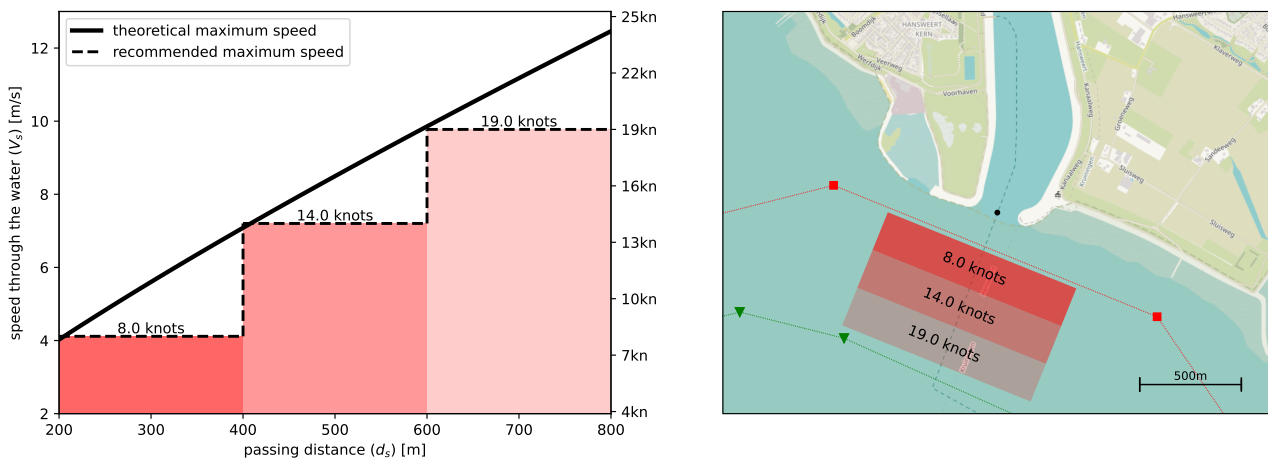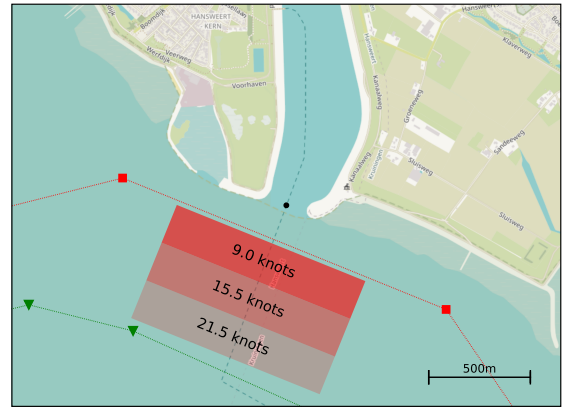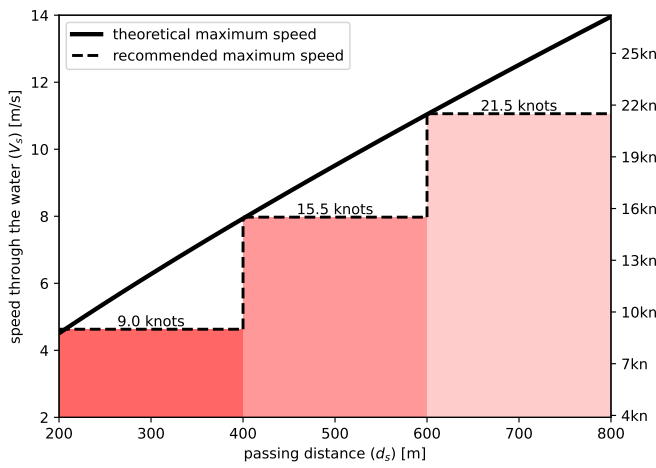


Figure N.4: Critical passing speed relative to the passing distance required to keep the drawdown height below the set maximum drawdown height. For the calculation of this example, $B_s = 40$m, $D_s = 12$m, $L_s = 340$m, $C_m = 0.975$, WL = -1mNAP, $h_s = 26$m and $\Delta h_{\text{max}} = 12$cm.
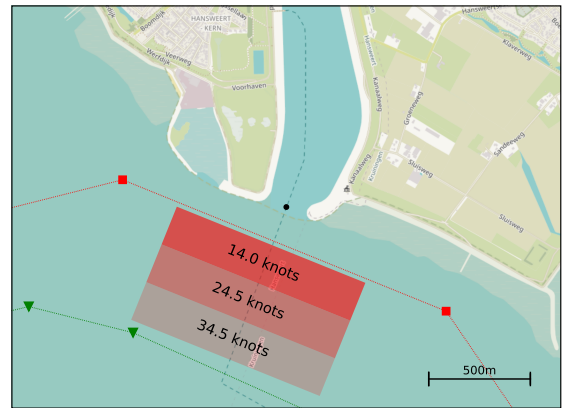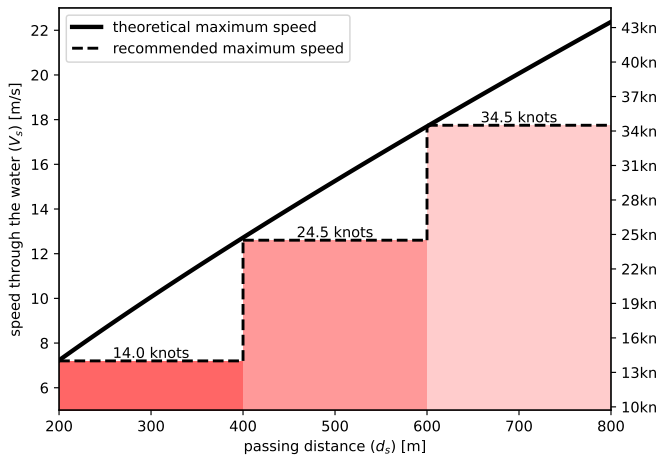
Figure N.5: Critical passing speed relative to the passing distance required to keep the drawdown height below the set maximum drawdown height. For the calculation of this example, $B_s = 40$m, $D_s = 11$m, $L_s = 300$m, $C_m = 0.975$, WL = -0.5mNAP, $h_s = 24$m and $\Delta h_{max} = 12$cm.



Figure N.6: Critical passing speed relative to the passing distance required to keep the drawdown height below the set maximum drawdown height. For the calculation of this example, $B_s = 30$m, $D_s = 10$m, $L_s = 180$m, $C_m = 0.975$, WL = 3.0mNAP, $h_s = 24$m and $\Delta h_{max} = 12$cm.

# Appendix O: Visualization of outliers

This appendix visualizes the water level fluctuations of the outliers discussed in Section 8.2.4 and provides the corresponding parameters describing the passage.
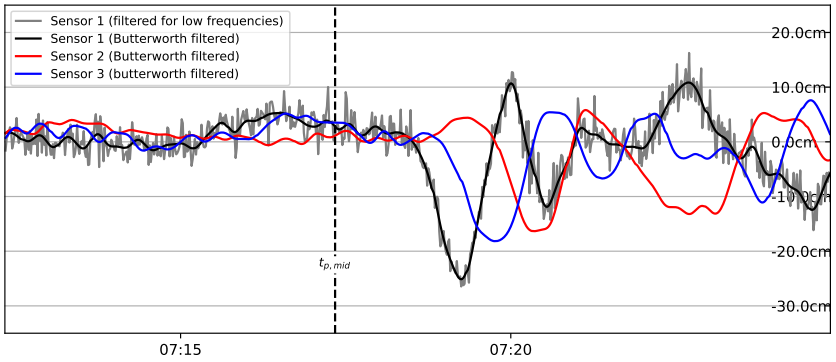


| | |
|---|---|
| date and time | 2023-07-14 07:17 |
| vessel name | Hermann Schulte |
| vessel length | 275m |
| vessel width | 40m |
| vessel draught | 11.9m |
| speed over ground | 8.8m/s (17.1kts) |
| speed through water | 8.0m/s (15.5kts) |
| passing distance | 431m downstream |
| under keel clearance | 7.4m |
| water level | -1.9mNAP |
| current speed/dir | 0.9m/s at 285° |
| wind speed | 5.6m/s at 213° |

Figure O.1: Water level fluctuations as measured during the passage of the Hermann Schulte on the 14th of July.
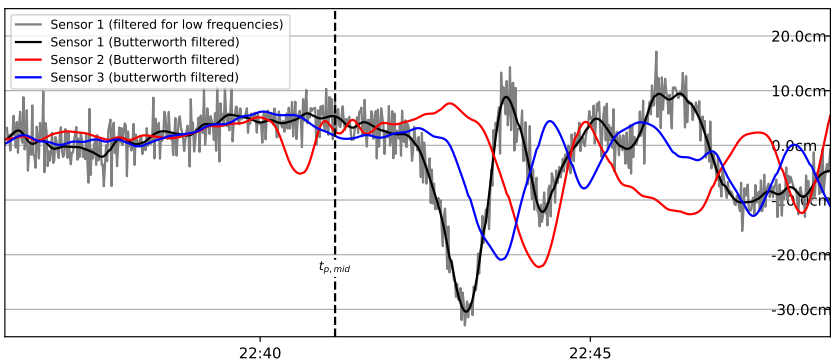


| | |
|---|---|
| date and time | 2023-07-15 22:41 |
| vessel name | MSC Tianping |
| vessel length | 334m |
| vessel width | 41m |
| vessel draught | 11.9m |
| speed over ground | 8.0m/s (15.5kts) |
| speed through water | 8.7m/s (16.9kts) |
| passing distance | 427m downstream |
| under keel clearance | 8.8m |
| water level | -0.9mNAP |
| current speed/dir | 0.7m/s at 106° |
| wind speed | 5.9m/s at 235° |

Figure O.2: Water level fluctuations as measured during the passage of the MSC Tianping on the 15th of July.
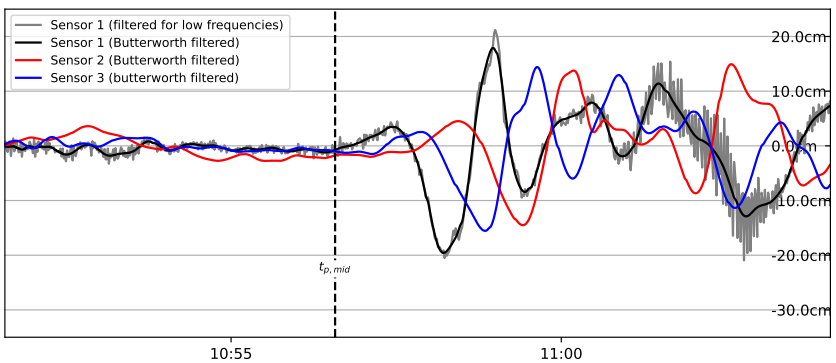


| | |
|---|---|
| date and time | 2023-07-20 10:56 |
| vessel name | CMA CGM Iskenderun |
| vessel length | 247m |
| vessel width | 32m |
| vessel draught | 10.4m |
| speed over ground | 10.4/s (20.3kts) |
| speed through water | 9.5m/s (18.5kts) |
| passing distance | 290m downstream |
| under keel clearance | 14.0m |
| water level | -1.5mNAP |
| current speed/dir | 0.9m/s at 280° |
| wind speed | 1.9m/s at 192° |

Figure O.3: Water level fluctuations as measured during the passage of the CMA CGM Iskenderun on the 20th of July.
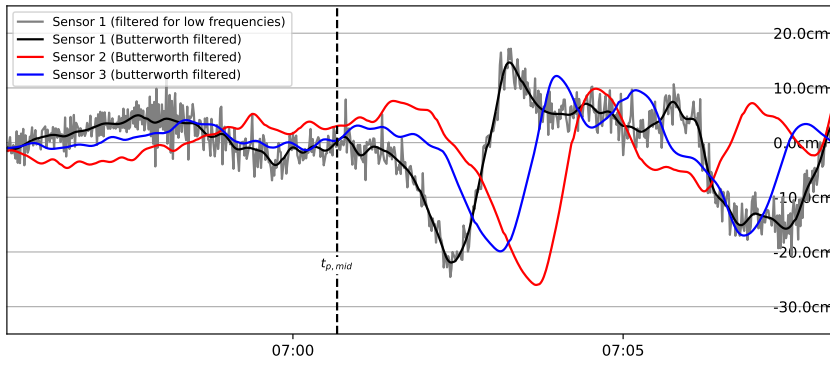
| | |
|---|---|
| date and time | 2023-07-13 07:00 |
| vessel name | HMM Helsinki |
| vessel length | 400m |
| vessel width | 61m |
| vessel draught | 13.4m |
| speed over ground | 6.4/s (13.2kts) |
| speed through water | 6.3m/s (12.3kts) |
| passing distance | 343m downstream |
| under keel clearance | 11.4m |
| water level | -1.6mNAP |
| current speed/dir | 0.5m/s at 290° |
| wind speed | 8.0m/s at 238° |

Figure O.4: Water level fluctuations as measured during the passage of the HMM Helsinki on the 13th of July.

*Return to Section 8.2.4.*